Peptide-coated microneedles for antigen specific immunotherapy of type 1 diabetes

A thesis submitted for the degree of Philosophiae Doctor in

Cardiff University

by

Xin Zhao

June 2015

Cardiff School of Pharmacy and Pharmaceutical Sciences

Cardiff University

DECLARATION

This work has not been submitted in substance for any other degree or award at this or any other university or place of learning, nor is being submitted concurrently in candidature for any degree or other award.

Signed ……Xin Zhao…… (candidate) Date ……28/08/2015……

STATEMENT 1

This thesis is being submitted in partial fulfillment of the requirements for the degree of PhD

Signed ……Xin Zhao…… (candidate) Date ……28/08/2015……

STATEMENT 2

This thesis is the result of my own independent work/investigation, except where otherwise stated.
Other sources are acknowledged by explicit references. The views expressed are my own.

Signed ……Xin Zhao…… (candidate) Date ……28/08/2015……

STATEMENT 3

I hereby give consent for my thesis, if accepted, to be available for photocopying and for inter-library loan, and for the title and summary to be made available to outside organisations.

Signed ……Xin Zhao…… (candidate) Date ……28/08/2015……

Acknowledgements

I would like to express my special appreciation and thanks to my supervisors: Prof. James C. Birchall, Dr. Sion Coulman from the School of Pharmacy and Prof. Colin Dayan and Prof. Susan Wong from the School of Medicine. Thank you all for offering me this great opportunity to explore the potential of using microneedle therapy for the treatment of T1D. Each of you has offered me an invaluable and unique perspective on this interesting topic and without your individual and collective help and expertise completion this project would never have been possible. Your expert guidance and individual enthusiasm for the work has been inspiring and motivating and I am pleased to have worked with each of you on individual aspects of the project and to have been part of a team involved in such an interesting and challenging project.

I would like to express my gratitude to Dr. Stephanie Hanna for your help and support with my experiments in immunology and for your useful advice on experimental design, along with as the camaraderie experienced working side-by-side with you on a daily basis

I would like to thank Dr. Danijela Tatovic for teaching me the fundamentals techniques of Human skin experiments and help with blood collection from donors.

To my colleagues, particularly Marc Pearton, Matt Ivory, Martha Stefanidou and Maria Dul in Pharmacy and Evy De Leenher, Joanne Davies, Larissa Carmago da Rosa, Ravinder Singh, Claire Hocter, James Pearson and Terri Thayer in Medicine. I am of course, grateful for every bit of help and advice, and I sincerely thank you for the friendship you have offered me in sharing our achievements, frustrations and tribulations together. Thanks for making me feel welcome.

Thanks to Dr. Catherine Naseriyan and Ms. Vicke Nixon for their help with flow cytometry, and to Dr. Chris von Ruhland and Mr. Kirk Scudder for their help with Electron and Light Microscopy.

Finally, thanks to my family for all of the love, encouragement and support. Thanks particularly to my parents for everything, and to my in-laws for the love and encouragement. I would like to give special thanks to my husband for his unending love and support as well as hours of proofreading, editing, and language advice.

Abstract

Type 1 diabetes is an autoimmune disorder caused by the destruction of insulin secreting ß cells in the pancreas. The aim of this project is to explore the potential of using solid-coated microneedles to target skin dendritic cells with an auto-antigen to induce tolerance for the treatment of type 1 diabetes.

A novel coating formulation has been developed to accommodate peptides with different lipophilicities. The optimised coating formulation and electro-polishing of the microneedle surface were key factors which enhance the efficiency of peptide delivery. Optimised coating formulation did not show adverse effects on peptide bioactivity or trigger a pro-inflammatory response.

The delivery route (microneedle vs. intradermal injection) was shown to be the main factor that influenced the clearance of peptide from murine skin *in vivo*. Other factors such as temperature, skin hydration state and peptide solubility were also shown to have effects on peptide clearance.

Two autoantigens were used to induce tolerance in non-obese diabetic mice – a potent mimotope m31 and endogenous antigen WE14. The proliferation profile of transferred carboxyfluorescein succinimidyl ester labelled BDC2.5 T cells in pancreatic lymph nodes in non-obese diabetic mice was used as a readout for the development of immunological tolerance. The results herein provide the first demonstration that WE14-coated microneedles were able to induce tolerance *in vivo*, showing reduced proliferation of BDC2.5 T cells.

Additionally, this project examined the potential of short-term topical application of betamethasone to enhance peptide-induced tolerance. Both human and mouse dendritic cells showed a pro-tolerogenic state after treatment with topical application of betamethasone *in vitro*. However, full dose betamethasone was shown to have systemic toxicity *in vivo*, resulting in depletion of $CD11c^+$ dendritic cells and $CD4^+$ T cells. Diluted topical betamethasone facilitated a small effect on BDC2.5 proliferation; however no advantage on enhancing antigen specific immunotherapy was observed.

Table of Contents

ABBREVIATIONS I

LIST OF FIGURES V

LIST OF TABLES IX

LIST OF EQUATIONS X

REAGENTS XI

MATERIALS AND EQUIPMENT XVI

CHAPTER 1 GENERAL INTRODUCTION 1

1.1 A BRIEF INTRODUCTION TO TYPE ONE DIABETES 1

1.2 BASIC CONCEPTS OF THE IMMUNE SYSTEM AS RELATING TO T1D 4

1.3 DENDRITIC CELLS (DCS) AND T CELL CROSS-TALK 5

1.4 T CELLS AND AUTOIMMUNITY 10

1.4.1 CD4 T cell subsets and their functions *10*

1.4.1.1 Effector T cells 11

1.4.1.2 Regulatory T cells (Tregs) 13

1.4.1.3 Markers of $CD4^+$ T cells 16

1.5 CENTRAL TOLERANCE, PERIPHERAL TOLERANCE AND AUTOIMMUNITY 19

1.5.1 Central tolerance *19*

1.5.2 Peripheral tolerance *21*

1.6 THE NOD (NON OBESE DIABETIC) MOUSE 23

1.6.1 Pathology of T1D in NOD mouse *23*

1.6.2 The BDC2.5-TCR (T cell receptor)-Tg (transgenic) mouse *26*

1.6.3 Auto-antigens in the NOD mouse *28*

1.7 ANTIGEN SPECIFIC IMMUNOTHERAPY (ASI) 31

1.7.1 Antigen Specific Immunotherapy (ASI) *31*

1.7.2 Non-antigen based therapy *34*

1.8 SKIN STRUCTURE AND SKIN IMMUNITY 36
1.9 ADMINISTRATION OF DRUGS USING MICRONEEDLES (MNS) 40
1.9.1 Drug administration methods, ... *40*
1.9.2 A brief introduction to MNs *41*
1.9.3 MN types *42*
1.9.4 MN safety *46*
1.9.4.1 Poration and microbial infection 46
1.9.4.2 Pain sensation 48
1.9.5 MNs used for drug delivery *50*
1.9.5.1 Vaccine delivery using MN 50
1.9.5.2 Peptide delivery using MN 52
1.10 AIMS AND OBJECTIVES 56
CHAPTER 2 MN DESIGN AND COATING FORMULATION 59
2.1. INTRODUCTION 59
2.1.1. Choice of MNs for ASI *59*
2.1.2. Coating formulation for solid-coated MNs *61*
2.1.3. Solid MN geometry and drug transportation *62*
2.2. OBJECTIVES 64
2.3. METHODS 65
2.3.1. Preparation of human skin explants *65*
2.3.2. Imaging MNs using Scanning Electron Microscopy (SEM) *65*
2.3.3. OCT (Optical Coherence Tomography) imaging *66*
2.3.4. Skin delivery using hollow MNs *68*
2.3.5. Coating procedure for solid MNs *68*
2.3.6. Imaging the MN after coating *69*
2.3.7. Skin delivery using solid MNs *70*
2.3.8. Quantification of delivery efficiency of 5-TAMRA conjugated peptide using UV-vis absorbance *70*

2.3.9. Skin histology *71*

2.3.10. Measurement of pH value of acetic acid solution *73*

2.3.11. Electro-polishing stainless steel MNs *73*

2.4. RESULTS 75

2.4.1. Choice of MNs for targeting skin DCs *75*

2.4.1.1. Delivery depth, solid versus hollow MNs 75

2.4.1.2. Skin disruption using solid MNs of different length 79

2.4.2. Development of a novel coating formulation *81*

2.4.2.1. Peptide properties 81

2.4.2.2. Choice of solvent for coating hydrophobic peptides 81

2.4.2.3. Choice of formulation excipients 84

2.4.3. Factors that influence skin delivery efficiency *86*

2.4.3.1. Excipients in the coating formulation 86

2.4.3.2. The effect of MN surface properties 87

2.4.3.3. Delivery efficiency as a function of hydrophobicity of peptide 91

2.4.3.4. Effect of skin species on skin delivery 93

2.4.3.5. Effect of needle numbers on delivery efficiency 94

2.4.4. Design and manufacture of solid-coated MN systems suitable for both human and mouse skin models *94*

2.4.5. Validation of new MN designs for peptide coating and delivery *97*

2.5. DISCUSSION 99

2.5.1. Targeting skin DCs with minimal damage *99*

2.5.2. Coating formulation for hydrophobic peptides *101*

2.5.3. Factors that influence delivery efficiency using solid-coated MNs *106*

2.5.4. Design of solid MNs for minimally invasive delivery of peptide in both human and mouse skin models *111*

2.6. CONCLUSIONS 115

CHAPTER 3 INDUCING TOLERANCE *IN VIVO* USING SOLID-COATED MN ARRAY 116

3.1. INTRODUCTION 116

3.1.1. Animal models for study of T1D 116

3.1.1.1. NOD-SCID mouse 116

3.1.1.2. Foxp3-FIR (Foxp3- internal ribosomal entry site-linked monomeric red fluorescent protein) mouse 117

3.1.2. CD4+ T cell function and proliferation assays 117

3.2. OBJECTIVES 120

3.3. METHODS 121

3.3.1. Mice 121

3.3.2. Preparation of a single cell suspension from murine SP (spleen) and LNs (lymph nodes) 121

3.3.3. In vitro BDC2.5 T cell proliferation 122

3.3.4. Evaluating the effect of MN coating formulation on m31 bioactivity 123

3.3.5. Cytokine detection of IFNγ using ELISA (enzyme linked enzyme-linked immunosorbent assay) 123

3.3.6. Intravital imaging of peptide clearance from murine skin. 124

3.3.7. Optimising CFDA-SE labelling conditions and concentration for BDC2.5 T cells using an in vitro assay 126

3.3.8. Investigating the time and minimum CFSE+BDC2.5 T cell number required for in vivo studies. 127

3.3.9. CD4+ T cell isolation using MACs kit 127

3.3.10. Using Flow cytometry to identify cell phenotypes 128

3.3.11. Trafficking of m31 in vivo 129

3.3.12. Administration of peptides 129

3.3.13. Inducing tolerance in vivo 130

3.3.14. Foxp3+BDC2.5 T cells suppressive effect in vivo 130

3.4. RESULTS 132

3.4.1. Characterization of BDC2.5 T cells 132

3.4.2. Evaluating the effect of MN coating formulation on m31 bioactivity 134

3.4.3. Clearance of peptide from skin 135

3.4.3.1. Effect of environmental temperature on m31-5TAMRA peptide clearance from mouse skin 135

3.4.3.2. Effect of peptide solubility and administration method on clearance 136

3.4.3.3. Local effect of pre-treatment of skin with BD cream on m31-5TAMRA peptide clearance from skin 137

3.4.4. Optimising the CFSE labelling protocol for monitoring m31 trafficking and BDC2.5 T cell proliferation in vivo 142

3.4.4.1. MACs sorting purity check 142

3.4.4.2. Optimizing CFDA-SE labeling conditions and concentration for BDC2.5 T cells using an in vitro assay 143

3.4.4.3. Optimizing the proliferation time required for transferred CFSE$^+$BDC2.5 T cells in vivo 146

3.4.4.4. Titrating the minimum number of CFSE labeled BDC2.5 T cells required for in vivo tolerance study 147

3.4.5. Tracking m31 in vivo using CFSE labelled BDC2.5 T cells 148

3.4.6. Inducing peripheral tolerance in vivo 152

3.4.6.1. Expanding antigen specific Tregs in the BDC2.5 TCR-Tg.Foxp3-FIR mouse 152

3.4.6.2. CD4$^+$Foxp3$^+$ BDC2.5 T cells suppress the immune response in vivo 153

3.4.6.3. Peripheral tolerance could be induced in NOD mice by using WE14 delivered by solid-coated MNs, showing a dose sparing effect compared to ID injection. 156

3.5. DISCUSSION 159

3.5.1. Characterization of the BDC2.5-TCR-Tg mouse 159

3.5.2. Evaluating the effect of coating formulation on m31 bioactivity 159

3.5.3. Pharmacokinetics of peptide administered by solid-coated MNs or ID injection 160

3.5.3.1. Factors that influence the in vivo clearance of peptides from mouse skin 160

3.5.3.2. Trafficking of the m31 peptide in vivo 164

3.5.4. Optimise CFSE labelling protocol for the analysis of cell proliferation 166

3.5.5. Peripheral tolerance could be induced in NOD mice by using WE14 delivered by solid-coated MNs, showing a dose-sparing effect compared to ID injection. .. *168*

3.6. CONCLUSION 172

CHAPTER 4 EFFECT OF SHORT TERM TOPICAL BETAMETHASONE ON ASI 174

4.1. INTRODUCTION 174

4.1.1. Topical glucocorticoid and its local effect on immune cells *174*

4.1.1.1. Effect on DCs 175

4.1.1.2. Betamethasone 176

4.2. OBJECTIVES 178

4.3. METHODS 179

4.3.1. Preparation of human epidermal cells *179*

4.3.2. Human peripheral blood mononuclear cell (PBMC) preparation *179*

4.3.3. Intradermal Betamethasone delivery using a topical cream or solid-coated MNs *181*

4.3.4. Ex vivo human skin explant culture *181*

4.3.5. Quantification of BSP using HPLC (high pressure liquid chomography) *182*

4.3.6. Preparation of mouse epidermal cells *182*

4.3.7. Imaging mouse LCs in an epidermal sheet *183*

4.3.8. Evaluating the effect of betamethasone on the phenotype of human epidermal DCs *183*

4.3.9. Evaluating the effect of betamethasone on human epidermal cells using the Mixed Lymphocyte Reaction (MLR) assay *184*

4.3.10. Assessing the effect of topical BD cream on murine epidermal cells *184*

4.3.11. Titrating topical BD cream for in vivo study *185*

4.3.12. Topical BD effect on local antigen presentation *185*

4.3.13. Determining the dose of BD cream *186*

4.3.14. Topical BD effect on inducing tolerance in vivo *186*

4.4. RESULTS 187

4.4.1. Effect of topical steroid on epidermal cells in both human and mouse skin models *187*

4.4.1.1. Quantification of BSP using HPLC 187

4.4.1.2. Effect of steroid on human epidermal cells 188

4.4.1.3. Effect of topical steroid on mouse epidermal cells 191

4.4.2. Titration of topical BD cream for in vivo study *193*

4.4.2.1. Short term effect of topical steroid on local and systemic antigen presentation 193

4.4.2.2. Effect of BD cream on cells in LNs 195

4.4.2.3. Titration of topical steroid for murine study 196

4.4.3. Effect of short term topical BD on inducing antigen specific tolerance in vivo *201*

4.5. DISCUSSION 203

4.5.1. Effect of BD cream on epidermal cells *203*

4.5.2. Titration of topical steroid for murine study *204*

4.5.3. Effect of topical BD cream on inducing antigen specific tolerance in vivo *206*

4.6. CONCLUSION 209

CHAPTER 5 GENERAL DISCUSSION 211

5.1. BRIEF OVERVIEW 211

5.2. SIGNIFICANCE, LIMITATIONS AND FUTURE WORK 211

5.2.1. MN design and coating formulation *211*

5.2.2. Inducing tolerance in vivo using solid-coated MNs *215*

5.2.3. Effect of short term topical BD on ASI *220*

5.3. CONCLUDING REMARKS 222

BIBLIOGRAPHY 224

Abbreviations

Abbreviation	Full name
2M2B	2 methyl 2 butanol
AIRE	Autoimmune regulator
ALN	Axillary lymph node
ANOVA	Analysis of variance
ASI	Antigen specific immunotherapy
AUC	Area under curve
BD	Betamethasone dipropionate
BSA	Bovine serum albumin
BSP	Betamethasone sodium phosphate
CD	Cluster of differentiation
cDC	Conventional/Classic dendritic cell
CFDA	Carboxyfluorescein diacetate
CFDA-SE	Carboxyfluorescein diacetate succinimidyl ester
ChgA	Chromogranin A
CLN	Cervical lymph node
CMC	Carboxymythyl cellulose
CPM	Counts per minute
CTL	Cytotoxic T lymphocyte
CTLA-4	Cytotoxic T-lymphocyte-associated protein 4
DC	Dendritic cell
DI water	Deionised water
DMEM	Dulbecco's Modified Eagle's Medium Base
EDTA	Ethylenediaminetetraacetic acid

ELISA	Enzyme-linked immunosorbent assay
FCS	Foetal calf serum
FIR	Foxp3-IRES-mRFP
Foxp3	Forkhead box P3
G	Gauge (hypodermic needle)
GC	Glucocorticoid
GITR	Glucocorticoid-induced TNFR-related protein
HA	Sodium hyaluronate
H&E	Haematoxylin and eosin
HLA	Human leukocyte antigen
HPLC	High-performance liquid chromatography
HRP	Horseradish peroxidase
ICA69	Islet cell autoantigen 69 Kda
ID	Intradermal
IFA	Incomplete Freund's adjuvant
IFNγ	Interferon gamma
IHC	Immunohistochemistry
IL	Interleukin
ILN	Inguinal lymph node
IM	Intramuscular
IRES	Internal ribosomal entry site (linked)
iTreg	Induced Tregs
LN	Lymph node
m31	BDC2.5 mimotope 1040-31
mDC	Myeloid dendritic cell
MFI	Mean fluorescent intensity
MHC	Major histocompatibility complex

MLR	Mixed Lymphocyte reaction
MN	Microneedle
mRFP	Monomeric red fluorescent protein
mTEC	Medullary thymic epithelial cells
NF-kappaB	Nuclear factor kappa-light-chain-enhancer of activated B cells
NOD	Non-obese diabetic
NRI	Normalised relative intensity
nT	Naïve T cell
nTreg	Naturally occurring thymic-derived Tregs
OCT	Optical coherence tomography
OVA	Ovalbumin
p	Probability value
PaLN	Para-aortic lymph node
PBMCs	Peripheral blood mononuclear cells
PBS	Phosphate-buffered saline
pDC	Plasmacytoid dendritic cell
pH	H^+ potential
PHA	Phytohaemagglutinin
PI	Isoelectric point
PK	Pharmacokinetics
PLGA	Poly(lactic-co-glycolic acid)
PLN	Pancreatic lymph node
PTH1-34	Parathyroid hormone 1-34
PVA	Polyvinyl alcohol
PVP	Polyvinylpyrrolidone
NRI	Normalised relative intensity

ROI	Region of interest
SC	Subcutaneous
SCID	Severe combined immunodeficiency
SD	Standard deviation
SEM	Scanning electron microscope
SI	Stimulation index
SP	Spleen
Stat	Signal transducer and activator of transcription
T1D	Type 1 diabetes
TAMRA	Carboxytetramethylrhodamine
Tcm	Central memory T cell
TCR	T cell receptor
Teff	Effector T cell
Tem	Effector memory T cell
TEWL	Transepidermal water loss
TGase	Transglutaminase
TGFβ	Transforming growth factor beta
Th1,2 or 17	Helper T cell type 1, 2 or 17
TMB	3,3',5,5'-Tetramethylbenzidine
TNFR	Tumour necrosis factors receptor
TNFα	Tumour necrosis factors alpha
Tol-DC	Tolerogenic dendritic cell
Treg	Regulatory T cell
VAS	Visual analogue scale
VLPs	Virus-like particles
wire-EDM	wire-Electric discharge machining

List of Figures

FIGURE 1.1 SCHEMATIC VIEW OF CELLULAR MECHANISMS OF T1D AND ANTIGEN SPECIFIC IMMUNOTHERAPY (ASI). 5

FIGURE 1.2 INTERACTION BETWEEN DCS AND $CD4^+$ T CELLS. 7

FIGURE 1.3 $CD4^+$T CELL SUBSETS.. 10

FIGURE 1.4 FOUR BASIC MECHANISMS THAT TREG UTILISE TO REGULATE IMMUNE RESPONSES. 15

FIGURE 1.5 SKIN ANATOMY AND SKIN DCS. 37

FIGURE 1.6 SCHEMATIC VIEW OF DELIVERY METHOD USING FOUR TYPES OF MNS. ..45

FIGURE 1.7 SCHEMATIC VIEW OF USING SOLID-COATED MN TO INDUCE TOLERANCE *IN VIVO*. 57

FIGURE 2.1 SCHEMATIC VIEW OF MICRONJET® MN APPLICATION TO HUMAN SKIN ... 68

FIGURE 2.2 SCHEMATIC DIAGRAM SHOWING THE COATING PROCESS USING A TIP COATING METHOD. 69

FIGURE 2.3 SOLID MN ASSEMBLY AND APPLICATION METHOD ON MOUSE. 70

FIGURE 2.4 SCHEMATIC VIEW OF THE MN ELECTRO-POLISHING PROCESS. 74

FIGURE 2.5 IMAGES OF NANOPASS 450µM MN AND DERMAROLLER® MN..... 76

FIGURE 2.6 HUMAN VS. MOUSE SKIN STRUCTURE. 78

FIGURE 2.7 DELIVERY DEPTH OF PEPTIDES USING HOLLOW MN AND SOLID MN IN HUMAN AND MOUSE SKIN. 79

FIGURE 2.8 SKIN DISRUPTION IN HUMAN VOLUNTEERS BY SOLID MNS IMAGED BY OCT. 80

FIGURE 2.9 FLUORESCENT IMAGES OF COATING ABILITY OF PROINSULIN B9-23-FITC IN FORMULATION WITH DIFFERENT EXCIPIENTS. 86

FIGURE 2.10 EXCIPIENT EFFECT ON DELIVERY EFFICIENCY OF WE14-5TAMRA USING 500µM DERMAROLLER® MNS. 87

FIGURE 2.11 SEM IMAGES OF SOLID MN SURFACE MORPHOLOGY. 88

FIGURE 2.12 DELIVERY EFFICIENCY OF WE14-5TAMRA USING ELECTRO-POLISHED MNS. 88
FIGURE 2.13 MN DIMENSIONS BEFORE AND AFTER ELECTRO-POLISHING. 89
FIGURE 2.14 IMAGES SHOW MN PENETRATION AND WE14-5TAMRA (PINK) RELEASE INTO HUMAN SKIN EXPLANTS AFTER 10 MINUTES APPLICATION.. 90
FIGURE 2.15 EFFECT OF SURFACE MORPHOLOGY ON THE DELIVERY EFFICIENCY OF WE14-5TAMRA IN HUMAN SKIN. 91
FIGURE 2.16 EFFECT OF PEPTIDE HYDROPHOBICITY ON DELIVERY EFFICIENCY IN HUMAN SKIN EXPLANTS USING ELECTRO-POLISHED 500µM MN. 92
FIGURE 2.17 EFFECT OF PEPTIDE HYDROPHOBICITY ON DELIVERY EFFICIENCY IN MOUSE SKIN USING ELECTRO-POLISHED 500µM MN. 93
FIGURE 2.18 THE DELIVERY EFFICIENCY OF WE14-5TAMRA IN HUMAN AND MOUSE SKIN USING ELECTRO-POLISHED 500µM LONG MNS. 93
FIGURE 2.19 THE EFFECT OF DISTRIBUTING THE COATING ON DIFFERENT NUMBERS OF MNS ON DELIVERY EFFICIENCY OF M31-5TAMRA IN MOUSE SKIN. 94
FIGURE 2.20 DESIGN OF MNS SUITABLE FOR BOTH HUMAN AND MOUSE STUDIES. ... 96
FIGURE 2.21 COATING REPEATABILITY OF M31-TAMRA USING IN HOUSE DESIGNED SOLID-COATED MNS. 98
FIGURE 2.22 DELIVERY EFFICIENCY RANGE OF M31-TAMRA AND WE14-TAMRA USING IN HOUSE DESIGNED MNS. 98
FIGURE 2.23 EQUILIBRIUM TERNARY SYSTEM OF WATER, ACETIC ACID AND TERT-AMYL ALCOHOL AT 298K. 105
FIGURE 2.24 DISTRIBUTION OF INSULIN WITHIN SKIN FOLLOWING DELIVERY VIA MNS. 113
FIGURE 3.1 SCHEMATIC VIEW OF KODAK *IN VIVO* IMAGING SYSTEM. 126
FIGURE 3.2 IDENTIFICATION OF BDC2.5 T CELLS. 133
FIGURE 3.3 A GRAPH TO ILLUSTRATE THE IMPACT OF THE MN COATING PROCESS ON THE BIOACTIVITY OF THE M31 PEPTIDE. 134

FIGURE 3.4 A GRAPH TO COMPARE THE BIOACTIVITY OF THE 1NG M31 PEPTIDE, BOTH WITH AND WITHOUT 5-TAMRA CONJUGATION. 135
FIGURE 3.5 REPRESENTATIVE FLUORESCENT INTRAVITAL IMAGE FOR ANALYSING PEPTIDE-5TAMRA CONJUGATE CLEARANCE FROM THE SKIN. 139
FIGURE 3.6 CLEARANCE CURVE OF INJECTED PEPTIDE-5TAMRA WITHIN THE SKIN. 140
FIGURE 3.7 AUC GRAPH SHOWING THE FACTORS THAT INFLUENCE THE OVERALL CLEARANCE RATE OF PEPTIDE FROM THE SKIN..... 141
FIGURE 3.8 PURITY OF $CD4^+$ T CELLS AFTER USING A MACS CD4 ISOLATION KIT.. 143
FIGURE 3.9 OPTIMISATION OF CFDA-SE LABELLING PROTOCOL TO MONITOR M31 TRAFFICKING AND BDC2.5 T CELL PROLIFERATION *IN VIVO*. 145
FIGURE 3.10 REPRESENTATIVE FLOW CYTOMETRY PLOT SHOWING THE TIME COURSE OF $CD4^+CFSE^+$ T CELLS *IN VIVO* PROLIFERATION IN PLN. 147
FIGURE 3.11 TITRATION CFSE LABELLED CELLS *IN VIVO*..... 148
FIGURE 3.12 REPRESENTATIVE FLOW CYTOMETRY PLOTS OF $CD4^+CFSE^+$ BDC2.5 T CELL PROLIFERATION PROFILES IN DIFFERENT LNS AND THE SP THREE DAYS AFTER TRANSFER. 150
FIGURE 3.13 TRACKING THE DISTRIBUTION OF M31 *IN VIVO* USING CFSE LABELLED BDC2.5 T CELLS..... 151
FIGURE 3.14 EXPANDED ANTIGEN SPECIFIC TREG CELL POPULATION IN BDC2.5 TCR-TG.FOXP3-FIR MOUSE FOLLOWING A SINGLE DOSE OF WE14 DELIVERED BY ID INJECTION. 153
FIGURE 3.15 BDC2.5 $FOXP3^+$ TREGS SUPPRESS THE ANTIGEN SPECIFIC IMMUNE RESPONSE *IN VIVO*.. 155
FIGURE 3.16 PERIPHERAL TOLERANCE WAS SHOWN TO BE INDUCED IN NOD MICE BY USING WE14 DELIVERED BY SOLID-COATED MNS, SHOWING A DOSE SPARING EFFECT COMPARED TO ID INJECTION. 158
FIGURE 4.1 BASIC MECHANISMS OF ACTION FOR GCS ON IMMUNE CELLS. 175

FIGURE 4.2 HPLC QUANTIFICATION OF BSP DOSE DELIVERED TO HUMAN OR MOUSE SKIN USING SOLID-COATED MN. 187
FIGURE 4.3 EFFECT OF BETAMETHASONE ON HUMAN EPIDERMAL DCS. 190
FIGURE 4.4 THE EFFECT OF SHORT-TERM TOPICAL BD CREAM ON MOUSE EPIDERMAL CELLS. 192
FIGURE 4.6 EFFECT OF 0.05%W/W BD CREAM ON LOCAL AND SYSTEMIC ANTIGEN PRESENTATION, REFLECTED BY A CHANGE TO THE PROLIFERATION PROFILE OF TRANSFERRED BDC2.5 T CELLS. 194
FIGURE 4.7 EFFECT OF BD CREAM ON T CELL AND DC POPULATION IN THE ALN AND PLN. 196
FIGURE 4.8 BD EFFECT ON $CD4^+$ T CELL POPULATION. 198
FIGURE 4.9 EFFECT OF SHORT TERM TOPICAL BD ON CD4+ T CELL PHENOTYPES. 199
FIGURE 4.10 EFFECT OF BD ON $CD11C^+$ DCS POPULATION IN ALN AND PLN. 200
FIGURE 4.11 EFFECT OF TOPICAL BD PRE-TREATMENT ON INDUCING ANTIGEN SPECIFIC TOLERANCE *IN VIVO*. 202

List of Tables

TABLE 1.1 $CD4^+$ MEMORY T CELL FUNCTION AND HOMING. 12

TABLE 1.2 CD4+ T CELL MARKERS. 16

TABLE 1.3 AUTO-ANTIGENS FOUND IN THE NOD MOUSE, WHICH HAVE A ROLE IN T1D DEVELOPMENT. 30

TABLE 2.1 PEPTIDE PROPERTIES.. 81

TABLE 2.2 CHEMICALS PHYSICAL PROPERTIES. 83

TABLE 2.3 COATING FORMULATION COMPOSITION FOR THREE PEPTIDES. 84

TABLE 2.4 EXCIPIENTS TESTED AS COMPONENTS IN THE COATING FORMULATION TO IMPROVE COATING ABILITY. 85

TABLE 2.5 ANATOMICAL DIFFERENCES BETWEEN MOUSE AND HUMAN SKIN 110

TABLE 3.1 ABBREVIATIONS FOR LNS USED IN EXPERIMENTS. 122

TABLE 3.2 ANTIBODY PANEL AND DYES FOR CELL STAINING USED TO IDENTIFY CFSE LABELLED $CD4^+$ T CELL PHENOTYPE BY FLOW CYTOMETRY. 129

TABLE 4.1 POTENCY AND PHARMACODYNAMICS OF BETAMETHASONE COMPARED WITH OTHER GCS. 177

TABLE 4.2 HPLC MOBILE PHASE GRADIENT FOR DETECTING BSP. 182

TABLE 4.3 ANTIBODY LIST FOR EXAMINING THE EFFECT OF BETAMETHASONE ON THE PHENOTYPE OF HUMAN EPIDERMAL CELLS. 184

TABLE 4.4 ANTIBODY LIST TO ANALYSE THE EFFECT OF BD CREAM ON THE PHENOTYPE OF LOCAL AND SYSTEMIC $CD4^+$ T CELLS. 185

TABLE 4.5 EFFECT OF TOPICAL BETAMETHASONE ON CD4+T CELL AND ITS SUBPOPULATIONS. 200

List of Equations

EQUATION 2.1 CALCULATING THE MASS OF PEPTIDE THAT REMAINED ON SOLID MNS. 71

EQUATION 2.2 CALCULATING THE DELIVERY EFFICIENCY OF PEPTIDE USING SOLID MNS. 71

EQUATION 3.1 EQUATION USED TO CALCULATE STIMULATION INDEX (SI) FROM CPM. 122

EQUATION 3.2 EQUATION USED TO CALCULATE NORMALISED RELATIVE INTENSITY (NRI). 125

Reagents

Reagent	Company	Country
(2-hydoxypropyl)-ß-cyclodextrin, powder, BioReagent	Sigma	UK
0.25% trypsin with 0.02% EDTA	Sigma	UK
2-Mercaptoethanol (55mM), Gibco®	Life Technologies	UK
2-methyl-2-butanol, ReagentPlus®, ≥99%	Sigma	UK
2-Propanol, BioReagent, ≥99.5%	Sigma	UK
Acetic acid, ACS reagent, ≥99.7%	Sigma	UK
Acetonitrile	Fisher	UK
Antibiotic-Antimycotic (100X) (10,000 units/mL of penicillin, 10,000 µg/mL of streptomycin, and 25 µg/mL of Fungizone® Antimycotic)	Life Technologies	UK
BDC2.5 mimotope (YVRPLWVRME), >95% purity	GLs	China
BDC2.5-5TAMRA (YVRPLWVRME-5TAMRA), >95% purity	GLs	China
Betamethasone sodium phosphate	Sigma	UK
Biotin Rat Anti-Mouse IFNγ	BD Biosciences	UK
Bovine Serum Albumin, powder, 96%	Fisher	UK
Carbonate-Bicarbonate Buffer, capsule	Sigma	UK
CD4+ T Cell Isolation Kit, mouse	Miltenyi Biotec	UK
Collagenase, Type IV, powder,	Life Technologies	UK

Gibco®		
Deoxyribonuclease I, lyophilized powder, Protein ≥85 %, ≥400 U/mg	Sigma	UK
DI water	Fisher	UK
Dimethyl Sulfoxide, 100ml, Molecular Biology Grade	Fisher	UK
Diprobase Cream	Merck Sharp & Dohme Limited	UK
DiproSone®0.05%w/w Cream (0.05% w/w betamethasone as dipropionate)	Merck Sharp & Dohme Limited	UK
Dispase® II (neutral protease, grade II), ≥0.8 U/mg	Roche	UK
Dulbecco's Modified Eagle's Medium Base, D 5030	Sigma	UK
Dulbecco's Phosphate Buffered Saline, liquid, sterile-filtered, -Ca2+, -Mg2+	Sigma	UK
Ethanol absolute 99.8+%	Fisher	UK
Ethylenediaminetetraacetic acid disodium salt solution (EDTA) 0.5M	Sigma	UK
Faramount Mounting Medium, Aqueous	Dako	UK
Fetal Bovine Serum, sterile-filtered	Sigma	UK
Ficoll® solution, Type 400, 20% in H2O	GE healthcare	UK
Fluorescence Mounting Medium, 15ml	Dako	UK

Glycerol, analytical grade	Fisher	UK
Hematoxylin, 85%, pure, Acros Organics	Fisher	UK
Heparin Sodium (preservative free), 1000 I.U./ml	Wockhardt	UK
HEPES, 1M, Gibco®	Life Technologies	UK
Human IL-10 ELISA Ready-SET-Go kit	e-bioscience	UK
Human serum, Type AB, sterile-filtered	Sigma	UK
Proinsulin B9-23-FITC (SHLVEALYLVCGERG-FTIC), >95% purity	GLs	China
L-Glutamine, 200mM, 100x, Gibco®	Life Technologies	UK
Mouse IL-10 ELISA Ready-SET-Go kit	e-bioscience	UK
OCT cryoembedding Matrix	Fisher	UK
Ortho-phosphoric acid (85%) 1.69 S.G.	Fisher	UK
PEG (MW 1450)	Sigma	UK
Penicillin-Streptomycin (10,000 U/mL), Gibco®	Life Technologies	UK
Phytohemagglutinin, M form (PHA-M)	Life Technologies	UK
Pluronic® F-127	Sigma	UK
Pluronic® F-68	Sigma	UK
Purified Rat Anti-mouse IFNγ	BD Biosciences	UK
PVA (MW 2000)	Sigma	UK

RPMI 1640, without L-Glutamine	GE healthcare	UK
Shandon Eosin Y aqueous CE-IVD	Fisher	UK
Soybean trypsin inhibitor, powder	Life Technologies	UK
Streptavidin, horseradish peroxidase (HRP) conjugate, Molecular Probes®	Life Technologies	UK
Thymidine, [Methyl-3H]- Specific Activity: 20Ci/mmol	PerkinElmer	UK
TMB Substrate Reagent Set	BD Biosciences	UK
Trypan Blue solution, 0.4% in phosphate buffered saline	Thermo Scientific	UK
Vybrant® CFDA SE Cell Tracer Kit	Life Technologies	UK
WE14 (WSRMDQLAKELTAE), >95% purity	GLs	China
WE14-5TAMRA (WSRMDQLAKELTAE-5TAMRA), >95% purity	GLs	China

Species	Antibody /Dye	Fluorophore	Clone	Company	Country
Mouse	CD62L	APC	MEL-14	Biolegend	UK
	CD25	Pacific Blue	PC61	Biolegend	UK
	CD4	PE Cy7	RM4-5	Biolegend	UK
	CD44	Percp cy5.5	IM7	Biolegend	UK
	Vβ4 TCR	FITC	A95-1	BD bioscience	UK
	CD62L	PE	MEL-14	ebioscience	UK
	CD69	PB	H1.2F3H 1.2F3	Biolegend	UK
	GITR	Alex Fluor 488	YGITR765	Biolegend	UK
Human	HLA DR	Percp Cy5.5	L243	Biolegend	UK
	Langerin	PE	10E2	Biolegend	UK
	CD1a	eFluor® 450	HI149	ebioscience	UK
Mouse /human	Viability	eFluor® 780	-	ebioscience	UK

Materials and Equipment

Name/Model	Company	Country
12mm adhesive carbon tab, G3347N	Agar Scientific	UK
1ml Luer syringe	BD Biosciences	UK
27 Gauge needle (short)	BD Biosciences	UK
32 x 10 mm aluminium specimen stubs, G318	Agar Scientific	UK
Centrifuge 5810 R	Eppendorf	UK
Contura Clipper	Wella	UK
Costar 3799, 96 U bottom plate	Corning	UK
Cryotome FSE	Thermo Scientific	UK
EMscope sputter coater	Agar Scientific	UK
F96 CERT Maxisorp plate	Thermo Scientific	UK
FACs tube	BD Biosciences	UK
FACSAria III	BD Biosciences	UK
Flow cytometer, Canto II	BD Biosciences	UK
Frost glass slides	Fisher	UK
Harvester	Tomtec	UK
HPLC 1200 UV	Agilent	UK
HyperClone, ODS C18 Gemini 5µm	Phenomenex	UK
Insulin inject syringe (U-100, 0.5ml, 28G x 1/2 in)	BD Biosciences	UK
Kodak FX Pro	Carestream	UK
Leica DM IRB Microscope	Leica	UK

Leit-C Conducting Carbon Cement, G3300	Agar Scientific	UK
Lens tissue	Fisher	UK
MACs Separation Columns (LS)	Milteny	UK
MicroBeta Counter	Perkin Elmer	UK
Microtome blade, MB35 Premier	Thermo Scientific	UK
Millipore® Millicell® cell culture plate inserts 12mm	Sigma	UK
MN holder	Made in house	UK
Multiwave plate reader	Thermo Scientific	UK
NanoVue Plus Spectrophotometer	GE lifesciences	UK
Olympus BX50 Microscope	Olympus	UK
Optical coherence tomography system	Vivosight	UK
Pasteur pipette	Fisher	UK
pH meter 4521	Hanna	UK
Raw MNs	Made in house	UK
Research plus 0.1-2.5µl pipette	Fisher	UK
SEM, JSM-840A	JEOL	UK
Sterile Cell Strainer 40µm	Fisher	UK
Sterile cell strainer 70µm	Fisher	UK
Superfrost Plus glass slide	Thermo Scientific	UK
Sure one 0.1µl-10µl ultra long tip	Fisher	UK

Chapter 1 General Introduction

1.1 A brief introduction to type one diabetes

Type one diabetes (T1D) is an autoimmune disorder which is caused by the destruction of insulin secreting beta-cells in the islets of Langerhans in the pancreas (van Belle et al., 2011). The first primary pathology of the pancreas in human T1D was documented by Gepts (Gepts, 1965). His work demonstrated that the loss of pancreatic beta cell mass occurs prior to the clinical presentation of the disease.

Insulin, an endocrine hormone, is responsible for regulating the uptake of blood glucose by cells, which is broken down within cells to produce energy. In response to elevated blood glucose levels beta cells secrete insulin, which is stored in granules in the beta cells. In order to compensate for the consumption of insulin, proinsulin is converted into insulin and C-peptide (Uchizono et al., 2007). Hyperglycaemia, caused by dysregulation of glucose in the system, can cause damage to several organs and can lead to complications such as retinopathy (eye disease), nephropathy (nerve disease), and cardiovascular disease (Forbes and Cooper, 2013).

Classified as a metabolic disease, T1D can be diagnosed clinically by a raised blood glucose level. This is associated with reduced C-peptide concentration, the presence of beta cell-reactive T cells, and the presence of antibodies against insulin, IA-2 and GAD65 (American Diabetes, 2010). T1D has also been referred to, in the past, as juvenile diabetes, as many patients are diagnosed with T1D at a young age. Approximately 10% of the diabetic population have T1D with a ~4% increase in incidence every year (Harjutsalo et al., 2008, Taplin et al., 2005).

With the development of scientific techniques and an improved understanding of autoimmunity, it was in the 1970s that T1D was classified as an autoimmune disease (Cudworth and Woodrow, 1977, Irvine, 1977). The understanding of the immunological pathogenesis of the disease rapidly improved with the development of animal models, such as the biobreeding rat and the non-obese diabetic (NOD) mouse. The development of the NOD mouse in 1980 (Makino et al., 1980) was particularly important due to its ability to develop T1D which is comparable to human disease.

Currently, the most common treatment for T1D is the subcutaneous injection of insulin. Although this approach reduces the risk of microvascular complications, patients are required to constantly monitor the blood glucose level, which can fluctuate, in order to avoid hypoglycaemia. The use of insulin can help reduce acute complications and prolong patient life span, however, it does not provide a cure for T1D. Patients, especially those diagnosed at a young age, need to rely on insulin treatment for the rest of their life span. The need for daily insulin injections (the current delivery method of choice for patients) coupled with the need to be extremely vigilant with diet and lifestyle adjustments reduces patients' life quality and may make tasks which are relatively simple for non-diabetic individuals. Despite careful management, patients are often still susceptible to glucose level fluctuations and are therefore vulnerable to the acute effects of hypoglycaemia, which can cause damage to the heart and brain and can be life threatening, even in well-controlled diabetes. This possibility may also place an emotional burden on the family and loved ones of patients, as they can have no control over such events. The desire to improve life expectancy and reduce impediment to the life style of patients has led to forty years of T1D research undertaken mainly to elucidate the mechanisms of cellular immunology and

genetic susceptibility factors. Despite this work, there currently remains no cure for this chronic disease. (Pettus and von Herrath, 2013).

1.2 Basic concepts of the immune system as relating to T1D

As a defence system, the immune system consists of the innate immune system and the adaptive immune system. Apart from physical barriers, cells of the innate immune system are the first to respond to pathogens. The innate immune response is quick and non-specific, and typically involves mast cells, macrophages, leukocytes, dendritic cells, natural killer cells, basophils and eosinophils (Storey and Jordan, 2008). The adaptive immune system provides a second layer of immune protection and is an antigen-specific process, which involves T cells and B-lymphocytes. T1D is an autoimmune disease caused mainly by the dysregulation of immune tolerance which involves an imbalance of pathogenic T cells and regulatory T cells (Tregs). One of the cellular mechanisms of T1D is that under proinflammatory conditions DCs take up beta cell antigens, which are released due to the damage of beta cells, and become fully mature. These mature DCs differentiate naïve $CD4^+$ T cells into antigen specific pathogenic $CD4^+$ effector T cells (Teff). These $CD4^+$ Teffs then help the activation of $CD8^+$ cytotoxic T cells, which infiltrate the pancreas and induce apoptosis in beta cells. Without the paired (accompanying) tolerogenic mechanism, such as $CD4^+$ Tregs, this diabetogenic process progresses unhindered and eventually causes tissue damage. On the other hand, together with appropriate regulatory signals, DCs can differentiate naïve $CD4^+$ T cells into Tregs, which prevent the development of Teffs and thereby protect beta cells from damage by cytotoxic $CD8^+$ T cells (Figure 1.1). One potential therapy for T1D is to use the regulatory properties of DCs and Tregs in a beta-cell-antigen-specific manner, i.e. antigen specific immunotherapy (ASI). Therefore, it is important to understand the role of DCs and T cells, especially $CD4^+$ T cells, in T1D. By directing DCs and T cells toward different developmental pathways, it is

possible to provide a therapy, which works by re-inducing balance using tolerogenic dendritic cells and regulatory T cells.

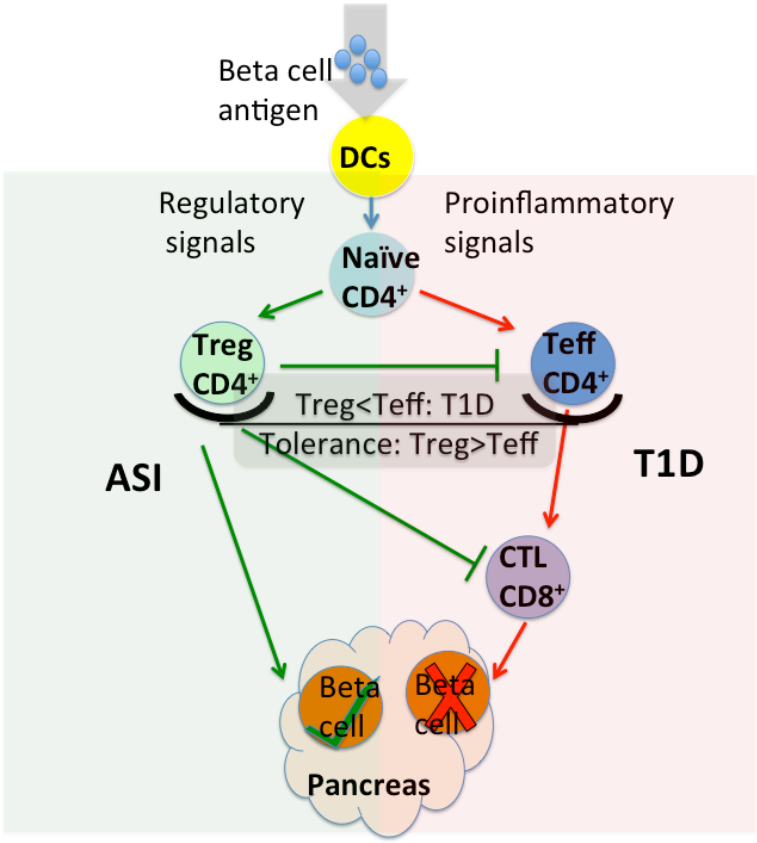

Figure 1.1 Schematic view of cellular mechanisms of T1D and antigen specific immunotherapy (ASI). Naïve $CD4^+$ T cells can be differentiated into either Teff or Treg under different immune signals. Autoimmunity can occur when the regulatory mechanism is out of balance. An organ specific immunotherapy (ASI) can be used to re-induce tolerance, which can prevent or delay the development of T1D. Teff=Effector T cell, Treg=Regulatory T cell, CTL=cytotoxic T cell, ASI= antigen specific immunotherapy, T1D=type one diabetes.

1.3 Dendritic Cells (DCs) and T cell cross-talk

DCs are a special type of antigen presenting cell (APC). DCs provide an important bridge between the innate immune system and adaptive immune system by capturing, processing and presenting antigens to T lymphocytes (Inaba et al., 1993, Moll et al., 1993, Reis e Sousa et al., 1993).

DCs were first identified in secondary lymphoid organs (spleen (SP) and lymph nodes (LNs)) in 1973 and named 'Dendritic Cells' due to their branched morphology (Steinman and Cohn, 1973). There are two major DC subsets: conventional or classical DCs (cDC) and plasmacytoid DCs (pDC). pDCs represent a small proportion of the total DC population, whose main function it is to respond to viral infection. pDCs can be identified by their secretion of type one interferons and low expression of major histocompatibility complex II (MHC II) and CD80/CD86 co-stimulators (Reizis et al., 2011). Unlike pDCs, cDCs express high levels of CD11c and MHCII and can be identified using these two surface markers (Miloud et al., 2010). Resident in both lymphoid and non-lymphoid tissues, cDCs constantly sample their surroundings for foreign antigens or self-antigens (Merad and Manz, 2009). Therefore, cDCs play an important role in priming T cells to induce immune responses to foreign antigens or inducing tolerance to self-antigens.

DCs are a highly heterogeneous group of cells that are able to perform different functions. They can either prime T cells to induce immunity or educate T cells to have a tolerogenic function. DCs are able to communicate with T cells using a number of different signals as illustrated in Figure 1.2.

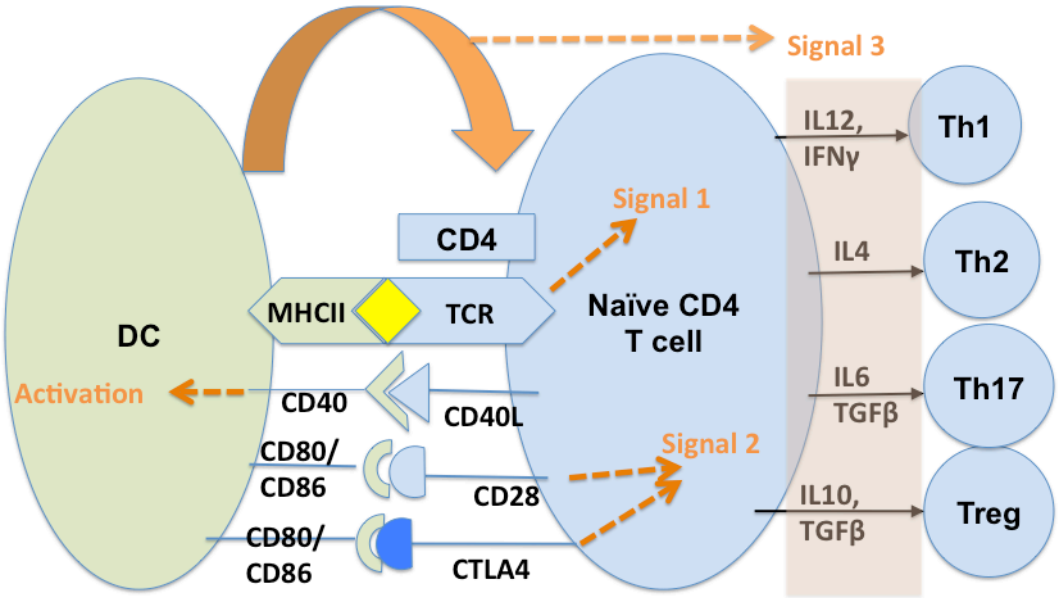

Figure 1.2 Interaction between DCs and CD4$^+$ T cells. Three signals are involved in DC and naïve T cell interaction, which helps the differentiation of naïve CD4$^+$ T cells into different subsets. The first signal is through MHCII-peptide complex to TCR in an antigen specific manner. The second signal from DC is through costimulators (CD80/CD86) to CD28, which is expressed by T cells and up-regulates activation signals in T cells. When lacking co-stimulatory signals, naïve T cells become anergic. CTLA4 expressed by T cells can also interact with CD80/CD86 and compete with CD28 binding. CTLA4 is not able to induce activation signals but can induce a regulatory signal. The third signal involved in DC/T cell interaction is via cytokines. Proinflammatory cytokines, such as IFNγ, IL4 and IL6 differentiate naïve T cells into effector T cell subsets: Th1, Th2 and Th17. Regulatory cytokines, such as IL10 and TGF-β help with Treg differentiation. Furthermore, the binding of CD40 and CD40 ligand (CD40L) gives positive feedback to DCs and promotes the activation of DCs (Merad et al., 2013).

In the steady state, immature DCs are constantly sampling the surrounding environment for pathogens. After phagocytosis, DCs digest pathogens into small protein or peptide fragments. These fragments then bind with MHC molecules creating MHC-peptide complexes, which can then be translocated to the cell surface. Intracellular pathogens, such as viruses, are processed in the cytoplasm and loaded on MHC I, which presents to CD8$^+$ T cells. On the other hand, extracellular pathogens, processed in endosome/lysosome, are loaded onto MHC II and presented to CD4$^+$ T cells (Savina and Amigorena, 2007).

DCs are activated and become fully matured once they encounter a pathogen, which is recognised through pattern recognition receptors, such as toll like

receptors (TLRs) (Hoarau et al., 2006). Fully mature DCs undergo a phenotypic change (expressing high MHCII and CD80/CD86) and migrate to the draining lymph node where they are able to activate T cells through signals from MHCII, CD80/CD86 and pro-inflammatory cytokines, such as TNFα and IL12 (Romani et al., 2001, Kurita et al., 2006).

In the steady state, DCs are resident in tissues and remain immature, with low expression of MHCII and costimulators (CD80, CD86) on the cell surface (Mommaas et al., 1995). In the absence of costimulators (CD80, CD86), DCs stimulate T cells in a tolerogenic manner, inducing anergy (Appleman and Boussiotis, 2003). It was suggested that by injection of a soluble antigen, DCs can avoid activation and thus induce T cell anergy (Miller et al., 2007). DCs also play an important role in the maintenance of the T cell repertoire. In the steady state, DCs constantly monitor T cells through self-peptide MHCII/TCR interaction. If a TCR has high affinity for self-peptide MHCII, T cells will be programmed to undergo apoptosis. T cells with a low or intermediate affinity will survive, enabling successful antigen recognition (Garbi et al., 2010).

DCs play an important role in maintaining peripheral tolerance. DCs carrying self-antigen migrate to LNs without activation, showing a semi-mature state with high expression of MHCII and CD80/CD86 but low pro-inflammatory cytokine expression (Lutz and Schuler, 2002). Instead of activating T cells, these semi-mature DCs express IL10 and induce Tregs (Akbari et al., 2001). These semi-mature DCs have therefore been referred to as tolerogenic DCs (tol-DC), indicating their function in inducing tolerance. Several factors have been investigated to determine their influence in educating DCs into tol-DCs. Vitamin D3 can differentiate DCs into tol-DCs, which then promote the secretion of IL10 and the apoptosis of mature DCs (Szeles et al., 2009, Penna and Adorini, 2000).

TNFα plays a critical role in inducing tol-DCs by vitamin D3. Vitamin D3 treated DCs failed to induce Tregs when membrane bound TNFα (insoluble) was blocked (Kleijwegt et al., 2010). Dexamethasone is another immune regulator that was used to induce tol-DCs. Like vitamin D3, dexamethasone can modulate DCs into a semi-mature phenotype and these tol-DCs have been shown to induce IL10 secreting Tregs (Unger et al., 2009).

1.4 T cells and autoimmunity

1.4.1 CD4 T cell subsets and their functions

T cells are derived from bone marrow and undergo maturation in the thymus, whereby they become single positive CD4 or CD8 T cells. $CD8^+$ T cells are cytotoxic T cells, which eliminate cells infected with intracellular pathogens, such as viruses (Zhang and Bevan, 2011). CD8 T cell receptors recognise major histocompatibility complex class I (MHCI) and cytosolic pathogen fragments. $CD4^+$ T cells are responsible for the elimination of intracellular pathogens, which can recognise MHCII / antigen complexes. $CD4^+$ T cells can be subdivided into effector T cells (helper T cell type (Th) 1, Th2, Th9, Th13 and Th17) and regulatory T cells (Tregs) (iTreg, Tr1, and Th3) according to their cytokine production and their function (Luckheeram et al., 2012) (Figure 1.3).

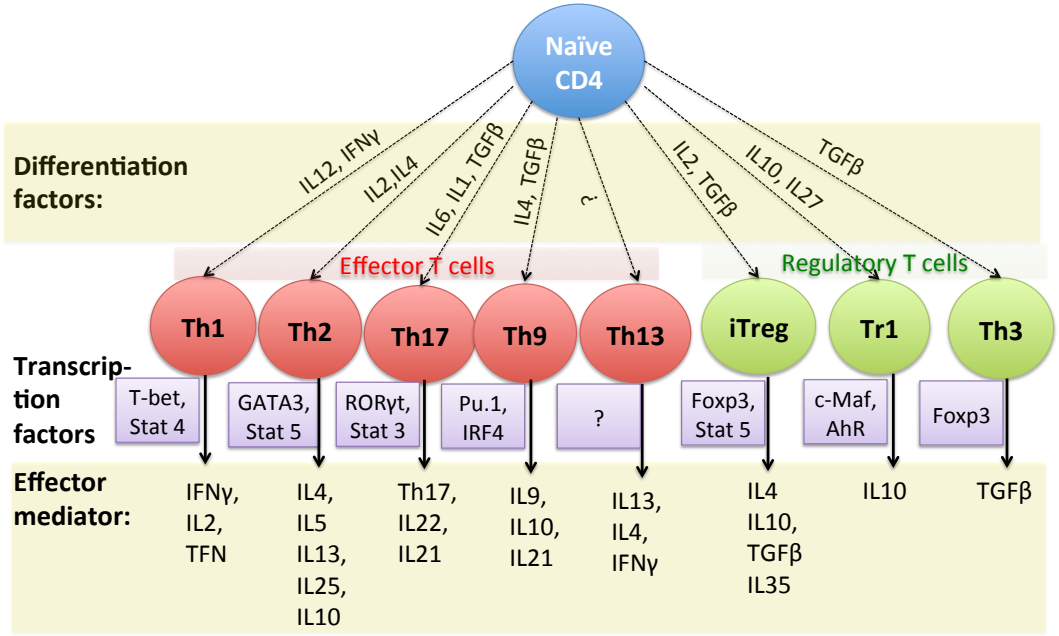

Figure 1.3 $CD4^+$ T cell subsets. After encountering antigen presenting DCs, naïve $CD4^+$ T cells can differentiate into effector T cells and regulatory T cells. Differentiation factors (cytokines in the surrounding micro-environment) play a key role in the differentiation of T cells subtypes in response to different immune stimuli. Transcription factors can then further promote and regulate the differentiation process. $CD4^+$ T cell subsets then exert their effect through secretion of cytokines which mediate the function of other immune cells (Zhu and Paul, 2008, Gerlach et al., 2014, Geginat et al., 2014, Palucka et al., 2009, Luckheeram et al., 2012).

1.4.1.1 Effector T cells

It was in 1986 that activated $CD4^+$ T cells were subdivided into two groups, Th1 and Th2 (Mosmann et al., 1986). The Th1 T cell subset differentiates from naïve T cells due to the presence of IL12 (which is released by APCs), and can be identified by the release of cytokines such as IFNγ (Romagnani, 1999). IFNγ is a proinflammatory cytokine, which is predominantly secreted by Th1 $CD4^+$ and $CD8^+$ T lymphocytes and natural killer T cells (NKTs). It is an important factor for activation of macrophages (Dinarello, 2000). Other cytokines are released by Th1 T cells, including IL2, which is a growth factor required for T cell proliferation. Th1 cells are effector $CD4^+$ T cells, which respond to intracellular pathogens (Del Prete, 1992). Th1 cells elicit activation of macrophages and proliferation of CD8 T cells. It was shown that Th1 cells play an important role in the development of T1D and can induce diabetes in NOD-SCID mice following adoptive transfer (Bradley et al., 1999).

Naïve CD4 T cells differentiate into Th2 cells in the presence of IL2 and IL4. IL4 is also a major cytokine released by Th2 cells. Th2 cells respond to extracellular parasites and help B cells to secrete antibodies, especially IgE (Del Prete, 1992). Allergies and asthma are shown to be closely related to Th2 reactivity (Azar et al., 1999). It is widely accepted that Th1 and Th2 cells are able to counter balance each other with the cytokines they release. IFNγ released by Th1 cells inhibits the proliferation of Th2 cells, while Th1 cell proliferation can be inhibited by IL4 and IL10, which are released by Th2 cells (Luckheeram et al., 2012).

Many cytokines contribute to the differentiation of Th17 cells, such as IL6, IL21, IL23, and TGFβ, among which TGFβ is critical for development of Th17 cells (Zhu and Paul, 2008). Interestingly, TGFβ was also shown to be an important cytokine for differentiation of Tregs. When naïve T cells are stimulated with a low

concentration of TGFβ and other cytokines such as IL6, naïve T cells differentiated to IL17-secreting Th17 effector cells (Luckheeram et al., 2012, Hatton, 2011). On the other hand, when TGFβ is present at high concentration, it induces Foxp3, which differentiates naïve T cells into Tregs (Hatton, 2011). Th17 cells mediate immune function against extracellular bacteria and fungi as well as inducing autoimmunity. In NOD mice, which can develop T1D spontaneously, a high concentration of IL17 was observed in the pancreas and islet antigen specific CD4 T cells were shown to be Th17 cells, which are known to induce diabetes in NOD-SCID mice (Shao et al., 2012).

After activation, $CD4^+$ Teffs go through different immune phases, including clonal expansion, contraction due to apoptosis and the memory phase. These memory $CD4^+$ T cells survive apoptosis after activation and preserve the antigen specificity and can be activated more quickly than naïve T cell when re-challenged with the same antigen (MacLeod et al., 2009, MacLeod et al., 2010, Ammirati et al., 2012, Correia et al., 2014). $CD4^+$ memory T cells can be divided into two subsets: effector memory T cells and central memory T cells, as listed in Table 1.1 .

Table 1.1 $CD4^+$ memory T cell function and homing. Tcm=central memory T cells, Tem=effector memory T cells. (MacLeod et al., 2009, MacLeod et al., 2010, Ammirati et al., 2012, Correia et al., 2014).

	Tcm	Tem
Function	Absence of immediate effector function	Immediate effector function
Anatomic location	Lymph nodes, Blood	Lung, liver and gut
Migration	Secondary lymphoid organs	Peripheral site of inflammation, non-lymphoid tissues
Proliferation	High	Low
Cytokine production	IL2	IL4, IL17, IFNγ

1.4.1.2 Regulatory T cells (Tregs)

Regulatory T cells (Tregs) play an important role in controlling ongoing immune response and silencing self-reactive T cells in peripheral tolerance. There are two main Treg subsets: naturally occurring thymic-derived Tregs (nTregs) and antigen induced Tregs (iTregs) (Shevach and Thornton, 2014). These Treg subsets are identified based on their expression of cell surface markers, production of cytokines, and mechanisms of action (Jonuleit and Schmitt, 2003).

Differentiated in the thymus, nTregs are a group of polyclonal Tregs with a TCR repertoire which can effectively bind MHC/self-antigen complex (Hsieh et al., 2004). Naturally occurring thymic-derived $CD4^+CD25^+$ Tregs (nTreg) are characterized by their constitutive expression of the transcription factor forkhead box P3 (Foxp3) and inhibitory cytokines such as IL10 and TGFβ. Foxp3 plays a very important role in both the development and function of nTreg (Hori and Sakaguchi, 2004). Foxp3 expressed by mTEC (medullary thymic epithelial cells) in the thymus plays a key role in Treg development in the thymus (Liu et al., 2008, Aschenbrenner et al., 2007). The importance of Foxp3 in Treg function was demonstrated by depletion of $Foxp3^+$ T cells to induce autoimmune disease and disease was prevented when antigen specific Tregs were introduced (Kim et al., 2009a, Brode et al., 2006). Two mechanisms are thought to be involved in nTreg suppression: Firstly, Tregs inhibit the differentiation of Naïve T cells into Teff and therefore prevent the expansion of Teff population. Secondly, nTregs exert their tolerogenic effect on DCs through CTLA4, IL10 and TGFβ and indirectly inhibit fully differentiated Teffs through tolerogenic DCs (Shevach and Thornton, 2014).

As well as deriving from the thymus, Tregs can also be generated by tolerogenic cytokines, IL10, TGFβ, or tol-DCs in the periphery (Matsumura et al., 2007,

Kushwah and Hu, 2011). These antigen/cell specific T cells are referred to as induced Tregs (iTreg). It was thought that iTregs retain similar functionality to nTregs. In an *in vitro* experiment, TGF-beta, retinoic acid, and IL-2 were used to generate iTregs, which showed a suppressive effect on antigen-specific effector T cells in an experimental autoimmune encephalomyelitis (EAE) model (Zhang et al., 2010).

It is thought that there are four basic mechanisms in the regulation of immune response which involve Tregs (Vignali et al., 2008, Schmetterer et al., 2012). These are demonstrated in Figure 1.4 as follows: **1,** Suppression of Teff proliferation by inhibitory cytokines, such as IL10 and TGF, which control the inflammatory response and inhibit Teff function. **2,** Induction of Teff apoptosis by metabolic disruption due to competitive deprivation of the growth factor IL2. **3,** Induced apoptosis through secretion of granzyme A or B, which causes cytolysis of Teff cells. **4,** Indirect inhibition mediated through DC and Treg amplification loop. Cytotoxic T-lymphocyte antigen 4 (CTLA4) is expressed on Tregs and interacts with CD80/CD86 on DC, up-regulating the expression of indoleamine 2,3-dioxygenase (IDO); an enzyme that degrades tryptophan. IDO was demonstrated to inhibit Teff functions as well as help naïve T cells to differentiate into Tregs (Mellor and Munn, 2004).

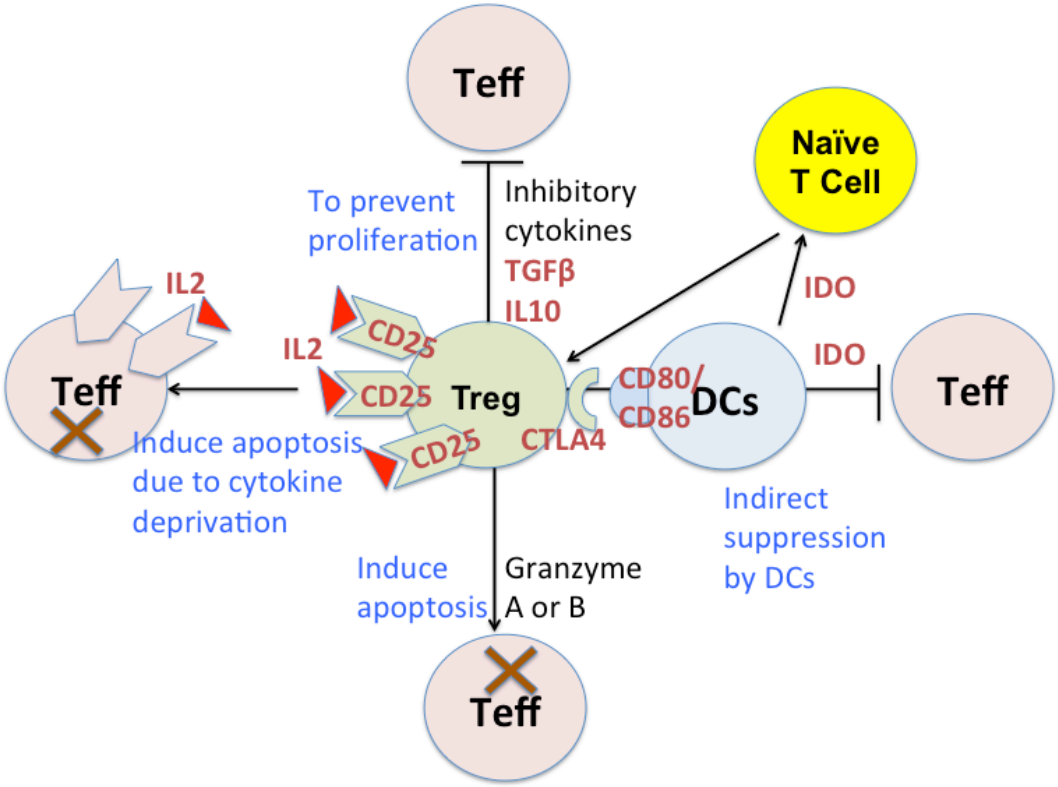

Figure 1.4 Four basic mechanisms that Treg utilise to regulate immune responses. Tregs regulate immune response by the direct prevention of proliferation or by inducing apoptosis. Tregs also can prevent Teff function indirectly through DCs (Vignali et al., 2008, Schmetterer et al., 2012).

As described above, Tregs are important in maintaining peripheral tolerance. Both antigen-specific and polyclonal Tregs have a role in regulating the immune system in the prevention of autoimmune disease. In a model of EAE, using a transgenic mouse model, Hori et al. demonstrated that both antigen-specific Tregs and polyclonal Tregs prevented EAE development with equivalent efficacy (Hori et al., 2002). Thus, Tregs can be a useful tool in the therapy of autoimmune disease. Young patients with T1D who received *in vitro* expanded Tregs in a clinical trial showed a reduced blood glucose level and an increased Treg population in the blood for two weeks following treatment. No adverse effect was demonstrated over a year following treatment (Marek-Trzonkowska et al., 2012). However, these fundamental insights are not yet ready to be utilized as an effective clinical therapeutic intervention, due to factors such as Treg purity, dosage, specificity and dynamics (Tang and Bluestone, 2013).

1.4.1.3 Markers of CD4$^+$ T cells

Apart from their functions, CD4$^+$ T cell subsets also can be recognised by their phenotypic characteristics such as surface and intracellular markers. Some of these markers are listed in Table 1.2.

Table 1.2 CD4+ T cell markers. Tn=Naïve T cell, Teff=Effector T cell, Treg=Regulatory T cell, Tem=Effector memory T cell, Tcm=Central memory T cell, N/K=not known.

Name	Expression	Function	Tn	Teff	Treg	Tem	Tcm
CD69	Surface	Activation and memory marker	-	+++	-	-	-
CD44	Surface	Cell adhesion	+	+++	-	+++	+++
CD62L	Surface	Homing	+++	-	+++	+/-	+++
CD25	Surface	IL2 receptor	-	++	+++	-	-
GITR	Surface	Activation	+	+++	+++	N/K	N/K
Foxp3	Intracellular	Suppressive function marker	-	+	+++	N/K	N/K

CD62L is L-selectin which is expressed on T cells and controls T cell migration to secondary lymphoid organs. Upon activation, T cells in circulation migrate to both lymphoid and non-lymphoid organs and down-regulate CD62L. A high expression of CD62L was found on naïve T cells and less on activated effector T cells (Klinger et al., 2009). CD62L-expressing CD4 T cells prevented development of T1D and restored normal glycaemia in a mouse model, thus demonstrating a regulatory function (You et al., 2004, Ermann et al., 2005, Tarbell et al., 2007).

CD44 is a surface molecule expressed on a wide range of cells. In T lymphocytes, it is responsible for adhesion, activation, migration and proliferation (Graham et al., 2007). CD44 is upregulated when T cells are activated and a high expression on memory T lymphocytes is retained. It has been shown that CD44 plays an important role in Th1 cell survival (Baaten et al., 2010)

CD69 is a type II integral membrane protein belonging to the C-type lectin superfamily (Natarajan et al., 2000). It is an early T cell activation marker, and is shown to be upregulated rapidly approximately 3-4 hours after activation. Expression of CD69 declines after 24 hours if the stimulus is removed (Testi et al., 1994). The level of CD69 expression was shown to be correlated with T cell activation and proliferation, and has been analysed quantitatively using flow cytometery (Lindsey et al., 2007, Caruso et al., 1997). It was shown that CD69 influence the differentiation of Th17 cells through the Jak3/Stat5 signalling pathway (Martin et al., 2010). CD69 was also shown to alter the Th2 cell migration to the asthmatic lung by altering the expression of VCAM-1 (Miki-Hosokawa et al., 2009). This indicated that CD69 is related to CD4 T cell differentiation and migration which further influence the inflammatory response.

GITR (glucocorticoid-induced TNFR family related gene) is a member of the TNFR (tumour necrosis factor receptor) super family. GITR is upregulated when T cells become activated and it was shown to be involved in the control of glucocorticoid-induced T cell apoptosis (Zhan et al., 2004). GITR also plays an important role in $CD4^+CD25^+$ regulatory T cell expansion and suppressive functions. $CD4^+CD25^+$ T cells were shown to lose their regulatory function when GITR was knocked out (Ronchetti et al., 2004). However, it was found that GITR has effects on both Teffs and Treg and promotes function in both types of T cell (Shevach and Stephens, 2006).

CD25 is a transmembrane protein, which acts as an alpha chain of receptor for the cytokine IL2, a T cell growth factor. CD25 was shown to have a low affinity with IL2. However, when combined with IL2 receptor gamma chain CD122, CD25 has a high affinity for IL2 (Letourneau et al., 2009). Treg cells were shown to express a high level of CD25, which was thought to compete with effector T cells for IL2, when IL2 is in low concentration. IL2 starvation caused by Treg with high expression of CD25 was thought to be one of the mechanism by which Treg suppresses Teff functions (for detail see section 1.4.1.2, and Figure 1.4). CD25 is not expressed on resting T cells but is upregulated when T cells become activated (Nelson and Willerford, 1998). T cells also express a high level of CD25 during the early development stages in the thymus (Godfrey and Zlotnik, 1993). CD25 In the periphery, nTregs can be identified by high expression of CD25 on $CD4^+$ T cells (Letourneau et al., 2009).

Foxp3 is a protein belonging to the forkhead family of transcription factors. Foxp3 plays a key role in Treg development and function (Hori et al., 2003). Expression of Foxp3 is associated with the upregulation of other Treg markers such as CD25, CTLA4 (Cytotoxic T-lymphocyte-associated protein 4) and GITR (Hori and Sakaguchi, 2004). In T1D, $Foxp3^+$ Tregs were able to protect against the destruction of pancreas in NOD mice by adoptive transfer and depletion of $Foxp3^+$ Treg could lead to fatal autoimmunity in mice at 3-4 weeks of age (Petzold et al., 2013).

1.5 Central tolerance, peripheral tolerance and autoimmunity

Another mechanism used by the immune system to distinguish between self and non-self is by self-tolerance, a mechanism that protects self-tissue against immune response. There are two stages of tolerance: central tolerance and peripheral tolerance. During these tolerance processes, self-reactive cells are depleted, become anergic or are regulated.

1.5.1 Central tolerance

T cells are first selected in the thymus by positive and negative selection, in a process called central tolerance. T cells are selected in central tolerance depending on the affinity between their TCR and self-peptide/MHC complex.

Derived from bone marrow progenitors, T thymocytes initially lack T cell receptors (TCR) or CD4 and CD8 markers; at this stage they are termed “double negative”. Double negative T thymocytes then undergo proliferation when TCR are rearranged and they become $CD4^{+}CD8^{+}$ double positive thymocytes. At this stage TCRs have random specificity with a broad TCR repertoire (Hogquist et al., 2005). In the cortex, double positive T cells interact through TCRs with cortex epithelial cells, which express MHCI, MHCII and self-peptide. T thymocytes with TCR which do not bind self-peptide/MHC complex is undergo apoptosis due to neglect (Xing and Hogquist, 2012). T thymocytes with TCR that weakly bind with self-peptide/MHC complex survive and migrate to medulla where they become single CD4 or CD8 positive. This selection process is called positive selection, during which the TCR is selected to recognize self-peptide/MHC complex.

In the medulla, an inner region of the thymus, single positive CD4 and CD8 T cells are further selected during the negative selection process. During negative

selection, T cells with TCR that can recognize self-antigen/MHC complexes with high affinity will be deleted from the T cell repertoire (McCaughtry and Hogquist, 2008). This process is also referred to as clonal deletion. The fine threshold of affinity between TCR and self-peptide/MHC distinguishes between positive selection and negative selection (Palmer and Naeher, 2009). It is thought that polyclonal T cell progenitors are deleted during positive selection in the cortex and tissue specific progenitors are deleted during negative selection in the medulla (Xing and Hogquist, 2012). Two types of cells in the thymus are involved in clonal deletion: mTEC and DCs. mTECs express a protein called autoimmune regulator (AIRE), which is involved in regulating the expression of tissue specific antigens. It has been demonstrated that tissue specific self-antigen in the thymus is controlled by the AIRE gene (Liston et al., 2003). A mutation in this gene can lead to autoimmune disease.

In addition to clonal deletion, T thymocytes can also be diverted down a different developmental route during the negative selection period in a process called clonal diversion. During this stage, tissue-antigen specific Tregs are differentiated from T thymocytes. Several factors can determine the fate of T thymocytes, including TCR signal, signal through CD28 and cytokines: It was suggested that the generation of foxp3^{+} Treg is correlated with a weaker TCR signal compared to the negative selection process. The reduced expression of MHCII on mTEC was shown to prevent T thymocytes from being deleted (Klein et al., 2009). Apart from the TCR signal, signal from costimulator CD28 is also important in the generation of Tregs in the thymus. The intrinsic signal induced by CD28 was shown to be involved in generation of Foxp3^{-} Treg precursors (Lio et al., 2010). Signals from cytokines, such as IL2 and TGFβ, can help the survival of Tregs; IL2 was shown to promote the expression of Foxp3 on T thymocytes (Lio and Hsieh, 2008), whilst TGFβ was shown to be able to protect

Tregs from clonal deletion (Ouyang et al., 2010). The generation of Tregs in the thymus, i.e. nTreg, also plays a vital role on peripheral tolerance, which will be discussed in the next section, 1.5.2.

1.5.2 Peripheral tolerance

The processes that enable central tolerance are not able to eliminate all autoreactive T cells. This is because some T lymphocytes have a low affinity for MHC/self antigen and can escape central tolerance. Additionally, not all self-antigens are expressed in the thymus. T cells that escape the central tolerance mechanism can be further regulated by peripheral tolerance via inactivation or elimination.

TolDCs are important in the induction and maintenance of peripheral tolerance (details see Section 1.3). Inactivation is achieved by absence of activation signals from DCs (such as costimulators CD80/CD86), which induces T cell anergy. To be activated, T cells require signals from TCR, CD28 and inflammatory cytokines and therefore lack of a signal from CD80/CD86 to CD28 results in T cell anergy (Thompson et al., 1989, Sharpe and Freeman, 2002). Another important co-stimulator in T cell anergy is CTLA-4. CTLA-4 can down regulate the T cell activation process and block growth cytokine IL2 receptor expression, even when T cells are activated (Walunas et al., 1996). A lack of CTLA-4 has been shown to cause severe autoimmune disease in mice (Tivol et al., 1995).

Immune homeostasis can also be achieved with Tregs by cell-cell contact in the periphery (Takahashi et al., 1998). Both nTreg and iTreg (see section 1.4.1.2) are able to maintain peripheral tolerance. Tregs can directly induce Teff

apoptosis by metabolic disruption or enzyme cytolysis. Additionally, Tregs can secrete anti-inflammatory cytokines, such as TGFß and interleukin-10 (IL10), which have been shown to inhibit immune response *in vivo* (Hawrylowicz and O'Garra, 2005). The details of Treg regulatory mechanisms were introduced in the previous section 1.4.1.2.

A process, which causes an imbalance during any of these regulatory processes, may lead to the development of an autoimmune disorder, and such is the case for T1D. A detailed pathology of T1D in animal model will be introduced in the next section, 1.6.1.

1.6 The NOD (Non Obese Diabetic) mouse

The causes of T1D are complex. Therefore, models are needed to help understand the mechanisms behind this chronic disease. The use of efficient, convenient, cost effective and appropriate animal models is important in assisting the development of a potential prevention or intervention for the treatment of T1D. Two animal models, which spontaneously develop diabetes, have been widely used for study of T1D: the Biobreeding rat and the NOD mouse (King, 2012). The most commonly used of these two models is the NOD mouse. The Biobreeding rat is most useful for studying environmental influences on T1D and pancreatic transplant intervention studies (Mordes et al., 2004, King, 2012). One disadvantage of the Biobreeding rat is that it can develop T cell lymphopenia, which is not found in the NOD mouse or in human patients with T1D (Mordes et al., 2004).

1.6.1 Pathology of T1D in NOD mouse

The NOD murine subline was originally developed in order to study cataract disease (Leiter et al., 1987). NOD mice were also shown to develop T1D spontaneously in a manner similar to human T1D, *via* genetic and cellular mechanisms (Serreze and Leiter, 1994, Atkinson and Leiter, 1999, Leiter, 2001). There are differences in rates of disease incidence between males and females. Approximately 60-80% of female NOD mice develop disease between 12-14 weeks old, while only 10-20% of male mice become diabetic at a comparable ages. (Markle et al., 2013, Bao et al., 2002, Baxter et al., 1991).

Insulitis in the NOD mouse is initiated by APCs, together with the death of beta cells. A wave of beta cell death occurring at 1-2 weeks of age was observed in a rat model (Scaglia et al., 1997). This was thought to be part of a process called

"tissue remodelling", a renovation process which occurs during the neonatal stage of development, in order to maintain the mass of beta cells. This process has also been observed in the Biobreeding rat and NOD mouse models. Rapid beta cell apoptosis was observed at 13 days of age in both models (Trudeau et al., 2000). The increased number of dead cells and/or dead cell fragments during tissue remodelling in these developing neonatal tissues can potentially provide both an activation signal and self-antigenic fragments to APCs. APCs can engulf beta cell antigens in the pancreas and prime T cells in PLNs (pancreatic lymph nodes).

Enhanced APC ability of DCs was found in NOD mice. It was suggested that elevated expression of NF-κB (nuclear factor kappa-light-chain-enhancer of activated B cells) on mDCs (myeloid DCs) was associated with the increased expression of TNFα and also increased ability to prime T cells (Poligone et al., 2002). Following depletion of mDCs from NOD mice, reduced T cell activation was observed (Saxena et al., 2007). Interestingly, a DC subtype, pDC (plasmacytoid DC), was able to counter-regulate the activation process. Absence of pDCs can accelerate diabetes progression in NOD-SCID mice and local regulation was restored when pDCs were re-introduced (Saxena et al., 2007).

During maturation, DCs migrate to the pancreatic lymph nodes (PLN) where they prime naïve T cells. T cells play a key role in insulitis during the development of T1D. It was shown that T cells infiltrate the pancreas of NOD mice at the age of 3-4 weeks and cause onset of diabetes by the age of 12 weeks (Leiter, 2001). T1D can be induced by transferring T cells ($CD4^+$ and $CD8^+$) from diabetic NOD mice to NOD-SCID mice; this can be prevented by depletion of T cells, which can be achieved by using anti-CD3 antibody to treat NOD mice (Christianson et al.,

1993, Chatenoud et al., 1994). This evidence indicates that T1D in NOD mouse is a T cell-mediated disease. Loss of central and peripheral tolerance in the NOD mouse enables the escape and activation of diabetogenic T cells. Abnormal migration of thymocytes in the NOD mouse was shown to be due to the reduced expression of integrin-type fibronectin receptors, VLA-4 and VLA-5 (Cotta-de-Almeida et al., 2004). Although research has shown that the total T cell migration from the NOD mouse thymus was not different from a control strain, a greater proportion of $Foxp3^+$ T cells were shown to remain in the thymus in NOD mice (Mendes-da-Cruz et al., 2008). Failure of depletion is also related to the insufficient expression of self-antigens in the thymus. AIRE (autoimmune regulator) is a transcription factor that regulates expression of self-antigen in the thymus, and was shown to down-regulate ICA69 (islet cell autogantigen 69 KDa) in NOD thymus, which may explain the inefficient depletion of autoreactive T cells in the NOD thymus (Bonner et al., 2012).

Activation of naïve diabetogenic T cells by DCs occurs in the PLN. Removing PLNs before the age of 3 weeks protected NOD mice from developing T1D (Gagnerault et al., 2002). However, further insulitis could not be prevented by the removal of PLN alone in mice that were more than 10 weeks old (Gagnerault et al., 2002). Several factors influence the activation of the autoreactive T cells in the NOD mouse. $I\text{-}A^{g7}$, an MHCII molecule expressed on the surface of DCs, was found to have an unusual β chain, which is associated with diabetes susceptibility (Acha-Orbea and McDevitt, 1987). $I\text{-}A^{g7}$ lacks an aspartic acid residue at position β-57 and has a larger pocket at P9 compared with another MHCII molecule $I\text{-}A^{d}$ (Corper et al., 2000, Stratmann et al., 2000). These features enable enhanced binding between the autoantigen (originating from GAD65 protein) and the MHCII molecule, which further provides a strong activation signal to T cells. Another activation signal is through co-stimulators,

CD80/CD86 on DCs. CTLA4 expressed on CD4 T cells can compete with CD28 by binding with CD80/CD86 and providing a negative signal to T cells, which inhibits T cell activation (Walunas et al., 1996). Loss of CTLA4 can result in unregulated T cell activation, which could contribute to the development of autoimmune disease (Tivol et al., 1995). In NOD mice the susceptibility to T1D could also be associated with a lack of the CD80/CD86 ligand-binding domain on CTLA4 (Ueda et al., 2003)

After activation, T cells homing back to the pancreas showed up-regulation of CD44 and down-regulation of CD62L. These activated T cells kill beta cells by Fas/FasL, release of perforin and granzymes, and release of cytokines to create an inflammatory environment (Pirot et al., 2008).

1.6.2 The BDC2.5-TCR (T cell receptor)-Tg (transgenic) mouse

It has been widely accepted that T1D is a T cell mediated autoimmune disease both in humans and in the NOD mouse (van Belle et al., 2011, Phillips et al., 2009, Roep, 2003, Sakumai et al., 2007). Interestingly, diabetic T cells have been isolated in order to understand the molecular and cellular mechanisms of T1D disease progression. The first islet antigen-specific T cell clone isolated from the NOD mouse (BDC2.5) was a CD4 T cell clone (Haskins et al., 1988). This BDC2.5 T cell was shown to be highly reactive to islet antigens and was shown to be pathogenic and able to infiltrate the pancreas *in vivo* (Haskins et al., 1989). The TCR was subsequently cloned and a BDC2.5-TCR-Tg-mouse was first reported by Katz and colleagues (Katz et al., 1993). $CD4^+$ T cells from these mice express the TCR genes Vα1 and Vβ4. It has been suggested that BDC2.5 T cells are positively selected in the thymus and comprise over 95% of $CD4^+$ T cells in the Tg-mouse. The BDC2.5 T cells from the Tg mouse shows a naïve

phenotype compared with the cloned T cells, which display an effector/memory phenotype (Dobbs and Haskins, 2001). Both types of BDC2.5 T cell appear to be biochemically similar, which suggests that BDC2.5 T cells from the TCR-Tg-mouse are present in their activated state. BDC2.5 TCR-Tg-mice with the NOD genetic background had a lower diabetes incidence compared with those on the $B6^{g/7}$ congenic background (Gonzalez et al., 1997). This could be due to an inhibitory effect on disease progression by $CD4^{+}DX5^{+}$ T cells (Gonzalez et al., 2001). NOD-SCID recipients, adoptively transferred with BDC2.5 T cells isolated from a TCR-Tg-mouse, were shown to develop diabetes rapidly (Peterson and Haskins, 1996). These studies demonstrate that the BDC2.5-TCR-Tg mouse is a useful tool for the study of T1D pathology and these mice provide a valuable model for use in studies designed to improve understanding of tolerance in this autoimmune model.

It was not until recently that Chromogranin A (ChgA) was identified as an autoantigen for the BDC2.5 T cell and WE14 (WSRMDQLAKELTAE), derived from ChgA, is the natural antigenic epitope that stimulates the BDC2.5 T cell receptor (Stadinski et al., 2010). However, WE14 has a low affinity for the BDC2.5 TCR and thus has a low potency for BDC2.5 T cell stimulation. A further study suggested that transglutamination is a key post-translational modification required to generate pathogenic peptides. After transglutaminase (TGase) modification, WE14 becomes 10 times more potent in stimulating BDC2.5 T cells *in vitro.* NOD-SCID mice developed T1D quicker when transferred with BDC2.5 T cells and stimulated with TGase modified WE14 than when transferred with cells stimulated with untreated WE14 (Delong et al., 2012). The BDC2.5 mimotope 1040-31 (m31) (YVRPLWVRME) is a synthesized peptide, which mimics the sequence of the autoantigen (GAD65 fragments) but has a greater affinity for the TCR (Judkowski et al., 2001). BDC2.5 T cells can respond to m31

at a concentration of less than 10ng/ml (Montero-Hadjadje et al., 2002, Curry et al., 2002), whereas WE14 has a low potency and requires a 1000 fold greater dose than the m31 in order to activate BDC2.5 T cell clones *in vitro* (Stadinski et al., 2010, Delong et al., 2013).

1.6.3 Auto-antigens in the NOD mouse

As T1D is mainly mediated by T cells, it is important to identify their auto-antigenic targets. Depletion of $CD4^+$ and $CD8^+$ T cells using antibodies, conferred prolonged protection of T1D in NOD mice and resulted in an increased population of $CD4^+CD25^+$ Treg in PLN but not in the SP (Yi et al., 2012). Following the isolation of BDC2.5, several diabetogenic T cell clones have been isolated from NOD mice indicating that more than one autoantigen contributes to the destruction of beta cells (Babad et al., 2010). A summary of the autoantigens isolated to date is listed in Table 1.3.

As described in the previous section, 1.6.2, ChgA (Chromogranin A) is a newly discovered autoantigen of T1D, which can be isolated from secretory granules of a beta cell (Stadinski et al., 2010). WE14, a natural cleavage product of ChgA, binds weakly to the MHCII I-Ag^7 molecule (Curry et al., 2002, Stadinski et al., 2010). As ChgA is not exclusively expressed in beta cells, this has raised questions as to why there are no other organs targeted and therefore no pathology related to ChgA has been demonstrated outside of the pancreas in T1D. One potential explanation was that organ specific post-translational modification of ChgA had occurred in the pancreas, which could contribute to its inflammatory state. It was suggested that WE14 could have been modified using transglutaminase, resulting in a modified molecule capable of stimulating BDC2.5 T cells more potently than original WE14 peptide (Haskins and Cooke, 2011,

Delong et al., 2012). NOD-SCID mice transferred with BDC2.5 T cells pre-cultured with transglutaminase-treated WE14 developed disease more rapidly than using WE14 pre-treated BDC2.5 T cells (Delong et al., 2012). Although the BDC2.5 T cell clone derived from the NOD mouse can respond to ChgA and WE14, it was necessary to confirm that ChgA and WE14 are also human autoantigens, due to species differences. In a recent study, CD4 T cells from a newly diagnosed T1D patient (<1 year) were shown to respond to WE14 at a concentration of 40μM while transglutaminase-treated WE14 stimulated the CD4 T cells at both 20μM and 40μM. Average IFNγ ELISPOT counts of PBMCs in response to TGase-treated WE14 were elevated in the T1D patient group compared to a healthy control group (Gottlieb et al., 2014). These data indicated that ChgA and WE14 are autoantigens in the NOD mouse model as well as in human patients newly diagnosed with T1D.

Table 1.3 Auto-antigens found in the NOD mouse, which have a role in T1D development. (Roep and Peakman, 2012)

Autoantigen	Tissue distribution	Mice	
		Auto Abs	T cells
Pre-proinsulin	β cells, thymus	Yes	CD4
Glutamic decarboxylase 65 (GAD65)	Islet cells, adrenal gland, CNS, neurons, testis, ovary	No	CD4
GAD67	Islet cells, neurons	No	CD4
Tyrosine phosphatase like autoantigen or insulinoma antigen-2 (IA-2; ICA512, PTPRN)	Islets	Yes	CD4
IA-2 β (Phogrin, PTPRN2)	Islets	No	CD4
Islet cell antigen-69 (ICA69)	Pancreas, heart, and brain	No	No
Zinc transporter-8 (ZnT8)	β cells		
Chromogranin A	Neuroendocrine cells	No	CD4
38 kDa granule antigen	Neuroendocrine cells	No	?
Peripherin	Neurons	No	CD4
Islet amyloid polypeptide (ppIAPP)	Islets	No	CD4
Carboxypeptidase H/E	Neuroendocrine cells; adrenals	No	No
Heat shock protein 60 (hsp60)	Ubiquitous (mitochondria)	No	CD4
IGRP; islet-specific glucose-6-phosphatase catalytic subunit-related protein	Islets	No	CD8
Sulfatide	Ubiquitous	No	No
Ganglioside	Ubiquitous	No	No

1.7 Antigen specific immunotherapy (ASI)

1.7.1 Antigen Specific Immunotherapy (ASI)

ASI is a type of immunotherapy targeting specific immune cells in an antigen-specific manner (Sabatos-Peyton et al., 2010). One approach to ASI is to target immature DCs using an endogenous antigen (Anderson and Jabri, 2013). During this process, DCs are maintained in an immature or semi-mature state, thus boosting antigen-specific Treg population *in vivo* (Lutz and Schuler, 2002) (section 1.3 and 1.4.1.2.). As the mechanism of Treg suppression requires cell-cell contact and it is required at the site of inflammation (Vignali et al., 2008, Schmetterer et al., 2012), an autoantigen which was involved in the inflammatory autoimmune response, should be used in order to home back to the disease organ and target the source from which antigens originated, in the case of T1D, beta cells in the pancreas. More than one autoantigen has been shown to contribute to the development of T1D (Table 1.3). Whether one or several antigens should be targeted in therapy remains unanswered. The growing number of antigens with a role in T1D necessitates a selective approach to the discussion of antigen therapy, as presented here. Therefore one of the main autoantigens, insulin, is discussed in further detail to demonstrate the efficacy of the ASI approach. A recently discovered auto-antigen, WE14, which is used in this project, is also discussed.

Single antigen therapy has been used for ASI in animal and clinical studies. In the early 90's, insulin was shown to protect NOD mice when delivered either subcutaneously or orally (Atkinson et al., 1990). Following these observations proinsulin B9-23 was identified as an autoantigen for T1D, stimulating several islet reactive T cell clones. Proinsulin B9-23 has been delivered via. subcutaneous or intranasal routes to induce tolerance in NOD mice (Daniel et al.,

1995, Daniel and Wegmann, 1996). This promising pre-clinical data led to the use of insulin and its peptides in clinical trials.

The administration of insulin or insulin-peptide by different routes has resulted in different clinical outcomes. When insulin autoantibody levels were used as the end point, an oral insulin clinical trial showed no effect on prevention or intervention of T1D (Skyler et al., 2005, Chaillous et al., 2000). However, when using plasma C-peptide as readout, a positive result was achieved. Newly diagnosed T1D patients were either treated with 1mg/day or 10mg/day oral insulin. Follow-up results showed that patients in different age groups responded to varying insulin doses differently. A high dose was more effective in reducing the loss of C-peptide in patients younger than 20 years old, while a low dose was more effective in reducing the loss of C-peptide in patients more than 20 years old (Ergun-Longmire et al., 2004).

Relatives of patients with T1D who were positive for IA-2 antibodies; an indicator of T1D susceptibility, were recruited for another clinical study. Insulin was administered subcutaneously twice daily for 36 months, and no differences in T1D prevention were observed (Vandemeulebroucke et al., 2009). Rather than using subcutaneous delivery, a phase I trial used pro-insulin C19-A3 peptide, administered intradermally, which can target the DC-rich skin region. Long-standing T1D patients with human leukocyte antigen (HLA)-DRB1*0401 genotype were selected and split into two groups, injected with C19-A3 either at a low dose (10μg) or at a high dose (100μg) repeated monthly for 3 months. Both dose regimes were well tolerated. Interestingly, the low dose (10μg) treatment group showed increased levels of C19-A3-specific T cells (which secrete IL10) at the 3 month time point in 4 out of 18 cases. This may suggest that such an immunotherapeutic approach to T1D treatment is promising,

however; this conclusion can only be speculative as the study was not designed to elucidate the immunological mechanism of the patients' response (Thrower et al., 2009).

Another approach to target mucosal DCs is to administer antigen intranasally. The early nasal administration of insulin was performed on infants and their siblings with two positive T1D antibodies and HLA-DQB1 susceptibility. No prevention of T1D was observed; however, this approach changed the insulin autoantibody level (Nanto-Salonen et al., 2008). A recent study suggested that targeting mucosal DCs with insulin could induce tolerance. Patients diagnosed with recent-onset T1D but with no dependence on exogenous insulin were recruited and nasal insulin was administered for 12 months. With 24 months follow-up, the insulin antibody level was retarded and IFNγ released by T cells in response to pro-insulin was reduced in patients treated with nasal insulin; however, no preservation of beta cell function was observed using this approach, (Fourlanos et al., 2011). This tolerogenic effect can be enhanced by combination with an adjuvant. IFA (incomplete Freund's adjuvant), together with proinsulin B9-23 has been injected intramuscularly. After 2 years follow up, it was shown that insulin B-chain-specific $CD4^+$ T cells isolated from the proinsulin-B9-23 treated group showed a tolerogenic phenotype and function (Orban et al., 2010). These studies suggested that by carefully choosing the targeting autoantigen, the ASI approach did not cause any adverse effect in patients and was well tolerated. Peripheral tolerance could be enhanced, which is demonstrated by reduced insulin autoantibody levels, reduced proinflammatory cytokine (IFNγ) levels and increased regulatory cytokine (IL10) levels. Importantly to this study, the aforementioned studies suggested that delivery route, i.e. oral, subcutaneous, intranasal or intradermal, may also influence the ASI outcome.

Chromogranin A (ChgA) has been shown to be an autoantigen for pathogenic BDC2.5 T cell clones *in vitro* and *in vivo* and these cells also respond weakly to its naturally occurring proteolytic cleavage peptide, WE14 (Curry et al., 2002, Stadinski et al., 2010) (for detailed introduction see section 1.6.3). This weak affinity peptide has been shown to be able to induce tolerance *in vivo*. Using an adoptive transfer model, a subcutaneous injection of WE14 was shown to delay the progress of transferred T1D in NOD-SCID mice (Haskins et al., 2012). A more recent study suggested that ChgA is an antigen in human patients (Gottlieb et al., 2014). These promising findings suggested that ChgA and its peptides could be used in future intervention trials.

ASI has been shown to be efficient in prevention of T1D in animal models. However, there are still hurdles to overcome when translating these findings into effective human therapy. Parameters such as the timing of treatment, dose regime and frequency still need to be optimised. One clinical risk of using autoantigen for ASI is the potential for boosting effector T cells; therefore control of the DC signal is of key importance. This can be controlled by delivery route (intranasal, oral, subcutaneous or intradermally), or using a tolerogenic adjuvant (Incomplete Freund's Adjuvant or an alum-formulation) (Ludvigsson et al., 2008, Ludvigsson et al., 2014, Fousteri et al., 2010).

1.7.2 Non-antigen based therapy

One immunotherapeutic approach is to suppress the systemic immune response by utilising a general suppressive drug, such as cyclosporin A and anti-CD3 to down- regulate the immune response systemically. Both approaches achieved a degree of success in animal models, however, no obvious benefits were observed in clinical T1D prevention trials (Herold et al., 2002, Daifotis et al.,

2013, Herold et al., 2013, Lernmark and Larsson, 2013, De Filippo et al., 1996). Furthermore, immunosuppressive drugs do not specifically target diabetogenic cells; rather they suppress the entire immune system. Therefore, when treated with therapies, which involve systemically immunosuppressive drugs, the ability of the body to defend against pathogens is reduced and patients may become more susceptible to infection.

In this study, in order to avoid the problems associated with general suppression, antigen/organ specific therapy was utilised. In order to maximise the opportunity for antigen to be taken up by DCs, we chose the skin as the target organ for delivery. Skin is not only an easy to access organ but it is also densely packed with DCs, especially Langerhans cells. Therefore, the next section will introduce the structure and immunology of the skin.

1.8 Skin structure and skin immunity

The skin is the largest organ in the human body and functions as the first line of the body's defence system. It consists of three main layers, the epidermis, dermis and hypodermis (Widelitz et al., 1997). The hypodermis is a fatty tissue where nutrients are stored and body temperature is regulated (Kanitakis, 2002). The dermis is a supportive layer between the hypodermis and epidermis, containing sweat glands, blood vessels and lymphatic vessels. The epidermis is the outermost layer; which functions as a barrier for maintaining hydration and excluding pathogens. As a protective organ, the skin protects the body from pathogens not only by providing a physical barrier (i.e. the stratum corneum) but a fully functional immune network.

Keratinocytes are the major cell type in the epidermis, which exhibit the full range of innate immune functions. Keratinocytes can express toll like receptors (TLC) and CD1d, which can recognise microbes, kill invaders and release pro-inflammatory cytokines and chemokines (Pivarcsi et al., 2004). Transplantation experiments have revealed that keratinocytes have a non-professional antigen presentation function with the expression of MHC II (Nickoloff and Turka, 1994). Hapten-modified Ia+ keratinocytes were shown able to help generate Treg *in vitro* and reduce the contact allergy *in vivo* (Gaspari and Katz, 1991). Keratinocytes were also demonstrated to play an important role in skin DC maturation. Type one IFNs and IL18 secreted by keratinocytes could assist the DCs to polarise into a matured state, which can further induce Th1 response (Lebre et al., 2003).

Human skin DCs can be categorised into two main groups according to their location: epidermal DCs and dermal DCs (Figure 1.5).

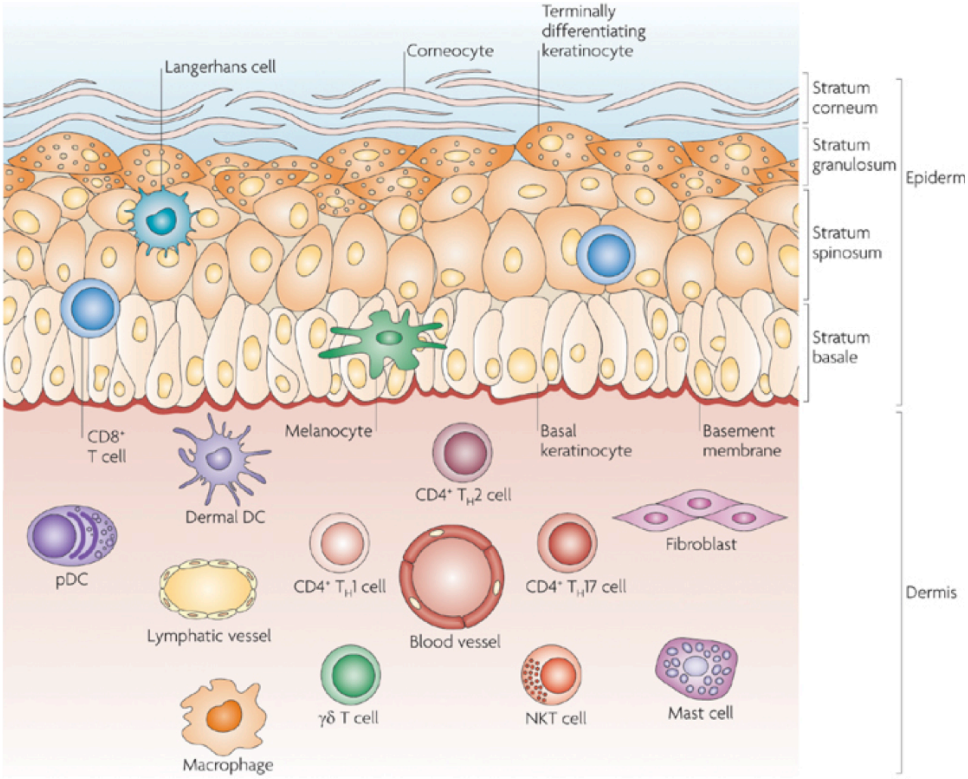

Figure 1.5 Skin anatomy and skin DCs. LCs are resident in the epidermis (most prominently in the stratum spinosum) and form a network within a layer of densely packed keratinocytes. Dermal DCs are mainly located in the same level as capillaries and the upper dermis. Figure copied from Nature Reviews Immunology 9, 679-691, doi:10.1038/nri2622 (Nestle et al., 2009)

Langerhans cells (LCs) are a type of DC located in the epidermis, within which they form a network to defend the body from intruders. LCs were first described by Paul Langerhans in 1869 (Jolles, 2002). It was thought LCs can be recognised by the expression of a surface marker CD1a, CD207 (langerin) and MHCII and are characterised by a distinctive intracytoplasmic marker, the Birbeck granule (Nestle et al., 2009, Kashihara et al., 1986, Valladeau et al., 1999). LCs are capable of engulfing and processing pathogens they encounter which triggers the maturation of the LCs. The matured LCs then migrate across the basal membrane and migrate into the lymphatic vessels resident in the dermis. During this migration process, LCs firstly detach from adjacent keratinocytes by down regulation of E-cadherin expression and become mobile (Kissenpfennig et al.,

2005, Konradi et al., 2014). LCs and other epidermal cells then secrete collagenase IV to enable LCs to cross the connective tissue matrix in the dermis (Kobayashi, 1997). It was suggested that LCs can cross-prime naïve $CD8^+$ T cells (Nestle et al., 2009). However, another research suggested that it was $Langerin^+$ dermal DCs cross present to $CD8^+$ T cells (Seneschal et al., 2014). Under certain conditions, such as treatment with glucocorticoid or vitamin D3, human LCs can be educated to induce a tolerance effect. For example, after treatment with vitamin D3, LCs can express TGF-ß cytokine and induce $Foxp3^+$ T cells (Palomares et al., 2011). Compared with dermal DCs, LCs were thought to be more tolerogenic (Shklovskaya et al., 2011). Bacteria-primed LCs showed a relatively poor stimulation of memory T cells and Teffs, compared with dermal DCs; rather they induced bacteria specific $Foxp3^+$ regulatory T cells (van der Aar et al., 2013). Unlike LCs, which have been shown to have a regulatory function, dermal DCs were thought to be more immunogenic. It was suggested that dermal DCs but not LCs isolated from draining LNs after initial challenge were able to activate T cells *in vitro*, which indicate the role of dermal DCs in immune response (Fukunaga et al., 2008)

Apart from differences in biological function, LCs and dermal DCs also show different migration abilities, either during steady state or the migration stage. It has been shown that dermal DCs begin to migrate to skin draining LNs 24 hours after skin was painted with a fluorescent dye and the number of DCs migrating to LNs peaks at 2 days (Kissenpfennig et al., 2005). In the same study, LCs have been shown to achieve peak migration number in LNs 4 days after stimulation. It was suggested that LCs and dermal DCs migrate to different compartment of LNs. Dermal DCs were shown to migrate to the outer paracortex, which near the B cell follicles, while LCs migrate into the paracortex, a T cell rich region (Kissenpfennig et al., 2005).

These results indicated that by targeting different skin DC subtypes may result in a different outcome. In this project, we would like to induce tolerance by utilizing tol-DCs, therefore, it is rational to target LCs rather than dermal DCs. However, it is technically difficult to target only specific cell type without modifying the peptide, which is outside of the scope of this study. In previous studies, glucocorticoid has been shown able to induce tol-DCs *in vitro* and *in vivo* (Moser et al., 1995). Therefore, in this project a topical application of glucocorticoid, betamethasone, was used to 'pre-educate' skin DCs to a tolerogenic state (presented in Chapter 4).

Other immune cells such as skin resident T cells ($CD8^+$, $CD4^+$ and NKT cells) and macrophages form an effective immune network by protecting the body from infection and trauma, as well as maintaining the homeostasis of the skin immune system.

1.9 Administration of drugs using Microneedles (MNs)

1.9.1 Drug administration methods,

Drug delivery is the method or process of administering a pharmaceutical compound to achieve a therapeutic effect in humans or animals. Drugs can either be delivered through enteral routes (sublingual, oral and rectal) or parenteral routes (intravascular, intra/transdermal injection, intramuscular, subcutaneous and inhalation). The route of administration is determined not only by the physical characteristics of the drug, but also the site of action, which may, in turn determine the speed at which the drug is absorbed and subsequently released.

The oral route is the most commonly used, due to its many advantages such as the low cost, high patient compliance and large absorption area. There are, however, limitations of the oral route, including the first-pass effect, local irritation to the gastric mucosa and degradation of certain drugs; such as peptides and proteins (Morishita and Peppas, 2006, Gupta et al., 2009a). Intravascular delivery has the advantages that it is precise, accurate, high dosage and the drug can take effect almost instantly. Some of the difficulties associated with intravascular delivery include the lack of controlled release and a relatively high risk of acute overdose, compared with other delivery methods.

As a large and accessible organ, the skin is an interesting target for drug delivery. The main obstacle for delivery drug through skin is the protective mechanisms of skin. One such important mechanism is offered by the stratum corneum, which provides a significant physical barrier to drug ingress. There are two types of skin delivery routes: transdermal and intradermal (ID). Delivery by the transdermal route involves delivering active ingredients across the skin for

systemic distribution. Drug can either pass through transcellular or intercellular pathways. The aim of ID injection is to inject a small amount of the drug locally, i.e. ID injection is not useful for systemic administration. This type of injection has several uses; including allergy tests and vaccinations.

In this project, a delivery method was required for targeting skin DCs locally in a minimally invasive manner in order to deliver a 'negative' vaccination signal. Therefore, the ID delivery is the chosen method for this purpose.

1.9.2 A brief introduction to MNs

MNs are needle-like structures with diameters in the order of microns and lengths of up to 1mm. These structures are used to penetrate the upper layer of the skin to enable dermal/transdermal drug delivery and for taking biological samples via the skin. The major advantage of using MNs for drug delivery is their ability to pierce the skin in a relatively non-invasive and painless way. The first MN was designed and patented in 1976 (Gerstel, 1976). Since then, MNs have been produced in various geometries and using different materials such as silicon, metals and polymers (Chandrasekaran et al., 2003, Chu et al., 2010, Jing Ji, 2006, Lee et al., 2008, Martin et al., 2012, N Wilke, 2007). Drugs, including oligonucleotides, desmopressin, human growth hormone, insulin and DNA have been delivered using MNs. There are, however some significant barriers, such as health and safety regulation and mass manufacture costs, which will need to be overcome before a MN based drug delivery or monitoring device is marketable.

MNs can be useful for systemic and local skin delivery. This project focuses on the delivery of autoantigen to skin by locally targeting DCs with a minimally invasive approach.

1.9.3 MN types

There are four general approaches to dermal drug delivery by different types of MNs: 'poke and flow' (hollow type), 'poke and patch' (solid/patch type), 'coat and poke' (solid-coated type) and 'poke and release' (solid/dissolvable type) (Kim et al., 2012) (Figure 1.6).

Hollow MNs function in a similar manner to hypodermic needles when used as a drug delivery device. They deliver drugs via the 'poke and flow' approach, facilitating force-driven fluid flow, thereby allowing a faster rate of delivery and larger volume than solid MNs. Another advantage of hollow MNs is that the dose of the desired drug in solution can currently be more easily controlled compared with other MN systems (Wang et al. 2006). Hollow MNs have some intrinsic disadvantages. Because of their hollow structure, there is risk of the hole clogging during insertion, causing a blockage. Blocked needles can potentially lead to leakage or prevent drug from being released and thereby cause inaccurate dosage. The hollow structure of this MN design also offers reduced mechanical strength, compared against solid MNs with the same geometry (Kim et al., 2012).

Solid/patch MNs are applied to puncture the skin creating micropores, allowing drug incorporated in a patch or topical formulation to bypass the stratum corneum and diffuse into the skin, i.e. the 'poke and patch' approach Figure 1.6. Compared with intact skin, the permeability coefficient of calcein (MW = 622.55)

was significantly increased by 104 to 105 times on skin pre-punched with 150um length MNs (Wu et al. 2008). For the 'poke and patch' approach to be effective, it is very important that the micropores stay open during the drug application period. Micropores are shown to close very rapidly *in vivo*, taking approximately 15 minutes (Milewski et al. 2010). Various approaches have been used to improve the lifetime of micropores. Maintaining hydration and occlusion is important because water has been shown to influence signalling during the skin repair process. Microchannels remained open for 24 hours (in some cases up to 72 hours) after MN treatment coupled with treatment to ensure the maintenance of hydration (Kalluri et al. 2011; Li et al. 2010). The 'poke and patch' approach is a simple way to achieve extended drug delivery via the skin. It enables the potential for delivery of drugs with high molecular weight, which are difficult to deliver successfully by other methods whilst maintaining their function. On the other hand, the lack of precise dosing and the low loading of drug, which can limit the effective dose delivered *per* treatment, has previously limited the usefulness of this method (Tuan-Mahmood et al., 2013).

Another way of delivering drugs by the 'poke and release' approach utilises dissolvable or biodegradable MNs. Polymer and sugar based MNs are able to encapsulate drugs in their needle matrix. The hypothesis is that encapsulated drugs can be released as the MN dissolves or degrades *in situ*. BSA encapsulated dissolving MNs made from carboxymethyl cellulose (CMC) and amylopectin have been produced, and were shown to dissolve completely in porcine skin within 1 hour (Park et al., 2006). A similar release rate for protein was found using dextran MNs (Ito et al., 2011a). Controlled release can be achieved by using dissolvable MNs. Extended release was achieved applying Gantrez® AN13 (a type of poly(methylvinyl ether/maleic anhydride) to deliver encapsulated theophylline into porcine skin (Donnelly et al., 2011). Dissolving

MNs can also be used for vaccination and delivery of peptides, such as human growth hormone (Lee et al., 2011). There are obstacles which need to be resolved before this technology can be widely used: These include low dosing, high fabrication temperature (during manufacture process) causing peptide to break down and low mechanical strength, which can be inadequate to reliably penetrate skin. A sugar based MN array was reported recently which was fabricated under vacuum conditions at low temperature (Martin et al., 2012). Due to the more amenable conditions used to produce these MNs, this approach could enable encapsulation of easily denatured or deactivated drugs, such as peptides and proteins.

An alternative approach to the 'solid/patch' method is using the 'solid-coated' approach. Solid MN arrays are coated with drug and deliver the drugs when inserted into the skin. Compared with hollow and solid/patch MNs, solid-coated MNs do not require additional equipment such as a pump, syringe or patch. Furthermore, solid-state drugs coated on MNs have a longer shelf life and no need for special storage compared to drugs in solution. One key benefit of solid-coated MNs is therefore relatively low cold chain costs.

A key step for the 'solid-coated' approach is the drug coating step. Various coating procedures, formulations and coating devices have been developed. The coating efficiency is influenced by the rate of solvent evaporation, wettability, viscosity and de-wetting (Gill and Prausnitz 2007a). To create a near-optimal coating formulation, it is important to decrease the surface tension and increase the viscosity of the coating formulation. Coating solutions have been developed for the 'dip-coating' method. A coating solution comprising 1% CMC and 0.5% Lutrol F-68 was shown to form a uniform thin film on solid stainless steel MN surfaces (Gill and Prausnitz 2007a). For hydrophobic drugs, 5% PVP in ethanol

has been used (Gill and Prausnitz 2007a). The aqueous coating solution was applied to deliver influenza virus-like particles and whole attenuated virus using the coat and poke approach (Marc 2010; Zhu et al. 2009) (Figure 1.6). It was thought that use of pre-coatings on the surface of MNs, such as PLGA or chitosan, could improve coating efficiency (Gill and Prausnitz 2007a). The dip-coating method has some drawbacks. It requires an excess volume of coating solution, causing wastage during preparation. The immersion and removal process must also be repeated several times in order to ensure sufficient coating. Other coating methods have been developed as an approach, which ensure uniform coating and may also be scalable. In one example, silicon MNs were sprayed with hydroxypropylmethyl cellulose or CMC (McGrath et al. 2011). A micron-scale thickness film was coated uniformly on MNs treated in this way (McGrath et al. 2011).

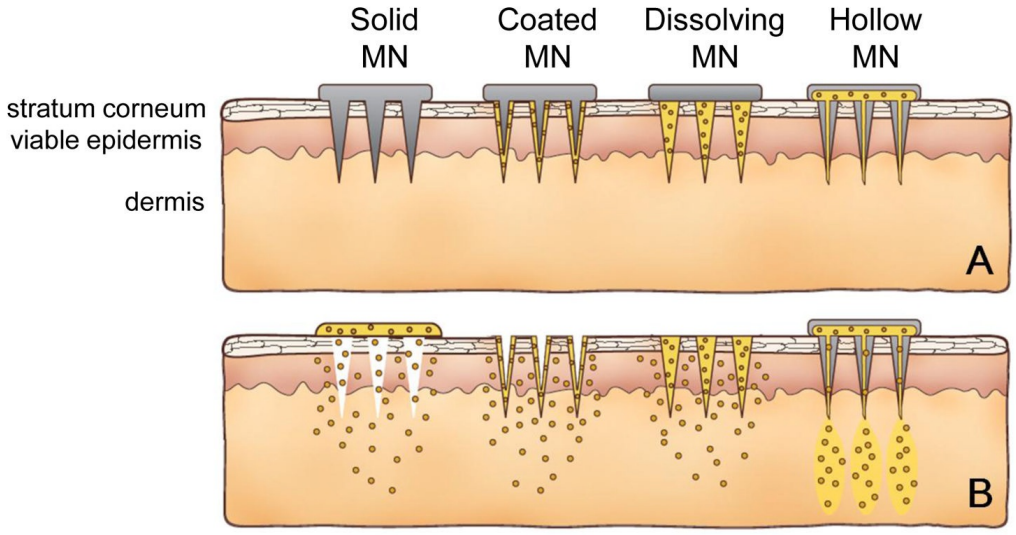

Figure 1.6 Schematic view of delivery method using four types of MNs. **A.** Drug deposition for four different types of MN before drug is released into skin. **B.** Drug diffusion within skin after MN application. Solid MNs can be used to create microconduits and drug can be delivered by applying a drug-encapsulated patch over the microconduits. Delivery of coated MN can be achieved by pre-coating solid MN with a layer of drug and drug can be released into skin during the MN penetration period. Drug can also be encapsulated into a dissolvable material and moulded into a dissolvable MN. Drug can be released into skin upon the dissolution of the needle within skin. Hollow MNs deliver drug in a fashion similar to conventional hypodermic needle. Drug solution can be pre-loaded in a syringe and injected into the skin using back pressure (Kim et al., 2012).

1.9.4 MN safety

1.9.4.1 Poration and microbial infection

Effective skin penetration is directly related to the length of the MN that is used. Two lengths of stainless steel MNs (200μm and 400μm) were tested on human volunteers to assess skin irritation and pain sensation. As predicted, the TEWL (transepidermal water loss) value increased when using 400μm long MNs compared with 200μm and started to drop back to baseline after two hours in both cases. Interestingly, no difference in skin redness or blood flow was observed between the two lengths, which are used as indicators of skin irritation. It was suggested that use of 400μm long MNs will effectively penetrate skin without causing significantly increased skin irritation (Bal et al., 2008). Both needle length and density were also shown to be linked to the degree of damage caused by MNs. Short MNs (100μm or 200μm) were not able to induce sufficient drug flux even with low needle density (Yan et al., 2010). Long MNs, greater than 600μm, effectively penetrated the skin when needle density was less than 2000 needles/cm^2 (Yan et al., 2010). TEWL values have indicated that 400μm long MNs are able to penetrate skin but no drug flux was observed if the needle density was greater than 60000 needles/cm^2 (Yan et al., 2010).

The size of the skin microconduit has been shown to be related to the radius or base width of the needle. MNs made of maltose with a 213±12μm base width created 60μm diameter open channels in hairless rat skin (Kalluri and Banga, 2011). A similar poration size was found using 770μm long metal MN with 140μm base width; a pore with a 70μm open conduit was observed in hairless rat by using calcein imaging (Kalluri et al., 2011). It has also been suggested that the ability of skin to regenerate its barrier function was not related to the needle

length used. In the cases of 370μm and 770μm lengths of MN, TEWL recovered to baseline levels 4-5 hours post treatment (Kalluri et al., 2011).

One concern is that microbes might travel through the conduits created by MN insertions; either transferred directly from the MN surface during insertion or transferred from the environment after MN removal (Donnelly et al., 2009b). Two *in vitro* skin models have been used to demonstrate the movement of dry state microbes on the skin into the skin substructure during the application of MNs: a 50μm thick Silescol® was used to mimic the intercellular liquid pathway and 400μm thick neonatal porcine skin was used to represent human skin. Three species of microbes, which are commonly found on human skin, were tested: Staphylococcus epidermidis, Candida albicans, and Pseudomonas aeruginosa. Results demonstrated that MNs caused less microbial penetration in both skin models than use of a 21G hypodermic needle. Therefore it was suggested that MNs could be used clinically with low risk of local and/or systemic infection (Donnelly et al., 2009b).

Another *in vivo* study was designed to investigate the flux of Staphylococcus aureus in solution through conduits after very short MN (70-80μm long) treatment. It was demonstrated that the MN treatment did not cause an increase in white blood cell counts, leukocytes and neutrophils in blood, which was thought to be due to the minimal damage caused to the dermal layer. On the other hand, damage caused by a 1500μm long needle on the skin enabled the transport of microbial load through the skin and showed an increased level of immune cells in the blood (Li et al., 2010). Their study also assessed skin damage by testing fibronectin level. Fibronectin–EIIIA and EIIIB were not found in undamaged rat skin as well as the short MN treated rat skin, indicating that damage caused by short MNs was minimised (Li et al., 2010).

The self-sealing ability of the skin is important in order to prevent unwanted infection after MN treatment. It has been shown that skin-resealing time is related to MN density, base width and length. Density played an important role on the rate of skin resealing. Skin resealed almost 6 times quicker when using 10 needles compared with 50 needles. Thick and wide needles were shown to prolong the skin resealing time. Furthermore, skin sealed 35% faster when using short (500μm) rather than long (750μm) needles (Gupta et al., 2011a).

1.9.4.2 Pain sensation

VAS (visual analogue scale) has been used to measure the pain sensation during MN application. Silicon MNs with 180μm long and 400/9mm^2 density were tested on volunteers compared with a smooth surface control and a 26G hypodermic needle. It was reported that no significant difference was observed between smooth surface and MN treatment with mean scores as 0.42 and 0.67 relatively, while hypodermic needles scored as high as 23.9 (Kaushik et al., 2001).

Pyramidal silicon MNs with 180μm and 280μm length were tested on human volunteers to investigate the pain sensation as compared with 25G hypodermic needles, using the McGill Pain Questionnaire Short Form and VAS. Both lengths of MNs caused less pain than a hypodermic needle. Furthermore, on average, the 280μm long MN was described as less painful than 180μm long MN (Haq et al., 2009). This was reported to be due to the need for the clinician to push harder with the shorter length MN device to ensure sufficient skin penetration.

It has been demonstrated that the VAS pain score for application of MNs is related to the geometry of MNs used. Stainless steel electro-polished MNs were fabricated with different length (l), thickness (t), base width (w) and density (n). The most painful type of MN was the longest, with dimensions of 1500(l) x75 (t) x200 (w) n=10, followed by the thick and dense MNs (750(l) x125 (t) x500 (w) n=50). The least painful MNs were shown to be those with shorter needles (500(l) x125 (t) x500 (w) n=50) or those of lower needle density (750(l) x75 (t) x200 (w) n=10). All MNs scored lower than the 26G hypodermic needle used in the same test (Gupta et al., 2011a).

Pain sensation induced by hollow MNs has been thought to be attributed to the liquid infusion as well as MN puncture. A small volume of methyl nicotinate (1µl) was injected in volunteers' forearms using silicon hollow MNs and a sensation of pressure but not pain was reported (Sivamani et al., 2005). Hollow MN delivery of insulin was reported to be less painful than catheter based devices but caused a tingling feeling when injection flow rate was at 1ml/minute. This tingling sensation was not noticeable when injection flow rate was less than 0.5ml/minute (Gupta et al., 2009c). A further study investigated the relationship between MN injection volume and pain sensation. In accordance with the previous observations, flow rate was shown to be positively related with the degree of pain sensation. Low flow rates (0.1ml/min) caused significantly less pain than high flow rates (1m/min), when the injection volume is high (1ml). Injection volume itself, however, was suggested not to be the main contributory factor to the pressure and pain sensation. Similarly, observations seen in solid MN penetration tests demonstrate that long hollow macro needles (1mm) caused more pain than short MNs (500µm) (Gupta et al., 2011b).

1.9.5 MNs used for drug delivery

MNs have been used for delivery of different drugs, such as, DNA (Coulman et al., 2006, Pearton et al., 2012); nanoparticles (Coulman et al., 2009); influenza vaccine (Pearton et al., 2010b, Song et al., 2010); siRNA (Chong et al., 2013); proteins such as botulinum toxin A (Torrisi et al., 2013) and recombined human growth hormone (Ameri et al., 2014); and peptides such as exenatide (Zhu et al., 2014), salmon calcitonin (Tas et al., 2012) and cosmetically relevant peptides (Mohammed et al., 2014). As this project is related to inducing immune response using a peptide (autoantigen), two main applications of MNs are of particular relevance here: vaccines and peptides.

1.9.5.1 Vaccine delivery using MN

Use of a hollow MN (1mm long, 34G) was studied for delivery of vaccines intradermally compared with an intramuscular (IM) injection using a 30G hypodermic needle. Three different vaccines were delivered: whole inactivated virus, trivalent human vaccine and DNA plasmid vaccine. Delivery using hollow MNs was shown to be dose-sparing for all three types of vaccines compared with IM delivery (the dose required to elicit a specific immune response was shown to be much lower for MN delivery as compared to IM delivery) (Alarcon et al., 2007). It was shown that the delivery route and delivery depth are important factors in inducing immune response. The dimensions of MNs used in this study were on the upper borderline of acceptable dimensions for a MN as defined earlier in this chapter (Alarcon et al., 2007). A phase II clinical study was carried out using this microinjection device for delivery of influenza vaccine compared with a licensed IM vaccination. ID (intradermal) injection of vaccine was shown to induce a similar immune response to IM injection, but using a smaller volume (0.1ml vs. 0.5ml) at a lower dose (9μg vs. 15μg). No adverse effects were observed using MNs in this 3-year follow up clinical study (Beran et al., 2009). Another shorter

hollow MN, which comprised of four 450μm long silicon needles, was also used in a clinical trial for the delivery of influenza vaccine. A low dose (3μg or 6μg) of hemagglutinin was delivered using MN, and a full dose (15μg) hemagglutinin was delivered using a 25G needle by IM injection. Both low doses delivered by MN were shown to be able to elicit immunogenic responses similar to a full dose IM injection. Furthermore, MN injection was demonstrated to be less painful than IM injection. At the same time, MN injection did cause a mild response, resulting in localised redness and swelling, which may have been due to liquid diffusion as discussed above (Van Damme et al., 2009).

Dissolvable MNs made of CMC (carboxymythylcellulose) have been tested in mice for inducing immune response. After a 10 minute application on the ventral side of the ear, MNs were seen to have dissolved, and the vaccine was therefore assumed to have been delivered. Both OVA and influenza vaccine were able to induce similar immune response when using dissolvable MNs compared to IM injection. The MN, however, was shown to require almost 45 times less influenza vaccine than IM injection, which was thought to be due to the targeting of skin DCs with these short needles (80μm long on average) (Raphael et al., 2010). Similar observations were made with another dissolvable MN made of a water-soluble polymer, PVP (polyvinylpyrrolidone). Dissolvable MNs can induce a robust humoral and cellular response in mice with a single-dose immunisation compared to IM injection using the same dose (Sullivan et al., 2010).

As previously mentioned, one important consideration using solid-coated MNs is the choice of coating formulation. It was shown that by adding trehalose to the coating formulation, improved influenza vaccine stability was observed (Quan et al., 2009). Using this coating formulation, 0.4μg of inactivated influenza vaccine was coated on 700μm long stainless steel MNs. Compared with IM injection,

using the same dose regime, MN immunisation showed a similar humoral response and an improved cellular response (Kim et al., 2009b). A long lasting humoral and cellular response was also observed using virus-like particles (VLPs). Influenza H5 VLP coated MNs were shown to be able to elicit higher levels of antibodies, when compared with traditional IM injection in mice, even at 8 months post-vaccination. Both MN and IM injection were shown to protect mice against lethal challenge 16 weeks after vaccination (Song et al., 2010).

As the skin DCs, especially LCs in the epidermis play an important role in both innate and adaptive immunity, it is important to understand the role of these DCs during the vaccination processes. Pearton *et al.* demonstrated that LCs changed their morphology after the delivery of VLP vaccine using ID or MN injection. More LCs migrate from the epidermis 48 hours after treatment when using MN rather than using ID, indicating that MN delivery is more efficient to target epidermal LCs (Pearton et al., 2010a). An in depth understanding of the immunological response to subunit influenza vaccine coated MN treatment has also been investigated. It was suggested that IM vaccination increased IgG1 antibody levels, while MN vaccination induces IgG2 antibodies, which indicates a Th1 response. MN treatment has been shown to enhance protection by rapid virus clearance, which contributed to the activation of an adaptive immune response (Koutsonanos et al., 2012). One interesting observation was that after lethal challenge, mice treated with MNs had higher IL10 levels in the lung than a comparable IM treated group, which consequently resulted in reduced lung inflammation (Koutsonanos et al., 2012).

1.9.5.2 Peptide delivery using MN

Peptides have been successfully delivered using a dissolvable MN system. Leuprolide acetate, a GnRH (gonadotropin-releasing hormone) agonist, was

encapsulated in a dissolvable MN, which was shown to be stable for 3 months when stored at ambient and low temperatures. However, low bioavailability was observed when using MN delivery, which was thought to be due to the degradation of leuprolide acetate within the skin (Ito et al., 2011b). Another peptide, exenatide, was also delivered using dissolvable MNs. MNs made of low-molecular-weight sodium hyaluronate (HA) can quickly dissolve in rat skin within 2 minutes following insertion time. Using these MNs, exenatide showed comparable pK compared with subcutaneous injection (Zhu et al., 2014).

Several peptides have been delivered using solid-coated MNs, such as desmopressin, PTH-1-34, salmon calcitonin and group of cosmetic peptides (Cormier et al., 2004) (Daddona et al., 2011) (Tas et al., 2012, Mohammed et al., 2014). Desmopressin coated MN arrays have been administered to hairless guinea pigs. High delivery efficiency (85%) can be achieved when using low drug loading and an application time of 15 minutes. Approximately 10% of drug was found on the skin surface, regardless of drug loading. This was thought to be due to the coating technique. The non-homogenous coating and drug coated on the base of MNs caused insufficient and inconsistent delivery (Cormier et al., 2004).

Using an improved coating technique, PTH1-34 (parathyroid hormone 1-34) was administered for Phase I and II clinical studies. The site of application was shown to have an impact on the bioavailability of PTH. Using the same dose of peptide, the AUC (area under curve) of PTH was found to be highest when delivered to the skin of the abdomen (65.7 pg*h/mL), followed by the skin of the upper arm (46.5 pg*h/mL), and the lowest was on the skin of the thigh (29.9 pg*h/mL). MN delivery, however, showed lower bioavailability when using the same dose as the standard subcutaneous (SC) injection. Thereafter PTH coated

on to MNs at double the dose (40μg) was compared with 20μg SC injection. MN delivery of PTH not only increased spine bone mineral density, but also, increased bone mineral density in the hip bone, which was not shown in control patients, treated using standard SC injection (Daddona et al., 2011).

Salmon calcitonin was also delivered using a solid-coated MN approach. The coating formulation for salmon calcitonin was prepared with a mixture of CMC, trehalose and Lutrol F-68. Coated MNs were applied on the dorsal side of rat ear for 20 minutes and the concentration of salmon calcitonin in serum was analysed for pK study. MN delivery of salmon calcitonin was able to achieve Cmax quicker than subcutaneous injection, which was thought to be due to the quicker absorption from dermal capillaries when using MN delivery. The choice of coating formulation is important. It has been shown that the loss of bioactivity of salmon calcitonin during formulation preparation and coating process contribute to the low bioavailability when using MNs (250ng/mL*min), compared to subcutaneous injections (403ng/mL*min) (Tas et al., 2012).

These studies have demonstrated that there is potential to successfully deliver peptides using MNs. However, because each peptide has different physical and chemical properties, there is no universal solution to deliver peptides using MNs. Furthermore, improving the low bioavailability of peptide using MNs, which could due to the stability of the peptide within the coating formulation and the solubility of peptides, still remains a difficult challenge. For this project, two auto-antigenic peptides were to be delivered using a solid-coated MN system. However, the physical and chemical properties of these two peptides make them difficult to deliver using any previously published coating formulation. The second obstacle is delivering the desired amount of peptide *in vivo*, due to a number of factors such as low solubility of peptide and hydration state of skin (as discussed in

section 2.4.2. and section 2.5.2. . As an added concern, the additives in published coating formulations may trigger an unwanted inflammatory immune response, which could counteract the desired effects of the ASI. Therefore, newly designed coating formulation specific to the peptide to be delivered was required for this project. The detailed aims and objectives for this project are listed in the next section.

1.10 Aims and objectives

T1D is an autoimmune disease caused by self-destruction of insulin secreting beta cells. One approach for potential treatment of this disease is ASI. However, one potential problem with using an ASI approach is controlling T cell polarisation. ASI treatment poses a risk of inducing Teff rather than Treg, which may cause further damage to the pancreas. In this project, we believe using a minimally invasive delivery method (MN) and targeting skin DCs, could reduce the risk of side effects whilst enhancing the effect of ASI to induce peripheral tolerance. We also investigated whether solid-coated MN delivery of autoantigen combined with use of a topical application of glucocorticoid could enhance the peripheral tolerance induced using a solid-coated MN approach. The schematic in Figure 1.7 illustrates the intended mechanisms underlying the approach taken for this project.

Therefore, the hypotheses for this project are:

1. Solid-coated MN delivery of autoantigen can enhance peripheral tolerance.
2. Topical application of glucocorticoid can enhance the effect of tolerance when combined with solid-coated MN delivery of autoantigen.

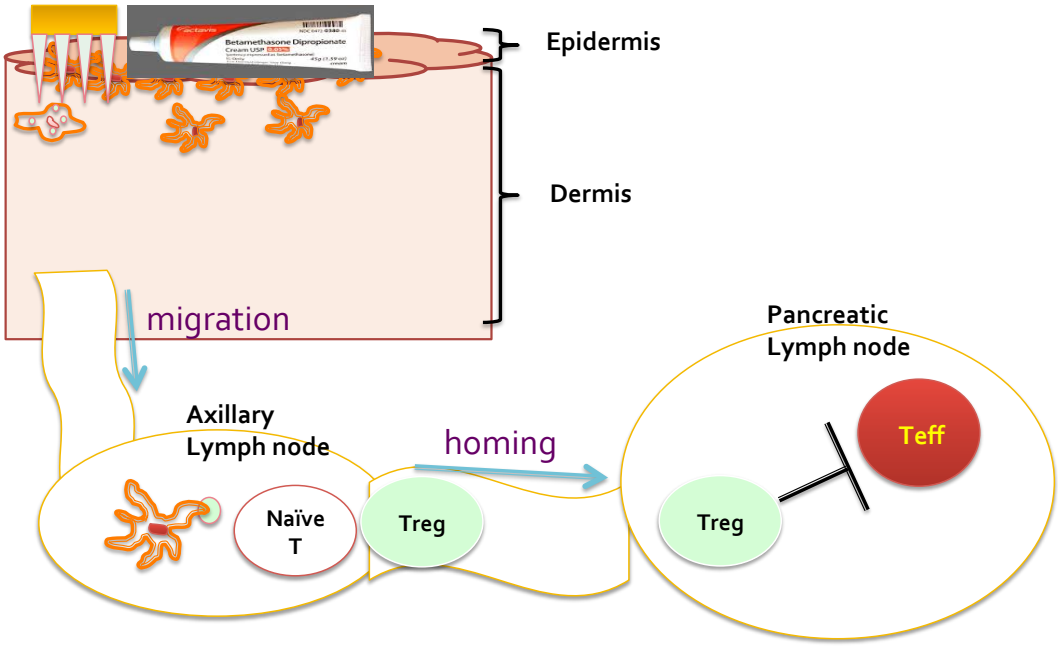

Figure 1.7 Schematic view of using solid-coated MN to induce tolerance *in vivo*. MNs were loaded with beta cell autoantigen and delivered to the skin. Autoantigen was then engulfed and processed by skin DCs, which then migrate to draining LNs (axillary lymph nodes) and present antigen to naïve T cells. Without full maturation, these skin DCs can induce antigen specific Tregs in skin draining LNs, axillary LNs (ALNs). These antigen specific Tregs home back to the PLN, where antigen specific Tregs deplete or anergise Teffs in PLN.

The aim of this project is to investigate the potential of ASI for the treatment of T1D using solid-coated MNs with or without the assistance of pre-treatment with a glucocorticoid cream.

Specific experimental objectives are as follows:

- Design and manufacture a solid-coated MN system suitable for both human and mouse skin
- Design a universal MN coating formulation system suitable for both hydrophobic and hydrophilic peptides
- To investigate the clearance of peptide delivered using MNs vs ID injection in mouse skin
- To investigate the potential of inducing tolerance in NOD mice *in vivo* using MN or ID injection of antigen
- To investigate the effect of short term topical application of glucocorticoid (betamethasone dipropionate (BD)) pre-treatment on enhancing ASI *in vivo*

Chapter 2 MN design and coating formulation

2.1. Introduction

2.1.1. Choice of MNs for ASI

As introduced in section 1.9.3, four approaches are commonly used for the intradermal or transdermal delivery of active pharmaceutical ingredients (APIs) by MN; solid/patch, solid-coated, dissolvable and hollow MNs (Figure 1.6). However, each MN type has its limitations as listed below.

The solid/patch method involves two separate processes: firstly creating micron-dimensioned pores in the skin using MNs and then delivering APIs through these pores using a topically applied carrier (e.g. patch, hydrogel, suspension or solution) (Bal et al., 2010, Wermeling et al., 2008, Pearton et al., 2008). There are two major limitations to using this method. Firstly, it is difficult to control the dose of API which penetrates the skin, and secondly, any excipients contained in the carrier may trigger an unwanted immune response. Therefore, solid/patch MN approach was not chosen for this project.

Dissolvable (or degradable) MNs encapsulate APIs in the body of the needles allowing APIs to be released into the skin when the needle is inserted into a hydrated environment (i.e. the dermis). One drawback to this approach is that APIs may lose their activity during the needle encapsulation process (Donnelly et al., 2009a). For this project, a minimum excipient content is required to minimise the potential inflammatory effect of excipient. This is also important to isolate the solo effect of antigen and delivery route on ASI output. Therefore the dissolvable MNs are not suitable for this project due to their high excipient to drug ratio.

Hollow MNs can deliver APIs into skin in a similar fashion to hypodermic needles, but with less pain and a more precise delivery depth. The advantage of hollow MNs is that they can deliver a large volume of drug solution with a precise dose (Norman et al., 2013, Gupta et al., 2009b). One type of hollow MN, MicronJet® (NanoPass, Israel) has shown efficacy in clinical trials in inducing immune response following influenza vaccination. Compared with full dose intramuscular injection, ID injection using MicronJet® showed a similar immunogenic response at a reduced dose, demonstrating the dose-sparing potential of a MN delivery system (Kenney et al., 2004, Van Damme et al., 2009). Therefore Micronjet® was chosen to compare with solid-coated MNs in this project.

An alternative approach to the 'solid/patch' method is the 'solid-coated' approach. Solid MN arrays are coated with drug which is delivered when the MNs are inserted into the skin. Compared with hollow and solid/patch MNs, solid-coated MNs do not require extra equipment such as a syringe or additional patch. Furthermore, solid-state drugs coated on MNs have a longer shelf life compared with drugs in solution. Solid MNs can be manufactured in a desired shape and length for different purposes but without losing their mechanic strength like hollow MN and dissolvable MN. Solid-coated MNs have been shown to target skin DCs and LCs effectively, which results in a dose-sparing effect on vaccination using solid-coated MN (for details see section 1.9.5). By targeting DCs locally, a systemic response can be avoided. This targeted delivery method provides a safe and efficient strategy for ASI without causing systemic suppression. For these reasons, solid-coated MNs were chosen for this project.

2.1.2. Coating formulation for solid-coated MNs

A fundamental step for the 'solid-coated' approach is the coating procedure. Various coating formulations and coating devices have been developed. The coating is influenced by the rate of solvent evaporation, wettability, and viscosity. Therefore, for a coating solution, it is important to decrease the surface tension and increase the viscosity in order to form a film during the coating process. After drying, this film will solidify and deposit APIs on the surface of the needle. Coating solutions have been developed for the 'dip-coating' method, whereby MNs are repeatedly introduced into the drug formulation. For example, a formulation comprising 1%w/v CMC and 0.5%w/v Lutrol F-68 was shown to form a uniform thin film on solid stainless steel MN surfaces (Gill and Prausnitz, 2007c). For the coating of hydrophobic drugs, 5%w/v PVP (Polyvinylpyrrolidone) in ethanol was employed as a solvent and inactive additive. The aqueous coating solution was used to deliver influenza virus-like particles (VLPs) and whole attenuated virus using the solid-coated approach (Zhu et al., 2009, Marc, 2010). It has also been reported that pre-coatings on the surface of MNs, which alter MN surface properties, such as PLGA or chitosan, can improve coating efficiency (Gill and Prausnitz, 2007a). However, the dip-coating method has some drawbacks. The method requires an excess volume of coating solution, causing wastage during preparation. The immersion and removal process needs to be repeated several times to ensure sufficient coating for an adequate dose. Other coating methods have been developed for uniform MN coating, which may also be scalable in the commercial context. In one example, silicon MNs are sprayed with hydroxypropylmethylcellulose or CMC. Using this approach a micron scale thickness film was coated uniformly on MNs (McGrath et al., 2011).

Compared with hydrophilic drugs, there are only few publications which discuss coating formulations for hydrophobic drugs. Two strategies were used by Gill and Prausnitz to encapsulate hydrophobic drugs in a coating formulation; 1) the use of organic solvents and 2) the use of low melting point polymers (Gill and Prausnitz, 2007c). Ethanol and acetonitrile were used as solvents for the preparation of the hydrophobic drugs, curcumin and sulforhodamine. Polyethylene glycol (MW1500) was melted and solid sulforhodamine was suspended in the liquid polymer, which was then coated on MNs. Both methods have the disadvantage that they only provide low drug loading dose, 0.01-0.1%(w/v). In another study, ketoprofen gel was coated onto solid MNs and the pharmacokinetics were tested *in vivo* following delivery (So et al., 2009). In this study, ketoprofen was encapsulated in a hydrogel mixture with a loading efficiency of 24mg/kg. The AUC (area under curve) of ketoprofen in the plasma of rats was shown to be higher when using coated MNs than using gel alone. However, the delivery efficiency of ketoprofen using coated MNs was not reported in this paper. The difficulty in delivering hydrophobic drugs is not just related to the dosage. In another study an aqueous coating formulation, salmon calcitonin (with a solubility of 1mg/ml in water) partially lost its activity during the dissolution and coating process (Tas et al., 2012).

2.1.3. Solid MN geometry and drug transportation

Several studies have been performed to determine the effect of MN geometry on skin puncture and drug transportation. Dermaroller® MNs of different needle length have been analysed for their ability to penetrate skin to deliver insulin *in vivo* to diabetic rats (Badran et al., 2009, Zhou et al., 2010). MNs with a needle length of 500μm were sufficient to increase drug flux without causing significant skin damage. MN safety studies have also been undertaken on human

volunteers (Coulman et al., 2011). Skin redness and dermal blood flow have been measured to indicate the degree of irritation caused by MN puncture. It was postulated that increasing the length of needle would increase the likelihood of induced redness of the skin. There was, however, no difference in blood flow or pain scoring with MNs between 200μm and 400μm long (Bal et al., 2008).

Needle interspacing is also an important parameter to enable successful MN penetration of the skin. In MN arrays, needle interspacing of less than 150μm requires an increased penetration force to enable successful penetration due to skin deformation and distribution of application force (Olatunji et al., 2013). Analytical models have been developed to study the combination of MN parameters such as dimensions and spacing on the skin damage and drug transportation. In skin pre-treated with silicon MN arrays, acyclovir fluxes increased with the increment of needle length. This effect, however, is reduced when needle density is greater than 2000/cm^2 (Yan et al., 2010). Sharpness of the needle also influences drug transportation. Increased tip radius, i.e. blunt MNs, can increase the damage to the skin, which will increase drug flux through skin. However, blunt MNs also need more application force to enable successful penetration (Olatunji et al., 2012), whereas sharper needles are able to penetrate the skin relatively easily. Coated MNs of different shapes have been analysed for their effect on insulin delivery and subsequent insulin concentration in blood. One report suggested that 'rocket' shaped MNs can distribute insulin evenly across the skin whilst a conical shape results in the least even dispersal of delivered load (Al-Qallaf et al., 2009). These studies provide some insight, which can guide MN design, and help prediction of drug transportation dynamics in the skin using these MNs.

2.2. Objectives

- To develop a formulation system which is suitable for peptides with a wide spectrum of solubilities.
- To determine the factors which influence the delivery efficiency of peptide via coated MNs
- To design a coated MN system that is suitable for both human and murine studies for the efficient targeting of skin DCs

2.3. Methods

2.3.1. Preparation of human skin explants

All human skin samples were obtained from female patients undergoing mastectomy or breast reduction surgery under informed patient consent and local ethical committee approval (South East Wales Ethics Committee Ref. 08/WSE03/55). Excised skin was transported from surgery to the laboratory at 4˚C in Dulbecco's Modified Eagle's Medium Base 5030 (DMEM 5030), supplemented with 1% penicillin/ streptomycin (100IU/ml), as described in a previous study (Ng et al., 2009). The subcutaneous fat was trimmed off of the skin using blunt dissection. The skin was then stretched to approximately its normal tension using pins on a cork dissection board.

2.3.2. Imaging MNs using Scanning Electron Microscopy (SEM)

SEM is an imaging technology that can be used to image the topology of an appropriately prepared sample. A scanning electron microscope utilises an electron beam which scans the object (sample) surface, producing signals such as secondary electrons emitted from atoms of objective surface (which is the primary signal used for normal SEM imaging), as well as backscattered electron and X-rays, which also have some imaging and analytical utility. The resolution of a modern SEM image can be better than 1nm, with a typical working resolution suitable for prepared samples in the micron range. Samples prepared for SEM can be relatively large in three dimensions and sample preparation is usually relatively simple, particularly for metallic, mineral and dehydrated samples. Preparation typically involves sputter coating with a heavy metal such as gold, which provides a good source of secondary electrons as well as dispersing any localised surface charging from the incident electron beam. Its resolution, analytical capabilities and ease of use make SEM, a relatively simple and useful

technique to examine surface morphology in great detail (Jensen, 2012). For SEM observation, MNs were carefully mounted on 32 x 10 mm aluminium specimen stubs (Agar Scientific, G318). A small piece of a 12mm adhesive carbon tab (Agar Scientific, G3347N) was cut to shape and placed underneath the MN to provide an appropriate angle for observation in the SEM. Leit-C Conducting Carbon Cement (Agar Scientific, G3300) was then used to secure the specimen in place. Mounted samples were then placed in an EMscope sputter coater under a low pressure argon atmosphere and coated with gold (Agar Scientific, AGB7184) to improve surface conductivity and increase generation of secondary electrons, thereby improving the signal/noise ratio. Samples were observed in a JEOL JSM-840A scanning electron microscope (JEOL, Tokyo, Japan) operating at 5kV. Images were captured using a SIS ADDAII Image grabber with analysis software (Soft Imaging System GmbH, Munster, Germany).

2.3.3. OCT (Optical Coherence Tomography) imaging

OCT is a non-invasive medical imaging system, which is mainly used in the diagnosis of ocular and skin diseases (Chen and Lee, 2007). OCT maps the biological tissues by collecting signals from backreflected and backscattered low frequency lights (i.e. infrared), using a principle similar to ultrasonography. Compared with other systems such as MRI (magnetic resonance imaging) or X-ray, OCT has the advantage of providing higher resolution (<10μm/pixel) images (Huang et al., 1991). In recent studies, OCT has proven to be a useful tool to examine the penetration of skin by MNs, both *in vitro* and *in vivo* (Donnelly et al., 2010, Coulman et al., 2011). In this study, an OCT system (VivoSight, Germany) with a quoted resolution of 4μm/pixel was used to image MN insertion depth *in*

situ, and poration *in vivo*. Image processing was performed according to the manufacturers guidance.

To image MN insertion depth in human skin explants, the majority of the dermal layer was first carefully trimmed off using a pair of fine scissors. The resulting processed skin was approximately 2 mm thick, which matches the maximum imaging depth of the OCT device provided. MNs were inserted into the skin explants from the epidermal side. The MNs and skin were turned gently upside down, leaving the dermal side facing upward. The light source used in OCT cannot penetrate optically opaque objects, such as the MN base; therefore, the *in situ* images were taken from dermal side of the skin. In order to do so, the OCT scanning probe was carefully placed on the dermal side, and held still manually until one scan was completed.

Ethical approval for measuring MN penetration in human volunteers was obtained from The Cardiff School of Pharmacy and Pharmaceutical Sciences Ethics Committee. Human volunteers were recruited and provided written consent to the procedures. All MNs used in this study were sterilised with 70% v/v ethanol and then air dried. The skin area of interest was first cleaned with an isopropanol swab and then marked with a marker pen to ensure the scan area is consistent. OCT scans were performed before MN treatment and immediately after MN treatment.

All image data was analysed using ImageJ software to assess the degree of tissue damage.

2.3.4. Skin delivery using hollow MNs

To study the delivery depth and drug distribution using hollow MNs, an array of four 450μm long pyramid shaped silicon hollow MNs, MicroJet® (provided by NanoPass Technologies Ltd), was used. A 1 ml syringe was filled with the delivery material and attached to the hollow MNs. MNs were then inserted into the skin with an angle of approximately 60˚ with the bore-opening side facing the skin as illustrated in Figure 2.1 (Yeshurun et al., 2009). A successful injection should form a bleb on the skin surface, without rupturing or evidence of leakage of injectable from skin.

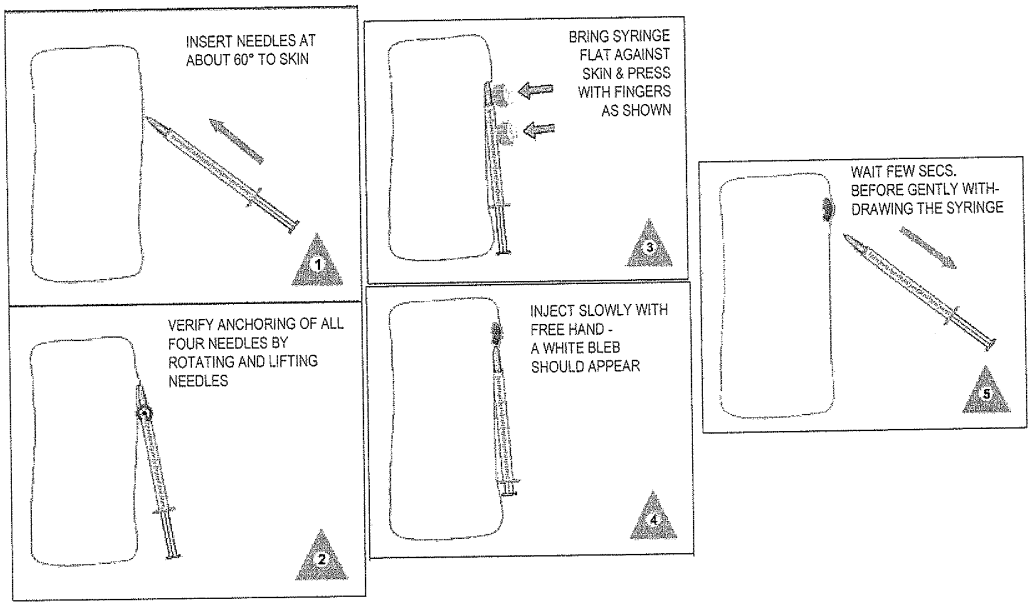

Figure 2.1 Schematic view of MicronJet® MN application to human skin (Yeshurun et al., 2009).

2.3.5. Coating procedure for solid MNs

To coat MNs, 0.4μl of the required formulation (which theoretically equates to 10μg peptide (25mg/ml)) was taken up using a pipette (range from 0.1μl-2.5μl) and 10μl ultra long tip. The tip was then carefully removed from the pipette ensuring that there was no loss of liquid. Peptide was then deposited onto

individual MNs by brushing the aperture of the pipette tip over the point of each needle (Figure 2.2). Due to adhesion/cohesion effects, a small amount of liquid is left on the surface of each needle. The needle can then be left to air dry, leaving peptide coated on the needle surface. This is repeated for three MN arrays (i.e. 30 needles in total) until all of the coating formulation had been coated onto the MN surfaces.

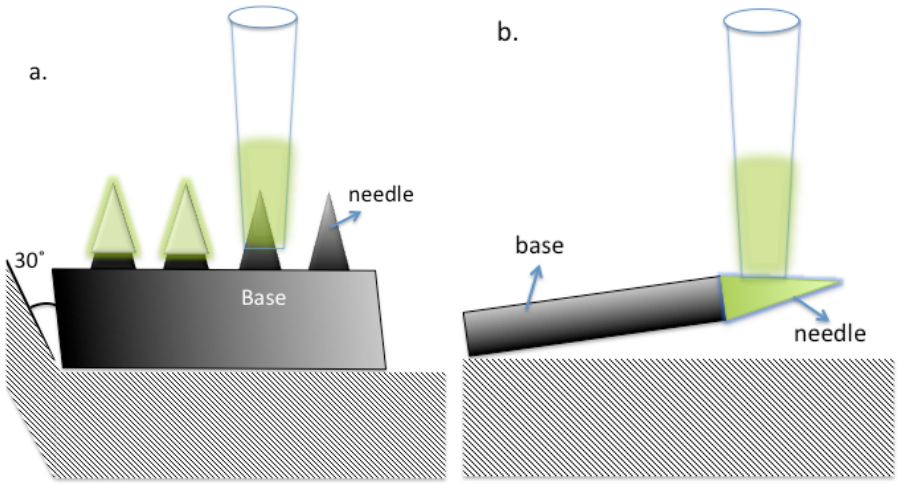

Figure 2.2 Schematic diagram showing the coating process using a tip coating method. 0.4µl (10µg peptide) coating formulation was taken for coating MNs (shown in green) and coated on MNs (black) surface by brushing liquid onto needle surface. **a.** Oblique view of coating process to show that needles can be precisely coated without depositing peptide on the base of MNs. **b.** Anterior view showing coating process.

2.3.6. Imaging the MN after coating

GeorgiaTech 750um MNs were coated, as described in section 2.3.5 with FITC-conjugated proinsulin B9-23-FITC, MNs were then imaged using a fluorescent microscope (Leica DM IRB Microscope, UK), to ensure coating quality and uniformity. The excitation and emission wavelengths of FITC are 490nm and 517nm respectively; therefore a blue excitation filter was used to detect the distribution of FITC conjugated peptide. During the imaging one MN array was placed on a glass slide and x4 and x10 magnification images were taken to

analyse the coating distribution and coating uniformity. Images were then processed using ImageJ software.

2.3.7. Skin delivery using solid MNs

Human skin explants were prepared using the method described in Section 2.3.1. MNs were firmly pressed into the skin by applying vertical pressure. The MNs were then held in place for 10 minutes before removal.

Three MN arrays were held together using a specially designed holder (Figure 2.3a). To apply MNs *in vivo*, a NOD mouse was shaved near the neck area using a clipper. MN arrays were then pinched and held against skin for 10 minutes with the mouse under general anaesthetic (Figure 2.3b).

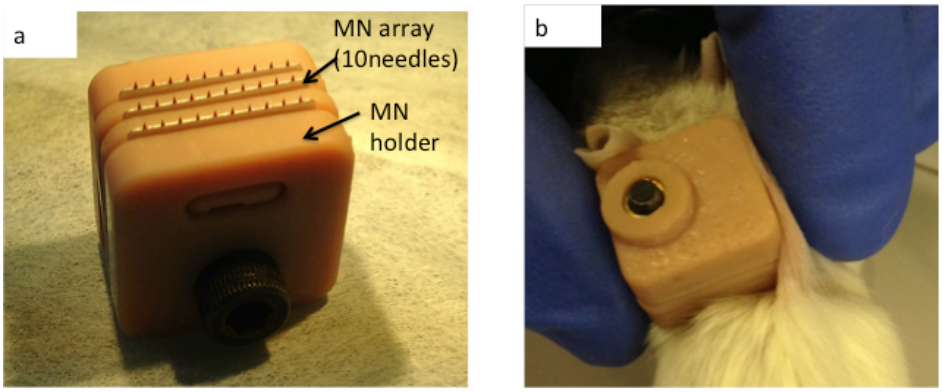

Figure 2.3 Solid MN assembly and application method on mouse. a. Three MN arrays (30 needles in total) assembled using a purpose built MN holder. Arrays were separated using a spacer and held together using a mini screw. **b.** *In vivo* MN application. The MN array was delicately pinched against shaved skin at the base of the mouse neck area and held still in order to maintain a stable delivery position.

2.3.8. Quantification of delivery efficiency of 5-TAMRA conjugated peptide using UV-vis absorbance

5-TAMRA is a pH sensitive photostable fluorophore. At pH7.0, Ex/Em (excitation and emission pair) is 553nm/576nm while in the solid state Ex/Em is 549nm/577nm. In 10%v/v acetic acid solution, its UV-vis peak absorbance

wavelength is 559nm. Using 5-TAMRA, different peptides can be quantified using the same UV-vis absorption, which provides a quick and reliable analytical method for different peptides.

The delivery efficiency of 5-TAMRA conjugated peptides was inferred by UV-vis spectrometry (NanoVue Plus Spectrophotometer, GE lifesciences) of the material remaining on the MNs after skin delivery. After skin insertion MNs were immersed in 100µl 10%v/v acetic acid in a sealed container and kept in the fridge for 15 minutes to wash off any residual peptide from the MNs. The absorbance of peptide-5TAMRA in the supernatant was then measured at 559nm using a NanoVue™ spectrophotometer and the concentration of residual peptide was then calculated using a calibration curve. This was repeated with MNs that had not been inserted into skin to determine the peptide loading of MNs. The residual mass of peptide on MNs and delivery efficiency were calculated using the equations below:

Equation 2.1 Calculating the mass of peptide that remained on solid MNs.

$$Mass\ (\mu g) = Concentration\ (\mu g/ml) * 0.1ml$$

Equation 2.2 Calculating the delivery efficiency of peptide using solid MNs.

$$Delivery\ efficiency\ (DE) = \frac{Mass\ before\ delivery - Mass\ post\ delivery}{Mass\ before\ delivery} X100\%$$

2.3.9. Skin histology

Skin tissue was immersed in optical cutting temperature embedding matrix at room temperature in a plastic mould with air carefully removed. This was then snap frozen using a mixture of methanol and dry ice. Sections (8µm thickness) were obtained using a Cryostat FSE (Thermo Scientific) with the chamber

temperature and the sample temperature set at -20˚C. Sections were collected on glass slides and kept at -80˚C for further use.

Haematoxylin and Eosin (H&E) staining is commonly used in the light microscopic study of histological specimens, and is a routine technique in diagnostic pathology. Haematoxylin, in the presence of aluminium salt, is a positively charged basic blue dye, which readily binds with molecules with a negative charge, such as DNA. For this reason nuclear material in an H&E histological section appears blue. Eosin is a pink/red negatively charged acidic dye, which binds with positively charged molecules such as arginine and lysine rich cytoplasmic protein and peptides. This is typically seen as pink connective, membranous and fibrous tissue in a prepared section (Fischer et al., 2008, Kuru, 2014).

Prior to H&E staining, cryosections were fixed in ice cold acetone for 10 minutes, then washed with PBS three times to remove OCT media. Sections were then stained in filtered Haematoxylin for 5 minutes before rinsing in running water for 2 minutes. Sections were decolourised by immersing in 1%v/v acid alcohol (1%v/v HCl in 70%v/v ethanol/water) for 1 second. Sections were then differentiated in eosin aqueous solution stain for 10 seconds before rinsing in running water until the water ran clear. Samples were dehydrated using an ethanol gradient; 10 seconds in 50%, 70%, 80%, 95% and 100% v/v alcohol sequentially. Slides were left in 100% alcohol for another 1 minute, cleared with xylene and mounted with a cover slip using mounting media. Once the mounting media was dry, the coverslip was sealed using clear nail varnish to improve the lifespan of the slide and prevent the section from becoming desiccated. Slides were stored at room temperature, in a slide box, avoiding light.

2.3.10. Measurement of pH value of acetic acid solution

Acetic acid was diluted in water to v/v dilutions of 20%, 12.5% and 10%. The pH meter was calibrated against standards. To test each solution, the pH probe was first washed in water, and then gently dried with a tissue paper. The probe tip was placed into the solution to be measured together with the temperature probe. The reading was allowed to stabilise and a recording was taken. After each measurement, the probe was washed in water, dried with a paper towel and stored immersed in 3M KCl solution.

2.3.11. Electro-polishing stainless steel MNs

Electro-polishing is a surface finishing process, which is able to remove surface imperfections (burrs) from a cut metal surface. As opposed to electroplating, metal on the anode side dissolves into electrolyte solution when a current is applied. On the irregular shaped metal surface the charge is concentrated on the protruding point resulting a rapid removal of metal atoms, therefore deburring the surface of metals and providing a smooth surface (Lee, 2000).

MNs were wire cut from stainless steel sheets using wire electrical discharge machining (wire-EDM) at the Cardiff School of Engineering. The MNs were then electro-polished using a method adapted from that described previously (Gill and Prausnitz, 2007a). An electrolyte bath was prepared containing glycerol, ortho-phosphoric acid (85%) and water in a volume ratio of 6:3:1. The cathode was connected to a copper plate and the anode was connected to a MN array. The electrolyte bath was heated to 70˚C and a magnetic stirrer was used to distribute the heat evenly. A current of 1.8 mA/mm^2 was applied for each MN array accordingly for 15 minutes coupled with the agitation of the MNs, by an agitating device (made in-house), which was used to remove bubbles (oxygen from the

anode, hydrogen from the cathode), increasing the efficiency of the process. After electro-polishing, the MNs were washed for 30 seconds in de-ionised (DI) water followed by 25%v/v nitric acid solution; these washing steps were repeated three times. MNs were then rinsed in hot running tap water before rinsing in DI water. MNs were then air dried, wrapped in lens tissue and kept in an airtight container to await further use.

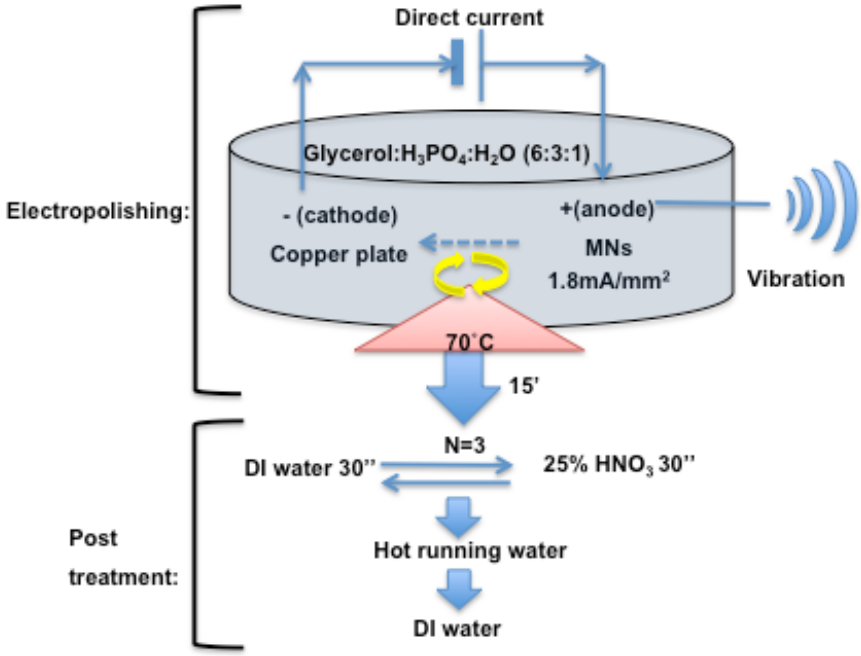

Figure 2.4 Schematic view of the MN electro-polishing process. The electro-polishing step uses a temperature controlled viscous acid bath (electrolyte solution) to remove uneven surfaces. Post treatment involves washing in nitric acid and water to give the desired finish.

2.4. Results

2.4.1. Choice of MNs for targeting skin DCs

2.4.1.1. Delivery depth, solid versus hollow MNs

In order to optimally target LCs in the skin, the delivery depth of two commercially available MNs was compared: Nanopass® MicronJet and Dermaroller®. Nanopass® 450μm consists of an array of hollow silicon MNs comprising four angled 450μm MNs in a row (Figure 2.5 A-D). Nanopass® MNs were attached to a conventional syringe and delivery was achieved by injecting a liquid formulation through the needles. Dermaroller® 500μm consists of two rows of 8 x 500μm length stainless steel MNs mounted on a plastic base (Figure 2.5 E-H). To achieve delivery using Dermaroller® solid MNs, deliverable drug was coated onto individual needles (see Section 2.2.5) which was then inserted into the skin to deliver drug load.

The morphology of both types of MNs were compared against a conventional 29G insulin injection needle (Figure 2.5 A&E). Both Nanopass® and Dermaroller® MNs had a much more refined structure than a conventional 29G needle. Nanopass® MNs were pyramid shaped with a bore-opening of 51.6μm (Figure 2.5 C&D). Dermaroller® MNs, on the other hand, were a conical shape with needle tip diameter of less than 10μm (Figure 2.5 G&H).

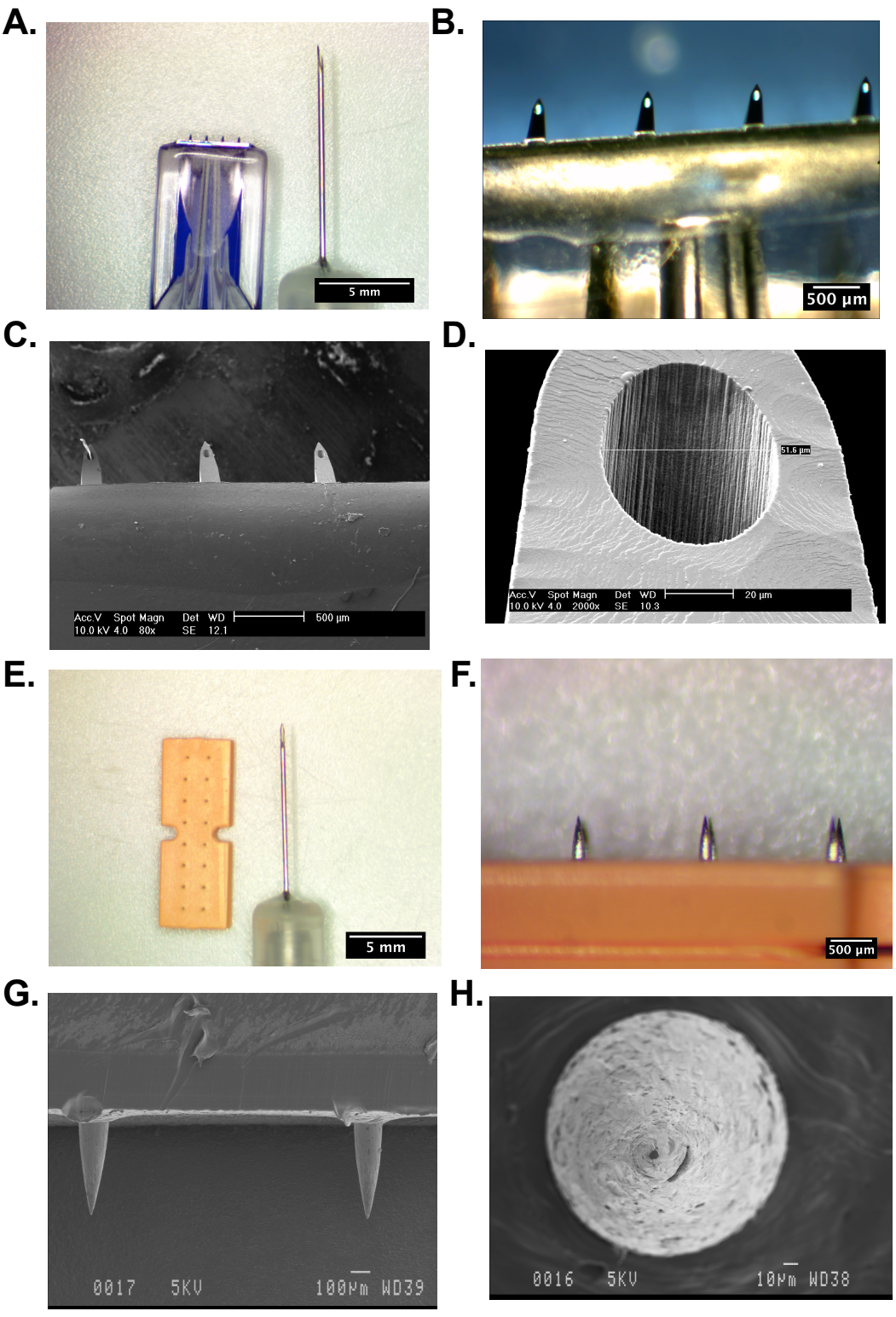

Figure 2.5 Images of Nanopass 450µm MNs and Dermaroller® MNs. A. Nanopass 450µm (left) compared with 29G Insulin injection needle (right), **B.** Magnified view of Nanopass MNs, **C.** SEM image of Nanopass 450µm and **D.** Needle opening and its size, **E.** Dermaroller® 500µm (left) compared with 29G Insulin injection needle (right), **F.** Magnified view of Dermaroller® MNs, **G.** SEM image of Dermaroller® 500µm side view and *en face* view (**H**).

Skin delivery depth was demonstrated histologically using H&E stained sections of human and mouse skin, as examined using light microscopy. Anatomical differences between human and mouse skin are shown in Figure 2.6. Following blunt dissection, the thickness of the human skin explants was approximately 2-3mm, with a densely packed epidermal layer measuring 60-100μm (Figure 2.6 A). Mouse skin on the other hand is much thinner (Figure 2.6 B). The total thickness of mouse skin is 200-300μm with a very thin layer of epidermis (20-30μm). Figure 2.7 A shows that 450μm hollow MNs delivered the majority of peptide (m31-5TAMRA, shown in red) into the lower dermis in human skin explant. Some peptide was left in the needle track when the needle was retrieved, but this only represents a small proportion of the total delivered peptide. When using mouse skin, most peptide (shown in green) was injected into the subcutaneous layer as well as the dermal layer. On the other hand, as shown in Figure 2.7 C, fluorescent peptide delivered using 500μm long solid-coated MNs was left in the epidermis and the uppermost layer of the dermis. For mouse skin, 500μm long solid MNs are able to target most dermal areas (Figure 2.7 D). The penetration depth of solid MNs in human skin was measured using the OCT imaging system. Dermaroller® MNs were inserted into human skin explants and imaged using OCT *in situ*. The insertion depth of 500μm Dermaroller® MNs measured in human skin explants was between 300-400μm.

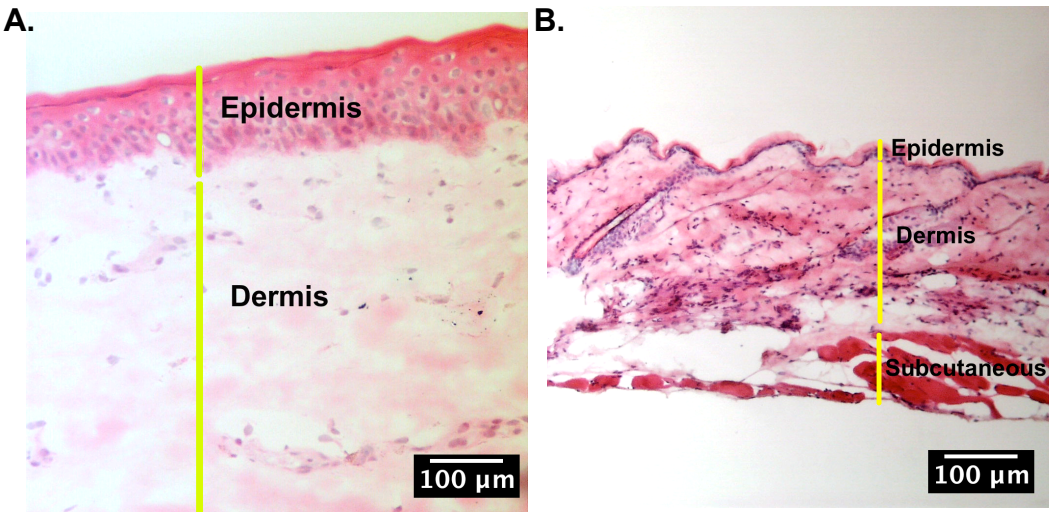

Figure 2.6 Human vs. mouse skin structure. Section was stained with H&E to distinguish cellular (blue) and connective tissue (pink). **A.** Human breast skin cross section. The thickness of human skin epidermis is between 60-100µm and densely packed with cells. The dermis is mainly constructed of connective tissues with scattered cells; **B.** Mouse flank skin cross section. The total thickness of mouse skin is between 200-300µm with a very thin epidermal layer (approximately 20µm).

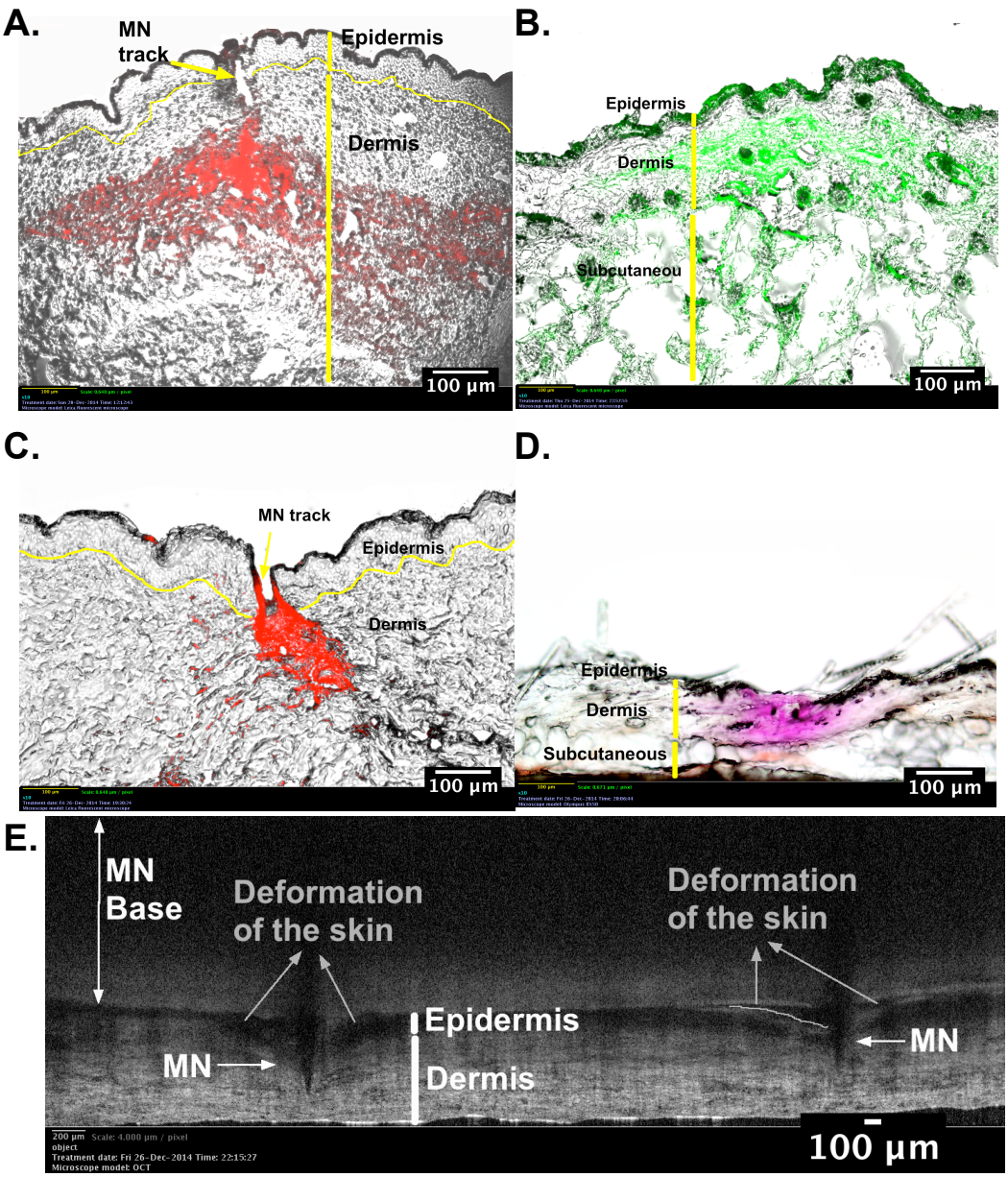

Figure 2.7 Delivery depth of peptides using hollow MN and solid MN in human and mouse skin. **A.** Hollow MN injection of fluorescent peptide (red) to human skin explant; **B.** Hollow MN injection of fluorescent peptide (green) to mouse skin; **C.** Fluorescent peptide (red) was coated on 500µm solid MN and delivered to human skin explant; **D.** Fluorescent peptide (red) was delivered to mouse skin using 500µm solid-coated MNs; **E.** *In situ* OCT image of 500µm solid MNs inserted into human skin explant.

2.4.1.2. Skin disruption using solid MNs of different length

OCT was used to determine MN disruption to human skin in human volunteers. Two solid metal MNs of different length were tested here: 500µm long Dermaroller® MNs and 750µm long GeorgiaTech MNs. Before MN treatment, the skin surface showed no signs of damage (Figure 2.8 A). After solid MN

treatment, pores caused by MN damage can be observed on the surface of the skin, and are indicated in the images presented by yellow arrows (Figure 2.8 B, D). There was no obvious difference in the pores created using 750μm long needles (Figure 2.8 B) or 500μm long needles (Figure 2.8 D) shown from the *enface* view of the skin. Cross-sections of the pores revealed the extent of skin disruption after MNs were removed. The damage track by 750μm long needles appeared to be deeper and wider compared with the damage created by 500μm long needles (Figure 2.8 C, E).

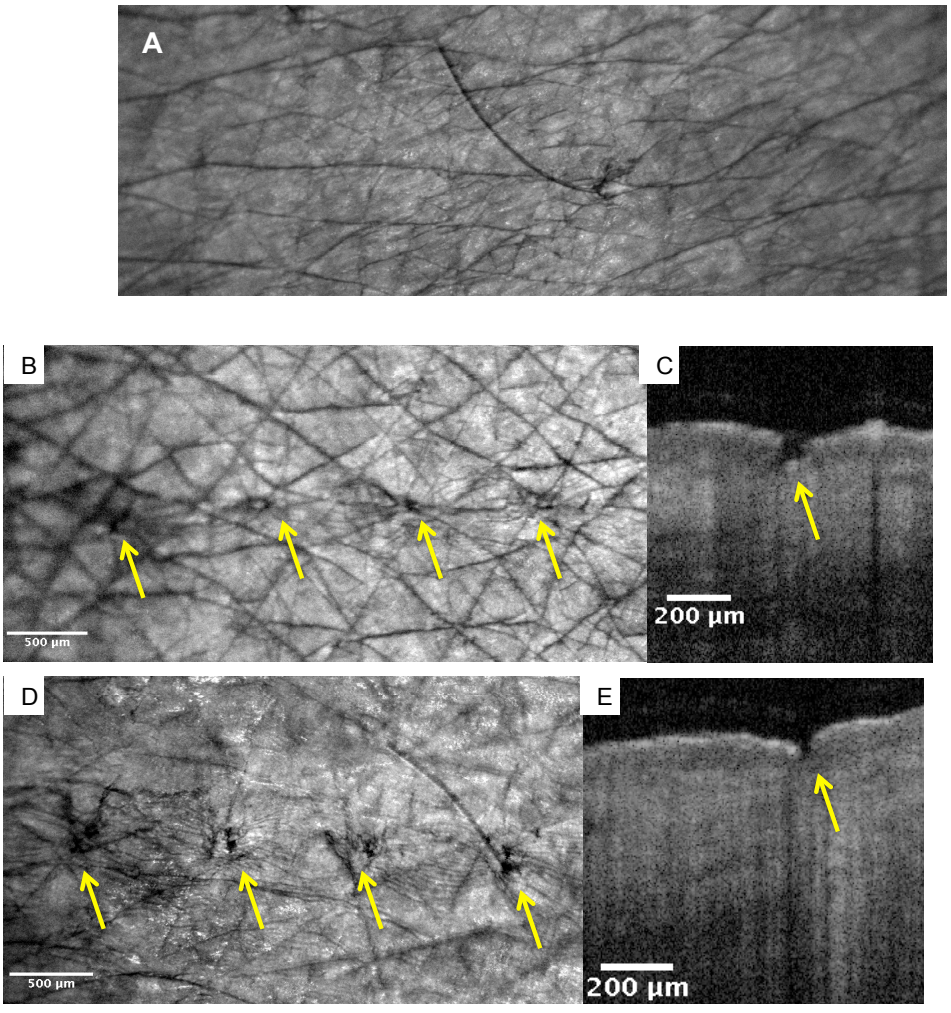

Figure 2.8 Skin disruption in human volunteers by solid MNs imaged by OCT. A. Skin surface features before treatment; **B.** Skin surface features after treatment with 750μm MNs. **C.** Cross-section of skin damage following removal of 750μm MNs from the skin. **D.** Skin surface features after treatment with 500μm MNs. Yellow arrows indicate the pore or skin disruption after application of MNs.. **E.** Cross-section of skin damage after 500μm MNs were removed from skin. Yellow arrows indicate the pore or skin disruption after application of MNs.

2.4.2. Development of a novel coating formulation

2.4.2.1. Peptide properties

Three different peptides were coated onto MNs. The amino acid sequence and properties of the peptides are listed below:

Table 2.1 Peptide properties. Peptide properties were generated using an online resource (https://www.genscript.com).

Peptide	Sequence	Charge	Isoelectric point	pH	Hydrophobicity (overall % Of hydrophobic and hydrophilic amino acids)
m31	YVRPLWVRME	1	9.3	Basic	Hydrophobic: 60% Hydrophilic: 30%
WE14	WSRMDQLAKELTAE	-1	4.43	Acidic	Hydrophobic: 43% Hydrophilic: 36%
Pro-insulin B9-23	SHLVEALYLVCGERG	0	5.48	Neutral	Hydrophobic: 40% Hydrophilic: 27%

All peptides included in this study are categorised as hydrophobic peptides. The solubility of these peptides in water is in the order WE14>M31>proinsulin B9-23. Preliminary studies showed that a previously reported MN coating formulation (Gill and Prausnitz, 2007c) was only able to dissolve low concentrations of WE14 and would therefore be unsuitable for coating MNs with these hydrophobic materials.

2.4.2.2. Choice of solvent for coating hydrophobic peptides

In order to coat a suitable amount of peptide onto MNs without overloading, a novel coating formulation was developed. Firstly, the desirable criteria of this formulation were identified to focus research effort:

- Water based system.

- Solvent used to dissolve the hydrophobic peptide should be, at least partially, miscible with water.
- Solvent will evaporate at room temperature and at atmospheric pressure, ideally with a similar vapour pressure to water.
- The coating formulation would not alter peptide bioactivity.
- The excipients in the coating formulation would not trigger a non-specific proinflammatory immune response.
- The amount of excipients should be minimised.
- Peptides should be soluble in the formulation at high concentration ≥ 10mg/ml.
- Formulation is able to be stored at -80˚C (i.e. has a melting point of > -80˚C).

In order to dissolve these hydrophobic peptides, the first approach used was to protonate water using acetic acid. Acetic acid has a low melting point, 16-17˚C, is miscible with water and will evaporate at room temperature. The pH of acetic acid solutions at concentrations of 1.9, 2.2 and 2.6 mol/L is 2.24, 2.21 and 2.17 respectively. All acetic acid solutions were able to dissolve WE14 resulting in concentrations ranging from 10mg/ml to 25mg/ml. Proinsulin B9-23 and m31 peptides were however not soluble enough in high or low concentration acetic acid solutions to produce peptide concentrations above 10mg/ml.

Alcohols were initially investigated as potential co-solvents as they are very commonly used for dissolving hydrophobic compounds and have relatively low toxicity. Within the series of ethanol, propanol, butanol and pentanol, only tert-butanol and tert-amyl alcohol have a melting point of greater than

80˚C. Table 2.2 lists some key physical properties of these two alcohols (tert-butanol and tert-amyl alcohol) compared with water. Containing one more methyl group, tert-amyl alcohol has a lower solubility in water than tert-butanol. The presence of a methyl group in these alcohols also alters the melting point, boiling point and vapour pressure. Both alcohols fit the criteria listed above which make them suitable candidates for further investigation for use in our coating formulation. Tert-butanol however was not able to dissolve proinsulin B9-23 at a high concentration (≥10mg/ml). Therefore tert-amyl alcohol was chosen as the solvent in coating formulations for hydrophobic peptides. The miscibility of tert-amyl alcohol with acetic acid/water mixtures was tested. Tert-amyl alcohol was able to dissolve in 1.7M-3.5M acetic acid/water mixtures at a ratio of 1:5v:v without visual observation of phase separation.

Table 2.2 Chemicals physical properties. The physical properties of acetic acid, tert-butanol and tert-amyl alcohol were compared with H_2O. All the data were cited from http://www.chemspider.com/

Compound	Molecular weight g/mol	Solubility in water / g/l	Melting point /˚C	Boiling point /˚C	Vapor pressure /Kpa (at 20˚C)
Acetic acid	60.05	Miscible	16 to 17	118 to 119	1.5
Tert-butanol	74.12	Miscible	25	82 to 83	4.1
Tert-Amyl alcohol	88.15	120	-9	101 to 103	1.6
H_2O	18	-	0	100	2.3

To dissolve the peptide it was crucial to disperse the peptide in a small volume of tert-amyl alcohol first, followed by the acetic acid solution. Three different concentrations of amyl alcohol and acetic acid solution were used for the three peptides listed in Table 2.2. The optimal combinations of coating formulation components for dissolving 1mg of peptide are listed in Table 2.3.

Table 2.3 Coating formulation composition for three peptides. The formulation was tested for its ability to dissolve 1mg of each peptide. Choice of excipients is listed in **Table 2.4**.

Peptide	Tert-amyl alcohol (v/v%)	Acetic acid Mol/L (v/v%)	Water (v/v%)	Peptide Conc. (mg/ml)	Excipient Conc. (mg/ml)	Volume to coat 10µg peptide (µl)
m31 mimotope	20	1.9 (11%)	69	25	2.5	0.4
WE14	-	2.6 (15%)	85	25	2.5	0.4
proinsulin B9-23	31.25	2.2 (12.5%)	56.25	12.5	1.25	0.8

2.4.2.3. Choice of formulation excipients

A range of further excipients were explored to 1) assist the dissolution of the peptide loaded onto MNs once in the *in vivo* environment and 2) stabilize the coating mixture (Table 2.4). As a previous study has shown the safety profile of 10µg pro-insulin C19-A3 in a Phase I clinical study (Thrower et al., 2009), it was decided that 10µg of peptide would be an appropriate dose to coat onto each MN array. Five excipients listed in Table 2.4 were tested individually to improve the coating ability (peptide alone was not able to coat the needle with the current coating method). 1µg of each excipient was used to provide a low excipient to drug ratio, 1:10w:w. The five excipients, from three main categories were; PVA (polyvinyl alcohol) and PEG (Polyethylene glycol), which were used as dispersants; Pluronic F68 and F127, which were used as surfactants, and finally 2HPßCD (2-hydroxypropyl-ß-cyclodextrin), which was used to form an inclusion complex with hydrophobic peptides in order to increase the peptide solubility.

Table 2.4 Excipients tested as components in the coating formulation to improve coating ability.

Excipients	Function	Properties
PVA (MW 2000)	Dispersant	Hydrogel
PEG (MW 1450)	Dispersant	Polymer
PF127	Nonionic Surfactant	Thermogel
PF68	Nonionic Surfactant	Thermogel
2-hydroxypropyl-ß-cyclodextrin	Form inclusion complex	Sugar ring

In order to develop the coating formulation, 1mg of proinsulin B9-23-FITC was initially dissolved in each of the solvents (as described in Table 2.3) prior to adding each additional excipient respectively. All excipients were able to assist peptide coating on MNs, resulting in a more uniform coating without overloading, as shown in Figure 2.9 (as a representative example).

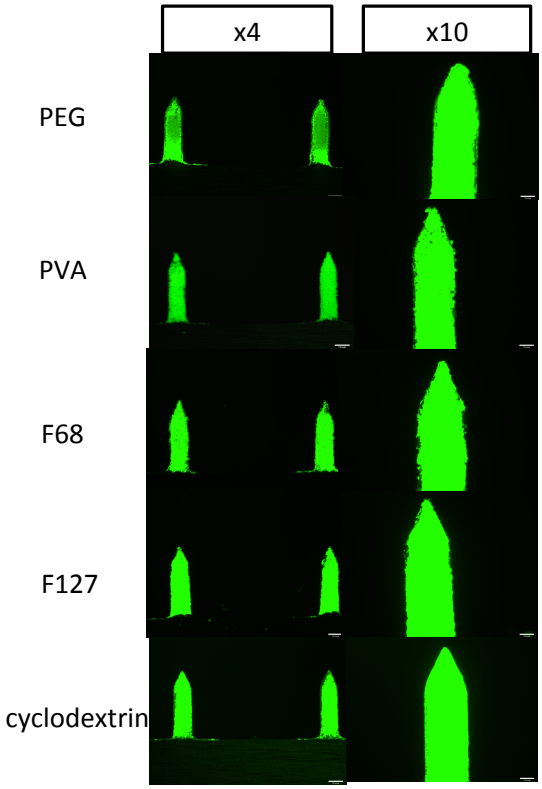

Figure 2.9 Fluorescent images of coating ability of proinsulin B9-23-FITC in formulation with different excipients. All excipients were able to assist coating of the peptide on the surface of the needle. Without the use of excipients, peptide was unable to coat MNs using the current coating method.

2.4.3. Factors that influence skin delivery efficiency

2.4.3.1. Excipients in the coating formulation

Coated MNs were then tested for their ability to deliver the coated material into human skin explants. Dermaroller® (500µm) MN arrays were coated with 1µg of excipient (as listed in Table 2.4) and 10µg of WE14-5TAMRA. MNs were inserted into human skin for 10 minutes. The amount of peptide remaining on the MNs was measured using UV-vis spectroscope (Nanovue™) with delivery efficiency inferred by subtraction using Equation 2.2. Both dispersants (PVA and PEG) improved delivery efficiency to skin, resulting in an overall delivery efficiency for WE14 peptide of greater than 40%. 2-hydroxypropyl-ß-cyclodextrin also assisted dissolution of the peptide from MNs, resulting in an overall delivery efficiency of 38%. Comparing excipients, PVA assisted WE14-5TAMRA release

into the skin more efficiently than other excipients and showed a significantly higher delivery efficiency than both the surfactants,PF68 and PF127.

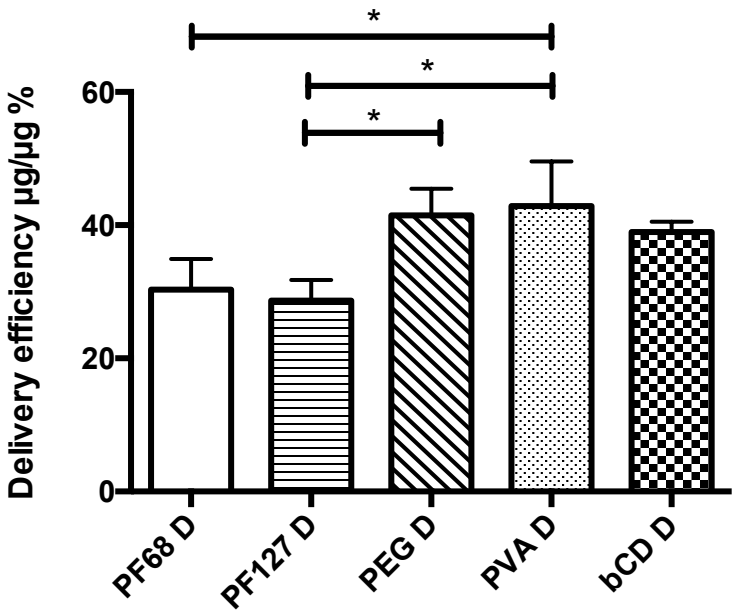

Figure 2.10 Excipient effect on delivery efficiency of WE14-5TAMRA using 500µm Dermaroller® MNs. MNs were coated with 10µg of WE14-5TAMRA and applied to human skin explants for 10 minutes before analysing the delivery efficiency. n=3. One way ANOVA with Tukey's post test. *p<0.05. D= peptide was delivered using 500µm long Dermaroller® MNs.

2.4.3.2. The effect of MN surface properties

In order to further improve the delivery efficiency, another MN device was tested. These MNs, supplied by Georgia Institute of Technology, were laser cut in-plane from stainless steel to create a row of 5 MNs of 750µm length. These MNs were already post treated by electro-polishing (Figure 2.11 B). Each MN array (5 needles) was coated with 10µg of WE14-5TAMRA and 1µg of excipient as described above, and inserted into human skin explants for 10 minutes. The delivery efficiency was measured using Nanovue™ and inferred by subtraction using Equation 2.2. Interestingly, all MNs were able to deliver over 80% of WE14-5TAMRA regardless of excipient effects (Figure 2.12). As the dispersant PVA (MW2000) was able to assist the release of peptide from MNs into the skin

in both polished and unpolished MNs this excipient was selected for further testing.

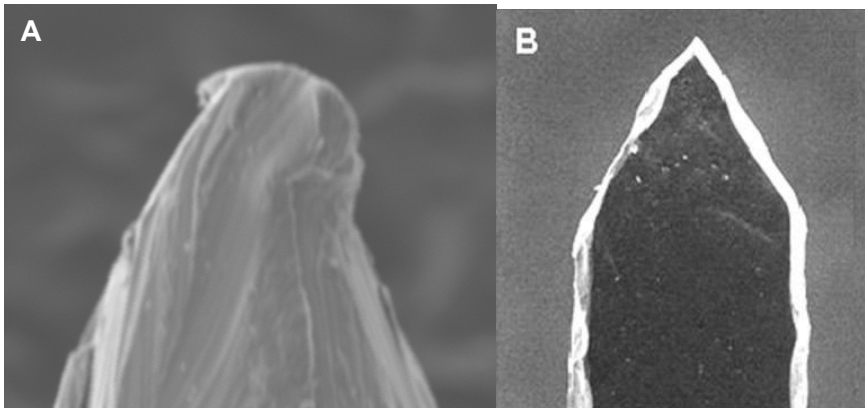

Figure 2.11 SEM images of solid MN surface morphology. A. Dermaroller® MN **B.** 750µm electro-polished MN from GeorgiaTech (Gill and Prausnitz, 2007b, Gill and Prausnitz, 2007a)

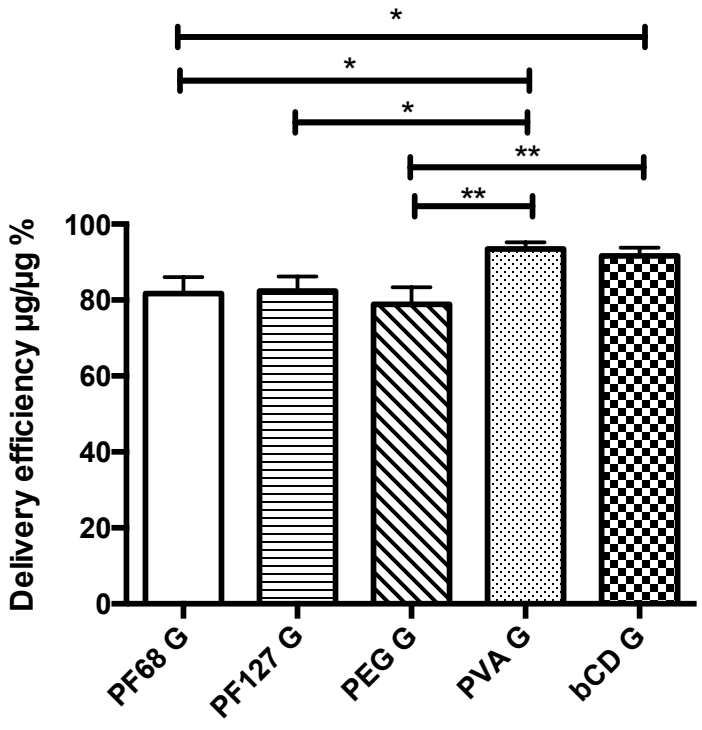

Figure 2.12 Delivery efficiency of WE14-5TAMRA using electro-polished MNs. MNs were coated with 10µg of WE14-5TAMRA and applied to human skin explants for 10 minutes before analysing the delivery efficiency. One way ANOVA, with Tukey post test. n=3. *p<0.05, **p<0.01

This dramatic change in delivery efficiency from the GeorgiaTech MNs could be due to altered MN length or altered MN surface properties, i.e. an effect of electro-polishing. As two variables were potentially responsible for this discrepancy, it was necessary to isolate the effects of electro-polishing and needle length. Therefore, in order to make a direct comparison, 5x500µm MN arrays were manufactured in-house by wire-EDM and electro-polished. After the electro-polishing process was complete, the dimensions of the MNs was shown to be reduced by approximately 12.5% in height and 23% in base width (Figure 2.13). In addition Dermaroller® MNs were used without further processing and following coating with gold using an EMtech sputter coater to modify surface properties.

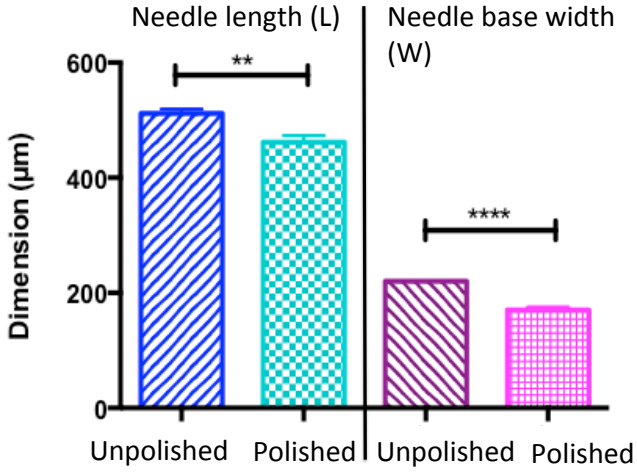

Figure 2.13 MN dimensions before and after electro-polishing. Stainless steel MN arrays (500µm long) were electro-polished and the dimensions of needles before and after electro-polishing were measured using ImageJ software. L=needle length, W=needle base width. n=10. Mean±SD. Tested with two tailed t test. **p<0.01, ****p<0.0001

Each array of MNs was coated with 10µg of WE14-5TAMRA and 1µg of PVA. Delivery efficiency was measured after MNs were inserted into human skin explants for 10 minutes (Figure 2.14). By visual observation alone it was obvious that unpolished MNs were able to deliver far less peptide than their electro-polished equivalent. This was confirmed quantitatively using UV-vis

spectrometry (Figure 2.15) where it was shown that delivery efficiency using electro-polished 500µm MNs was significantly greater than unpolished equivalents. The data showed no difference between gold coated and non-coated Dermaroller® MNs. Electro-polished MNs of 750µm length were able to achieve the highest delivery amongst all types of MNs and were able to deliver significantly more WE14-5TAMRA than Dermaroller® MNs. 500µm electro-polished MNs showed significantly lower delivery efficiency than 750µm long MNs (Figure 2.15).

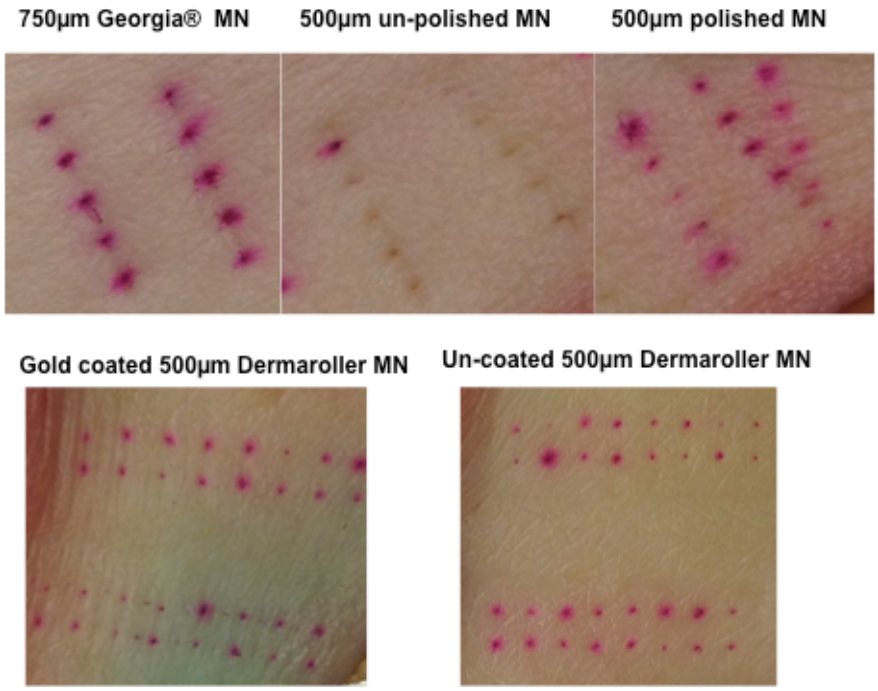

Figure 2.14 Images show MN penetration and WE14-5TAMRA (pink) release into human skin explants after 10 minutes application. MNs with five different surface properties were coated with same amount of WE14-5TAMRA (10µg) and applied to the human skin explant for 10 minutes. The penetration images were visualised using a stereo microscope and processed with ImageJ software.

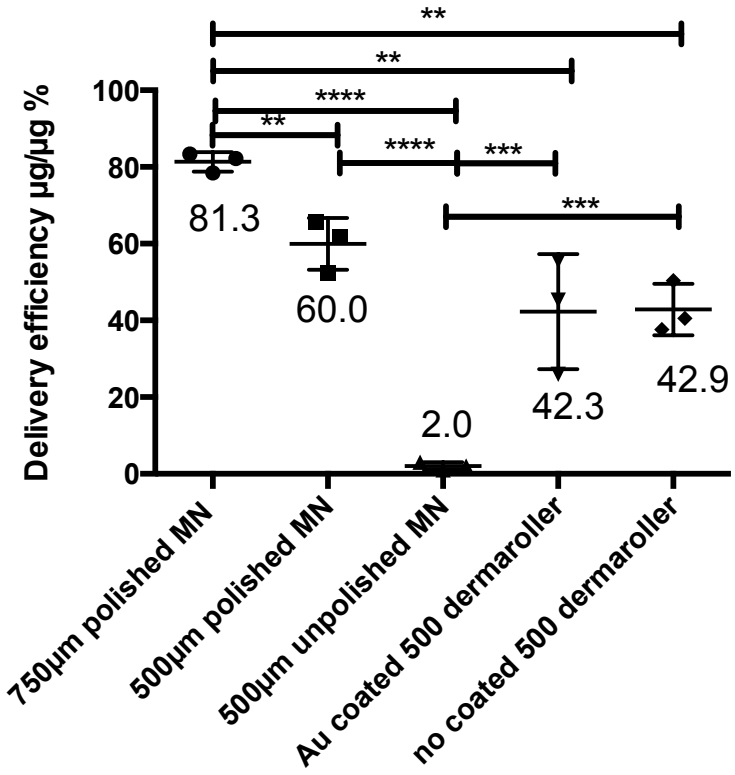

Figure 2.15 Effect of surface morphology on the delivery efficiency of WE14-5TAMRA in human skin. MNs with different surface morphology were coated with 10µg of WE14-5TAMRA and applied to human skin explants for 10 minutes before analysing the delivery efficiency. n=3, Mean±SD, One way ANOVA with Tukey post test. **p<0.01, ***p<0.001.

2.4.3.3. Delivery efficiency as a function of hydrophobicity of peptide

Delivery efficiency can also be influenced by the hydrophobicity of the peptide. Each set of 30 x 450µm long electro-polished needles was coated with a total of 10µg of peptide. Skin delivery efficiency was determined by applying MNs either to human skin explants or to the shaved neck area of a mouse for 10 minutes. The amount of peptide delivered was measured using a UV-vis spectrometer and delivery efficiency was inferred by subtraction (Equation 2.2). The delivery efficiency of the most hydrophilic peptide, WE14, was 80%. This was almost double the delivery efficiency of a very insoluble peptide, proinsulin B9-23 (Figure 2.16). Similar phenomena were observed when using the mouse skin model where a moderately hydrophobic peptide, m31, could only achieve 20% delivery,

whilst WE14 delivery efficiency was shown to go up to 60% in mouse skin (Figure 2.17.).

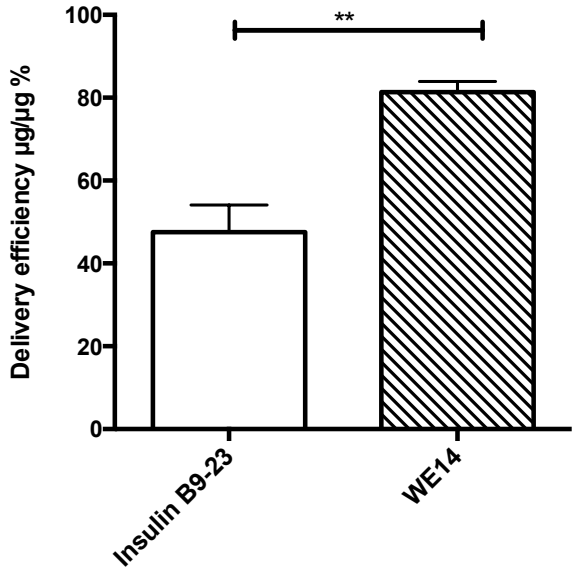

Figure 2.16 Effect of peptide hydrophobicity on delivery efficiency in human skin explants using electro-polished 500µm MNs. The same amount (10µg) of hydrophilic peptide, WE14, and hydrophobic peptide (proinsulin B9-23) was coated and delivered to human skin explants using 3 arrays of 500µm long electro-polished MNs. Delivery efficiency was then calculated after MN application. n=3. Mean±SD, Two-tailed t test. **p<0.01

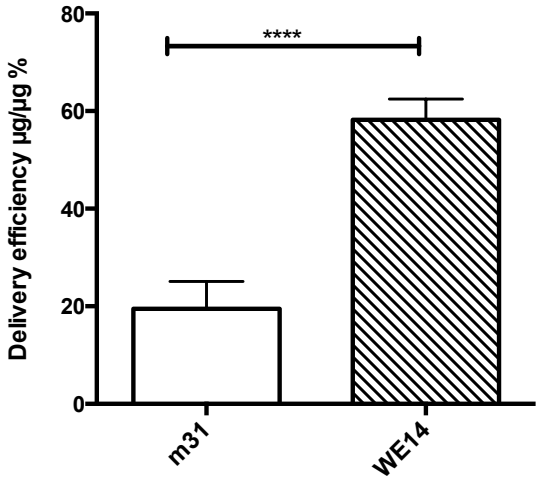

Figure 2.17 Effect of peptide hydrophobicity on delivery efficiency in mouse skin using electro-polished 500µm MNs. The same amount (10µg) of hydrophilic peptide, WE14, and hydrophobic peptide (m31) was coated and delivered to shaved mouse neck area using 3 arrays of 500µm long electro-polished MNs. Delivery efficiency was then calculated after MN application. n=3, Mean±SD, Two tailed t test. ****p<0.0001

2.4.3.4. Effect of skin species on skin delivery

In order to examine the effect of the skin model used on delivery efficiency, WE14-5TAMRA delivery efficiency was then compared in human skin and mouse skin (Figure 2.18). Using 500µm long electro-polished MNs, 80% of the WE14-TAMRA load can be delivered to human skin explant but only 60% of the load can be delivered to mouse skin.

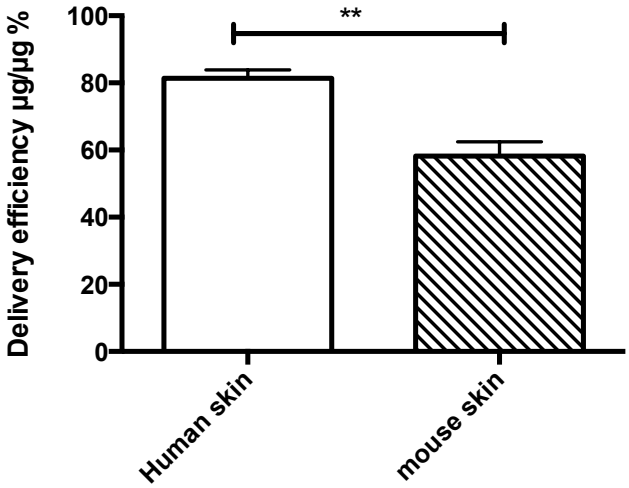

Figure 2.18 The delivery efficiency of WE14-5TAMRA in human and mouse skin using electro-polished 500µm long MNs. n=3. Mean±SD, two tailed t test, ** p<0.01 (Reanalysis of presented data from **Figure 2.16** and **Figure 2.17**)

2.4.3.5. Effect of needle numbers on delivery efficiency

To determine the effect of coating thickness on the delivery of peptide to skin, m31-5TAMRA (10µg) was coated onto 5, 15 or 30 electro-polished needles of 450µm length, i.e. the material was distributed over more MNs to reduce coating thickness per individual MN. As demonstrated in Figure 2.19, the delivery efficiency in mouse skin was almost three times higher when the material was distributed over 15 needles compared with 5 needles. When using 30 needles to deliver 10µg peptide, the delivery efficiency is approximately 20%, which is only 5% higher than when using 15 needles.

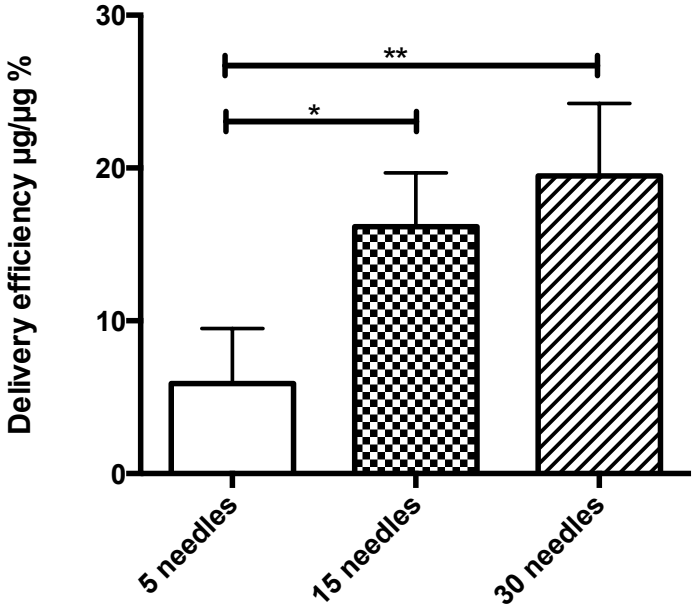

Figure 2.19 The effect of distributing the coating on different numbers of MNs on delivery efficiency of m31-5TAMRA in mouse skin. Electro-polished MNs with different needle number (5, 10 or 30) were coated with 10µg of m31-5TAMRA. Delivery efficiency of m31-5TAMRA was quantified after 10 minutes application in mouse skin. n=3, Mean±SD, one way ANOVA with Tukey post test. *p<0.1, **p<0.01

2.4.4. Design and manufacture of solid-coated MN systems suitable for both human and mouse skin models

As a result of the data presented in the previous results sections, solid MNs were designed and manufactured for use in both human and mouse skin. The following criteria were applied:

- ≤ 500μm long
- Sharp tip
- Electro-polished
- At least 30 needles per application
- Manufacturable in-house

According to these requirements, new MNs were designed with dimensions as shown in Figure 2.20. Each MN array was fashioned using wire-EDM from a 100μm thick stainless steel sheet, and contained 10 needles spaced 1 mm apart. Each needle is 500μm high and 200μm wide at the base. Five MN arrays were linked together using a breakable join during the cutting process to facilitate more efficient electro-polishing. Figure 2.20 C and D illustrate the MN surface morphology before and after electro-polishing. Prior to electro-polishing, the MN surface was uneven due to the heat generated during the cutting process (Figure 2.20 C). The debris was removed using electro-polishing (Figure 2.20 D) to produce a smoother surface finish with a sharpened tip. Each array of MNs contains 10 needles in a row. For *in vivo* applications, 3 MN arrays were assembled as shown in Figure 2.20 F using an application device, to provide a total needle number of 30 per application.

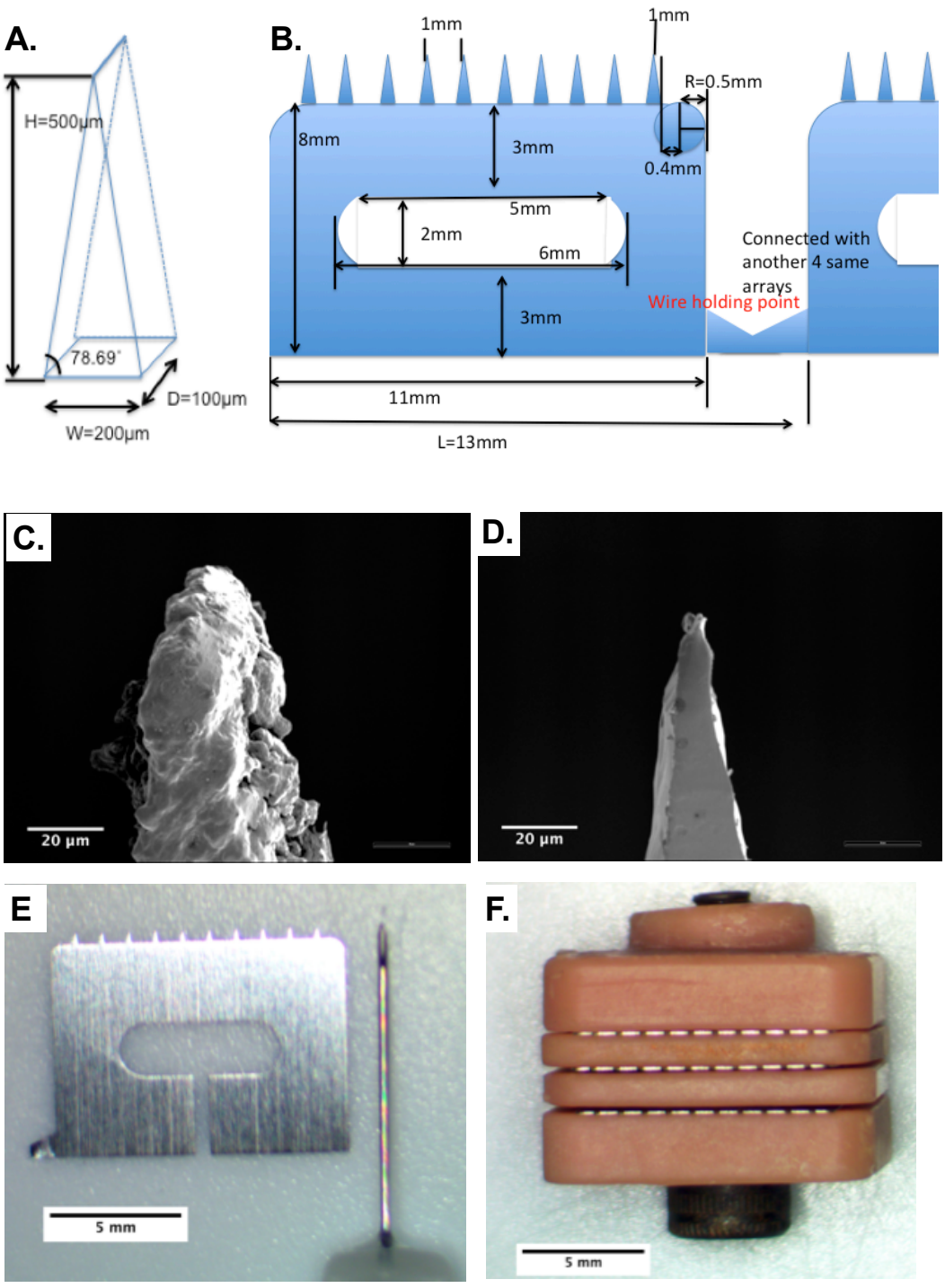

Figure 2.20 Design of MNs suitable for both human and mouse studies. **A**. Needle dimensions before electro-polishing (µm): 500, 200, 100, (L,W,D) L=length, W=width, D=depth; **B.** Dimensions of each MN array before electro-polishing. On each array, 10 needles are spaced with 1mm distance from point to point. Each array had a rounded end, the radius of which was 0.5mm. The hollow central structure enabled three arrays to be assembled together using a specially designed MN holder as shown in **F**. **C.** SEM image of needle tip before electro-polishing. **D.** SEM image of needle tip after electro-polishing. **E.** Finished single array stainless steel MN (left) compared with a 29G insulin injection needle (right). **F.** Three MN arrays were assembled together using a purpose built plastic holder for *in vivo* application.

2.4.5. Validation of new MN designs for peptide coating and delivery

To test the formulation uniformity and systematic error from pipetting, m31-5TAMRA (theoretically 10μg/0.4μl) was first air dried in Eppendorfs (200μl) and re-dissolved in 100μl 10%v/v acetic acid prior to quantification. The recovery of peptide was 9.76±0.54μg (n=6) (Figure 2.21). The coating repeatability was then measured by coating MNs with m31-TAMRA and washing this coating off using 100μl 10%v/v acetic acid. 9.37±1.1μg (n=3) m31-5TAMRA was shown to be coated onto the MNs (Figure 2.21). There was no significant difference between amount of peptide in the 0.4μl formulation and the amount coated on MNs, showing that a minimal amount of peptide was lost during the coating process. Delivery efficiency of m31-5TAMRA and WE14-5TAMRA were tested using mouse skin. After a 10 minute application to shaved mouse neck skin, 7.46±0.47μg m31-5TAMRA remained on the MNs; this means 1.91±0.47μg was delivered to mouse (n=10). This gives the delivery efficiency of m31-5TAMRA of 20.39±4.96% (Figure 2.22). Using the same method, delivery efficiency of WE14-5TAMRA to mouse skin was 58.21±4.26% (Figure 2.22).

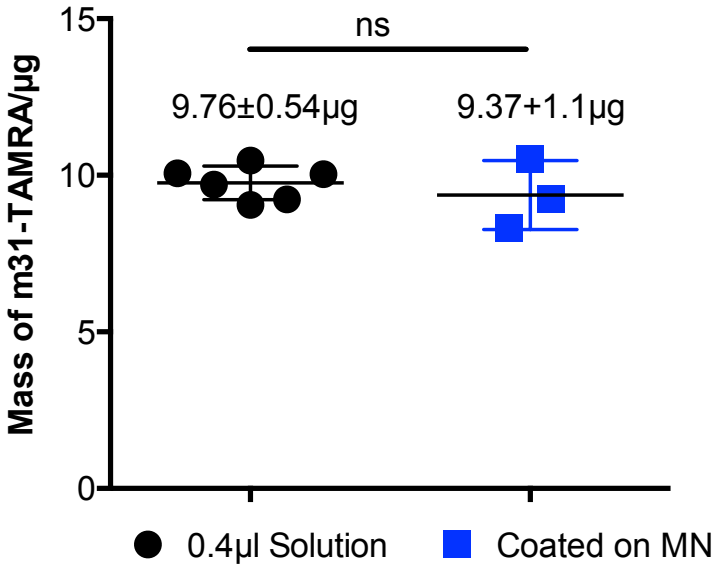

Figure 2.21 Coating repeatability of m31-TAMRA using in house designed solid-coated MNs. Three arrays of electro-polished 500µm long stainless steel MNs were coated with 10µg (theoretical) m31-TAMRA. Peptide mass coated on MNs was compared with mass of peptide within 0.4µl coating formulation. N≥3, Mean±SD, two tailed t test, ns.

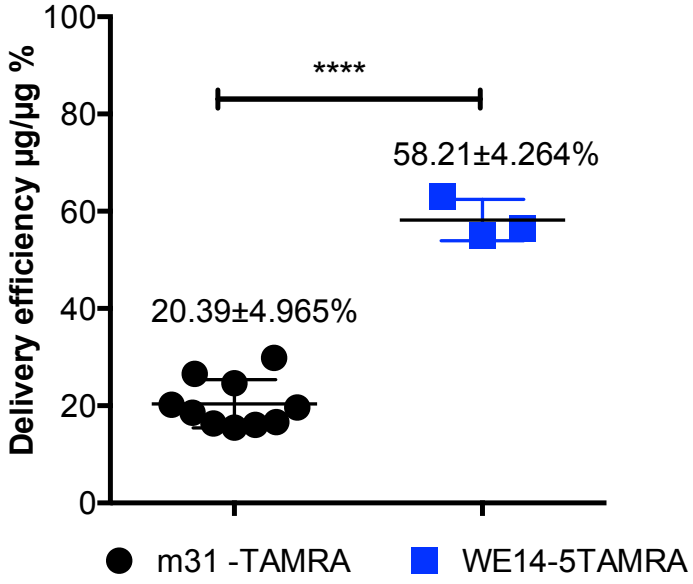

Figure 2.22 Delivery efficiency range of m31-TAMRA and WE14-TAMRA using in house designed MNs. Three arrays (30 needles) of electro-polished 500µm long stainless steel MNs were coated with m31-TAMRA or WE14-5TAMRA. MN arrays were then assembled using a MN holder and applied to shaved mouse neck skin area for 10 minutes. The delivery efficiency was calculated after MN application. n≥3, Mean±SD, two tailed t test. ****p<0.0001

2.5. Discussion

2.5.1. Targeting skin DCs with minimal damage

In initial targeting studies, two commercially available MNs were tested. NanoPass Technologies Ltd market the MicronJet® MN device as a hollow MN device for intradermal drug and vaccine delivery. The Dermaroller® MN device comprises solid MNs designed for skin puncture, skin repair and/or drug delivery. The MicronJet® MN consists of four 450μm long silicon needles, each with a bore-opening at the side of the MN tip (Figure 2.5). The device can connect via a Luer taper to a conventional syringe for simple patient injection. The delivery depth of peptides using this device is in the deep dermis in human skin and in the subcutaneous layer in mouse skin (Figure 2.7). This may be because the bore-opening faces towards the dermis when the MNs are inserted correctly into skin and the injection pressure forces the material through the bore and into the dermis. Dermaroller® MNs consist of two rows of eight 500μm long conical shaped stainless steel needles (Figure 2.5). Peptide delivered by Dermaroller® MNs remained in the epidermal and upper dermal layers in the human skin model and in the epidermis and dermis in mouse skin, rather than in the deep subcutaneous layer (Figure 2.7). The penetration depth of Dermaroller® 500μm long MNs in human skin was imaged using OCT. The penetration depth in human skin explants was approximately 300-400μm, which represents 60-80% of the total needle length, when applied using moderate manual pressure. This incomplete insertion depth agreed with previous observations (Donnelly et al., 2010, Coulman et al., 2011). Factors that contribute to the incomplete penetration include, the sharpness of needle tip, needle shape, insertion force and the deformation of soft tissues, which is due to the biomechanical properties of the skin; elasticity and flexibility (Donnelly et al., 2010, Davis et al., 2004, Boonma et al., 2012).

The aim of this project is to target delivery to skin DCs that reside in the epidermis (LCs) and the upper dermis (dermal DCs). For this reason solid-coated MNs were selected for further functional studies. The degree of skin damage caused by solid MNs was investigated for needles of different lengths (500μm and 750μm). *En face* OCT images suggested no obvious differences in skin surface damage between 500μm and 750μm long needles. Previous studies have shown that skin reseals within 2 hours post MN treatment regardless of the needle length (Gupta et al., 2011a). Another study using SEM, a higher resolution methodology, to examine the effect of needle length on microporation suggested that longer needles were capable of generating larger pores (Kalluri et al., 2011). One concern could be that the physical insult caused by MN penetration increases risk of microbiological ingress. An *in vitro* experiment has been carried out to assess microbial penetration using solid MNs and hypodermic needles (Donnelly et al., 2009b). Fewer microorganisms were observed to penetrate through viable epidermis when using MN treatment compared against 21G hypodermic needle. Based on these observations, it has been suggested that MNs are less likely than hypodermic needles to cause local or systemic infections. The low risk of infection caused by MN damage is an important factor to this project. This could minimise the risk of the activation of the immune system and prevent a proinflammatory response from occurring. Therefore, delivery using solid-coated MN could help maintain skin DCs in an un-activated state and further benefit the generation of Treg and maximise the success potential of ASI.

2.5.2. Coating formulation for hydrophobic peptides

For this project three different peptides will be used in further studies: m31, WE14 and proinsulin B9-23. The peptides' physicochemical properties are shown in Table 2.2. WE14 and m31 were soluble in PBS at a concentration of 1mg/ml, while proinsulin B9-23 was only able to dissolve in PBS at a concentration of less than 0.5mg/ml. In a previous clinical study into ASI for T1D, 10μg of C19-A3 peptide delivered by ID injection was well tolerated (Thrower et al., 2009). We therefore considered 10μg to be a realistic target dose to coat onto and deliver via solid-coated MNs. Several coating formulations have been developed previously for solid-coated MNs. A coating formulation developed at GeorgiaTech was used to coat peptide, vaccine, BSA and plasmid DNA (Gill and Prausnitz, 2007b, Gill and Prausnitz, 2007c, Tas et al., 2012, Kim et al., 2010a, Kim et al., 2010b, Ludvigsson et al., 2014, Gill and Prausnitz, 2007a, Valladeau et al., 1999). This aqueous formulation typically contains 1% (w/v) carboxymethylcellulose sodium salt, 0.5% (w/v) Lutro F-68 NF and 15% (w/v) trehalose in PBS. If peptide were able to dissolve in this coating formulation at a concentration of 1mg/ml, i.e. 0.1% (w/v), then the API to excipient ratio would be 1:165, i.e. 1650μg of excipients would be co-coated with every 10μg of peptide. Excess excipient could overload the needles (data not shown), which could influence skin penetration, delivery and bioavailability (Widera et al., 2006, Cormier et al., 2004, Al-Qallaf et al., 2009). Other formulations for coating hydrophobic molecules have also been described. Gill et al. utilised organic solvents such as ethanol and acetonitrile to dissolve hydrophobic compounds for coating formulation (Gill and Prausnitz, 2007c). One disadvantage of these two solvents is their high volatility. As a result, it is difficult to control the stock concentration, which can then influence the accuracy and repeatability of coating. The authors also investigated a coating formulation for hydrophobic molecules

using a molten polymer, polyethylene glycol (MW. 1500). However, the high temperature, 45˚C, and low drug content employed (0.01%w/v), would make it impractical for this project. There was, therefore, a requirement in this project to develop a MN coating formulation suitable for both hydrophilic and hydrophobic peptides.

The desired formulation criteria were defined as:

- A predominantly water based system, in order to maintain maximum peptide activity without denaturation caused by organic solvent alone.
- Any organic solvent used as a co-solvent should be, at least partially, miscible with water, in order to ensure that there is no phase separation. Phase separation can cause the peptide to denature at the phase interface and could cause uneven peptide concentration (partitioning due to phase separation coupled with differential solubility of peptide).
- Solvent evaporation at room temperature and atmospheric pressure to allow for peptide coating under ambient conditions.
- Solvents with a similar vapourisation rate to water, in order to ensure that no phase separation occurs during storage. This is important to maintain homogeneity of the stock coating formulation during the coating process.
- The coating formulation does not alter peptide bioactivity.
- The excipients used in the coating formulation does not stimulate a proinflammatory immune response. Unlike vaccine delivery, this project aims to induce immune regulation, therefore it is important that the excipient itself causes minimal inflammation and minimises any other non-specific immune responses.
- The amount of excipients should be minimised to increase peptide to excipient ratio and to further minimise the biological effect of excipients.

This approach is to ensure the final read out is determined by the auto-antigen and delivery route. This is also to ensure the sharpness of needles is not influenced by the coaing.

- Peptides are soluble in coating formulation at a concentration ≥ 10mg/ml. This is a limitation of the coating method described above (Figure 2.2). After optimisation, the coating process took 15 minutes for each MN set and therefore concentrations lower than this would result in longer coating times. This may further increase the risk of formulation evaporation, altering the concentration of stock formulation during the coating process and therefore potentially introducing poor reproducibility.
- The formulation is amenable to frozen storage at -80˚C. This is mainly to reduce the cost and reduce the systematic error during the formulation preparation process. In order to facilitate storage at -80˚C, all liquid solvents used in the formulation should have a melting temperature of greater than -80˚C. Ideally, the systematic melting temperature of all reagents combined will fall within the range 0˚C to -20˚C. This could ensure that the formulation can be kept on ice during the coating process to minimise the error caused by evaporation and to avoid the freeze-thaw cycle.

The first approach in developing a formulation to meet these criteria was to use a pH modifier to increase peptide polarity and solubility. Acetic acid is a weak organic acid that has been widely used to dissolve hydrophobic peptides. The pH of 2M aqueous acetic acid solution is approximately 2. This pH change was enough to dissolve WE14, a peptide with less hydrophobic groups (43%), at a concentration of 25mg/ml. For the other two peptides, m31, a basic peptide with 60% hydrophobic groups, and proinsulin B9-23, a neutral peptide containing 40% hydrophobic groups, increasing ionisation

alone was not sufficient to ensure dissolution at the desired concentration. An organic solvent was therefore required to increase peptide dissolution.

DMSO (Dimethyl sulfoxide) is a commonly used solvent for dissolving hydrophobic peptides due to its low toxicity and good biocompatibility. DMSO is, however, not suitable for the MN coating formulation. DMSO can form suphoxide or disulphide bonds with amino acids, such as cysteine, methionine and tryptophan residues (Lipton and Bodwell, 1973). Both WE14 and m31 contain methionine and tryptophan, so DMSO should be avoided. Secondly it is very difficult to remove DMSO even under reduced pressure conditions, i.e. it is difficult to form a dry coating using DMSO under normal atmospheric pressure conditions. In researching more appropriate co-solvents we investigated the use of alcohols, since they are chemically stable and may offer a range of advantageous properties. The chain length of the carbon backbone was limited to below 5. This was because in compounds with carbon backbone chain lengths of greater than 5 (i.e. hexanol upwards), the hydrophobic effect of the chain structure becomes greater than the hydrophilic influence of the hydroxyl group, which makes the overall molecule immiscible with water. According to the above defined limiting conditions for vapour rate at RT and freezing temperature, two alcohols were selected: tert-butanol and tert-amyl alcohol. Tert-butanol however, was found to be unable to dissolve peptide at the desired concentration, even with the addition of acetic acid solution (data not presented). Tert-amyl alcohol was able to dissolve m31 at a concentration of 50mg/ml and proinsulin B9-23 at 25mg/ml. However as tert-amyl alcohol is only partially miscible with water, it was necessary to test the miscibility of the ternary system: water, acetic acid and tert-amyl alcohol. As shown in Figure 2.23, the ternary system of water, acetic acid and tert-amyl alcohol was able to form a uniform mixture when

their molar ratios fell beneath the plot curve (Fahim and Al-Muhtaseb, 1996). The optimised concentration of each component in the coating formulation to provide a miscible formulation is listed in Table 2.3. These ratios were all within the plot curve as shown in Figure 2.23, which demonstrated that the coating formulation is a uniform, equilibrated ternary system.

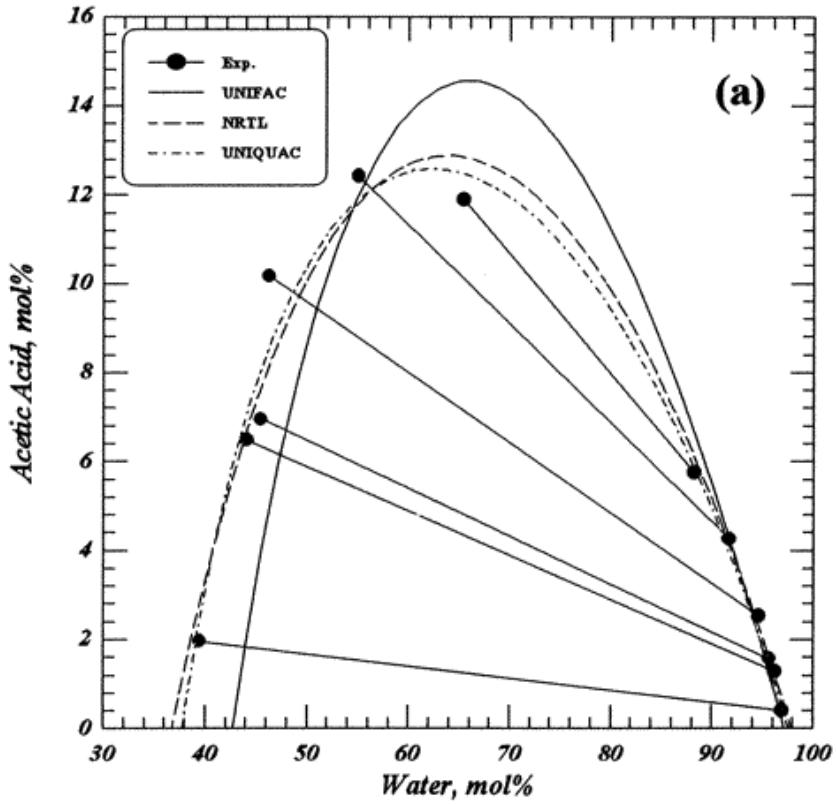

Figure 2.23 Equilibrium ternary system of water, acetic acid and tert-amyl alcohol at 298K. Curves of solid line, dash line and dash-dot line were calculated using URTL, UNIQUAC and UNIFAC equilibrium models. Data points were obtained by experimentation in the quoted publication (Fahim and Al-Muhtaseb, 1996).

In order to dissolve the peptide in a uniform solution, it was important to add tert-amyl alcohol, acetic acid solution and PVA/water sequentially. If the solution was premixed the peptide did not dissolve as expected. This might be because tert-amyl alcohol disperses the peptide into fine particles rather than larger aggregates. This approach increased the surface energy and contact area of

peptide to acetic acid, which charges the free peptide, increasing its solubility in water. PVA behaves as a stabiliser and a viscosity enhancer for the formulation.

Five excipients in three separate categories were tested: surfactant, dispersant and inclusion complex (Table 2.4). For every 10µg peptide, 1µg of excipient was co-coated onto each MN array. This resulting excipient:drug ratio was far lower than ratios reported in other studies using hydrophobic compounds (Gill and Prausnitz, 2007c). All excipients were able to assist the most hydrophobic peptide, proinsulin B9-23-FITC to coat onto MNs evenly without overloading or material flaking (Figure 2.9).

2.5.3. Factors that influence delivery efficiency using solid-coated MNs

The delivery of the peptide to skin using solid-coated MN can be achieved by two interactive processes: removal of peptide from MN surface and peptide re-dissolution into the skin. The efficiency of the first process was demonstrated earlier in this study to be related to the MN surface morphology. The efficiency of the second process is related to factors such as peptide solubility, the excipient, the thickness of the coating and the skin condition (for example, data obtained in human skin vs. mouse skin experiments illustrates this). The combined effect of these two processes determines the final delivery dose of coated peptide.

The delivery efficiency of a mildly hydrophobic peptide, WE14, was initially tested using Dermaroller® MNs. The delivery efficiency of coated peptide was tested using human skin explants, and mouse skin *in vivo*. UV-vis spectroscopy was used to quantify the amount of coated peptide delivered, or at least removed from the MN during skin insertion. Using 5-TAMRA as the probe for detection the

linear range of peptide-5TAMRA at 559nm is 6.25µg/ml to 400µg/ml when using UV-vis spectrometry.

Excipients were co-precipitated with peptides on MNs during the drying process to alter surface tension for coating and/or to promote de-coating *in situ.* Addition of the surfactants, PF68 and PF127, led to the delivery of 30% of the coated WE14-5TAMRA. The inclusion of the dispersants, PEG and PVA, increased the WE14-5TAMRA delivery to 40%. It was shown that the ability of peptide/coating formulation with the addition of 2HPßCD to assist MN de-coating was between that of surfactants (PF68 and PF127) and dispersants (PEG and PVA). The dispersant PVA showed the highest delivery efficiency among all five 'de-coating' excipients, possibly because PVA can dissolve more rapidly than other excipients and cause a 'burst release' of peptide into the skin. Based on these studies PVA (MW2000) was chosen as the final excipient for use in the coating formulation.

Dermaroller® MNs have been mainly used to create microchannels in the skin for transdermal delivery of materials that are applied after MNs are removed by patch or topical formulation, i.e. the poke/patch approach. Another solid MN array used in our laboratories, supplied by GeorgiaTech, previously achieved 90% delivery efficiency for the delivery of vitamin B coated onto the MN surface; the original loading was 3% w/v (Gill and Prausnitz, 2007a). Using these MNs the delivery efficiency of WE14-5TAMRA increased from approximately 40% with Dermaroller® MNs to ≥80% using GeorgiaTech MNs. This dramatic difference was generally independent of excipient effect, which indicated that it was probably due to the needle length or needle surface properties. As shown in Figure 2.11, electro-polished GeorgiaTech MNs have a much smoother surface compared to Dermaroller® MNs. To test the impact of surface finish, stainless steel MN arrays were manufactured and electro-polished in house. As a result of

the electro-polishing process, MN dimensions were reduced by approximately 12.5% (Figure 2.13). In addition Dermaroller® MNs were coated with 20μm thick gold using an EMtech sputter coater to modify surface properties.

WE14-5TAMRA peptide was not released from unpolished 500μm length MNs after skin insertion. Electro-polishing MNs of similar length was shown to increase the delivery efficiency from 3% to 60%. We propose that the change of surface properties following electro-polishing contributed to this change, by removing debris from needle surface and providing a more uniform, smooth surface, therefore absorption of the peptide on needle surface was minimised. Delivery efficiency using Dermaroller® MNs showed no difference before and after gold coating. The reduction of MN surface roughness acts to minimise the absorbance of the coating material to the needle surface, which enables efficient delivery of the MN load on insertion/ removal.

Peptide hydrophobicity is another factor, which may influence delivery efficiency. Using the human skin model, a less hydrophobic peptide; WE14, was delivered more efficiently than a more hydrophobic peptide, proinsulin B9-23 (Figure 2.16). This difference has also been observed when using the mouse skin model (Figure 2.17).

The skin model and species is also a factor, which has been shown to influence delivery efficiency. As shown in Figure 2.18, when using the same peptide, delivery efficiency was shown to be significantly different between human skin and mouse skin. This is probably due to the biomechanical, physical and biological differences between human and mouse skin (Ghosh et al., 2000, Bond and Barry, 1988, Wong et al., 2011). The major differences of skin between the two species are listed in the Table 2.5 (Wong et al., 2011). Several experiments

have shown interspecies variation on permeation of the skin by drugs between mouse and human. Narcotic analgesics were shown to permeate through hairless mouse skin quicker than human epidermis (Roy et al., 1994). Another drug, 5-fluorouracil, was shown to permeate mouse skin ten times quicker than in human models *in vitro* (Sherertz et al., 1990). Drug properties can also differentially influence skin permeation. In one study, it was demonstrated that hydrophobic drugs flux through mouse skin much quicker than in human skin, whereas no difference was observed using a hydrophilic drug (Ghosh et al., 1992). This study is the first to show differences in MN delivery efficiency caused by interspecies variation. As shown in Figure 2.6, the epidermis is between 60-100μm thickness in human skin compared to 20μm thickness in mouse skin. The thickness of the human dermis is between 1.6-2.6mm (Laurent et al., 2007) and the mouse dermis was measured to be 200-300μm thick Figure 2.6. The delivery depth of peptide using 500μm electro-polished, solid-coated MN was approximately 300-400μm in human skin (Figure 2.7), which targets the epidermis and the upper layer of the dermis. This delivery depth targets both the epidermal and the dermal layers in mouse skin. Therefore, mechanical and structural differences between species at this delivery depth may determine the delivery efficiency of peptide. The anatomical differences between human skin and mouse skin are listed in Table 2.5. The main factors that could contribute to the delivery efficiency differences are: skin thickness, skin stiffness and the hydration state of the skin. Other differences between human and mouse, however, may further influence the drug absorption and bioavailability.

Table 2.5 Anatomical differences between mouse and human skin (Wong et al., 2011).

	Mouse	Human
Hair cycle	Approximately 3 weeks	Highly variable, region-dependent
Epithelial architecture	No rete ridges	Rete ridges present
Apocrine sweat glands	Not present in skin, extensive in mammary glands	Present in axilla, inguinal, and perianal skin regions
Biomechanical properties	Thin, compliant, loose	Thick, relatively stiff, adherent to underlying tissues
Hypodermal thickness	Hair cycle-dependent	Less variable
Subcutaneous muscle layer	Present throughout as panniculosus carnosus	Present only in neck region as platysma
Major method of wound healing	Contraction	Granulation tissue formation and re-epithelialization

Formulation coating thickness has been shown to have an effect on the delivery efficiency of coated MNs (Cormier et al., 2004). The aforementioned publication demonstrated that an increased coating thickness was shown to result in reduced delivery efficiency when the same amount of desmopressin was delivered. To test this effect, 10µg of m31-TAMRA was coated on 5, 15 or 30 needles and delivered to mouse skin. As shown in Figure 2.19, spreading the peptide over 15 needles rather than just 5 needles tripled the delivery efficiency. Delivery efficiency was further increased when the formulation was coated over 30 needles. With the reduced thickness of the drug coating on each needle, several parameters may change accordingly. Firstly, with reduced coating thickness the sharpness of the needle would be better retained. Secondly, although the skin is hydrated, a significant fraction of the water in the skin is associated with tissues or held within cells, leaving only the water contained within the extracellular fluid as the mobile fraction, thus over a restricted time frame, the water content in skin

is effectively limited. This limitation on available water effectively limits the amount of peptide that is able to dissolve, reducing the peptides saturation threshold. Thin coating helps alleviate this problem by distributing the dry drug over a larger area, thereby reducing the possibility of creating a drug saturated pocket effect. Furthermore, when drug de-coats from MNs, it diffuses into the skin, creating a diffusion gradient. The concentration of drug is highest near the needle, which may achieve local saturation and thereby reduce the rate of diffusion. This is one mechanism by which, within a set time frame, more drug can be released into the skin from a thin, rather than a thick coating.

2.5.4. Design of solid MNs for minimally invasive delivery of peptide in both human and mouse skin models

This project aims to develop and test solid MNs that can target immune-processing cells in the epidermis and upper dermis. Several considerations need to be considered when designing MNs for specific indications including needle length, needle shape, needle spacing and needle number.

The total mouse skin thickness (epidermis plus dermis) is approximately the same as the human epidermal layer alone (including just the stratum corneum and viable epidermis), being approximately 60-100μm (Figure 2.6). In MN penetration depth studies, MNs with 500μm long needles have been shown to penetrate deep enough to target the human epidermal and upper dermal layer, whilst being superficial enough not to cause extensive damage to the dermis. Increased MN length can cause extended skin damage and create larger pores than MNs with the same shape but of shorter length (Donnelly et al., 2010). On the other hand, needle lengths of less than 300μm have been shown to cause inconsistent penetration in human skin (Verbaan et al., 2007). Dermaroller®

MNs of different lengths were tested for their ability to penetrate the skin whilst minimizing skin damage. It was suggested that 500μm long MNs were sufficient to increase drug flux through skin. Transepidermal water loss (TEWL) data suggested that skin surface damage caused by 500μm long MN sealed within 1-2 hours post MN treatment (Zhou et al., 2010, Badran et al., 2009).

The effect of MN geometry on insulin delivery and the resulting blood insulin concentration has been determined using a mathematical model (Figure 2.24). It was suggested that "rocket shaped" MNs were able to increase blood insulin concentration more efficiently than other shaped needles (Al-Qallaf et al., 2009). One limitation of this study is that it assumes there is no boundary effect between viable epidermis and dermis, thus the defined partition coefficient between these two layers was as one. Although this simple assumption did not reflect the structural differences between these two anatomically distinct layers, it provided a link between needle shape and drug diffusion pattern within the skin to a certain degree. It was shown that "wedge shaped" needles distributed more insulin in the top layer of the skin than other types of needles. In this project, we would like peptide to remain in the upper layers of skin for as long as possible to increase the probability of peptide uptake by skin resident DCs, especially epidermal LCs. Therefore, for this project, "wedge shaped" MNs were determined to be preferable.

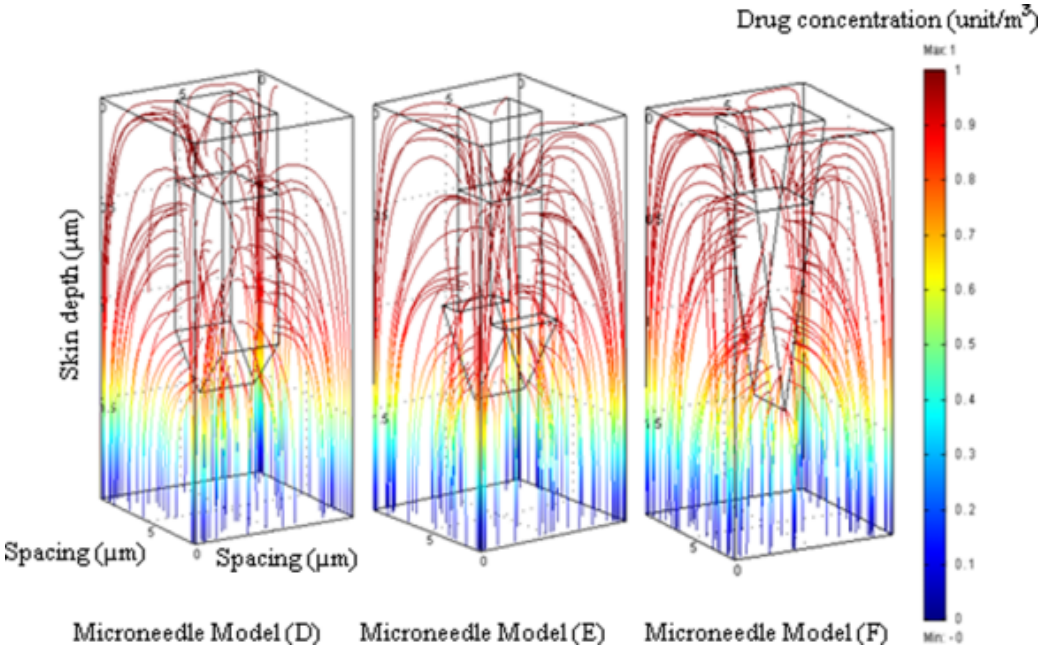

Figure 2.24 Distribution of insulin within skin following delivery via MNs. The penetration depth for all MNs was set to 140µm and insulin concentration gradient was calculated using a mathematic model in the quoted publication. As shown in the concentration rainbow scale (right), red colour indicates the highest concentration of insulin and the dark blue colour indicates the lowest concentration. Insulin concentration distribution is correlated to the shape of the needle with the same length. D. Rocket shaped needle; E. Arrow shaped needle, F Wedge shaped needle (Al-Qallaf et al., 2009).

Another MN modeling study suggested that MN sharpness inversely correlates with the amount of force needed to penetrate the skin and therefore correlates with the degree of skin deformation before MN penetration occurs. A sharp needle is able to penetrate the skin with less force than a blunt needle. An increase in pressure, as would be required to penetrate the skin with blunt needles, is likely to result in greater trauma. Therefore skin irritation and damage can be minimized by using sharper needles (Boonma et al., 2012).

In this study, MNs were designed to take into account the previous considerations. Each MN array contained 10 needles with 1mm needle center-center spacing to ensure efficient skin penetration (Figure 2.20 B). Each needle was wedge shaped with dimensions of 500x200x100 µm (H x L x D), providing a sharp needle tip (Figure 2.20 A). These stainless steel MNs were then electro-

polished to remove surface debris in order to provide a smooth surface, reducing the absorption of peptide to the MNs. Electro-polishing was shown to further sharpen the needle reducing the force required for effective skin penetration (Figure 2.20 C, D). For *in vivo* testing, 3 MN arrays were assembled together using a novel MN applicator to provide a total of 30 MNs.

The resulting stainless steel MN product was then tested for *in vivo* studies. Theoretically, 10μg of peptide was coated over 30 needles. From the calibration curve we calculated the actual mass of the peptide available for coating onto MNs was 9.8μg (n=6), with no significant within-group differences (Figure 2.21). This indicates that the coating formulation remains uniform during storage (at -80˚C) and during the coating procedure (at 4˚C for 3-4 hours). The mass of peptide recovered from MNs was 9.4μg (96% coating efficiency) (Figure 2.21). The small loss of peptide may be due to traces of peptide left on the pipette tip after coating. Two peptides were tested, WE14 and m31. WE14 (WSRMDQLAKELTAE) contains 43% hydrophobic residues and m31 (YVRPLWVRME) contains 60% hydrophobic residues. The delivery efficiency of m31-5TAMRA was 20.39±4.96% and the delivery efficiency was 58.21±4.26% for WE14-5TAMRA, despite using the same initial coating amount (10μg) and insertion time (10 minutes). The differences in the solubility of the two peptides accounted for the difference in both human and mouse skin delivery efficiency. This may be because solubility is an important parameter when delivering a dried material into a restricted volume aqueous compartment, as discussed in section 2.5.3. These results suggested that this design of MN could be used for mouse *in vivo* study and could deliver two peptides (m31 and WE14) for further study.

2.6. Conclusions

In this study, a solid-coated MN system (MN design, bespoke holder and formulation) was developed for the delivery of hydrophobic peptides into the skin, with the eventual aim of delivering peptide therapeutics to induce tolerance *in vivo*.

A novel coating formulation was developed which was suitable for hydrophobic peptides. This formulation contains tert-amyl alcohol, acetic acid, water and PVA. Results show that, using this formulation, peptides with a range of hydrophobicity can be coated onto MNs in a reproducible fashion.

Several parameters have been demonstrated to influence skin delivery efficiency using solid-coated MNs. These include the excipient used, the proportion of excipients in the coating formulation, MN surface properties, skin differences between species and the hydrophobicity of peptide. It is also likely that the delivered dose from solid-coated MNs can only be expressed as a dose range rather than a relative accurate dose, as would be achieved using traditional ID injection. For future clinical applications it might be necessary to examine how age, sex and skin conditions affect delivery, and to normalise the differences caused by any fluctuation of dosage.

Finally, a solid stainless steel MN array was designed for both human skin and mouse skin delivery. Using this system, skin damage can be minimised and skin DC targeting can be enhanced. The *in vivo* delivery study showed that this system was capable of delivering peptides, WE14 and m31 consistently.

Chapter 3 Inducing tolerance *in vivo* using solid-coated MN array

3.1. Introduction

3.1.1. Animal models for study of T1D

In addition to disease models such as NOD and BDC2.5 TCR-Tg mouse (see 1.1.3.), two other animal models were also used in this study, the NOD-SCID mouse and the Foxp3-FIR mouse.

3.1.1.1. NOD-SCID mouse

The SCID (severe combined immunodeficiency) mouse was reported to lack functional T and B lymphocytes due to a mutation in a gene in which codes for DNA repair enzymes (Bosma and Carroll, 1991). In SCID mice, other immune cells such as APC and NK cells remain functional. SCID mice with a NOD background are therefore useful for the study of autoimmune diseases, such as T1D. Successful disease transfer to NOD-SCID mice can be achieved using either splenocytes from newly diagnosed diabetic NOD mice or BDC2.5 T cells (Christianson et al., 1993). Without other regulation mechanisms as found in NOD mice, transferred islet specific effector T cells can be expanded rapidly in NOD-SCID mice. Therefore, this disease model requires less time to show insulitis and can develop diabetes rapidly (showing high blood glucose level within 7-10 days post transfer) compared to the NOD natural disease progression model (12 weeks). It has also shown a more consistent disease incidence compared to the NOD mouse.

3.1.1.2. Foxp3-FIR (Foxp3- internal ribosomal entry site-linked monomeric red fluorescent protein) mouse

Foxp3 (forkhead box P3) has been shown to be an important regulatory gene in the development of Tregs, such as the $CD4^+CD25^+$ population (Hori et al., 2003, Fontenot et al., 2003) (details see section 1.4.1.3). A mouse model was established within which Foxp3 locus was knocked in with a bicistronic reporter expressing red fluorescent protein (RFP) (Wan and Flavell, 2005). It has been shown that only $Foxp3^+$ cells co-express RFP. These $Foxp3^+$ RFP^+ Tregs have been shown to retain their normal regulatory function. The expression of RFP therefore can be used to quantitatively and qualitatively study $Foxp3^+$ Tregs. Foxp3-FIR mice backcrossed with either NOD mice or BDC2.5 mice can be useful tools to study the function of polyclonal Tregs and monoclonal Tregs.

3.1.2. $CD4^+$ T cell function and proliferation assays

After being primed by DCs, naïve $CD4^+$ T cells will undergo activation, differentiation and proliferation. $CD4^+$ T cell activation and differentiation are described in Section1.4.1. After differentiation, activated $CD4^+$ T cells proliferate in an antigen specific fashion (clonal expansion), secreting growth factor IL2. This occurs in the first 1-2 days after $CD4^+$ T cells are primed by DCs (Miller et al., 2004). In the later stage of the proliferation phase, 2-5 days post activation, $CD4^+$ T cells proliferate driven by IL2 and release the proinflammatory cytokine IFNγ (Mempel et al., 2004). Proliferation assays provide a consistent and reliable readout. Therefore, T cell proliferation assays are widely accepted as a useful measure of $CD4^+$ T cell activity.

The direct way to analyse T cell proliferation is to measure the change of cell numbers after activation. In an *in vitro* experiment, cells can be labelled with a radioactive compound, such as [^{3}H] thymidine, by direct addition to the culture

media. During mitotic cell division, [^{3}H] thymidine, a radioactive nucleoside, is incorporated into the nascent DNA that is synthesised. Therefore the radioactivity count is proportional to total proliferated cell number in each culture well (Murat et al., 1990, Mosmann, 1983, Gillis et al., 1978). One draw back of this method is that it measures the total cell number rather than a specific cell type. This assay may also have a high background due to the non-specific stimulation, such as FCS in the culture media.

A non-radioactive probe also can be used to label the T cell and monitor T cell proliferation *in vivo*, such as carboxyfluorescein diacetate succinimidyl ester (CFDA-SE). CFDA-SE is a fluorescent dye, which is able to passively diffuse through the cell membrane and thereby enter the cell. Within the cell, the ester end of CFDA-SE is cleaved by esterase and generates an amine reactive compound, carboxyfluorescein succinimidyl ester (CFSE) (Weston and Parish, 1990). CFSE is stable within cells and can be used for long term cell trafficking *in vivo*. When CFSE labelled cells divide, the fluorescent intensity is halved for next generation. Cells that need to be monitored *in vivo* can be labelled *in vitro* and transferred to the recipients. The cell division within the *in vivo* environment can be analysed using flow cytometry after cells are isolated from examined organ (Quah et al., 2007, Quah and Parish, 2012). In this way, a specific cell type and its sub generations can be analysed for their proliferation *in vivo*.

Another way to assess the function of $CD4^+$ T cells is by analysing the proinflammatory cytokines they release, such as IFNγ. As described in section 1.4.1.1, IFNγ is a proinflammatory cytokine released by Th1 effector T cells. IFNγ was shown able to promote $CD4^+$ T cell proliferation (Reed et al., 2008). Therefore, the IFNγ released by $CD4^+$ T cells is related to the activity of Teffs and therefore reflects the degree of inflammation or T cell activation present. One

way to quantify IFNγ is using enzyme-linked immunosorbent assay (ELISA). ELISA is an immunoassay, which can detect a specific substance in liquid solution by using antigen specific antibodies (Engvall and Perlmann, 1971, Yalow and Berson, 1960). The most widely used technique is a 'sandwich' ELISA assay, which uses two antibodies. The first antibody is used to capture the antigen on a solid surface. The biotin conjugated secondary antibody is then added to detect the antigen. An enzyme, horseradish peroxidase (HRP), is then linked to the detecting secondary antibody and 3,3',5,5'-Tetramethylbenzidine (TMB) is then added to produce a colour change. This enzyme reaction can be stopped using a strong acid solution, such as 2M H_2SO_4. ELISA is therefore useful for detecting cytokines, which are released by cells into the culture media (Leng et al., 2008).

3.2. Objectives

- To evaluate peptide bio-activity after coating onto solid MNs using the aforementioned coating formulation (Table 2.3), which is reflected in the change of IFNγ levels as seen in the BDC2.5 T cell *in vitro* assay.
- Using an intravital imaging system, to investigate factors that influence the clearance of fluorescent probe conjugated peptides from the skin of NOD mouse, following delivery by either MNs or ID injection
- To optimise the CFSE labelled BDC2.5 T cell proliferation assay for evaluation of induced tolerance, including:
    - Optimise the CFDA-SE labeling protocol to enable effective labeling and manitain the viability of labeled $CD4^+$ T cells
    - Optimise the CFSE labelled BDC2.5 T cell number which could be then used as a readout for induced tolerance
- To understand how local skin clearance influences the trafficking of peptide in a NOD mouse model, showing the change in proliferation profile of CFSE labelled BDC2.5 T cells in different lymphatic organs.
- Evaluate the efficacy of inducing peripheral tolerance in NOD mice using m31 and WE14, delivered either by solid-coated MNs or ID injection, showing the change in proliferation profile of CFSE labelled BDC2.5 T cells
- Evaluate the efficacy of inducing peripheral tolerance in NOD mice using m31 and WE14, delivered either by solid-coated MNs or ID injection, showing the change in phenotype of transferred BDC2.5 T cells.

3.3. Methods

3.3.1. Mice

NOD, NOD-SCID, BDC-2.5-TCR-Tg.NOD, BDC2.5 TCR-Tg.Foxp3-FIR, Foxp3-FIR.NOD mice were bred and maintained in a specific pathogen-free environment in the Joint Biological Services Unit at Cardiff University, U.K. All experimental procedures were carried out in accordance with guidelines, as provided by U.K. Home Office project license regulations and following approval by the Ethical Review committee at Cardiff University.

3.3.2. Preparation of a single cell suspension from murine SP (spleen) and LNs (lymph nodes)

Mice were sacrificed in a sealed chamber filled with CO_2. The SP and different LNs (table 3.1) were removed, according to the Van den Broeck's LN anatomy (Van den Broeck et al., 2006) and kept in RPMI1640 media on ice before use. LNs were placed in a petri dish and cells were released by mechanically dissociating LNs using 29G needles. Cells were then filtered through a 70µm cell strainer, to remove tissue residues, and filtrate was then suspended in 1ml RPMI1640 media, which were kept on ice prior to use. The SP was dissociated using a glass homogenizer and cells were filtered through a 70µm cell strainer into a 50ml falcon tube. Cells were then pelleted at 400G for 5 minutes, lysed with 900µl of de-ionised H_2O and immediately neutralized with 100µl of x10 PBS. Splenocytes were then filtered for a second time through a 70µm cell strainer and suspended in 20ml of RPMI1640 media and then kept on ice prior to use.

Table 3.1 Abbreviations for LNs used in experiments.

Abbreviation	Name
PLN	Pancreatic LN
ALN	Axillary LN (accessory)
CLN	Cervical LN
ParaLN	Para-aotic LN
ILN	Inguinal LN

3.3.3. *In vitro* BDC2.5 T cell proliferation

Single splenic cell suspensions (Section 3.3.2.) were prepared from BDC2.5-mice. $CD4^+$ T cells were then isolated using a mouse $CD4^+$ T Cell Isolation Kit, as described in Section 3.3.9. Single cell suspensions were also prepared from the SP of NOD mice and were irradiated using a gamma irradiator (delivering 2000rad) to prevent proliferation of T cells but preserve the function of APCs. These irradiated splenocytes were then used as APCs. $CD4^+$ T cells (200,000/well) were co-cultured with the irradiated splenocytes (100,000/well) and 0.1, 1 or 10 ng/ml of m31 or 10, 50 or 100µg/ml of WE14 in complete media (RPMI 1640 media supplemented with 5% FCS, 2mM L-glutamine, 50µM 2-Mercaptoethanol and 1U/ml penicillin/streptomycin) at 37˚C, using a 96-well round bottom plate. Cells were then labelled with 20µl of 0.05µCi/µl [^{3}H] thymidine in RPMI complete medium at days 0,1 and 2. Cells were harvested 16 hours after labelling, at each of these time points. Cell proliferation was expressed as radioactivity and read as CPM (counts per minute) using a beta counter (MicroBeta2, PerkinElmer, UK). The stimulation index was calculated using the following equation:

Equation 3.1 Equation used to calculate stimulation index (SI) from CPM.

$$SI = {[cpm\ (sample) - cpm(background)]}\Big/{cpm(backgroud)}$$

3.3.4. Evaluating the effect of MN coating formulation on m31 bioactivity

A coating formulation of m31 was prepared according to table 2.3 and MNs were coated with 0.4µl of coating formulation as described in 2.3.5. In order to evaluate whether the coating formulation influenced the bioactivity of m31, m31 peptide or air dried m31-formulation was dissolved to a concentration of 0.2, 2 or 20 ng/ml in RPMI 1640 media supplemented with 5% FCS, 2mM L-glutamine, 50µM 2-Mercaptoethanol and 1U/ml penicillin/streptomycin (complete media). Splenocytes (300,000/well), which had been obtained from BDC2.5-TCR-Tg.NOD mice were cultured in 96-well round bottom plates together with 100µl of complete media, to which 100µl of m31 solution was added to give a final concentration of 0.1, 1 or 10ng/ml respectively. The plates were incubated at 37˚C with 5% CO_2 for 3 days. IFNγ concentration in the supernatant was then analysed using ELISA.

3.3.5. Cytokine detection of IFNγ using ELISA (enzyme linked enzyme-linked immunosorbent assay)

In order to detect IFNγ secreted by T cells, purified Rat Anti-mouse IFNγ antibody was diluted 1/500v/v using a coating buffer (carbonate buffer). Diluted capture antibody (50µl) was then added into each well of a F96 CERT Maxisorp plate and the plate was then incubated at 4˚C overnight. The coated plate was then washed with washing buffer (1x PBS, 0.05%v/v Tween-20) three times and blotted dry on a tissue paper. The plate was then blocked by adding 100µl of blocking buffer (1%w/v BSA and 0.1%v/v tween-20 in PBS) to each well and incubated at 37˚C for 1 hour. The blocking buffer was then discarded; the plate was washed three times with washing buffer and subsequently blotted dry. To test the IFNγ level, 50µl of supernatant from cell culture or IFNγ standards using diluent (1%w/v BSA in PBS,) was then added to each well and incubated at

ambient temperature for 2 hours. The supernatant was then discarded; the plate washed three times and then blotted dry. The secondary antibody, biotin Rat Anti-Mouse IFNγ detection antibody (50µl/well), was then added and the plate was incubated at ambient temperature for 1 hour. The antibody solution was then discarded; the plate was washed three times and then blotted dry. To detect secondary antibody, 50µl of streptavidin, horseradish peroxidase (HRP) (1/4000v/v in diluent) was then added to each well and the plate was incubated at ambient temperature for 30 minutes. The streptavidin-HRP solution was then discarded, the plate was washed three times and then blotted dry. HRP was then reacted with 50µl 3,3,5,5-Tetramethylbenzidine (TMB) substrate solution in each well and the plate was incubated at ambient temperature for 5-15 minutes until the substrate was fully converted (conversion was indicated by blue colour). Once conversion had taken place, the reaction was stopped by adding 50µl of stopping agent (2M H_2SO_4). Data was then acquired using a Multiwave plate reader set at 450nm to obtain the OD (optical density) value.

3.3.6. Intravital imaging of peptide clearance from murine skin.

Mice were kept under general anaesthetic using isoflurane during all processes including shaving, injection, MN treatment and imaging. To minimise background signal, hair was removed from the back of the neck of NOD mice (5-7 weeks old) using a Contura Clipper. For ID injection, 5TAMRA (fluorescent probe) conjugated peptides were dissolved in PBS to a final concentration of 40µg/ml for m31-5TAMRA and 120µg/ml for WE14-5TAMRA. Then 2µg of m31 or 6µg of WE14 was administered by injecting a 50µl solution intradermally into the shaved skin area using a 0.5ml insulin injection syringe (29G x 0.5" x 100unit). For MN treatment, three 5TAMRA conjugated peptide coated MN arrays were assembled in a specially designed holder and applied by pressing and holding MNs against

the shaved skin area for 10 minutes. To image the treatment area, the mouse was placed onto the observation cabinet and Ex/Em 546nm/579nm pair was used to detect the 5-TAMRA-peptide (Figure 3.1). During the imaging process the observation cabinet was kept at ambient temperature. Mice were imaged before treatment then 0, 1, 4 and 24 hours post treatment. Between each time point, the mouse cage was maintained at 26±1˚C, unless otherwise stated. To investigate the effect of pre-treatment of mouse skin with topical application of BD cream, 0.1ml of DiproSone®0.05%w/w Cream was applied once per day for two days before peptide injection.

White light images were taken before fluorescent images to allow anatomical co-localisation. To minimise the fluorescent background noise from hair, for each displayed image the minimum fluorescent intensity of peptide-5-TAMRA was set as 50 and maximum intensity was set as 150. Images were then analysed using Carestream MI software. For each fluorescent image the same area of ROI (region of interest) was applied to the data. Net fluorescent intensity for the ROI was calculated by subtracting the net intensity of the skin prior to treatment from the observed values obtained from the treated area. The normalised relative intensity (NRI) for each tested mouse was then calculated using equation 3.2.

Equation 3.2 Equation used to calculate normalised relative intensity (NRI).

$$\mathrm{NRI}\ (\%\mathrm{max}) = \frac{\text{Net intensity at each time point}}{\text{Maximum net intensity for each tested mouse}} \times 100\%$$

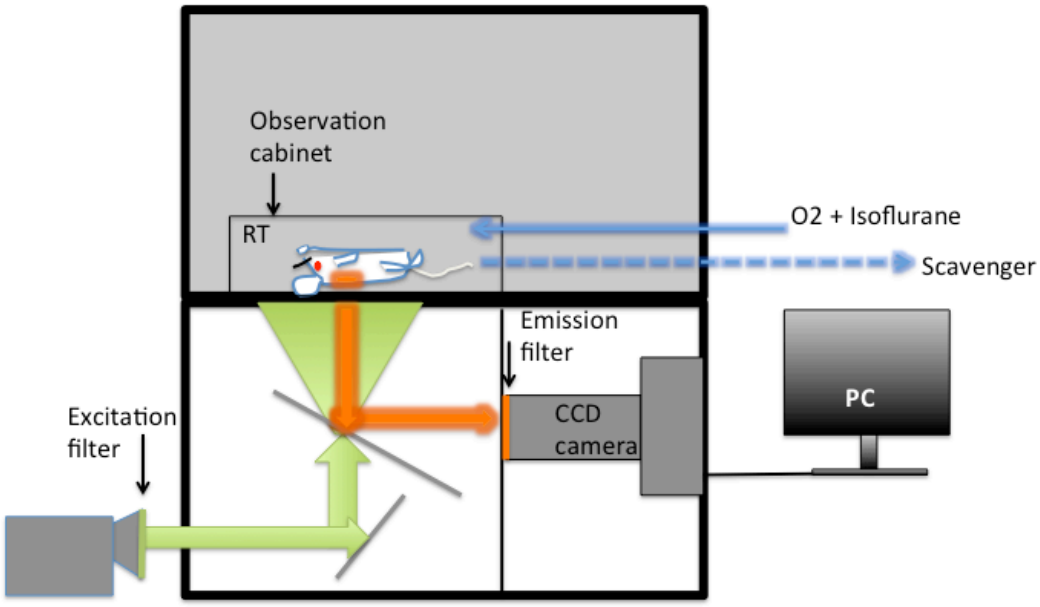

Figure 3.1 Schematic view of Kodak *in vivo* imaging system. The mouse was carefully placed in the observation cabinet with the treated area facing downwards. White light or fluorescent images were then taken by changing excitation and emission filters. The mouse remained under general anaesthetic to prevent movement for the duration of the imaging process.

3.3.7. Optimising CFDA-SE labelling conditions and concentration for BDC2.5 T cells using an *in vitro* assay

$CD4^+$ T cells were sorted from a population of BDC2.5 TCR-Tg mice splenocytes using a MACs $CD4^+$ isolation column, as described in Section 3.3.9. After sorting, cells were suspended at a concentration of 10^7/ml in RPMI1640 supplemented with 10%v/v FCS. Cells were then cultured in 10%v/v FCS/RPMI containing 0.1, 1, 3, 10 or 20μM of CFDA-SE for 5 minutes at ambient temperature, avoiding exposure to light. Cells were then washed twice with 10%v/v FCS/RPMI and pelleted at 400G for 5 minutes. After washing, CFSE labelled $CD4^+$ T cells (500,000/well) were co-cultured with irradiated splenocytes (500,000/well) together with 0.01, 0.1, 1 and 10ng/ml m31 in complete media for 3 days. After 3 days, cells were harvested, labelled with CD4 antibody (PE-cy7) and viability dye and the proliferation profile was then acquired using Flow Cytometry (Section 3.3.10.). To identify the CFSE labelled cell proliferation

profile, $CD4^+CFSE^+$ was first gated then the percentage of proliferated population was calculated by gating out the first generation, i.e. the percentage of cells with diluted CFSE labelling.

3.3.8. Investigating the time and minimum $CFSE^+$BDC2.5 T cell number required for *in vivo* studies.

To determine the time that adoptively transferred BDC2.5 T cells require to proliferate *in vivo*, NOD mice (female, 6-8 weeks old) were adoptively transferred with 10^7 CFSE labelled BDC2.5 T cells by injection into the tail vein. Mice were sacrificed at 1, 2, 3 and 4 days post transfer and cells from the PLNs were isolated (as described in section 3.3.2.). The proliferation profile of CFSE labelled cells were then analysed using flow cytometry (Section 3.3.10.).

To determine the minimum number of BDC2.5 T cells that were required for reliable analysis, NOD mice (female, 6-8 weeks old) were adoptively transferred with 10x, 4x, 2x and 1x 10^6 CFSE labelled BDC2.5 T cells through the tail vein. Mice were sacrificed three days post transfer and cells from PLNs were isolated (as described in section 3.3.2.) and the proliferation profile of CFSE labelled cells was analysed using flow cytometry (Section 3.3.10.).

3.3.9. $CD4^+$ T cell isolation using MACs kit

To obtain a purified population from a single cell suspension as prepared according to section 3.3.2. , $CD4^+$ T cells were sorted using $CD4^+$ MACs isolation kit (Miltenyi Biotec, UK) in a biosafety class II cabinet according to manufacturers instructions. Briefly, 10^7 single cells were suspended in 40µl MACs buffer (0.5% BSA, 2mM EDTA (Ethylenediaminetera acetic acid disodium salt solution)) and 10µl biotin-conjugated antibody cocktail solution (antibodies against CD8a,

CD11b, CD11c, CD19, CD45R (B220), CD49b (DX5), CD105, Anti-MHC-class II, Ter-119 and TCRγ/δ. (information obtained from http://www.miltenyibiotec.com)). Cells were incubated at 4˚C for 5 minutes. After incubation, cells were labelled with 30µl of MACs buffer and 20µl of anti-biotin magnetic beads per 10^7 cells. Cells were then incubated at 4˚C for another 10 minutes. One LS column, filled with ferromagnetic spheres, was used for every 10^8 labelled cells and the total cell number was less than $2x10^9$. The column was placed on MACs magnetic separators and then washed with 3ml cold MACs buffer. To isolate $CD4^+$ T cells, the cell suspension was then applied on the column and the column was washed three times with 3ml MACs buffer. $CD4^+$ T cells were washed through the column and collected in a 50ml falcon tube. Other (non-$CD4^+$) cells were collected by removing the column from the magnetic field and flushing using 5ml MACs buffer.

3.3.10. Using Flow cytometry to identify cell phenotypes

Single cell suspensions were prepared (see section 3.3.2.) and kept in ice cold staining buffer (1% w/v BSA and 0.1% sodium azide in PBS) at a concentration of 10^6/ml and were stained with both a viability dye and the relevant antibodies, as listed in Table 3.2, at 4˚C for 30 minutes in the dark. Cells were then washed with 2ml staining buffer (1% w/v BSA and 0.1% sodium azide in PBS), pelleted at 400G for 5 minutes and suspended in 200µl of staining buffer. Cells were kept on ice in the dark before analysis. Data were acquired using a CANON II FACs machine (BD Biosciences, UK) and analysed using software (FlowJo™).

Table 3.2 Antibody panel and dyes for cell staining used to identify CFSE labelled $CD4^+$ T cell phenotype by flow cytometry.

Ab/Dye	Fluorophore	Dilution v/v
CD62L	APC	1/400
CD25	Pacific Blue	1/100
CD4	PE Cy7	1/400
CD44	Percp cy5.5	1/400
Vb4	FITC	1/200
Viability	eFluor 780	1/1000
CFSE	CFSE	/

3.3.11. Trafficking of m31 *in vivo*

NOD mice were injected with 2µg of m31 either by ID injection or by MN administration. In order to examine m31 trafficking *in vivo*, either immediately or 7 days after m31 delivery, CFSE labelled BDC2.5 T cells were adoptively transferred. Briefly, splenocytes from BDC2.5-TCR-Tg.NOD mice were magnetically sorted using a $CD4^+$ isolation kit (Section 3.3.9.). Isolated $CD4^+$ T cells were labelled with CFSE (Section 3.3.7.). CFSE labelled $CD4^+$ T cells ($4x10^6$ cells/200µl) were adoptively transferred by intravenous injection, using a short 27G needle, to the tail veins of NOD mice (Female, 5-7 weeks old). Three days post transfer, ALNs, ILNs, CLNs, PLNs, SPs, and PaLNs (for abbreviations see Table 3.1) were mechanically dissociated and single cell suspensions were obtained. Cell phenotypes and proliferation profiles were then determined by flow cytometry (Section 3.3.10.).

3.3.12. Administration of peptides

To administer peptides by ID injection, peptides were dissolved in PBS to achieve concentrations of 40µg/ml and 120µg/ml for m31 and WE14 respectively. Mice were anesthetized using 2% isofluorane through an inhalation mask during the injection procedure. The hair of the neck area was then removed using an

electric clipper. 50µl of peptide solution was then injected intradermally to the shaved area using a 29G insulin injection needle.

To administer peptides by MNs, 10µg of peptide was coated on 3 arrays of solid stainless steel MNs with 30 needles in total (as described in section 2.3.5. Mice were anesthetized and the hair of the neck area was removed using an electric clipper. MNs were applied to the shaved area for 10 minutes (see section 2.3.7. Each MN application delivers, on average, 2µg m31 or 6µg WE14 (See Section 2.4.4).

3.3.13. Inducing tolerance *in vivo*

On day 0, NOD mice were anesthetised using 2% isofluorane through an inhalation mask and peptide was administered either by ID or solid-coated MN array to the shaved neck area as described in section 3.3.12. This was repeated on day 21. A week after the second peptide administration, $4x10^6$ CFSE labelled BDC2.5 T cells were transferred to mice through the tail vein using a 27G short needle. 3 days post transfer, mice were sacrificed and single cell suspensions were prepared from the ALN, PLN and SP. The BDC2.5 T cell proliferation profile was then analysed using flow cytometry 3.3.10.

3.3.14. Foxp3$^+$BDC2.5 T cells suppressive effect *in vivo*

$CD4^+$ T cells were isolated from either BDC2.5-Foxp3-Fir mice or NOD-Foxp3-Fir mice (Section 3.3.9. Then, $CD4^+Foxp3^+$ cells were sorted on a FACS AriaIII Cell Sorter. NOD-SCID mice were adoptively transferred with either 200µl saline containing $1.5x10^6$ $Foxp3^+BDC2.5^+$ T cells or $1.5x10^6$ $Foxp3^+CD4^+$ T cells intravenously through the tail vein using a 27G (1/4inch) needle. 24 hours after the initial transfer, the same mice were co-transferred with $1.5x10^6$/200µl

$CFSE^{+}BDC2.5^{+}$ T cells. BDC2.5 T cell proliferation was then analysed using a Canto II flow cytometer three days after the second cell transfer.

3.4. Results

3.4.1. Characterization of BDC2.5 T cells

$CD4^+$ T cell sub populations were compared between NOD mice and BDC2.5-TCR-Tg.NODmice. Splenocytes were stained with CD4 and Vβ4 antibodies to identify BDC2.5 T cells. Figure 3.2 A and B show that, approximately 85% of $CD4^+$ T cells were Vβ4 positive in BDC2.5-TCR-Tg.NOD mice splenocytes compared to approximately 10% in NOD mice. When BDC2.5 T cells were stimulated with m31 they proliferated dramatically compared with cells co-cultured with the WE14 peptide (Figure 3.2 C, D) (Sequence of m31 and WE14 see Table 2.1). BDC2.5 T cells were able to respond to 0.1ng/ml m31 after a three-day incubation time, the SI of which was 110 on average compared to background (background was 443 cpm). On the other hand, at least 50μg/ml WE14 was needed to stimulate BDC2.5 T cells. The SI of BDC2.5 T cells treated with 50μg/ml WE14 over 3 days had a mean value of 3.4, with an average background signal of 517cpm.

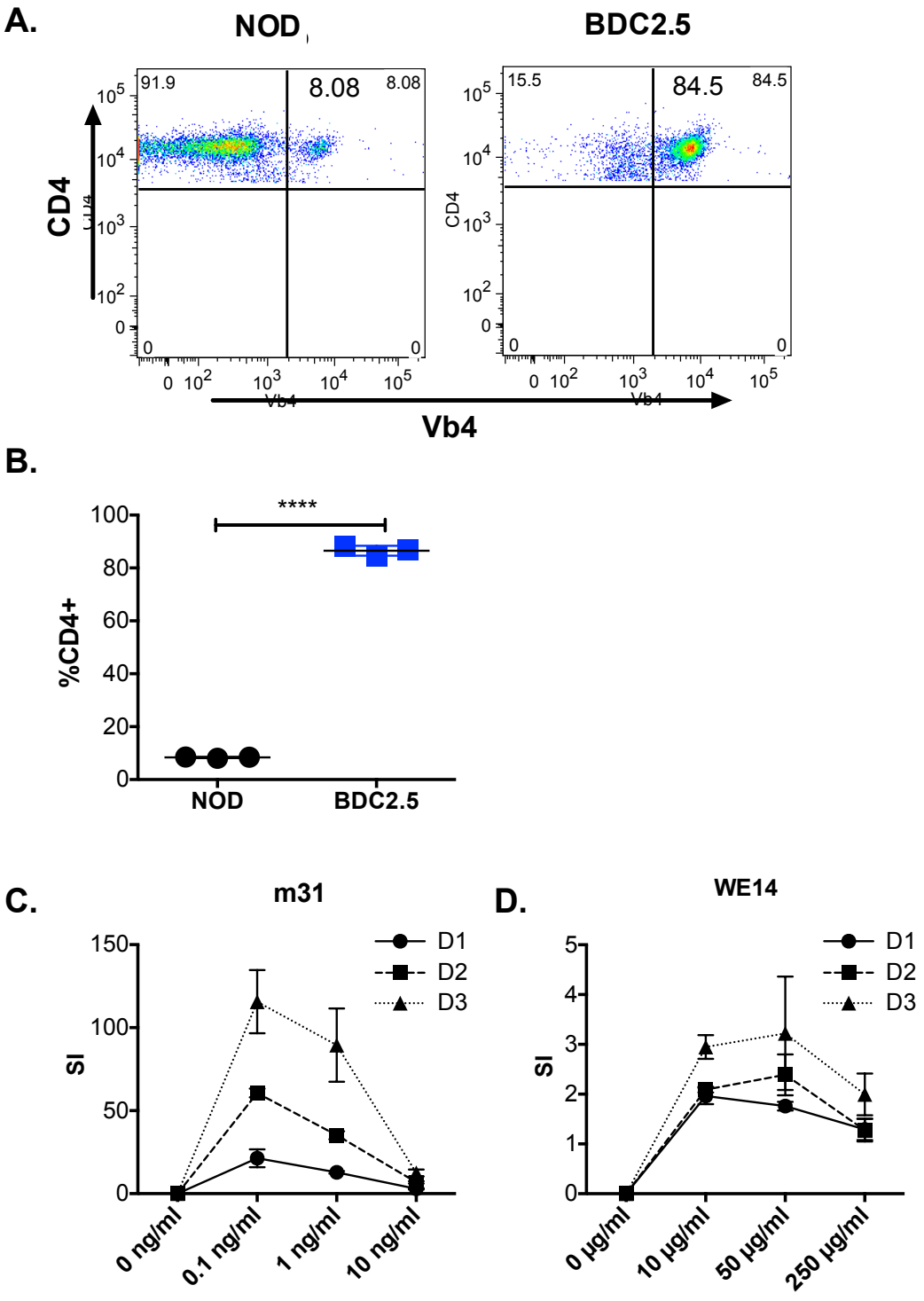

Figure 3.2 Identification of BDC2.5 T cells. **A.** Representative flow cytometry plot of BDC2.5 T cell population in total $CD4^+$ T cells from NOD mouse and BDC2.5-TCR-Tg.NOD mouse. **B.** A graph to illustrate differences in the percentage of BDC2.5 T cells detected in NOD and BDC2.5-TCR-Tg.NOD mouse SPs. **C.** Proliferation of BDC2.5 T cell to m31 *in vitro*. **D.** Proliferation of BDC2.5 T cell to WE15 *in vitro*. n≥3, Mean±SD, two tailed t test **** p<0.0001. D1,2 or 3= Day 1, Day 2 or Day 3. SI=stimulation index

3.4.2. Evaluating the effect of MN coating formulation on m31 bioactivity

M31 was coated on MNs and washed off to test whether the formulation and coating process altered the bioactivity of m31. Stock m31 solution or re-dissolved coating formulation were cultured with splenocytes of BDC2.5-TCR-Tg mice. The bioactivity of the m31 was reflected by the level of IFNγ detected in the supernatant, which was released by BDC2.5 T cells. The MN coated m31 showed no significant differences at 10, 1 and 0.1 ng/ml when compared with relevant m31 controls. Trace IFNγ was released by BDC2.5 splenocytes without m31 (Figure 3.3). Cells cultured with blank formulation, i.e. formulation without m31, showed no activation over three days and there was no significant difference between splenocytes alone and blank control formulation.

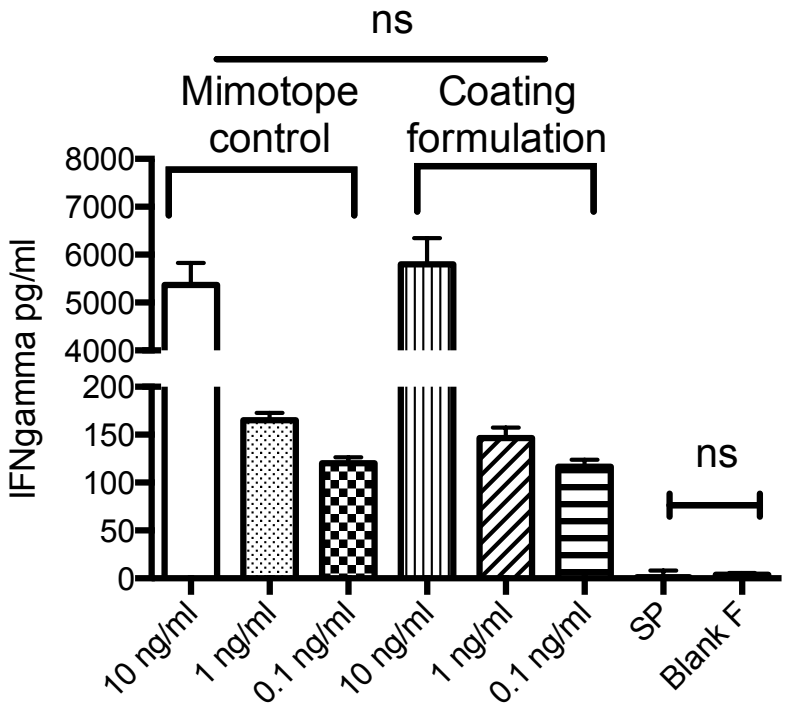

Figure 3.3 A graph to illustrate the impact of the MN coating process on the bioactivity of the m31 peptide. Three concentrations of m31 (10, 1 and 0.1ng/ml) were added to splenocytes, either before or after dry coating on a MN device. Stimulation of the cells by the peptide was determined by measuring IFNγ levels. SP=splenocytes alone. N=3, Mean±SD. Unpaired two tailed t-test; ns $p>0.05$. Data were compiled from two separate experiments.

3.4.3. Clearance of peptide from skin

In order to investigate the PKs of the peptide in the skin, a Kodak *in vivo* imaging system was used to visualise the clearance of a peptide conjugated with a fluorescent probe (5-TAMRA), from murine skin (Figure 3.5). The bioactivity of the conjugated peptide was tested and IFNγ ELISA results indicate that 5-TAMRA did not alter the bioactivity of m31 (Figure 3.4). Therefore, probe-conjugated peptide was considered to be a valid model to predict the skin clearance of the therapeutic peptide.

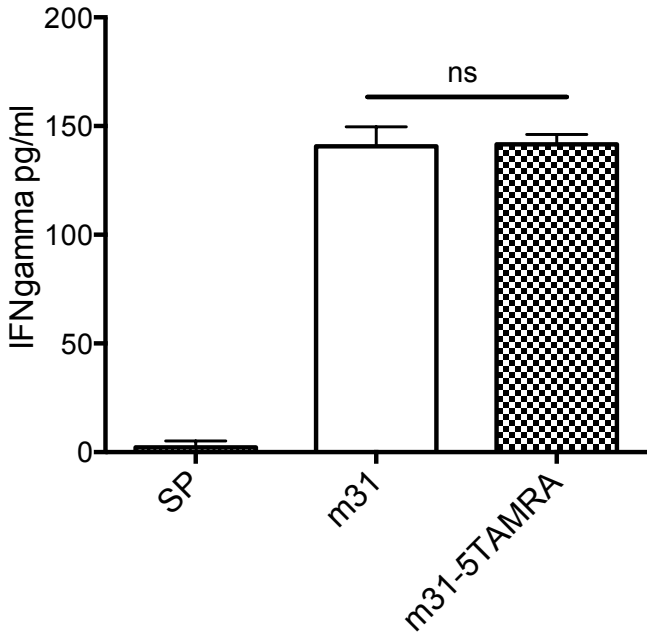

Figure 3.4 A graph to compare the bioactivity of the 1ng m31 peptide, both with and without 5-TAMRA conjugation. Bioactivity was determined by quantifying the IFNγ levels in BDC2.5 splenocyte cell culture 3 days after addition of the m31 peptide. SP = Splenocytes alone; m31 = Splenocytes cultured with m31 and m31-5TAMRA = Splenocytes cultured with m31-5TAMRA. n=3, Mean±SD, two tailed t test, ns, p>0.05.

3.4.3.1. Effect of environmental temperature on m31-5TAMRA peptide clearance from mouse skin

Mice were ID injected with m31-5TAMRA and either kept in a cool environment (22±1˚C) or in a warm environment (30±1˚C). At the lower temperature, the localised fluorescence intensity produced by the peptide was maintained for 1hr

and then quickly declined over the next 4 hours. Over the next 20 hours the clearance rate slowed (Figure 3.6 A). At a higher temperature (30˚C), there was a more rapid decline of fluorescence intensity during the first hour. After this the profile of peptide loss from the skin was comparable to the clearance at lower temperature (Figure 3.6 A). The area under curve (AUC) was calculated (Figure 3.7 A). AUC is inversely correlated with the clearance rate, therefore the higher the AUC the lower the clearance rate. At lower temperature, 22±1˚C, the AUC is significantly higher than at 30±1˚C. Based on this finding, it is important to control environmental temperature, particularly during the first 4 hours post delivery. The ambient temperature of the clearance experiments was generally controlled at 26±1˚C and thus the clearance of the peptide was measured at ambient temperature unless stated otherwise.

3.4.3.2. Effect of peptide solubility and administration method on clearance

To determine whether the inherent aqueous solubility of the peptide would influence its clearance rate in skin, two peptides with different solubility were used, WE14 and m31. When administered by ID, the NRI of WE 14-5TAMRA dropped sharply within 1 hour compared with m31-TAMRA. At the 4 hour point, WE14-5TAMRA was almost entirely eliminated from the skin, while m31-TAMRA was still traceable. Using MN delivery, both WE14-5TAMRA and m31-TAMRA showed similar local kinetics within the first hour. However, WE14-5TAMRA was cleared more quickly from the local area from 1 hour onwards (Figure 3.6 B).

The overall clearance rate from the skin was analysed using AUC. AUC of both peptides, m31-TAMRA and WE14-5TAMRA, was significantly higher for MN delivery than for ID delivery (Figure 3.7 B). The solubility of peptides was also shown to play a role in clearance over a 24 hour period. The MN delivery of

m31-5TAMRA showed a significantly higher AUC than the relatively more soluble WE14-5TAMRA. Although the AUC of ID delivery of m31-5TAMRA showed no significant difference compared to WE14-5TAMRA, a lower AUC of WE14-5TAMRA was observed compared to m31-5TAMRA (Figure 3.7 B).

3.4.3.3. Local effect of pre-treatment of skin with BD cream on m31-5TAMRA peptide clearance from skin

In order to precondition skin DCs, a topical steroid (0.05% w/v betamethasone dipropionate cream) was applied once every 24 hours for two days before m31-TAMRA administration. M31-5TAMRA was either delivered by ID injection or using a 10 minute application of a solid-coated MN array. Fluorescent images were taken using the Kodak *in vivo* imaging system at 0, 1, 4 and 24 hours.

For peptide administered by ID injection, the maximum fluorescent intensity occurred immediately after injection (0 hour time point) and is shown as 100% (Figure 3.6 C). At the 1 hour time point, NRI dropped to 80% without pre-treatment and to approximately 40% with pre-treatment. Within 4 hours, in both mice with and without pre-treatment, both NRIs drop down to near baseline levels (Figure 3.6 C). As shown in Figure 3.6 C, a peptide deposition was clearly observed post MN treatment. The maximum fluorescent intensity of peptide administered by MN was measured at 1 hour post delivery (Figure 3.6 C). The trend of NRI is to increase by approximately 30% during the first hour, followed by a decline to ~50% of maximum NRI during the following 3 hours. NRI then gradually declined to baseline levels within a 4 to 24 hour period (Figure 3.6 C). There was no statistically significant difference in NRI over the time period when comparing mice pre-treated with steroid and those without, except the initial NRI was slightly higher (60%) with preconditioning than without preconditioning (40%). Topical application of BD cream pre-treatment showed no influence on

clearance of peptide delivered either by MNs or ID injection, demonstrated by the non-significant difference observed in the total clearance rate of treated and un-treated groups over a 24 hour period (Figure 3.7 B).

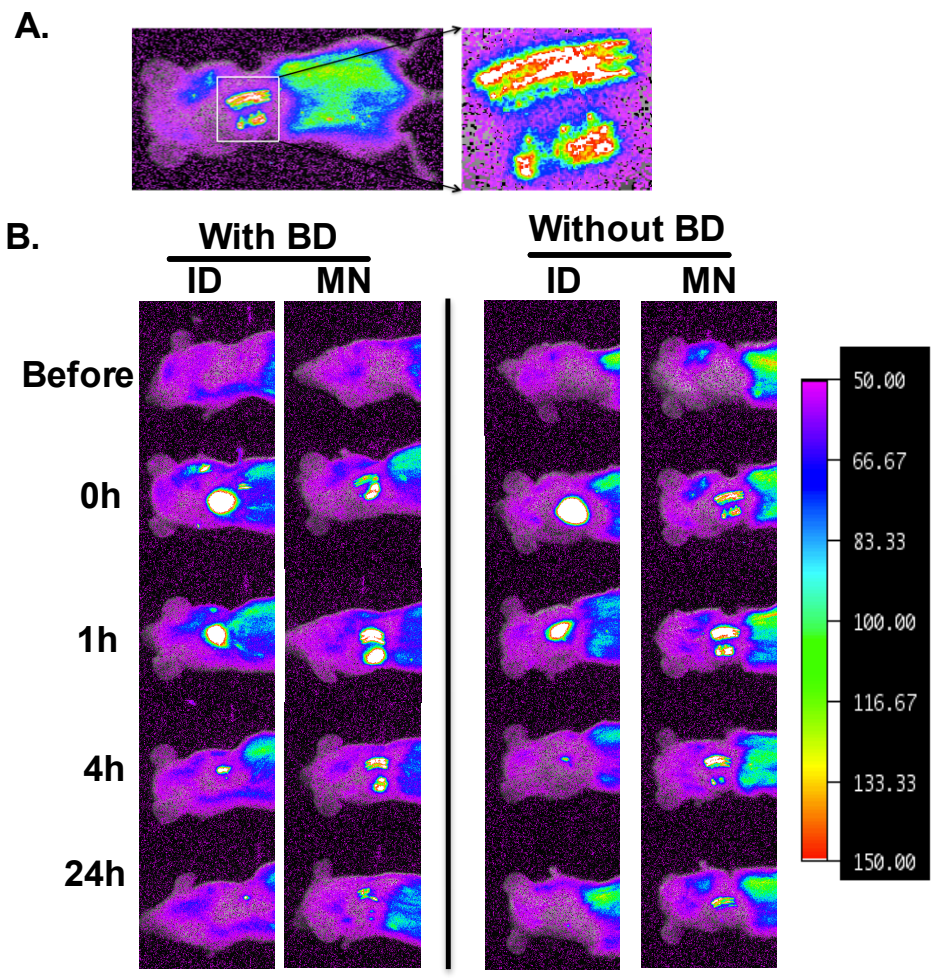

Figure 3.5 Representative fluorescent intravital image for analysing peptide-5TAMRA conjugate clearance from the skin. Hair from the back neck area of NOD mice was removed using a clipper and 5-TAMRA conjugated peptides were administered to this area either using ID injection or MNs. In order to study the clearance of peptide from skin, fluorescence intensity was measured at 0, 1, 4, and 24 hours post treatment. **A.** Representative fluorescent image of m31-TAMRA delivered by MN 0hr post delivery. The higher magnification image shows the MNs footprint at the 0 hour post delivery time point; **B.** Representative fluorescent images of m31-5TAMRA in skin before treatment, and at 0, 1, 4 and 24 hours post treatment. M31-TAMRA and WE14-5TAMRA were administered either by ID injection or MNs, with or without pre-treatment with topical application of BD cream.

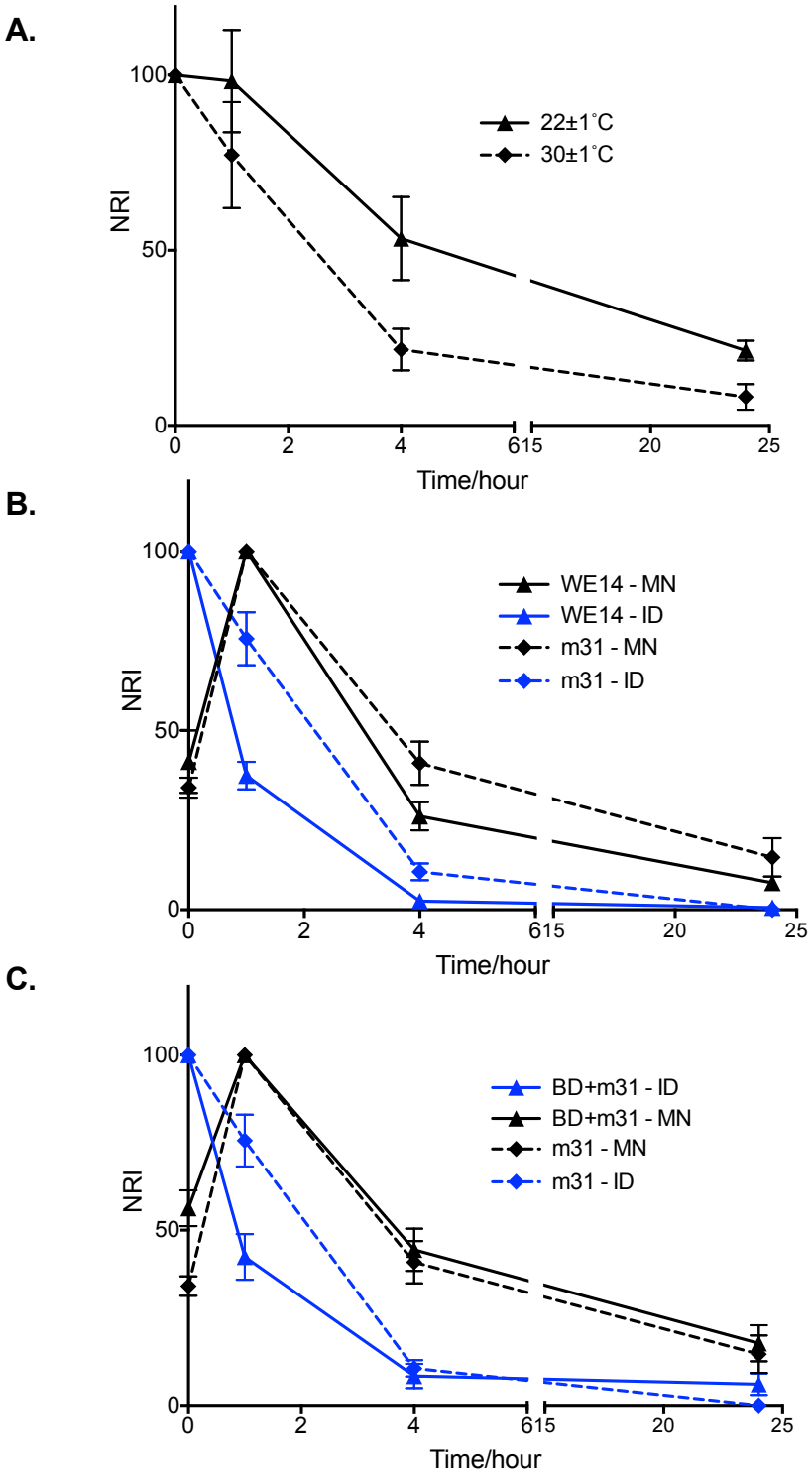

Figure 3.6 Clearance curve of injected peptide-5TAMRA within the skin. NRI of each treated area shown in **Figure 3.5** was calculated for each treated mouse. **A.** The effect of environmental temperature on clearance rate of m31-5TAMRA at 22±1˚C or 30±1 ˚C; **B.** Effect of peptide solubility on clearance. WE14-5TAMRA was compared with m31-5TAMRA administered either by ID injection or MNs. (m31-5TAMRA treatment n=6, WE14-5TAMRA treatment n=3); **C.** Effect of pre-treatment with BD cream on clearance of m31-5TAMRA from skin. Peptide was administered either by ID injection or MNs two days after BD cream pre-treatment (n=6). Mean±SD. Data were compiled from four separate experiments. NRI=net relative intensity

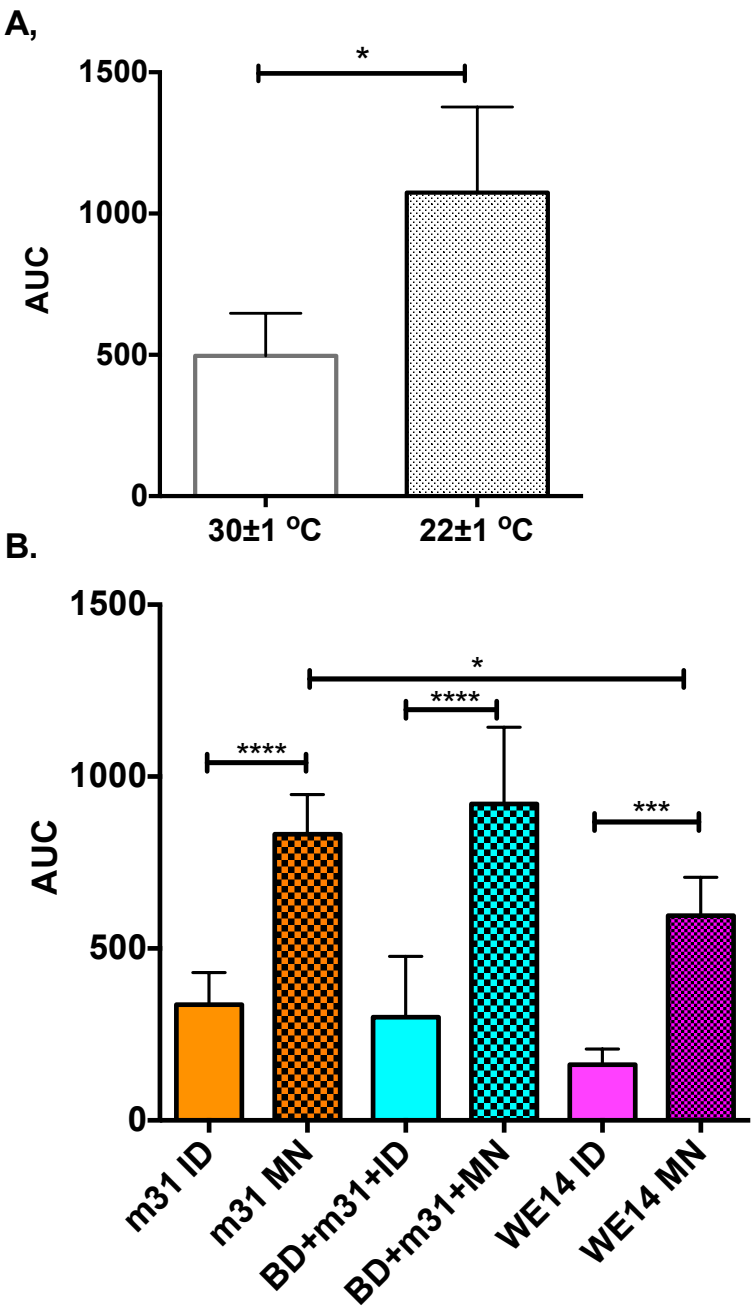

Figure 3.7 Graph showing the factors that influence the overall clearance rate of peptide from the skin. **A.** AUC of graph **Figure 3.6** A. showing the effect of environmental temperature on clearance. Two tailed t test. *p<0.05. **B.** AUC of graph **Figure 3.6 B** and **C**, showing the relationship of peptide solubility, delivery method and pre-treatment of BD cream on overall clearance rate. Mean±SD. One way ANOVA with Tukey post test. *p<0.05, ***p<0.001, ****p<0.0001. AUC=area under curve

3.4.4. Optimising the CFSE labelling protocol for monitoring m31 trafficking and BDC2.5 T cell proliferation *in vivo*

3.4.4.1. MACs sorting purity check

In order to obtain purified $CD4^+$ T cells from BDC2.5 mice, splenocytes from BDC2.5 mice were sorted using a MACs CD4 isolation kit. Before sorting, $CD4^+CD8^-$ T cells comprised approximately 30% of total splenocytes, of which, the majority were B cells and APCs (data not shown). After sorting, a purified $CD4^+$ T cell population was obtained with purity in the range of 85-90% of total live cells (Figure 3.8 A). The majority (90-95%) of these purified $CD4^+$ T cells were demonstrated to express the $CD4^+V\beta4^+$ phenotype (Figure 3.8 B), which identified these cells as BDC2.5 T cells. Therefore, in this project, purified $CD4^+$ T cells from BDC2.5 TCR-Tg mouse's splenocytes were considered to be pure BDC2.5 T cells.

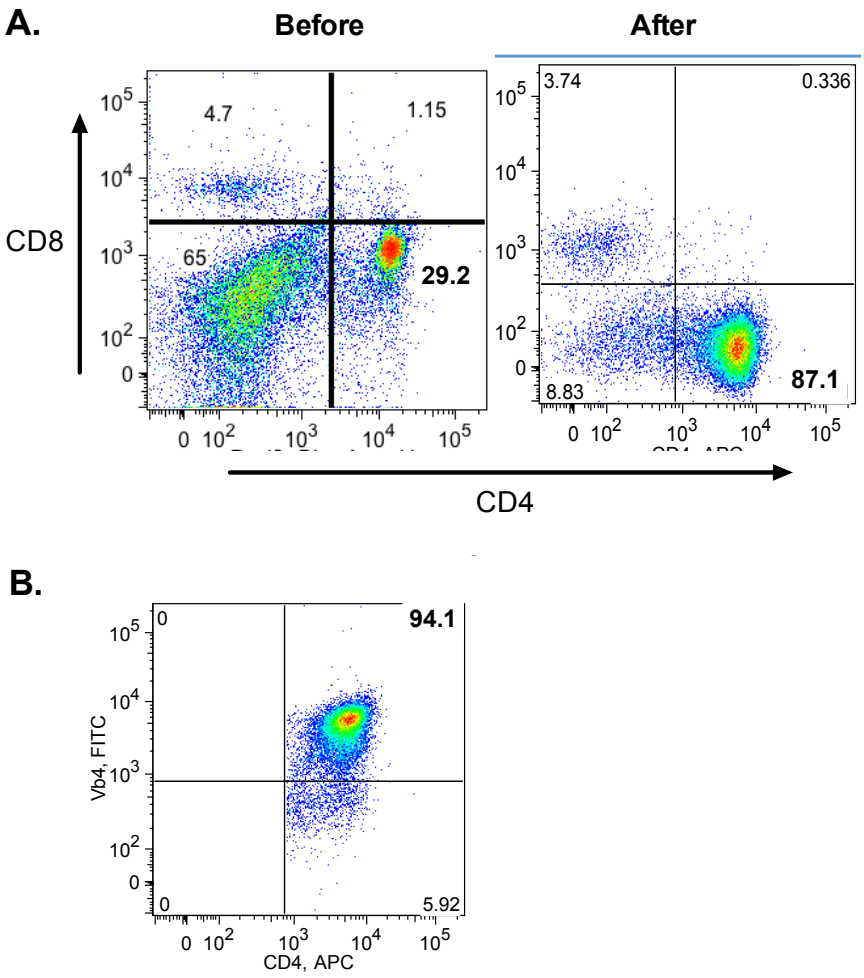

Figure 3.8 Purity of CD4$^+$ T cells after using a MACs CD4 isolation kit. A. Representative flow cytometry plot showing the percentage of CD4$^+$ T cell population before and after splenocytes were sorted with MACs CD4$^+$ isolation kit. **B.** Representative flow cytometry plot showing the percentage of CD4$^+$Vβ4$^+$ (BDC2.5) T cell subset in whole CD4$^+$ T cell population, after splenocytes were sorted with MACs CD4$^+$ isolation kit.

3.4.4.2. Optimizing CFDA-SE labeling conditions and concentration for BDC2.5 T cells using an in vitro assay

After purification, BDC2.5 T cells were labelled using a fluorescent dye (CFDA-SE), which enabled the proliferation of BDC2.5 T cells to be monitored, either *in vitro* or *in vivo*. When cells were stained according to the manufacturer's instructions, i.e. cells were stained in PBS (37˚C) containing 1μM CFDA-SE dye for 15 minutes, low cell viability was observed (Figure 3.9 A). After optimising the incubation time (5 minutes) and incubation media (10%v/v FCS/RPMI) according

a method by Quah, B.J. *et.al*, the viability of $CD4^+$ cells after labelling was improved to over 90% (Figure 3.9 B) (Quah and Parish, 2012, Quah et al., 2007). Cells also showed increasing fluorescent intensity when using increasing concentrations of CFDA-SE dye for labelling (Figure 3.9 C). Both 10μM and 20μM CFDA-SE were able to label cells sufficiently to differentiate them from the unstained control, providing separation of the sub-populations for proliferation analysis. After CFSE labelling, BDC2.5 T cells were stimulated with m31 and were allowed to proliferate over a three-day incubation period. A concentration of 20μM CFDA-SE produced a sub-generation of BDC2.5 T cells with sufficient resolution from the untreated sample (Figure 3.9 D). Therefore for *in vivo* proliferation experiments, 20μM of CFDA-SE was used to stain every 10^7/ml $CD4^+$ T cells.

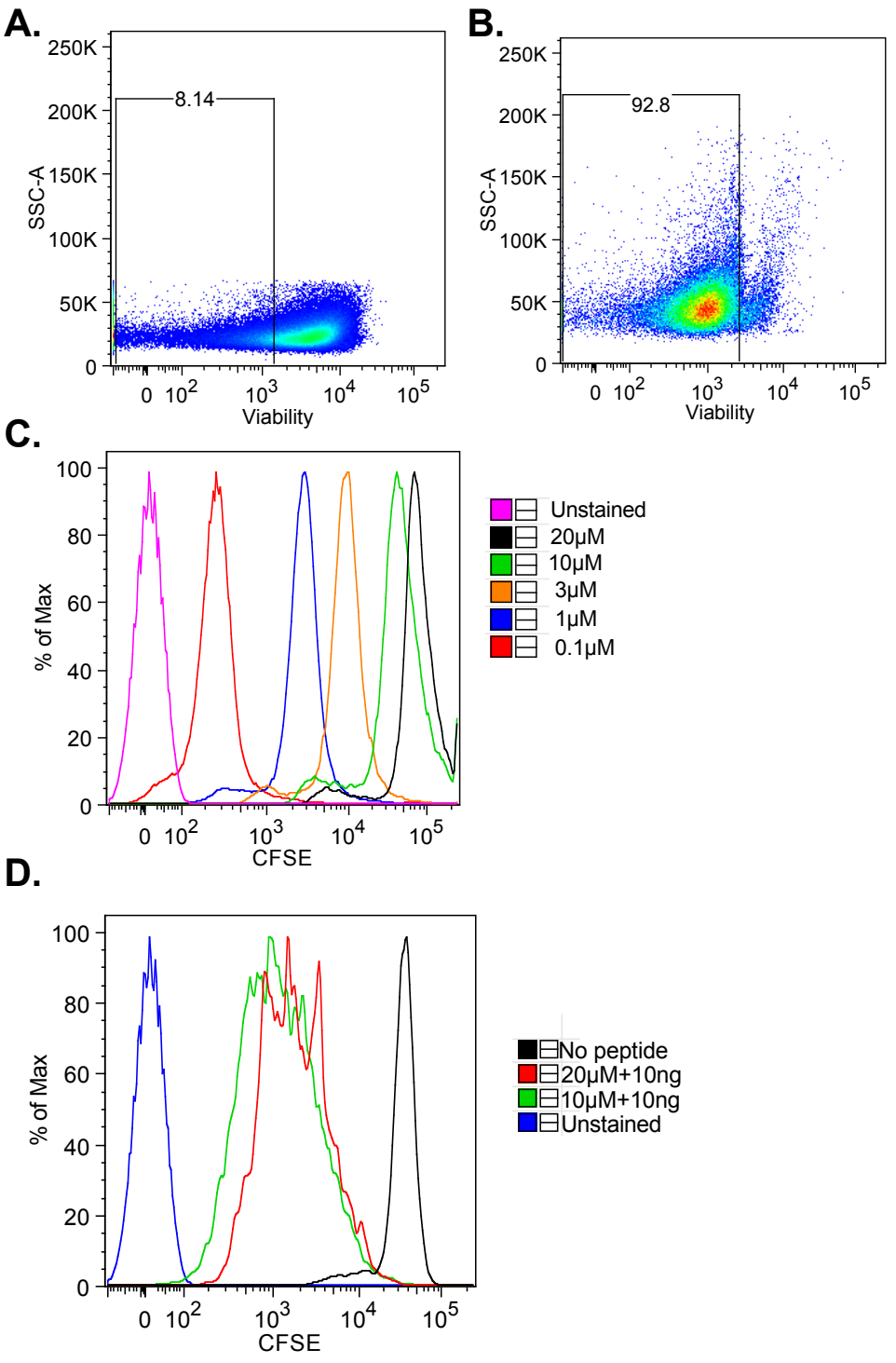

Figure 3.9 Optimisation of CFDA-SE labelling protocol to monitor m31 trafficking and BDC2.5 T cell proliferation *in vivo*. The toxicity of CFDA-SE dye was determined by testing the viability of BDC2.5 T cells after labelling. Representative flow cytometry plot showing the percentage of viable BDC2.5^{+}CD4^{+} cells after labelling using either **A.** according to manufacture's protocol or **B.** optimised protocol. A serial concentration of CFDA-SE dye (0.1μM-20μM) was tested to determine sufficient staining. **C.** Fluorescent intensity of labelled BDC2.5 T cells using different concentrations of CFDA-SE dye were shown in histogram overlay. Both 10μM and 20μM were able to stain cells sufficiently without exceeding the detection limit of the flow cytometer used. **D.** Histogram overlay showing the generation peaks of BDC2.5 T cells labelled either with 10μM or 20μM CFDA-SE after co-culture with APCs and 10ng/ml m31 for 3 days.

3.4.4.3. Optimizing the proliferation time required for transferred CFSE$^+$BDC2.5 T cells in vivo

In order to investigate the time that T cells required to proliferate *in vivo*, 10x10^6 CFSE labelled CD4$^+$ (BDC2.5) T cells were transferred to female NOD mice (5-7 weeks old). After 1, 2, 3 and 4 days, cell proliferation in the PLNs was assessed. Endogenous antigen of BDC2.5 T cells is located in the pancreas and presented to T cells in the PLN, therefore the proliferation of transferred BDC2.5 T cells in the PLN represent the degree of the endogenous activation. Mice without cell transfer had no CFSE$^+$ labelled cells (Figure 3.10 A). One day after cell transfer, CFSE$^+$ cells were found in the PLN, but no clear cell division was observed. At least 4 generations of CFSE$^+$ CD4$^+$ T cells were detected in the PLN on day 2. On day 3, six generations were observed in the PLN and by the sixth generation the signal from CFSE stained cells was only slightly greater than that in unstained cells (Figure 3.10 B). On day 4 the detection limit was reached, which means the last two subgenerations of CFSE$^+$CD4$^+$ T cells could not be distinguished from the background unstained population (Figure 3.10 B). Therefore for these experiments, mice were only examined up to 3 days post CFSE transfer.

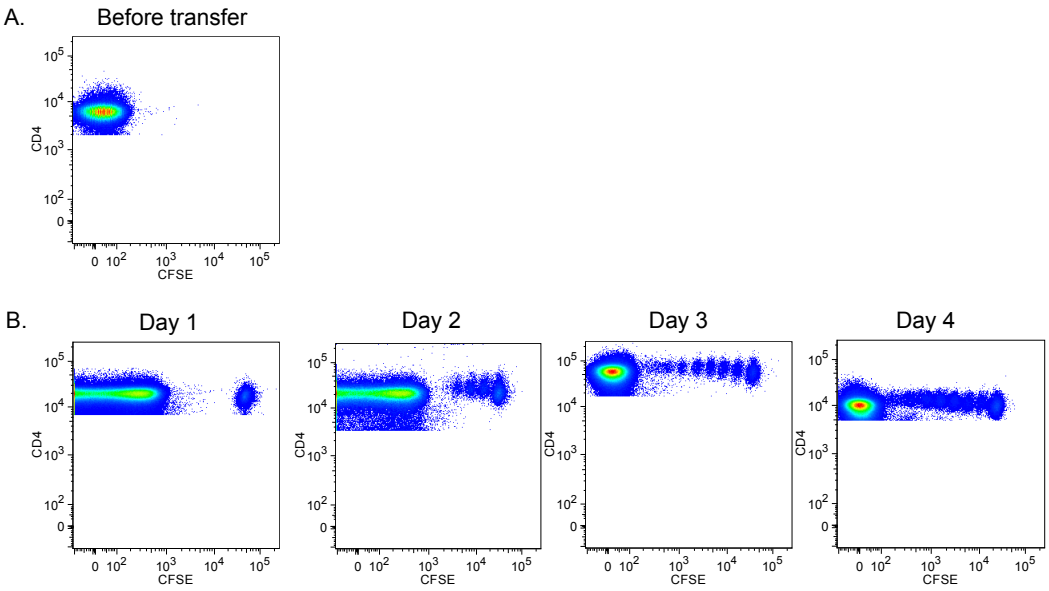

Figure 3.10 Representative flow cytometry plot showing the time course of CD4$^+$CFSE$^+$ T cells *in vivo* proliferation in PLN. A. Negative control mouse without CD4$^+$CFSE$^+$ cell transfer. **B.** CD4$^+$CFSE$^+$ proliferation profile in the PLN, 1, 2, 3 and 4 days post transfers.

3.4.4.4. Titrating the minimum number of CFSE labeled BDC2.5 T cells required for in vivo tolerance study

The minimum number of CFSE labelled CD4$^+$ T cells, which were required to generate a reliable signal was also tested. 10x, 4x, 2x or 1x10^6 CFSE labelled BDC2.5 T cells were adoptively transferred to NOD mice and endogenous proliferation in the PLN was analysed. Three days post transfer, CFSE labelled BDC2.5 T cells were gated as shown in Figure 3.11 A. It was possible to distinguish transferred CFSE-labelled BDC2.5 T cells from the endogenous CD4$^+$ T cell population for each of the groups. The low initial cell numbers, 1 x10^6 and 2 x10^6, were unable to generate distinct subgenerations. When the transferred cell number was increased to 4 x10^6 and 10 x10^6, distinguished subgenerations could be observed. Transfer of 4 x10^6 cells resulted in, on average, 0.9% CD4$^+$ T cells in the PLN that were CFSE labelled, with a total recorded cell number of between 4000 and 5000 (Figure 3.11 B and C.). This provided enough cells in each generation to allow for adequate proliferation studies.

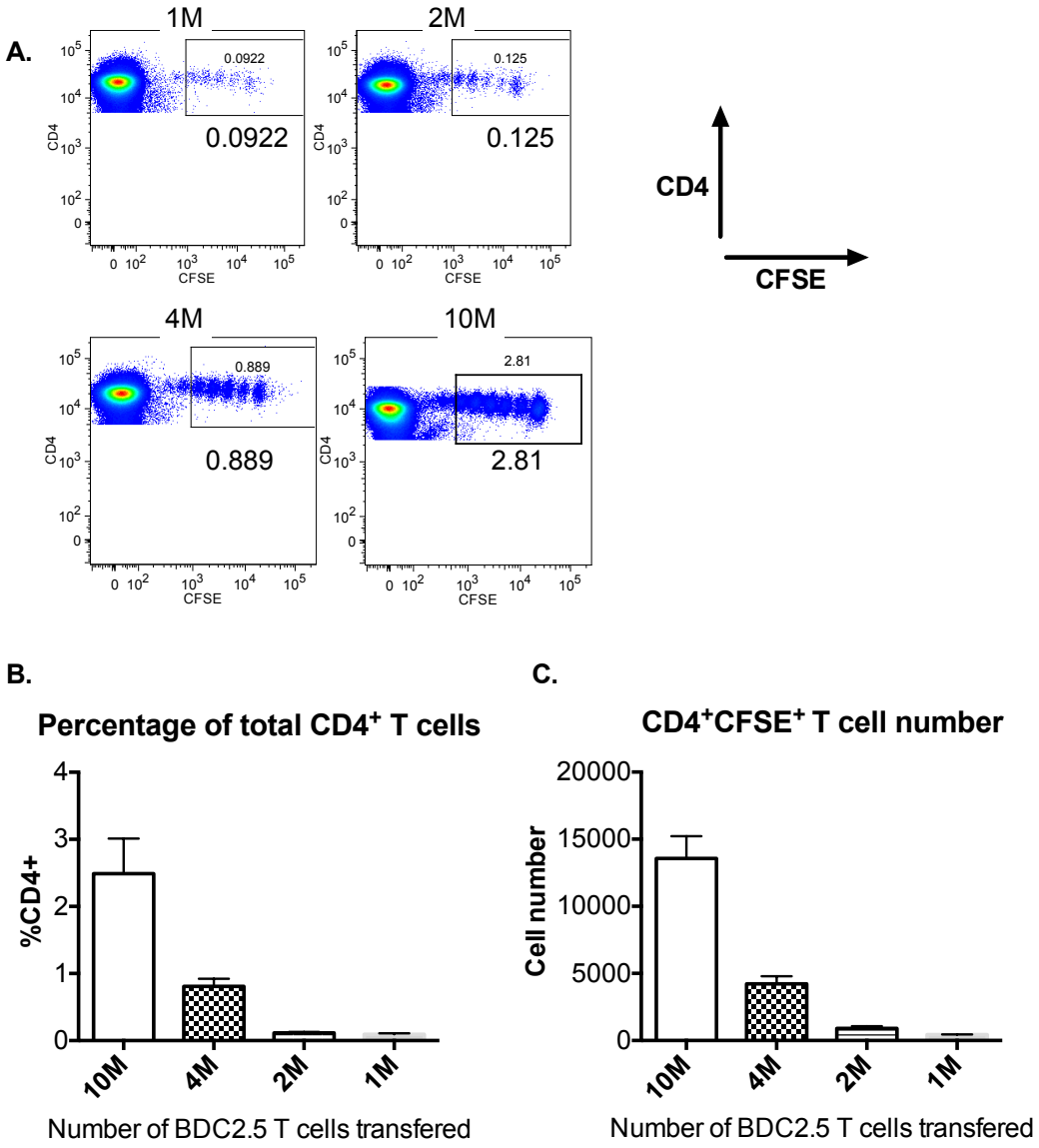

Figure 3.11 Titration CFSE labelled cells *in vivo*. A. Representative flow cytometry plot of $CD4^+$ cells in PLN. Gated population showed the percentage of $CFSE^+CD4^+$ cell three days after the NOD mouse was transferred with 10x, 4x, 2x or $1x10^6$ $CFSE^+$BDC2.5 T cell; **B.** $CD4^+CFSE^+$ as a percentage of total $CD4^+$ T cells in PLN; **C.** Absolute $CD4^+CFSE^+$ cell number in PLN three days post transfer. n=3. Mean±SD. $M=10^6$

3.4.5. Tracking m31 *in vivo* using CFSE labelled BDC2.5 T cells

Female NOD mice (6-8 weeks old) were treated with 2µg of m31; delivered either by ID injection or by solid-coated MNs, and mice were immediately adoptively transferred with CFSE labelled BDC2.5 T cells. Peptide distribution after delivery was determined by determining the proliferation of BDC2.5 T cell populations in different LNs and the SP. Without any exogenous antigen, BDC2.5 T cells only

proliferated in the PLN, where endogenous antigen was presented. No cell division was observed in other LNs or the SP (Figure 3.12). In the peripheral lymphoid organs, 3-4% $CFSE^{+}CD4^{+}$ T cells were demonstrated to have proliferated, which was considered to be a non-specific proliferation response. For mice treated with 2µg of m31 (by either ID injection or MNs), proliferation of BDC2.5 T cells was not only observed in the PLN but also in the LNs that drained the treatment site; the skin of the neck, i.e. the ALN. There were no activated BDC2.5 T cells observed in other LNs, even in the ILN; another skin draining LN situated in the hind limb (Figure 3.12). Greater proliferation was also observed when m31 was administered by solid-coated MN array rather than by ID injection at both 3 and 10 days post injection (Figure 3.13 C). T cells also showed a more consistent proliferation profile between experiments for MN administration rather than ID administration. Both 3 days and 10 days post ID injection of m31, the proliferation profile of $CFSE^{+}CD4^{+}$ BDC2.5 T cells in the PLN was not significantly altered (Figure 3.13 D). No enhanced stimulation of transferred $CFSE^{+}CD4^{+}$ BDC2.5 T cell was observed in the PLN when m31 was administered using solid-coated MNs when compared with ID injection (Figure 3.13 D).

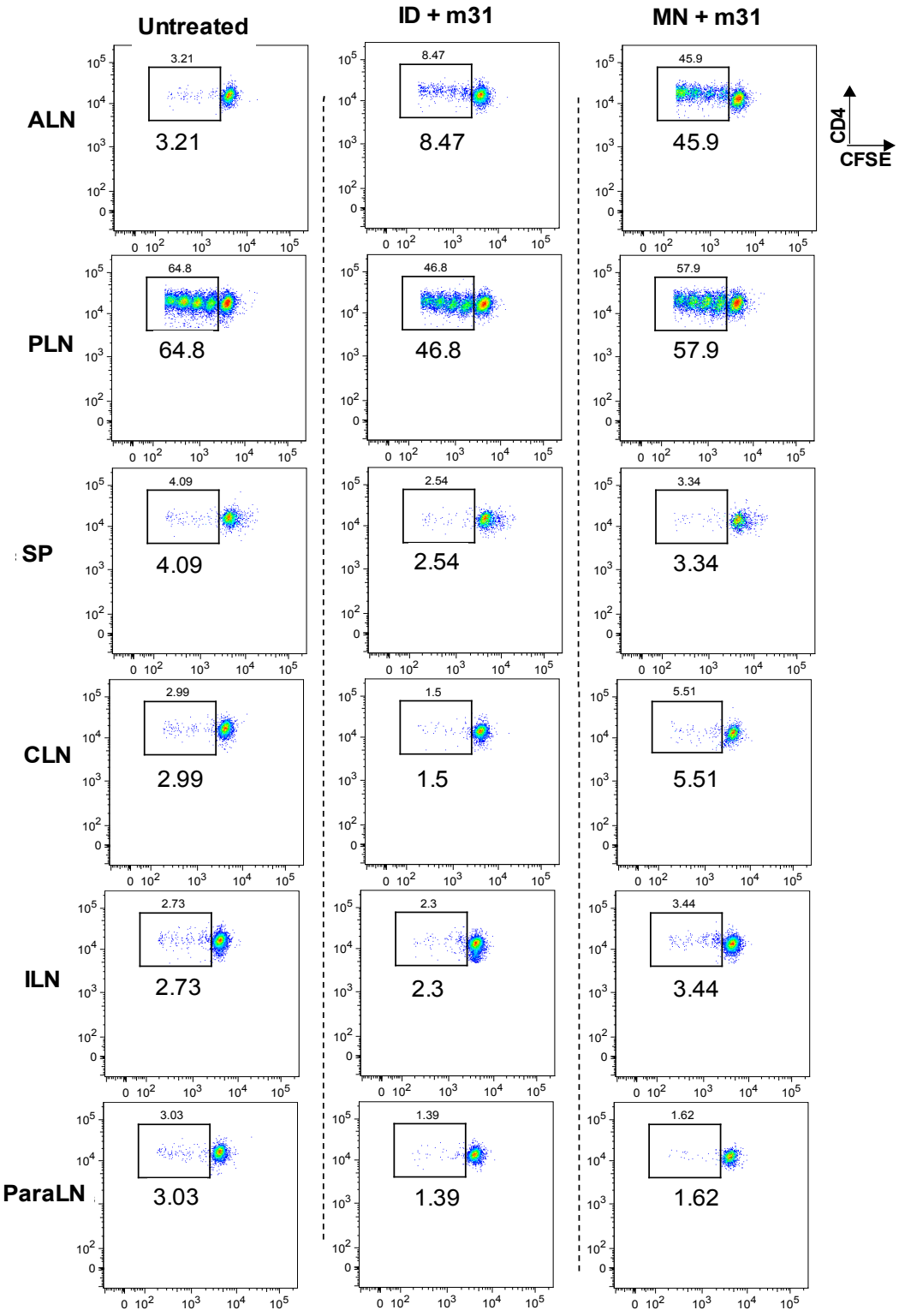

Figure 3.12 Representative flow cytometry plots of $CD4^{+}CFSE^{+}$ BDC2.5 T cell proliferation profiles in different LNs and the SP. NOD mice were treated with 2µg of m31 to the shaved neck area using either ID injection or solid-coated MN arrays. CFSE labelled BDC2.5 T cells ($4x10^{6}$) were then immediately transferred through the tail vein. Three days post-transfer, the proliferation profile of BDC2.5 T cells was analysed using Flow cytometry. The gate shows the divided population of transferred BDC2.5 T cells.

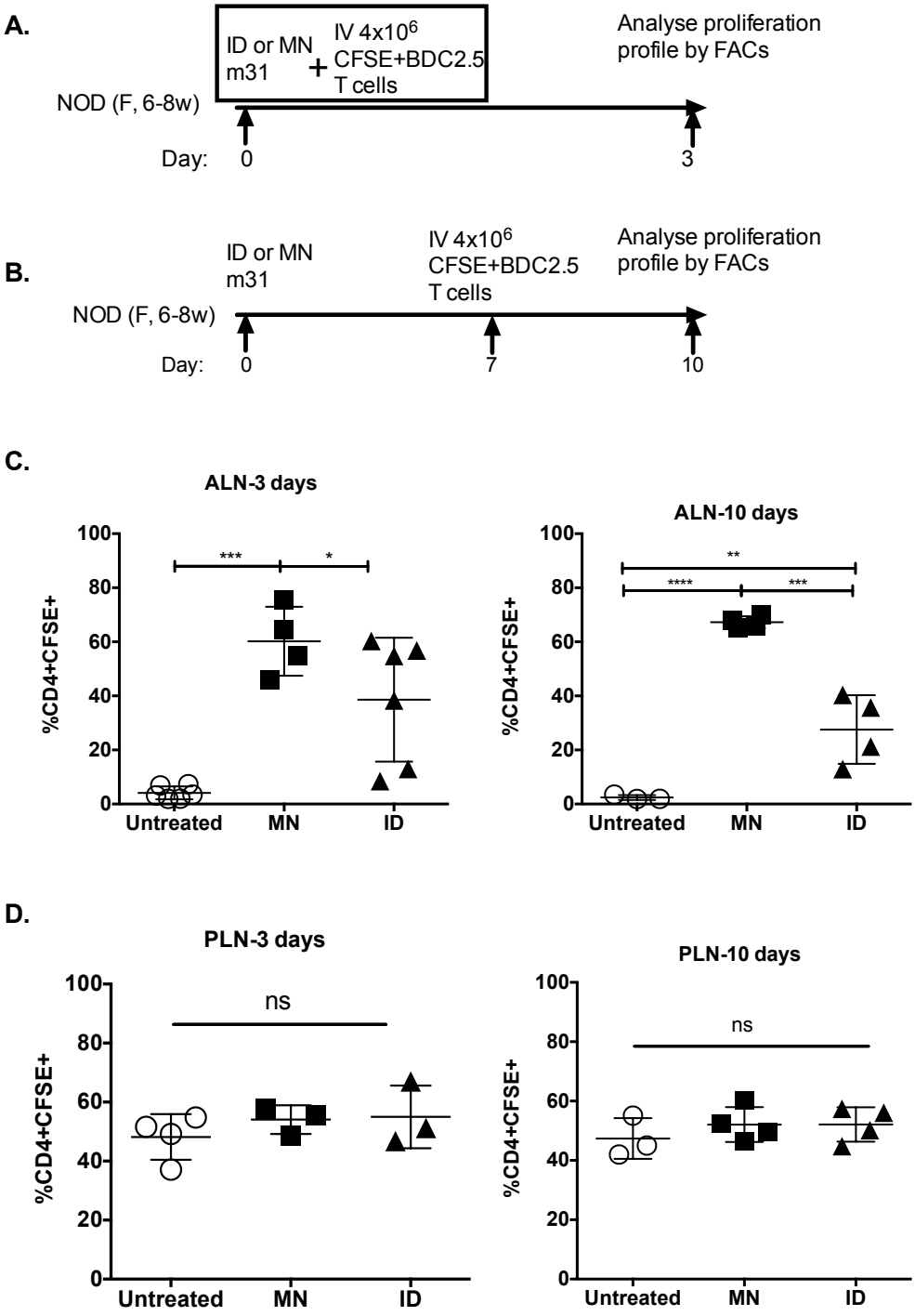

Figure 3.13 Tracking the distribution of m31 *in vivo* using CFSE labelled BDC2.5 T cells. **A.** and **B.** trafficking protocol at 3 or 10 days post m31 administration. BDC2.5 T cell proliferation profile in the ALN **(C.)** or the PLN **(D.)** was analysed 3 or 10 days post m31 administration. n≥3. Mean±SD. One way ANOVA with Tukey post test, *p<0.05, **p<0.01, ***p<0.001, ****p<0.0001. Data were compiled from four separate experiments

3.4.6. Inducing peripheral tolerance *in vivo*

3.4.6.1. Expanding antigen specific Tregs in the BDC2.5 TCR-Tg.Foxp3-FIR mouse

BDC2.5 TCR-Tg.Foxp3-FIR mice were used to determine the effect of administration of antigen WE14 (an endogenous antigen), *in vivo*. WE14, a weak stimulant of BDC2.5 T cells (section 3.4.1. was used to induce tolerance instead of a strong stimulant, m31, which is lethal for monoclonal Tg mouse, i.e. BDC2.5 TCR-Tg mice. BDC2.5 TCR-Tg.Foxp3-FIR mice were injected with 6μg of WE14 and 7 days later the phenotype of the $CD4^+$ cells was analysed (Figure 3.14 A). The $CD4^+Foxp3^+$ was thought to be a Treg marker as has been described in many publications. No significant difference was observed in $CD4^+Foxp3^+$ Treg populations in the PLN, ALN or SP before or after WE14 treatment. The subpopulations of $CD4^+Foxp3^+$ Tregs, such as $CD4^+Foxp3^+CD25^+$ and $CD4^+Foxp3^+CD62L^+$, were increased significantly in the PLNs of the WE14 treated group compared with controls (Figure 3.14 B). However, these two $CD4^+$ T cell subsets comprise a small percentage of the total $CD4^+$ T cell population, approximately 1.5% in the untreated group and 3% in the WE14 treated group. No difference was observed in the Treg population in the ALN or SP.

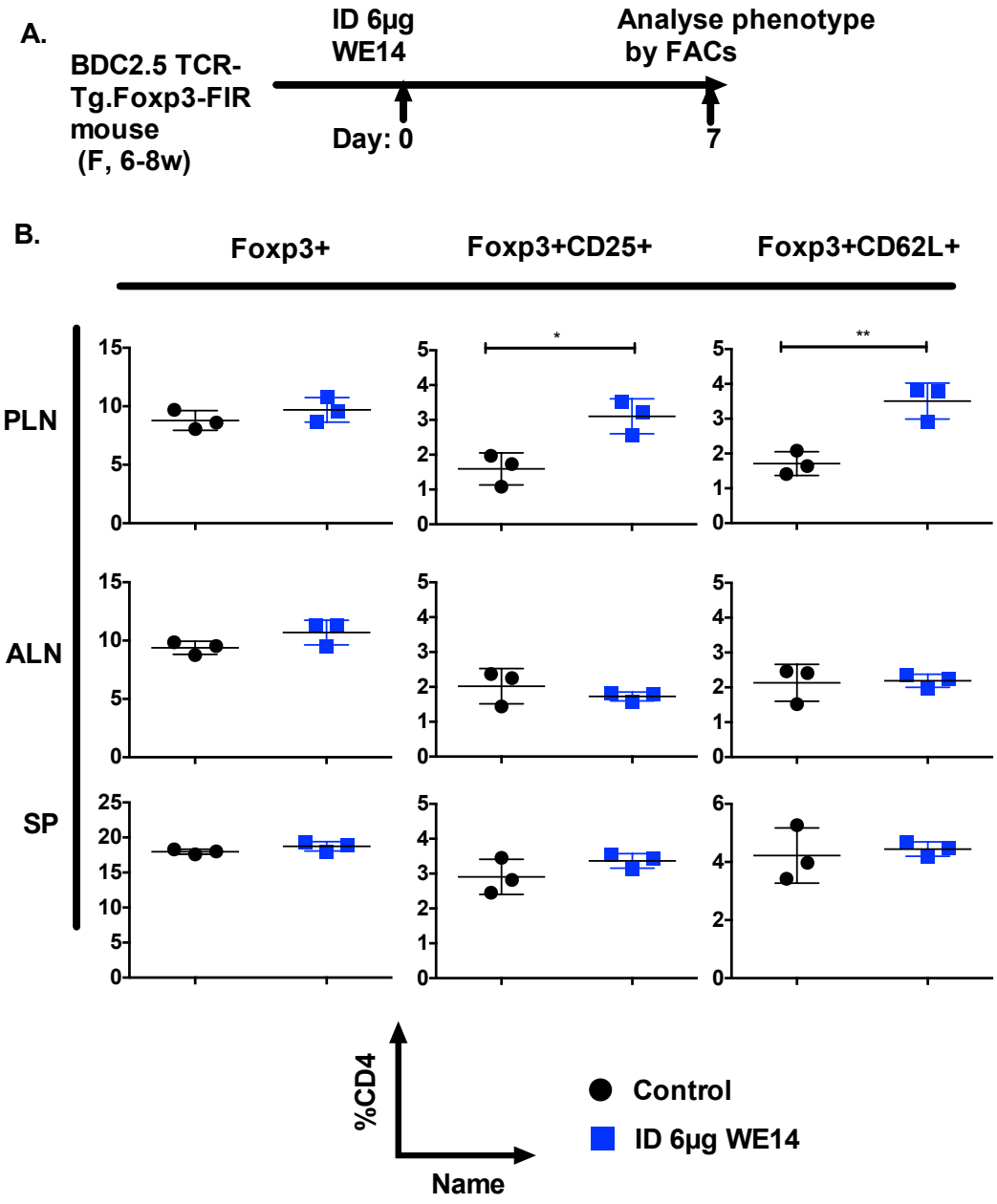

Figure 3.14 Expanded antigen specific Treg cell population in BDC2.5 TCR-Tg.Foxp3-FIR mouse following a single dose of WE14 delivered by ID injection. A. Protocol of expanding Treg *in vivo* in BDC2.5 TCR-Tg.Foxp3-FIR. **B.** $CD4^+$ Treg phenotype before and after WE14 treatment in PLN, ALN and the SP. n=3. Mean±SD. Two tailed t test, * $p<0.05$, ** $p<0.01$

3.4.6.2. $CD4^+Foxp3^+$ BDC2.5 T cells suppress the immune response in vivo

As demonstrated previously, WE14 was able to expand the $CD4^+$ T cell subpopulation, the phenotype of which was categorised as Treg. The next stage

was to determine whether these BDC2.5 T cells with a Treg phenotype possess regulatory function, showing prevention of transferred naïve BDC2.5 T cells from becoming effector T cells in NOD-SCID mouse. Secondly, we are interested in whether this inhibitory effect is TCR specific. In order to investigate the stated question, NOD-SCID mice were adoptively transferred with BDC2.5 T cells or co-transferred with $CD4^{+}Foxp3^{+}$ Tregs from Foxp3-FIR.NOD mice or BDC2.5 TCR-Tg.Foxp3-FIR mice. No change of proliferation profile of the transferred BDC2.5 T cells in NOD-SCID mice was observed when co-transferred with polyclonal $CD4^{+}Foxp3^{+}$ Tregs, compared to NOD-SCID mice without co-transferred with polyclonal Tregs. However, mice that were co-transferred with BDC2.5 $Foxp3^{+}$ Tregs, which shared the same TCR with Teffs (BDC2.5 T cells) showed a clear inhibition of proliferation *in vivo* (Figure 3.15 A). There were no obvious phenotype changes in total BDC2.5 T cell population in all three groups. Interestingly, CFSE labelled BDC2.5 T cells showed some shift in their phenotypes (Figure 3.15. C), with an increased expression of CD62L and decreased expression of CD44. There was also some change in the expression of CD25, however these changes were less clearly demonstrated.

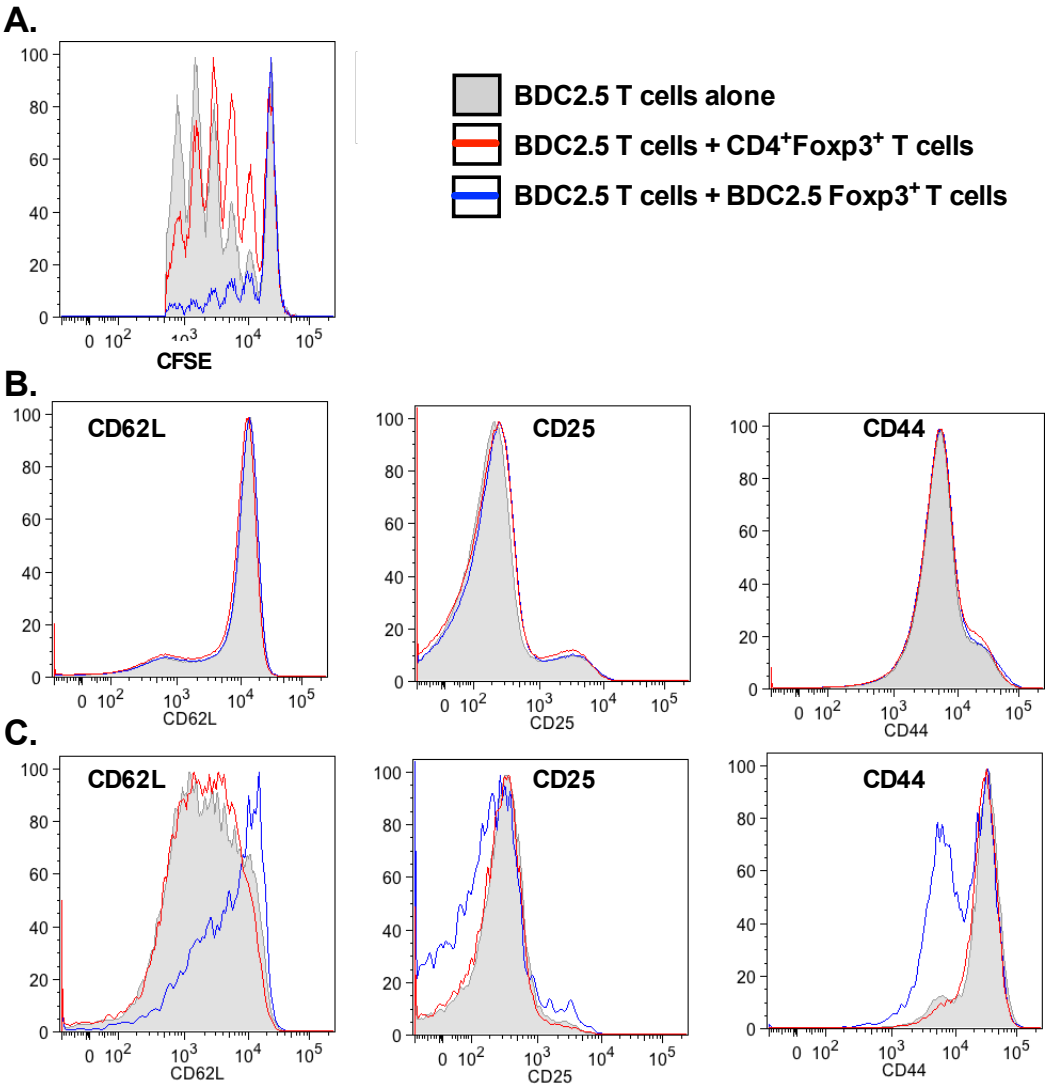

Figure 3.15 BDC2.5 Foxp3$^+$ Tregs suppress the antigen specific immune response *in vivo*. NOD-SCID mice were adoptively transferred with either 1.5x10^6 Foxp3$^+$BDC2.5$^+$ T cells or 1.5x10^6 Foxp3$^+$CD4$^+$ T cells intravenously. Twenty-four hours after the initial transfer, the same mice were co-transferred with 1.5x10^6 CFSE$^+$BDC2.5$^+$ T cells. BDC2.5 T cell proliferation in PLN was then analysed using a Canto II flow cytometer three days after the second cell transfer. **A.** Histogram overlay of CFSE labelled BDC2.5 T cell proliferation profile. Cells were isolated from the PLN of NOD-SCID mice co-transferred with CFSE$^+$ BDC2.5 T cells and Foxp3$^+$ BDC2.5 Tregs. The expression of CD62L, CD25, and CD44 was analysed for either all BDC2.5 T cells (**B**) or CFSE labelled BDC2.5 T cells (**C**).

3.4.6.3. Peripheral tolerance could be induced in NOD mice by using WE14 delivered by solid-coated MNs, showing a dose sparing effect compared to ID injection.

As demonstrated above, antigen specific Tregs were shown to have a suppressive effect on antigen specific Teffs *in vivo*, showing a reduction of transferred Teff proliferation. This provided a tool for understanding whether using an ASI approach to induce tolerance can be applicable in a more comprehensive T1D disease model, NOD mice. It was also important to understand whether a single antigen (rather than an antigen cocktail) could induce tolerance. Therefore, the aim of this section was to investigate whether tolerance can be induced using peptide coated MNs or ID injection in female NOD mice by analysing the proliferation profile of transferred BDC2.5 T cells in the PLN.

NOD mice (Female, 4-5 weeks old) were treated on two occasions with either m31 or WE14, with a three-week interval between treatments. A week after the second treatment, CFSE labelled BDC2.5 T cells were adoptively transferred through the tail vein to determine the proliferation profile (Figure 3.16 A). There was no significant reduction in BDC2.5 T cell proliferation in the PLN when using m31 antigen treatment compared with the untreated group (Figure 3.16 B). When using a 6µg dose of WE14, both solid-coated MNs and ID injection treatment groups showed a reduction in proliferation in the PLN, although only the solid-coated MN treated group showed a statistically significant difference to the control group. In general, 51.3% $CD4^+CFSE^+$ cells proliferated in the PLN of NOD mice without any treatment. After treatment with WE14, the 6µg ID injection showed a 9% reduction in proliferation while the solid-coated MN array treated group showed a 15% reduction. Increasing the WE14 dose further reduced BDC2.5 T cell proliferation. The proliferation of transferred cells was

reduced by 28.53% when the dose delivered by ID injection was increased from 6 µg to 50µg (Figure 3.16 C).

Phenotypic changes were also examined in order to further support the proliferation data. There was no difference observed in the level of $CD25^+$ expression within either intrinsic $CD4^+$ T cells or transferred $CD4^+CFSE^+$ T cell populations (data not shown). In consideration of the previous observation, the $CD62L^+CD44^-$ subpopulation (naïve T cells) was analysed for all $CD4^+CFSE^+$ cells (Figure 3.16 D). Before transfer, on average, 51.5% $CFSE^+CD4^+$ BDC2.5 T cells were shown as $CD62L^+CD44^-$. After transfer to NOD mice, without any treatment, only 22.8% of transferred $CFSE^+CD4^+$ BDC2.5 T cells retained their $CD62L^+CD44^-$ naïve phenotype. A higher percentage of $CFSE^+CD4^+$ BDC2.5 T cells were shown as $CD62L^+CD44^-$ (29.5%) when NOD mice were treated with two rounds of 6µg WE14 using solid-coated MNs (Figure 3.16 E). Using the same dose, WE14 administered by ID injection showed no significant change in BDC2.5 T cell phenotype (23.4%), when compared to the control. By increasing the dose to 50µg (ID), WE14 was shown to be able to preserve a significant proportion of naïve BDC2.5 T cells (35.5%) compared to control and low dose (6µg) groups.

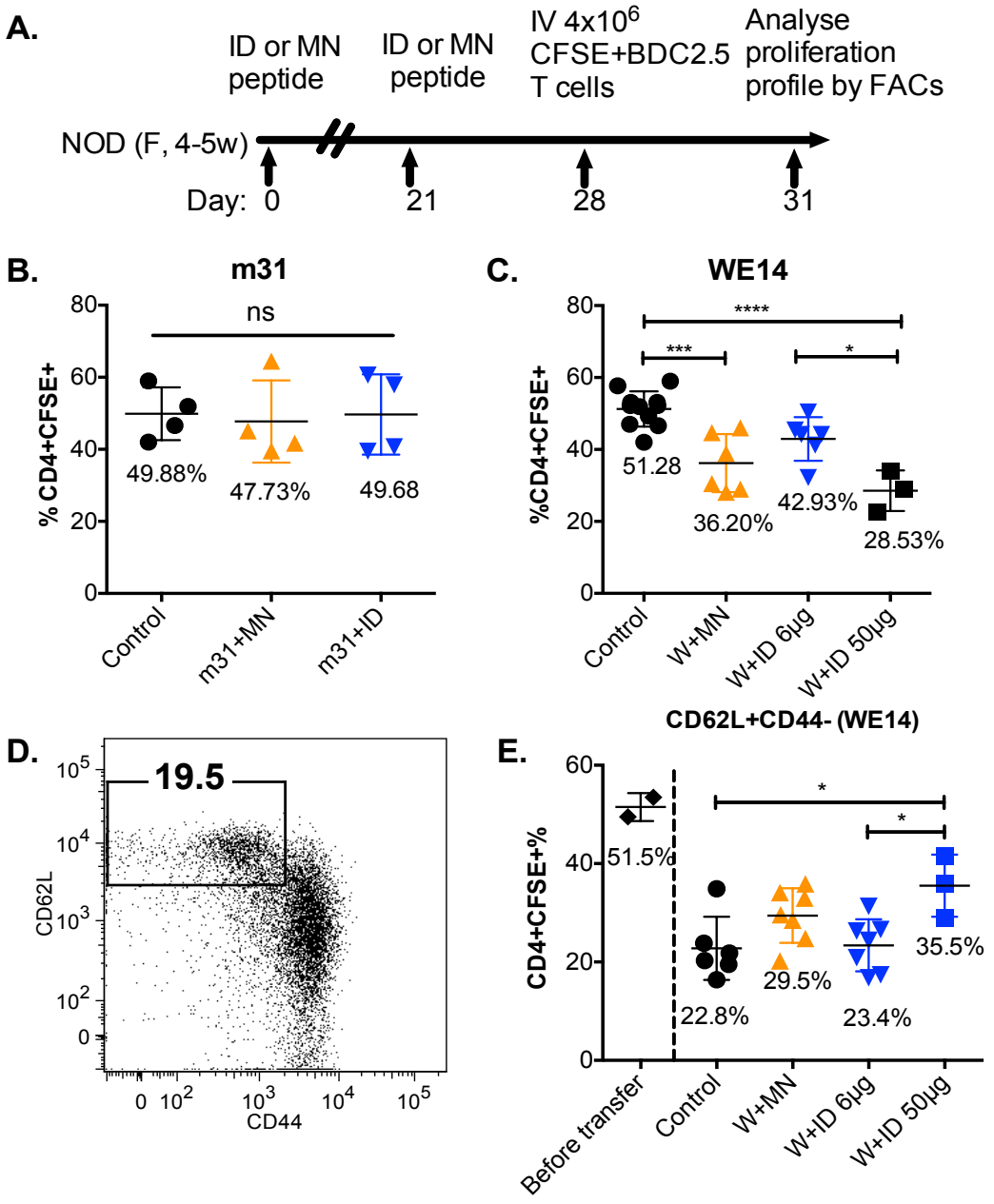

Figure 3.16 Peripheral tolerance was shown to be induced in NOD mice by using WE14 delivered by solid-coated MNs, showing a dose sparing effect compared to ID injection. **A.** Protocol for inducing tolerance in NOD mouse using m31 or WE14. Young female NOD mice were treated with two rounds of peptides and induced tolerance was reflected as a change in the proliferation profile of transferred $CFSE^+BDC2.5^+$ T cells. **B.** Proliferation profile of $CD4^+CFSE^+$ BDC2.5 T cells in the PLN was analysed in mice treated with 2µg of m31 either delivered by ID injection or MNs. **C.** Proliferation profile of $CD4^+CFSE^+$ cells in PLN was analysed in mice treated with 6 or 50µg of WE14 either delivered by ID injection or MNs. **D.** Gating strategy for $CD62L^+CD44^-$ population in $CD4^+CFSE^+$ BDC2.5 T cells. **E.** Phenotypic changes of $CD4^+CFSE^+$ BDC2.5 T cells after transfer to NOD mice with or without WE14 treatment. n≥4. Mean±SD. One way ANOVA with Tukey post test, *p<0.05, ***p<0.001, ****p<0.0001. Data were compiled from five separate experiments. Control=NOD mice without injection of peptides; m31+MN=NOD mice treated with m31 by solid-coated MNs; m31+ID=NOD mice treated with m31 by ID injection; W+MN=NOD mice treated with WE14 by solid-coated MNs; W+ID 6µg= NOD mice treated with 6µg of WE14 by ID injection; W+ID 50µg= NOD mice treated with 50µg of WE14 by ID injection.

3.5. Discussion

3.5.1. Characterization of the BDC2.5-TCR-Tg mouse

It was reported that the TCR of BDC2.5 T cells is composed of Vα1 and Vβ4 subunits (Haskins et al., 1989). A lack of a Vα1 antibody means that the $CD4^+V\beta4^+$ BDC2.5 T cell phenotypic feature was compromised in this project. Approximately 85% of $CD4^+$ T cells from BDC2.5-TCR-Tg mice were shown to be $V\beta4^+$, while in NOD mice only 10% were shown to be $V\beta4^+$. These $CD4^+V\beta4^+$ cells from BDC2.5 TCR-Tg mice were able to react with m31 in the presence of irradiated APC. M31 has been reported to be a strong stimulus for BDC2.5 T cells (Dai et al., 2005). The high reactivity of BDC2.5 T cells to m31 confirmed that the BDC2.5 T cells from mice which were bred in-house, were functional and were comparable with those in the published data. Another peptide, WE14 which has a lower affinity for BDC2.5 TCR has also been tested. At least 50µg/ml of WE14 was needed to promote the proliferation of BDC2.5 T cells *in vitro*. Therefore, because of the higher potency of m31, it was chosen as an indicator peptide to test for BDC2.5 T cell activity and peptide trafficking *in vivo* experiments. Both peptides were tested in the NOD mice for their ability to induce tolerance in following experiments.

3.5.2. Evaluating the effect of coating formulation on m31 bioactivity

IFNγ is a pro-inflammatory cytokine mainly secreted by Th1 and cytotoxic T cells or NK (natural killer) cells when they are activated by antigens, mitogens, or alloantigens (Schroder et al., 2004). M31 bioactivity was therefore quantified by culturing BDC2.5 T cells in the presence of m31 and quantifying IFNγ in the culture supernatant using ELISA. This was used to assess the bioactivity of m31 in a solid-coated MN coating formulation. There was no significant difference between coating formulation and the m31 PBS controls, as shown in Figure 3.3.

This indicates that the m31 did not lose its bioactivity during the formulation, preparation, storage or coating processes. Blank formulation, i.e. PVA2000 alone, did not trigger any non-specific proinflammatory immune response. PVA2000 is known to be a useful excipient for *in vivo* and *in vitro* medical applications due to its documented stability, biocompatibility and low toxicity (Alexandre et al., 2014). Low IFNγ levels therefore indicated that PVA did not cause a significant inflammatory response when it is used in a solid-coated MN formulation. Therefore, we would expect PVA 2000 to have a negligible effect in terms of its ability to trigger an inflammatory immune response in the *in vivo* experiments. This provides a safe foundation for solid-coated MN for inducing tolerance in the following experiments.

3.5.3. Pharmacokinetics of peptide administered by solid-coated MNs or ID injection

3.5.3.1. Factors that influence the in vivo clearance of peptides from mouse skin

One of the objectives of this project was to target skin DCs using different administration methods. It was thought that the longer the peptide remains in the skin the more likely it is that peptide can be taken up by skin DCs, especially LCs which have a slow migration rate and low regeneration rate ((Kissenpfennig et al., 2005, Rattanapak et al., 2014)). Therefore, it is necessary to understand the factors that influence the clearance of peptide from the local skin environment.

Body temperature was shown to be a factor which could influence local clearance of the peptide (Neelam, 2012). M31 was shown to be cleared from the skin more quickly when mice were kept at 30˚C rather than at 22˚C during a 24-hour monitoring period (Figure 3.6 A, Figure 3.7 A). This could be because an increase in temperature can increase the blood flow in the microcirculation of the

skin, which in turn increases the diffusion and distribution rate of compounds from the skin to the circulatory system (Neelam, 2012, Trabaris et al., 2012). In order to maintain experimental stability, mice were therefore kept at 22±1˚C in subsequent experiments.

Solubility of the drug itself and the administration route used were other factors which influence the clearance of peptides from the skin. The fluorescent signal of the peptide with higher solubility (WE14-5TAMRA) had declined more quickly than the lower solubility peptide (m31- 5TAMRA) four hours post administration by ID injection (Figure 3.6 B), however, no significant change in the AUC was observed (Figure 3.7 B). This may be because when using ID injection, WE14-5TAMRA and m31-5TAMRA were already in solution, which results in the effect caused by solubility difference being eliminated. Therefore, the rate of peptide diffusion from the skin to systemic circulation was the main contributor to the skin clearance rate. On the other hand, peptides delivered by solid-coated MN showed a different clearance profile. There are two factors, which may contribute to the skin clearance of peptides when using solid-coated MNs: dissolution rate and diffusion rate. Both rates were correlated with the solubility of peptide. Therefore, peptide with low solubility would remain in the skin longer over a 24-hour monitoring period than a more soluble peptide, which is reflected in significant differences on AUC, which inversely correlates with the overall clearance rate.

One of the striking observations was that the administration method was shown to be a major contributory factor to the rate of skin clearance. Compared with a matching dosage administered by ID injection, peptides, either m31-5TAMRA or WE14-5TAMRA, delivered using solid-coated MNs cleared from skin significantly more slowly than the same peptide delivered via ID injection (Figure 3.7 B). As

discussed above, the skin clearance rate of peptide administered by MN was determined by dissolution rate and diffusion rate. On the other hand, clearance following ID delivery was mainly determined by diffusion. When m31-5TAMRA or WE14-5TAMRA were delivered by solid-coated MNs, peptide concentration reached saturation in the local area of tissue due to the limited solubility of peptide in a restricted skin area. Therefore, any excess delivered peptide would remain in the solid state, thus acting as a reservoir and prolonging delivery. The rise of RNI one hour after solid-coated MN delivery further supports the hypothesis that peptide was delivered to the skin in the solid state. The excitation and emission pair of 5-TAMRA is different in solid state and in aqueous phase. The detector pair in the Kodak *in vivo* imaging system was set at 553nm/576nm, which does not image the solid-fraction of delivered peptide-5TAMRA. Another potential explanation for the rise of NRI is that the relatively densely packed probe (solid state) could have a self-quenching effect (Christie et al., 2009, Kuzmanich et al., 2011). Solid-state m31-TAMRA or WE14-TAMRA dissolves within the skin compartment due to tissue hydration, which results in a rise of RNI one hour after solid-coated MN treatment. The pocket deposition effect of solid-coated MNs therefore provides a prolonged release profile of peptide compared with ID injection. This results in slower skin clearance of peptide (Figure 3.7 B). The slowed release of peptide within skin enables skin DCs expose to the peptide for longer. This prolonged exposure time further enhanced the chance of the skin DCs uptake peptide/autoantigen (as discussed in section 3.5.3.2.).

In order to precondition the skin, a topical application of BD cream was used. GCs are a group of common immunosuppressive and anti-inflammatory drugs. Local treatment with GCs can influence the maturation of DCs and thereby induce Tregs (Kerzerho et al., 2012, Stary et al., 2011b, Koopman et al., 2001,

Pan et al., 2001a). The mechanism by which GCs induce Tregs is related to its dosage, local/systemic metabolism, and cell signalling. Short-term topical application of GC treatment is well tolerated, however long term treatment may cause a loss of Langerhans cells in the epidermis (Furue and Katz, 1989a, Belsito et al., 1982a, Ashworth et al., 1988, Grabbe et al., 1995). Within a short treatment window (24 hours) topical application of BD cream was shown to down regulate expression of HLA DR on human epidermal cells (Section 4.4.1.1.). BD cream was also shown to increase the secretion of IL10 in mouse epidermal cells (Section 4.4.1.3.).

In the first hour post treatment, a rapid decline of NRI was observed when mice were pre-treated with topical BD cream followed by ID injection of m31-5TAMRA (Figure 3.6 C). Increased liquid flux space created by ID injection together with the hydration effect created by the BD cream may have caused the increased rate of skin clearance. In order to minimise the hydration effect, dry peptide was delivered using coated MNs. With BD cream pre-treatment, a higher NRI is observed initially, which may be due to an increased rate of dissolution in the hydrated skin. This hydration effect caused by BD cream did not show a significant influence on the clearance of peptide over time when administered by solid-coated MNs. Although short term pre-treatment of BD cream showed some effect on clearance curve at individual time points, the hydration effect, did not show a significant effect on the overall skin clearance of peptide, which suggests that skin hydration, caused by the BD cream, was not the main factor in determining the rate of skin clearance of peptide (Figure 3.7 B). This finding provided the additional support for the use of BD cream in combined therapy with solid-coated MN for ASI.

3.5.3.2. Trafficking of the m31 peptide in vivo

As discussed in Section 3.5.4.2, solid-coated MN delivery was shown to prolong the retention of peptides within the skin. Therefore, it is important to understand how this prolonged effect influences local antigen presentation within the skin and whether this could result in different peptide trafficking.

In NOD mice, BDC2.5 T cells recognise antigens from the islet of Langerhans and therefore proliferate in the pancreas draining LNs, PLNs. When a strong stimulus such as m31 was introduced through the skin, BDC2.5 T cells also proliferated in the ALN, therefore confirming the exogenous nature of this antigen. One interesting observation was that BDC2.5 T cells proliferated more strongly when using MNs as a delivery method as compared to ID injection. This raised two questions: 1. Why, when using the same dose of peptide, did MN administration induce a greater proportion of antigen specific T cells to proliferate than ID administration? 2. How long does the peptide remain in the skin when using the two different methods of administration? The possible explanations are discussed next.

After delivery, peptides were trafficked to all secondary lymphoid organs within a few hours following ID injection in an *in vitro* study (data not shown). However, our *in vivo* study showed that BDC2.5 T cells only proliferated in the local skin draining LNs. In order to prime T cells in LNs, the antigen must first be taken up by DCs, which then migrate to the lymph nodes through the lymphatic vessels (Randolph et al., 2005). The observed presence of peptide in the local skin draining LNs may be explained by the migration of the peptide carrying DCs from skin to LNs. These DCs then present the peptide, rather than un-associated peptide trafficking, to T cells in LNs.

One potential explanation for increased proliferation in MN treated mice is that the MNs can target skin DCs more efficiently than ID injection, thereby inducing relatively higher levels of proliferation for the same dose of delivered peptide. When using the mouse skin model, solid-coated MN delivery can target both LCs in the epidermal layer and DCs in the dermal layer, as described previously (Section 2.4.1.2.). ID injection was by comparison more likely to deliver peptide to the deep dermal layer or even subcutaneously. Skin DCs can therefore be targeted more efficiently by using MN delivery and were thus exposed to more m31 peptide per dose when the peptide was delivered by MN. One study revealed that skin DCs are able to take up peptide between 40 and 360 minutes post treatment (Rattanapak et al., 2014). Skin DCs have also been observed in the draining LNs just 24 hours after the skin was painted with Rhodamine B (Randolph et al., 2005). These studies suggest that the kinetics of skin DC activity (uptake and migration) could contribute to our observed differences in the method of peptide delivery. Previous skin clearance data suggests that most peptide is cleared from the skin within 4 hours post ID injection, which limits the time available for antigen uptake. However skin DCs were exposed to m31 for a prolonged time when using the solid-coated MN delivery method, thus increasing the opportunity for antigen uptake and enabling more DCs to encounter the peptide. Epidermal LCs have different kinetics compared to dermal DCs. LCs showed a delayed migration compared with dermal DCs under inflammatory conditions (Kissenpfennig et al., 2005). This may imply that using a MN to induce tolerance is particularly beneficial when targeting tolerogenic epidermal LCs, due to the prolonged release profile.

An extended *in vivo* tracking study was also undertaken to provide further understanding of the benefit of using solid-coated MNs in skin targeted delivery. A proliferation profile of BDC2.5 T cells in the ALN was observed 10 days post

m31 delivery (Figure 3.13 D). A kinetic result has shown that antigen bearing LCs remained in the epidermis for 10 days after sensitization with Rhodamine B (van Wilsem et al., 1994). Therefore, the persistent response observed in our studies could be due to residual trace m31 in the skin and/or m31 bearing DCs that remain in the skin. In both 3 and 10-day trafficking studies, solid-coated MN delivery showed a more consistent response than ID injection between treatments. This can be explained by more targeted and persistent skin DC delivery when using MN rather than using ID injection. This prolonged exposure time may not only enhance the uptake, but may also reduce the trauma caused by repeated dosing, which reduces the chance of generating an inflammatory signal and therefore further benefits ASI approach.

3.5.4. Optimise CFSE labelling protocol for the analysis of cell proliferation

CFDA-SE is a well-documented cell tracing dye. After diffusion into the cell, CFDA-SE is cleaved by esterase enzymes and becomes CFSE, an amine reactive product. CFSE binds to lysine residues and has been used to analyse cell division by tracking the dilution of CFSE fluorescent intensity (Quah and Parish, 2012). CFSE, however, can be toxic to cells and may inhibit cell proliferation (Quah et al., 2007, Quah and Parish, 2012). The aforementioned article states that the degree of toxicity may differ for different cell types, therefore it was necessary to optimise the labelling protocol for BDC2.5 T cells.

In order to obtain good resolution of division peaks, 20μM CFDA-SE was used for 10^7 cells /ml. This is much higher than the manufacturers suggested concentration of 5μM, and could therefore result in an increased risk of toxicity. 10%v/v FCS was used to buffer the toxicity of CFSE during the labelling process and results showed that using optimised conditions, BDC2.5 T cells were still

functional and proliferated after labelling. Transferred BDC2.5 T cells showed proliferation for between 5-6 generations over three days *in vivo*. Transferred cell numbers for *in vivo* study were also titrated (Figure 3.11).

Tregs constitute a small proportion of the total T cell population in NOD mice (approximately 5% in circulation) (Kukreja et al., 2002, Girvin et al., 2000). In experiments that have attempted to show the suppressive effect of Tregs, the Treg:Teff ratio was set as high as 1:1. This was thought due to the low frequency of antigen specific Tregs in the polyclonal NOD mouse. It has also been shown that a reduced Treg:Teff ratio (<1:10) is appropriate when using a monoclonal BDC2.5-TCR-Tg mouse (Tang et al., 2004). In this project, it was shown that $Foxp3^{+}CD4^{+}$ T cells (nTreg) from a NOD mouse (polyclonal T cells) were not able to suppress proliferation of BDC2.5 T cells in SCID mice, but suppression was observed when using $Foxp3^{+}CD4^{+}$ BDC2.5 T cells (Figure 3.15).

The hypothesis for this project was that it would be possible to induce/expand peripheral antigen specific Tregs to generate peripheral tolerance using an autoantigen. However, expanding Tregs *in vivo* has proved to be difficult due to their anergic nature (Walker, 2004). As the antigen specific Tregs are anergic and low in frequency, the tolerance readout needs to be optimised in order to generate meaningful results. In this study iTreg induced tolerance is indicated by reducing the proliferation of antigen specific Teffs. CFSE labelled BDC2.5 T cells were used as responder cells to demonstrate the effect of the induced Treg population. However, due to the strongly diabetogenic nature of BDC2.5 T cells, it was necessary to titrate the transferred BDC2.5 cell number in order to enable the induced Tregs to generate a meaningful result.

A lower limitation was imposed by the need to provide a large enough initial (transferred) cell population to ensure resolution of cell division in subsequent generations. Results demonstrated that CFSE labelled BDC2.5 T cells could produce a clear proliferation profile, which was easily resolved for 5 to 6 generations in the PLNs of NOD mice transferred with $4x10^6$ BDC2.5 cells. Therefore, the proliferation of transferred $4x10^6$ BDC2.5 cells in the PLN of untreated NOD mice was calculated to provide a base line as an intrinsic response of BDC2.5 T cells to endogenous antigen from pancreas. If peptide delivered by MNs or ID injection induce antigen specific Tregs, these Tregs will home back to the site where the inflammation initiated, i.e. the pancreas, and its draining LN, PLN (Chow et al., 2015) The induced antigen specific peripheral tolerance could then be reflected as a reduced proliferation in PLN compare to the base line proliferation in untreated NOD mice as showed in following section.

3.5.5. Peripheral tolerance could be induced in NOD mice by using WE14 delivered by solid-coated MNs, showing a dose-sparing effect[1] compared to ID injection.

The m31 peptide has a strong affinity with MHCII and BDC2.5 TCR. BDC2.5 T cells pulsed with m31 *in vitro* can accelerate diabetes when introduced into NOD and SCID mice (Christianson et al., 1993). When m31 was injected into a BDC2.5-TCR-Tg mouse, it stimulated a fatal immune response. This could be due to the monoclonal diabetogenic T cells response in the BDC2.5-TCR-Tg mouse and the lack of other tolerogenic mechanisms. On the other hand, WE14 is a weak epitope of BDC2.5-TCR, and therefore this did not cause any adverse

[1] The term Dose-sparing effect herein refers to an improved therapeutic effect using a comparison dose. In this case solid-coated MN was able to improve induced peripheral tolerance compared to ID injection using the same dose, 6µg WE14, resulting in reduced BDC2.5 T cell proliferation in NOD mice.

effects to the BDC2.5-TCR-Tg mice. After treatment with WE14, two CD4 subpopulations, $CD4^+CD25^+Foxp3^+$ and $CD4^+CD62L^+Foxp3^+$, were increased compared to the untreated group. $CD4^+CD25^+Foxp3^+$ T cells are Tregs that can either be generated naturally or can be induced in the periphery. They can suppress antigen specific Teffs in a cell-cell contact fashion (Chatenoud, 2011, Feuerer et al., 2009). These $Foxp3^+CD4^+CD25^+$ BDC2.5 T cells were shown to prevent the progression of T1D in NOD mice (Jaeckel et al., 2005). Absence of $CD4^+CD25^+Foxp3^+$ Treg accelerates T1D in NOD mice, and recovery of antigen specific $CD4^+CD25^+Foxp3^+$ Treg could restore the balance (Brode et al., 2006). CD62L (L-selectin) is an adhesion molecule which is expressed on Leukocytes and regulates lymphocyte homing to secondary lymphoid organs (Bevilacqua et al., 1991). A low frequency of $CD62L^+$ Tregs is associated with T1D in both mouse models and human patients (Ryba et al., 2011, Kaminitz et al., 2014). Here, we have shown that WE14 was able to induce these antigen specific Tregs in the TCR-Tg mouse. This ability to induce both types of Tregs in BDC2.5-TCR-Tg mouse *in vivo*, indicates that WE14 could potentially be used as a therapeutic antigen for inducing tolerance.

To prove that $CD4^+Foxp3^+$ BDC2.5 Tregs are functional, SCID mice were co-transferred with $CD4^+Foxp3^+$ BDC2.5 Tregs and CFSE labelled BDC2.5 T cells. Subpopulations of $CD62L^+$ or $CD25^+$ of $CD4^+Foxp3^+$ cells were not sorted due to the low frequency of these two populations. In SCID mice, reduced proliferation was observed when using a 1:1 ratio of antigen specific $CD4^+Foxp3^+$ Treg to Teff rather than using polyclonal Tregs. This finding agreed with previous publications in regard to the role of antigen specific Tregs in suppressing Teffs. *In vitro* expanded BDC2.5 Tregs could suppress Teffs in a ratio as low as 1:9 in a $NOD.RAG^{-/-}$ transfer experiment,resulting in controlled blood glucose level of below 250mg/dL over a 105 day monitoring period (Tang et al., 2004). It has

also been reported that antigen specific Tregs were more effective than polyclonal Tregs in inducing tolerance to prevent the progression of T1D in $CD28^{-/-}$ NOD mice (Masteller et al., 2005). These publications together with the findings of this study suggest that if the proliferation of transferred BDC2.5 T cells were suppressed in NOD recipients, the Treg/tolerance induced is antigen specific.

Having demonstrated that it was possible to generate Tregs using WE14 in a monoclonal background, it was then important to demonstrate that WE14 could be administered intradermally to generate antigen specific Tregs *in vivo* in a polyclonal background. The use of WE14 to induce tolerance *in vivo* has previously been reported. In one investigation, splenocytes and cells from the PLN were taken from NOD mice, which had previously been injected intraperitoneally with either 50 or 100µg of WE14 and incomplete Freund's adjuvant. These cells showed a suppressive effect on inflammatory response in both $CD4^+$ and $CD8^+$ T cells *in vitro* (Haskins et al., 2012). They also showed that splenocytes from WE14-treated NOD mice can delay disease progression in SCID mice. Tolerance induced by WE14 can influence/reduce the recruitment and expansion of BDC2.5 T cells in the PLN, which was reflected in the rate of BDC2.5 proliferation in the PLN. Using skin targeted delivery by solid-coated MNs, a much lower dose of WE14 could be used (6µg on average) to achieve a similar outcome, due to the improved targeting of skin DCs. In our experiments significant suppression of BDC2.5 proliferation was observed when NOD mice were treated with WE14 solid-coated MNs. A reduced proliferation profile was also observed when using ID injection, but it was not as efficient as solid-coated MN administration. This could be due to the prolonged release of peptide in skin when using solid-coated MNs delivery, which can target skin DCs more efficiently than ID injection, as discussed in Section 3.5.3. This targeted and prolonged

delivery using solid-coated MNs provides a dose sparing effect in inducing tolerance when compared to ID injection. This is the first report on the dose sparing effect of solid-coated MN used to inducing tolerance. Other reports have previously demonstrated that MNs provide a dose sparing effect for vaccination applications (Kenney et al., 2004, Van Damme et al., 2009).

Apart from administration route, WE14 dosage was another factor that influenced the activation of transferred BDC2.5 T cells. Using ID injection, high dose (50µg) WE14 showed 16% greater reduction of proliferation than a low dose (6µg). Transferred cells also experienced a phenotypic shift, which was shown to be paired with their proliferation ability. When cells were recruited to the PLN, they lose L-selectin, resulting in half of transferred cells losing their naïve ($CD62L^{+}CD44^{-}$) state and becoming activated. Where tolerance was induced using WE14, more transferred T cells remained in their naïve state. As one of the functions of Tregs is to prevent the activation of naïve T cells through tolerogenic DCs (section 1.4.1.2), the preserved naïve T cell population further suggests that tolerance was induced using WE14.

3.6. Conclusion

Experiments in this chapter demonstrate that the MN coating formulation used does not alter peptide activity during the formulation preparation, coating and decoating processes. The excipient used in the formulation, specifically PVA2000, did not cause any non-specific inflammatory immune response, in the amounts that it was used.

Several factors influence the skin local pharmacokinetics of the delivered peptide, such as the environmental temperature, delivery method, hydration effect and hydrophobicity of the peptide. Increased environmental temperature increased the skin clearance rate of m31-5TAMRA which could be due to the increased microcirculation. It was shown that the administration route was the main factor that controls the peptide skin clearance rate. Peptide delivered by MNs using a solid-coated formulation remained in the skin significantly longer than a peptide solution delivered using ID injection. Another important contribution to the skin clearance of peptide is the solubility of peptides. Preconditioning of the skin using a BD cream was not shown to have any significant influence on the local kinetics. The clearance differences observed between delivery routes were then further tested to examine their effect on local antigen presentation and on inducing tolerance.

A prolonged release was reflected in an increased proliferation profile for BDC2.5 T cells in the draining LN at both 3 and 10 days post solid-coated MN treatment. MN administration of a solid-coated peptide formulation can therefore target skin DCs more effectively than ID injection of a peptide solution, thereby allowing for lower dosages to be used to induce tolerogenic effects, which can in turn reduce

the risk of inducing an undesirable proinflammatory immune response or causing systemic effects.

Using a low potency epitope; WE14, two types of Tregs, $CD4^+CD25^+Foxp3^+$ and $CD4^+CD62L^+Foxp3^+$ were shown to be induced *in vivo* in BDC2.5 TCR-Tg mice. These $CD4^+Foxp3^+$ BDC2.5 T cells were shown to suppress BDC2.5 T cell proliferation in the NOD-SCID mouse. It is therefore logical to use WE14 to induce peripheral tolerance. This is the first demonstration that intradermal delivery of WE14 using solid-coated MNs and ID injection can induce peripheral tolerance in a NOD mouse, resulting in a reduced proliferation profile of BDC2.5 T cells and preservation of $CD4^+CD62L^+CD44^+$ Naïve T cell populations Although both solid-coated MNs and ID injection can promote peripheral tolerance, results clearly demonstrated that MN administration was more reproducible and effective than ID injection. Furthermore, this induced antigen specific tolerance was dose responsive, showing a reduced proliferation when using higher dose, 50µg.

Chapter 4 Effect of short term topical Betamethasone on ASI

4.1. Introduction

4.1.1. Topical glucocorticoid and its local effect on immune cells

Glucocorticoids (GCs) are a class of small lipophilic compounds, which have medical use as steroid hormones. They are commonly used as anti-inflammatory or immunosuppressant drugs for the treatment of diseases such as asthma, rheumatoid arthritis, and inflammatory bowel disease. GCs exert their anti-inflammatory effect through binding with GC receptors within cells, which in turn regulate pro-inflammatory gene transcription (Danielsen et al., 1987, Barnes, 1998, Rhen and Cidlowski, 2005, Coutinho and Chapman, 2011).

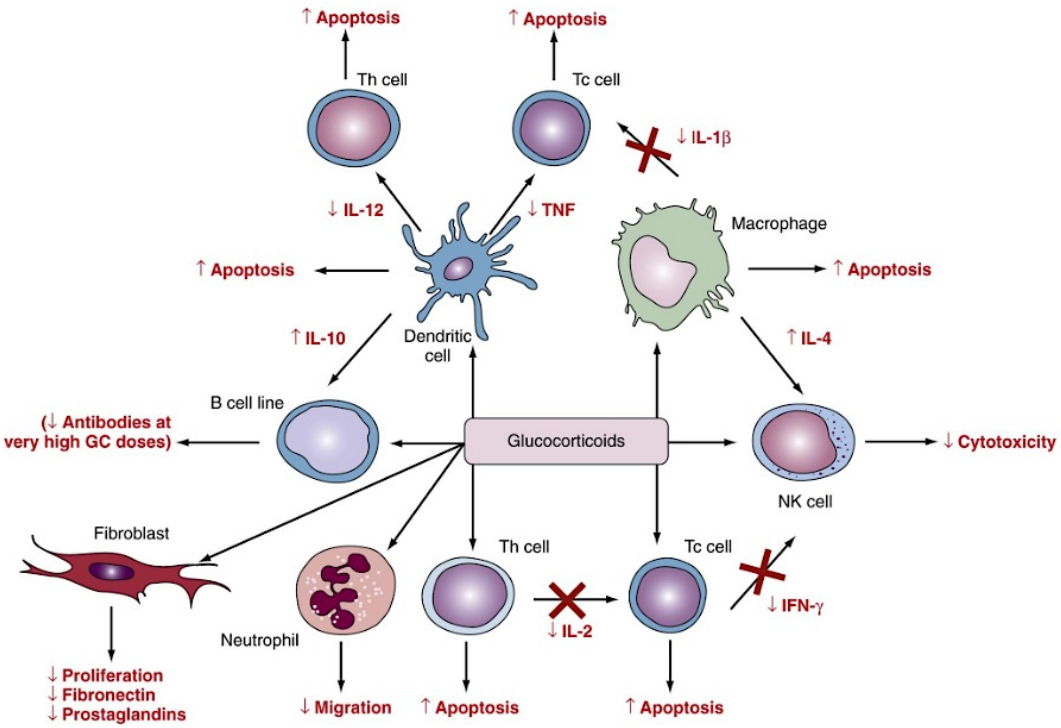

Figure 4.1 Basic mechanisms of action for GCs on immune cells. The GC receptor is widely expressed on cells such as DCs, T cells, B cells, NK cells, neutrophils, macrophages and fibroblasts. By binding to their receptors, GCs can suppress the immune response by inducing apoptosis either directly or indirectly, down regulating inflammatory cytokines, up regulating regulatory cytokines, and preventing proliferation either directly or indirectly (Gary, 2013).

4.1.1.1. Effect on DCs

GCs can suppress immune responses by changing the phenotype and functionality of DCs, which are mediatory cells, which create an important bridge between innate and adaptive immune systems. Maturation of DCs can be suppressed by GCs both *in vitro* and *in vivo*. In mouse studies, DCs, which have been treated with a GC, remain in an immature state when encountering an antigen and consequently show an impaired ability to stimulate T cells (Piemonti et al., 1999b, Moser et al., 1995). After co-culturing with GCs (betamethasone or dexamethasone), monocyte-derived human DCs showed an impaired stimulation of T cells, which was dose related (Kalthoff et al., 2003). Human DCs derived from cord blood showed a reduced expression of HLA DR and co-stimulators (CD86, CD83, and CD40) when co-cultured with GCs (Larange et al., 2012).

GCs also showed an inhibitory effect on antigen presentation of DCs through the MHCII pathway (Pan et al., 2001b). For epidermal LCs, GCs have the ability to promote production of tolerogenic cytokines and can induce Tregs *in vitro* (Stary et al., 2011a). Cytokine production was shown to be regulated by GCs by reducing pro-inflammatory cytokines, and promoting IL10 secretion (Almawi et al., 1996, Piemonti et al., 1999b). The combination of these mechanisms might contribute to inducing tolerogenic DCs (tol-DC) using GCs.

4.1.1.2. Betamethasone

Betamethasone is a potent synthetic GC that has been widely used as anti-inflammatory and immunosuppressive drug (Table 1.2). Its dipropionate form (betamethasone dipropionate, BD), which has poor water solubility but high skin penetration, has been used as a topical treatment for diseases such as allergic rhinitis, psoriasis, tinea pedis and dermatitis (Edwards, 1995, Menter et al., 2009, Smith et al., 1992, Lebrun-Vignes et al., 2000). For systemic treatment, a more soluble form is used, such as betamethasone disodium phosphate (BSP).

Our hypothesis for this section of the thesis is that topical betamethasone would precondition the skin to induce tol-DCs and thus enhance peptide specific immunotherapy.

Table 4.1 Potency and pharmacodynamics of betamethasone compared with other GCs. Betamethasone is a very potent and long acting GC with a biological half-life of between 36-54 hours (Gary, 2013).

	Equivalent Glucocorticoid Dose (mg)	Relative Glucocorticoid Activity	Relative Mineralo-corticoid Activity*	Plasma Half-Life (hour)	Biologic Half-Life (hour)
Short-Acting					
Cortisone	25	0.8	0.8	0.5	8-12
Cortisol	20	1	1	1.5-2	8-12
Intermediate-Acting					
Methylprednisolone	4	5	0.5	>3.5	18-36
Prednisolone	5	4	0.6	2.1-3.5	18-36
Prednisone	5	4	0.6	3.4-3.8	18-36
Triamcinolone	4	5	0	2->5	18-36
Long-Acting					
Dexamethasone	0.75	20-30	0	3-4.5	36-54
Betamethasone	0.6	20-30	0	3-5	36-54

4.2. Objectives

The aim of this chapter was to determine whether short-term topical BD treatment could condition skin DCs and create a tolerogenic environment, which would enhance the effect of ASI. The specific objectives of this chapter were set as follows:

- To investigate the effect of short term (two day) topical BD cream treatment on mouse epidermal cells, by analysing the change in IL10 levels in culture media.
- To investigate the effect of a single dose of topical BD cream vs a single application of betamethasone disodium phosphate (BSP) coated MNs on human epidermal cells The effect of this treatment was analysed by:
    a. Characterising epidermal DC phenotype with or without BD cream treatment by flow cytometry.
    b. Examining whether BD treatment affects the proliferation of MLR.
    c. Analysing the secretion of IL10 in MLR by BD and non-BD treated epdermal cells.
- To examine the effect of short term topical BD cream treatment on induction of tolDCs by analysing BDC2.5 T cell proliferation in skin draining LN (ALN) after m31 delivered either by MN or ID injection
- Examining the local and systemic effects of short term BD cream treatment on T cells and DCs in the lymphoid organs of NOD mouse by examining changes in the T cell and DC populations and phenotypes.
- Exploring the effect of short term topical BD cream on ASI *in vivo* using a BDC2.5 proliferation tolerance assay.

4.3. Methods

4.3.1. Preparation of human epidermal cells

All human skin samples were obtained from female patients undergoing mastectomy or breast reduction surgery with informed patient consent and local ethical committee approval.

Subcutaneous fat and most of the dermal layer was removed using a pair of surgical scissors leaving a thin layer of upper dermis and epidermis. The epidermal piece was then cut into thin strips and cultured in an enzyme cocktail (RPMI 1640 supplemented with 1mg/ml collagenase D, 20U/ml DNase I and 2.5mg/ml Dispase II) at 37˚C for 30-45 minutes. The epidermis was then peeled away from the upper dermis using a pair of fine forceps. Residual enzymes were neutralised by floating the piece of epidermis in 2mM EDTA/PBS solution. In order to obtain a single epidermal cell suspension, the epidermis pieces were incubated in 5 ml 0.25% trypsin (0.02% EDTA) at 37˚C for 35 minutes. After incubation, epidermal cells were released from the epidermal pieces by agitating using a 1 ml pipette. Trypsin was then neutralised by adding 5 ml of 1mg/ml soybean trypsin inhibitor solution. Cells were pelleted at 400G for 10 minutes and suspended in 0.025% DNase, 10%v/v FCS in PBS, then incubated at 37˚C for 1hr. Epidermal cells were filtered through a 70µm cell strainer into a 50ml falcon tube. Cells were pelleted at 400G for 5 minutes and washed twice with RPMI 1640 supplemented with 10%v/v FCS. For subsequent use, cells were centrifuged at 400G for 5 minutes and the supernatant was discarded.

4.3.2. Human peripheral blood mononuclear cell (PBMC) preparation

All human blood samples were obtained from healthy blood donors under informed donor consent and local ethical committee approval.

Peripheral blood (20ml) from a healthy donor was taken and placed into a 50 ml falcon tube prefilled with 500 units of heparin. The heparin was then mixed thoroughly with the blood by gently swirling. The blood was then mixed with 25 ml RPMI 1640 media supplemented with 1%v/v L-glutamine and 1%v/v Antibiotic-Antimycotic (100 units/mL of penicillin, 100 µg/mL of streptomycin, and 0.25 µg/mL of Fungizone® Antimycotic, Lifetechnologies, UK), which was pre-warmed in a 37˚C water bath. Ficoll solution (10ml) was added to an empty 50 ml universal sample tube. The blood/media mixture was added drop wise to the Ficoll solution without disturbing the interface between the Ficoll solution and the blood/media mixture. Red blood cells and mononuclear cells were then separated by centrifuging the universal tube at 400G on a 40-minute cycle, followed by progressive deceleration. The top layer containing plasma and white cells was removed using a Pasteur pipette and placed in an empty universal tube. The white cells were then suspended in 10 ml RPMI 1640 media supplemented with 1%v/v L-glutamine and 1%v/v Antibiotic-Antimycotic (100 units/mL of penicillin, 100 µg/mL of streptomycin, and 0.25 µg/mL of Fungizone® Antimycotic) and pelleted at 400G for 10 minutes, followed by progressive deceleration. White cells were washed with 10 ml RPMI 1640 media supplemented with 1%v/v L-glutamine and 1%v/v Antibiotic-Antimycotic and pelleted at 400G for 10 minutes followed by progressive deceleration. Cells were then suspended in complete media (RPMI 1640 media supplemented with 10%v/v human AB serum, 1%v/v L-glutamine and 1%v/v Antibiotic-Antimycotic (100 units/mL of penicillin, 100 µg/mL of streptomycin, and 0.25 µg/mL of Fungizone® Antimycotic) for further use.

4.3.3. Intradermal Betamethasone delivery using a topical cream or solid-coated MNs

To test the effect of topical application of BD cream, 0.1 ml of cream was applied onto a full thickness human skin explant, which was stretched to 2x1cm^2 on a cork board covered with tinfoil. The cream was manually massaged into the skin surface using the fingertip for 10 minutes to assist drug permeation.

For MN delivery, 1mg of BSP was first dissolved in 200µl 5mg/ml PVA200 solution and used as a coating formulation (50mg/ml BSP and 5mg/ml PVA). To coat MNs, 0.4µl of BSP coating formulation was coated onto three arrays of stainless steel MNs (see chapter 2). To test BSP coated MNs, MNs coated with BSP were inserted into human skin explants for 5 minutes, or shaved mouse skin for 10 minutes. MNs were then removed to analyse delivery efficiency.

4.3.4. *Ex vivo* human skin explant culture

A treated or untreated area of full thickness human skin explant was excised using an 8mm biopsy punch. Each skin biopsy was inserted in a Millicell Cell Culture Insert 12mm (base membrane was removed), with the epidermis facing up, exposed to the air, and the dermis facing down touching the liquid culture media. The inserts were then placed in a 24 well culture plate filled with 1ml of complete media (RPMI 1640 media supplemented with 10%v/v human AB serum, 1%v/v L-glutamine and 1%v/v Antibiotic-Antimycotic (100 units/mL of penicillin, 100 µg/mL of streptomycin, and 0.25 µg/mL of Fungizone® Antimycotic)) and cultured at 37˚C with 5% CO_2 for the required period.

4.3.5. Quantification of BSP using HPLC (high pressure liquid chomography)

BSP was quantified using an Agilent HP1200 UV reverse phase HPLC machine. The column used was an ODS C18 Gemini 5μm. HPLC running parameters were set as below:

Mobile phase A: Acetonitrile

Mobile phase B: 0.1%v/v phosphoric acid in DI water

Running time: 30min

Sample injection volume: 20μl

Detector wave length: 234nm

Post time: 5min

Gradient was shown in Table 4.2.

Table 4.2 HPLC mobile phase gradient for detecting BSP. A=Acetonitrile, B=0.1%v/v phosphoric acid in DI water

Time/min	A v/v%	B v/v%
0	30	70
25	50	50
26	30	70
30	30	70

4.3.6. Preparation of mouse epidermal cells

Mice were sacrificed using a sealed CO_2 chamber. Hair was removed from the treated skin area using a pair of curved forceps by pulling against the hair growth direction. Skin was then excised using an 8mm biopsy punch and subcutaneous fat was removed using a scalpel. Skin pieces were floated on 5ml of RPMI 1640 medium containing 2.14unit/ml dispase II and 0.25%w/v trypsin in a 50mm petri dish at 37˚C for 1 hour. After incubation, enzymes were washed off by rinsing the skin in 5%v/v FCS/PBS. The epidermis was then separated from the dermis

using a pair of fine curved forceps. The epidermal piece was then transferred to 500µl of complete media (RPMI 1640 supplemented with 5%v/v FCS, 1%v/v L-glutamine and 1%v/v Antibiotic-Antimycotic). Epidermal cells were then released by pipetting up and down using a 1 ml pipette until the culture media turned cloudy. The remaining portion of the epidermis was then carefully removed from the cell suspension.

4.3.7. Imaging mouse LCs in an epidermal sheet

Isolated mouse epidermal sheet was prepared as described in section 4.3.6. The epidermal sheet was then fixed in acetone at -20˚C for 15 minutes. In order to reduce non-specific staining, fixed epidermal sheets were incubated in a blocking agent; 5% w/v BSA/PBS and anti-CD16/32 mAb, for 1 h at ambient temperature. The epidermal sheet was then rinsed in fresh PBS three times to remove the blocking agent. To stain LCs, the epidermal sheet was incubated with CD207-PE mAb in 1%BSA in the dark at ambient room temperature for 1 hour. The epidermal sheet was then washed with PBS to remove excess antibody.

For imaging, the epidermal sheet was mounted on a glass slide using Dako fluorescence mounting media and covered with a glass coverslip. The slide was then sealed with nail polish after the mounting media was set. Fluorescent images were captured using a Leica DM IRB Fluorescence Microscope and processed using ImageJ software.

4.3.8. Evaluating the effect of betamethasone on the phenotype of human epidermal DCs

Human skin explants that had been treated with BD cream or BSP coated MNs were cultured *ex vivo* for 24 hours after treatment. Epidermal cells were then

isolated, stained with antibodies as listed in Table 4.3, and data were acquired using a CantoII Flow Cytometer. Mean fluorescent intensity (MFI) of $CD1a^{+}Langerin^{+}$ epidermal cells was analysed using FlowJo.

Table 4.3 Antibody list for examining the effect of betamethasone on the phenotype of human epidermal cells.

Ab	Fluorophore	Dilution v/v
HLA DR	Percp Cy5.5	1/200
Langerin	PE	1/200
CD1a	Pacific Blue	1/100
Viability	eFluor 780	1/1000

4.3.9. Evaluating the effect of betamethasone on human epidermal cells using the Mixed Lymphocyte Reaction (MLR) assay

In order to examine the effect of betamethasone on human epidermal DCs, human skin explants were first treated with either BD cream or BSP coated MNs as described in 4.3.3. Treated skin epidermal cells were then prepared as described in 4.3.1. In each well of a 96 round bottom plate, approximately 50,000 epidermal cells were seeded with 200,000 PBMCs in RPMI 1640 supplemented with 1%v/v L-glutamine, 1%v/v Antibiotic-Antimycotic and 10%v/v human AB serum. Cells were incubated at 37˚C, with 5% CO_2 for 30 hours. 100µl supernatant was then taken from each well and replaced with 100µl of fresh complete media.

4.3.10. Assessing the effect of topical BD cream on murine epidermal cells

Mouse epidermal cells were prepared as described in 4.3.6. BDC2.5 T cells were prepared as described in 3.3.9. Epidermal cells from each 8mm biopsy punch were co-cultured with 200,000 BDC2.5 T cells in the presence of 1ng/ml m31 in each well of the 96 round bottomed plate at 37˚C with 5% CO_2 for 3 days. After incubation, IL10 levels in the supernatant were analysed using ELISA (introduced in section 3.1.2.).

4.3.11. Titrating topical BD cream for *in vivo* study

DiproSone®0.05% w/w Cream was diluted 1/10, and 1/50 times in Diprobase Cream using geometric dilution. Geometric dilution was used to ensure the betamethasone was mixed uniformly in the Diprobase cream. Undiluted and diluted 0.1ml creams were applied to the shaved neck area of NOD mice once per day for two days. After treatment, single cell suspensions were prepared from the SP, ALN and PLN for analysis of changes to the $CD4^+$ T cell phenotype. Cells were then stained with antibodies (see table Table 4.4), and data was acquired using a CANTOII flow cytometer and data was analysed using FlowJo software.

Table 4.4 Antibody list to analyse the effect of BD cream on the phenotype of local and systemic $CD4^+$ T cells.

Ab	Fluorophore	Dilution v/v
CD62L	PE	1/400
CD69	PB	1/100
CD4	PE Cy7	1/400
CD44	Percp cy5.5	1/400
GITR	Alex Fluor 488	1/100
Viability	eFluor 780	1/1000

4.3.12. Topical BD effect on local antigen presentation

The neck area of NOD mice were shaved using an electric clipper and were treated with 0.1ml topical BD cream once per day for two consecutive days. Twenty-four hours after the second cream treatment, mice were adoptively transferred with 4 X 10^6 CFSE labeled BDC2.5 T cells through the tail vein and 2µg m31 by intradermal injection. Three days post injection, cells from the ALN and PLN were isolated and the cell proliferation profile from each organ was acquired using a CANTO II flow cytometer and analyzed using FlowJo software.

4.3.13. Determining the dose of BD cream

Aliquots of 0.1ml BD cream were measured onto a piece of grease proof paper, using a 1 ml syringe and weighed to determine the mass of 0.1ml BD cream. This allowed the mass of betamethasone in each 0.1 ml 0.05% w/w BD cream to be calculated.

4.3.14. Topical BD effect on inducing tolerance *in vivo*

NOD mice (Female, 4-5 weeks old) were treated with 0.1ml BD cream or 1/50 BD cream once a day for 2 days, then, 24 hours after the second treatment, mice were injected with peptide by either ID injections or via coated MNs at the site of topical steroid preconditioning. After 3 weeks, mice were treated again with BD cream for 2 days followed by peptide treatments using ID injection or MNs. A week after the second treatment, mice were transferred with $4x10^6$ CFSE labelled BDC2.5 T cells through the tail vein. Mice were then sacrificed 3 days post cell transfer and the cell proliferation profile was analysed using a CantoII Flow Cytometer and FlowJo software.

4.4. Results

4.4.1. Effect of topical steroid on epidermal cells in both human and mouse skin models

4.4.1.1. Quantification of BSP using HPLC

As discussed in Chapter 3, the hydration effect from BD cream treatment could change the rate of clearance of peptide delivered to the skin. MNs were used to deliver BSP to minimise the hydration effect of topical steroid delivery. Any BSP left on MNs after skin delivery was recovered and quantified using HPLC. As demonstrated in Figure 4.2 A, water-soluble BSP can be quantified using HPLC with a linear calibration range from 3.9μg/ml to 1000μg/ml. BSP (20μg) was coated on solid MNs and onto average (17.83±0.9)μg (88.71% delivery efficiency) was delivered to human skin and (10.6±3.9)μg (52.7% delivery efficiency) was delivered to mouse skin (Figure 4.2 B). The delivered dose of BSP was more consistent in human skin than in mouse skin.

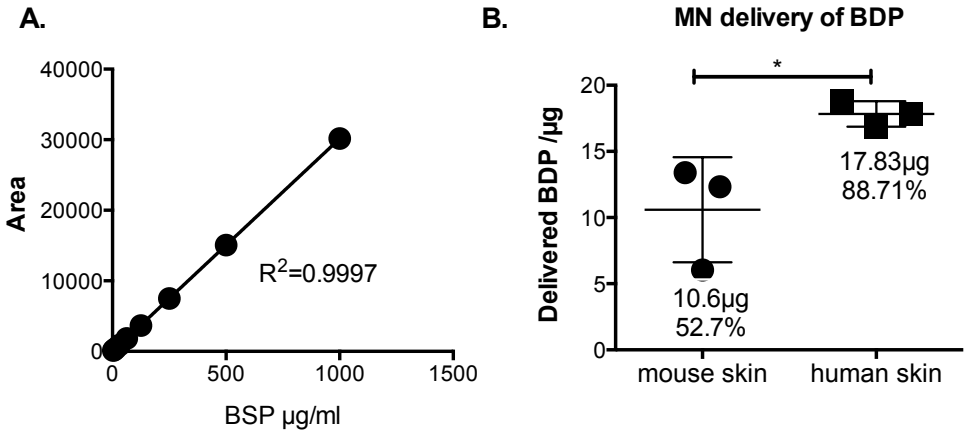

Figure 4.2 HPLC quantification of BSP dose delivered to human or mouse skin using solid-coated MN. A. Calibration range for BSP as quantified by HPLC (93.9μg/ml to 1000μg/ml). **B.** BSP delivery efficiency using solid-coated MNs to human skin explants or mouse skin *in vivo*. 20μg BSP was coated on solid MNs and delivered to either human or mouse skin, the delivery efficiency was reverse-quantified using HPLC. n=3, unpaired t test, * $p<0.05$, Mean±SD.

4.4.1.2. Effect of steroid on human epidermal cells

Topical application of betamethasone changed the expression of HLA DR on $CD1a^{+}Langerin^{+}$ epidermal DCs (Figure 4.3). As shown in Figure 4.3 A, $CD1a^{+}Langerin^{+}$ DCs accounted for approximately 2% of total epidermal cells. The effect of betamethasone on these DCs was measured by analysing the expression of HLA DR, a human MHCII cell surface receptor whose expression correlates with the level of stimulation (Fainaru et al., 2012, Matsuo et al., 2004, Berger et al., 2009, Chung et al., 2013). The absolute MFI of HLA DR expression on $CD1a^{+}Langerin^{+}$ is illustrated in Figure 4.3 B. Experiments that used the same skin donor were linked with a solid line. The baseline MFI for untreated skin samples varied between each donor, from 5999 to 61141, which is slightly greater than a 10-fold difference. Compared with the relevant controls, four out of seven of the BD cream-treated group showed a reduction in HLA DR expression, whilst one showed a small increase and the other two showed no change. The effect of MN-coated BSP on HLA DR was similar to BD cream, with five samples showing a decline in comparison with the relevant control sample. There was no obvious trend between BD cream and BSP-coated MN groups, with three skin samples showing more reduction when using BD cream compared with BSP-coated MNs. Three skin samples showed the opposite trend and one showed no difference between the two treatments. With blank MN treatment, three skin samples showed an increased stimulation response and two showed no difference compared with control. To provide an overall understanding of how betamethasone affected HLA-DR expression, the MFI of the experimental the group was normalised against its relative control (Figure 4.3 C). Both BD cream and BSP-coated MN-treated skin showed a significant reduction in HLA DR expression compared to untreated skin. Blank MN treatment alone showed no notable trend but there was a large standard deviation between specimens. This indicated that betamethasone can

normalised/conditioned the LCs to a state in which they expressed reduced HLA DR, i.e. an immature phenotype.

Epidermal DC function was also tested after BD treatment (Figure 4.3 D&E). By mixing epidermal cells with unmatched allogenic PBMCs, a non-specific lymphocyte reaction was triggered. Five negative controls were set as follows: epidermal cells alone, PBMCs alone, epidermal cells with blank MN treatment, epidermal cells with BSP-coated MN treatment and epidermal cells with BD cream treatment. The functionality of the PBMCs used in the MLR was confirmed by response to Phytohaemagglutinin (PHA) as positive control. In the proliferation assay, both BD cream and BSP coated MN treated skin epidermal cells produced a small reduction in proliferation compared with untreated epidermal cells. However, this was not reflected by a change in the IL10 level measured in the supernatant (Figure 4.3 D&E).

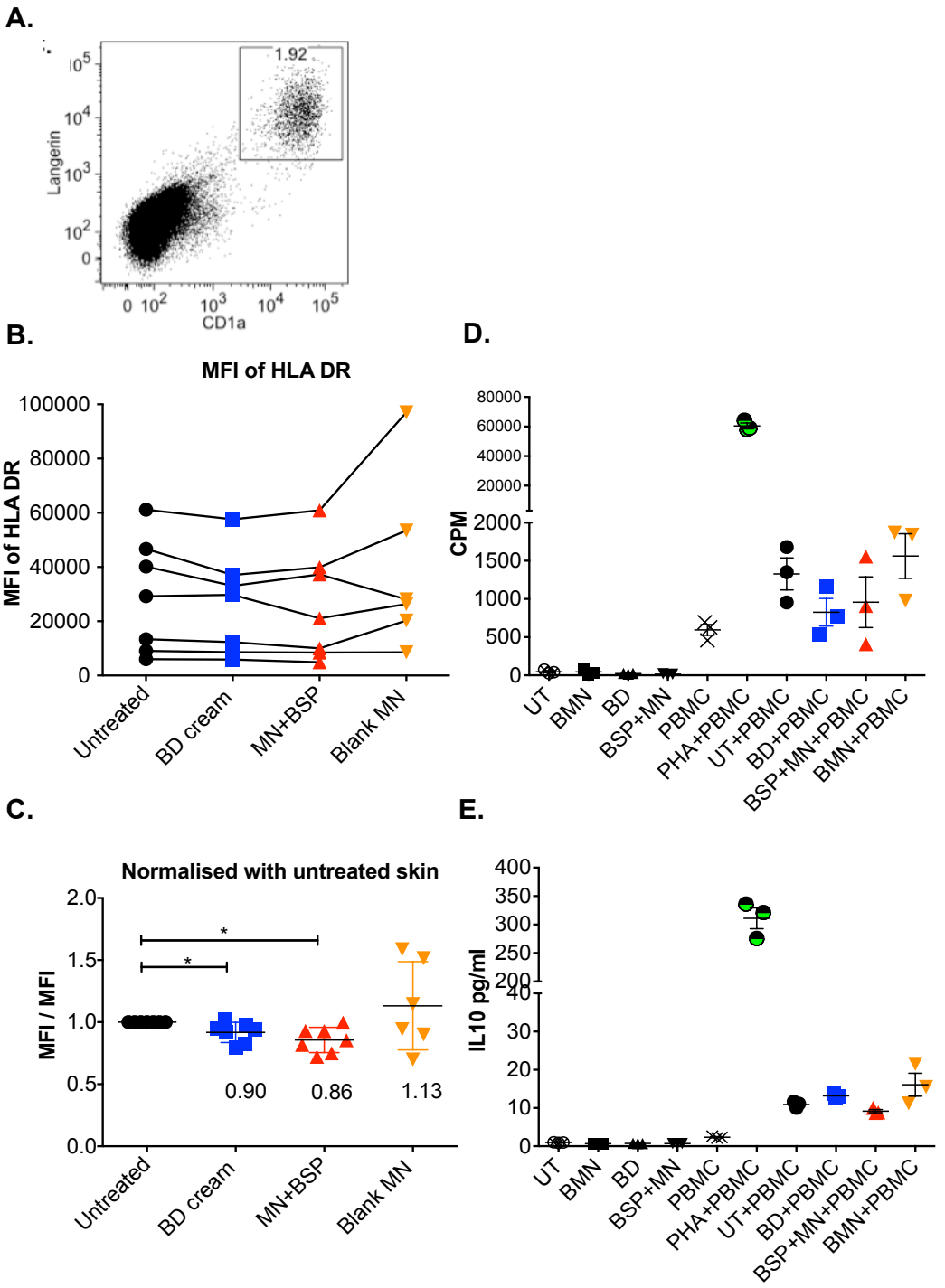

Figure 4.3 Effect of betamethasone on human epidermal DCs. **A.** Representative flow cytometry plot of $CD1a^{+}Langerin^{+}$ DCs in the human epidermal cell population. **B&C,** phenotypic change of LCs from skin explant cultured for 24 hours (data compiled from five separate experiments). **B.** Absolute MFI of HLA DR expressed on $CD1a^{+}Langerin^{+}$ cells. Experiments involving the same skin donor were linked using a solid line. **C.** Normalised MFI of betamethasone treated skin compared to untreated skin, n≥6. Mean±SD One way ANOVA, Wilcoxon matched pair test, *p<0.05. **D&E** MLR of epidermal cells and PBMCs. Skin explant was treated with betamethasone (cream or MN) and cultured for 24 hours. Epidermal cells were then isolated and co-cultured with PBMCs. IL10 level in supernatant was analysed using ELISA 54 hours post co-culture. Cells were pulsed with ^{3}H-Thymidine and proliferation was analysed 18 hours later. **D.** Radioactivity counts of MLR between epidermal cells and PBMCs, CPM (counts per minute). **E.** IL10 level in MLR supernatant, n=3, Mean±SD.

4.4.1.3. Effect of topical steroid on mouse epidermal cells

Because the mouse epidermis is very thin (around 20μm, see Chapter 1), the epidermis separation protocol (adapted from human epidermis separation) was validated to ensure LCs were not lost during the separation process. As demonstrated in Figure 4.4 A&B, LCs remained in the epidermis after enzyme digestion and separation from the dermis. On average, 48.73±3.72 μg of BD was applied topically to shaved mouse skin (Figure 4.4 C). After 2 days treatment with topical steroid, mouse epidermal cells showed higher capacity for releasing IL10 *in vitro* than untreated skin (Figure 4.4 D).

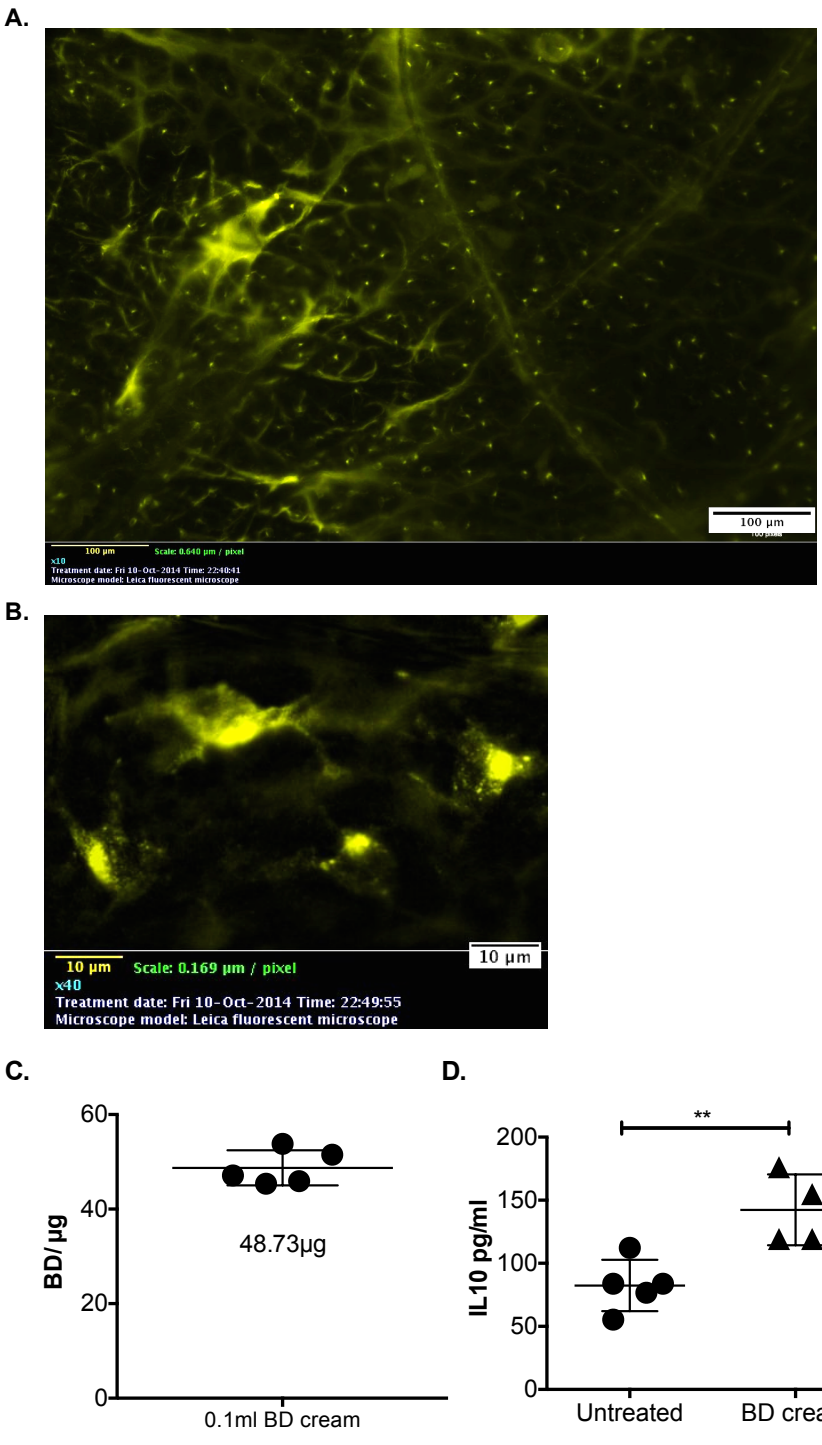

Figure 4.4 The effect of short-term topical BD cream on mouse epidermal cells. A&B Immunofluorescence images of CD207 antibody stained mouse epidermis. **A.** x10, scale bar=100µm**, B.** x45, scale bar=10µm. **C.** Average mass of BD applied to mice by measuring 0.1ml 0.05%w/v BD cream n=5, Mean±SD. **D.** IL10 level in the culture media. NOD mice were treated with 0.1ml BD cream once/day for two days. Twenty four hours after the second treatment, epidermal cells were isolated and co-cultured with 200,000 BDC2.5 T cells in the presence of 1ng/ml m31. The tolerogenic effect of BD cream on epidermal cells was measured as IL10 level in culture media, which was analysed using ELISA. **C&D** were compiled from two separate experiments. n=4, Mean±SD, unpaired t test, ** $p<0.01$.

4.4.2. Titration of topical BD cream for *in vivo* study

4.4.2.1. Short term effect of topical steroid on local and systemic antigen presentation

BD cream (0.05% w/w) was tested *in vivo* for its local or systemic suppressive effects. BD cream was applied once per day for two days followed by m31 treatment and BDC2.5 T cell adoptive transfer as seen in Figure 4.5 A. Effects of BD cream on the transferred BDC2.5 T cell proliferation in the ALN or PLN are presented in Figure 4.5 B. and C. BD cream did not cause any non-specific stimulation in the local draining lymph node, the ALN. It also did not have any significant effect on BDC2.5 T cell proliferation in the ALN. Interestingly, proliferation of BDC2.5 T cells was suppressed in the PLN in mice treated with BD cream (Figure 4.5 C.). BDC2.5 T cells in mice pre-treated with BD cream showed a significant reduction in proliferation compared to the untreated group. BD cream also impacted on BDC2.5 T cell proliferation in the PLN from mice treated with m31. The result in Figure 4.5 C suggested that topical BD cream alone suppressed the immune response in the PLN. The $CD4^+$ T cell population was analysed to check whether the suppression was due to induced tol-DCs or systemic suppression. It became apparent that full dose BD cream alone could cause the depletion of $CD4^+$ in both ALN and PLN (Figure 4.5 D.&E.). This effect lasted for four days post BD cream treatment. In order to minimise the systemic effect of BD cream, a reduced dose of betamethasone was required.

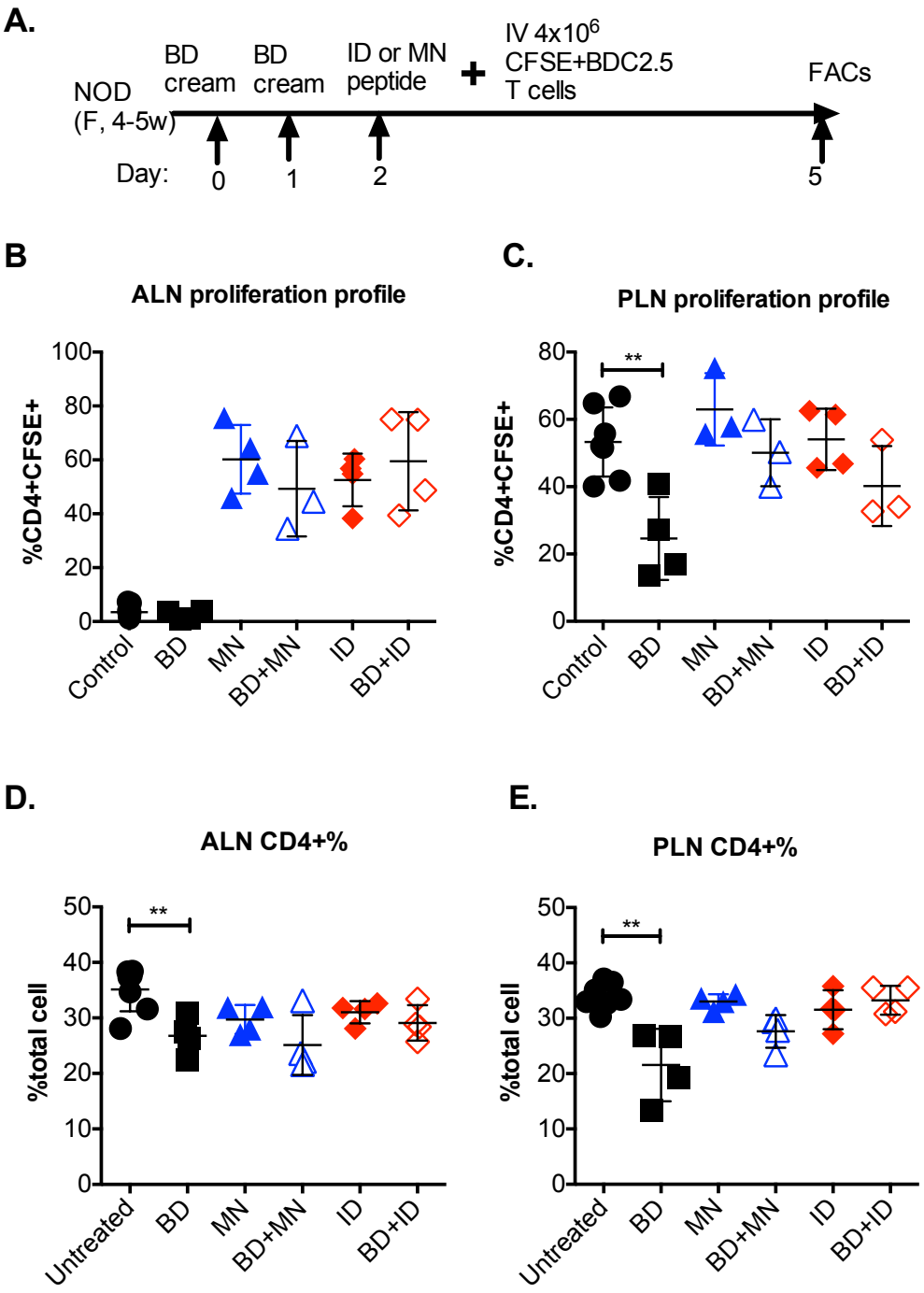

Figure 4.5 Effect of 0.05%w/w BD cream on local and systemic antigen presentation, reflected by a change to the proliferation profile of transferred BDC2.5 T cells. **A.** Protocol for testing the effect of BD cream *in vivo*. BD cream was applied two days before peptide treatment, followed with CFSE labelled BDC2.5 T cell adoptive transfer. Cell proliferation in the ALN and PLN were analysed using FACs. **B.&C.** Proliferation profile of BDC2.5 T cells in the ALN or PLN 3 days post peptide treatment. The proliferation profile was presented as percentage of $CFSE^{+}CD4^{+}$ apart from first generation to total $CFSE^{+}CD4^{+}$ cells. **D.&E.** Percentage of $CD4^{+}$ T cells in ALN or PLN 3 days after peptide treatment. Unpaired t test, **p<0.01. For all experiments, n≥3, Mean±SD. Data were compiled from two separated experiments.

4.4.2.2. Effect of BD cream on cells in LNs

As mentioned in the section 4.4.2.1, full dose topical BD showed depletion effect on both $CD4^+$ T cells and $CD11c^+$ DCs. In order to confirm this finding, a separate experiment was undertaken to examine the effect of BD cream on these two cell types without the three-day interval used in section 4.4.2.1 to enable $CFSE^+$ BDC2.5 T cell to proliferate. In order to do this, NOD mice were treated with BD cream for two days, and 24 hours post the second treatment, cells from the ALN and PLN were analysed using flow cytometry.

The result demonstrated that the effect of BD cream on T lymphocytes was focused on the $CD4^+$ population rather than $CD8^+$ cells. A significant reduction of $CD4^+$ T cells was observed after BD treatment, while there was no change in the $CD8^+$ T cell percentage (Figure 4.6). CD11c was used to identify DCs. BD cream did not have any effect on DC population in the skin draining LN, the ALN. However, in the PLN, the DC population was reduced by applying BD cream. This indicated that systemic suppression may be caused by the topical BD. As the intention was to use BD to educate local skin DCs rather than cause systemic suppression, a reduced dose of BD cream was required.

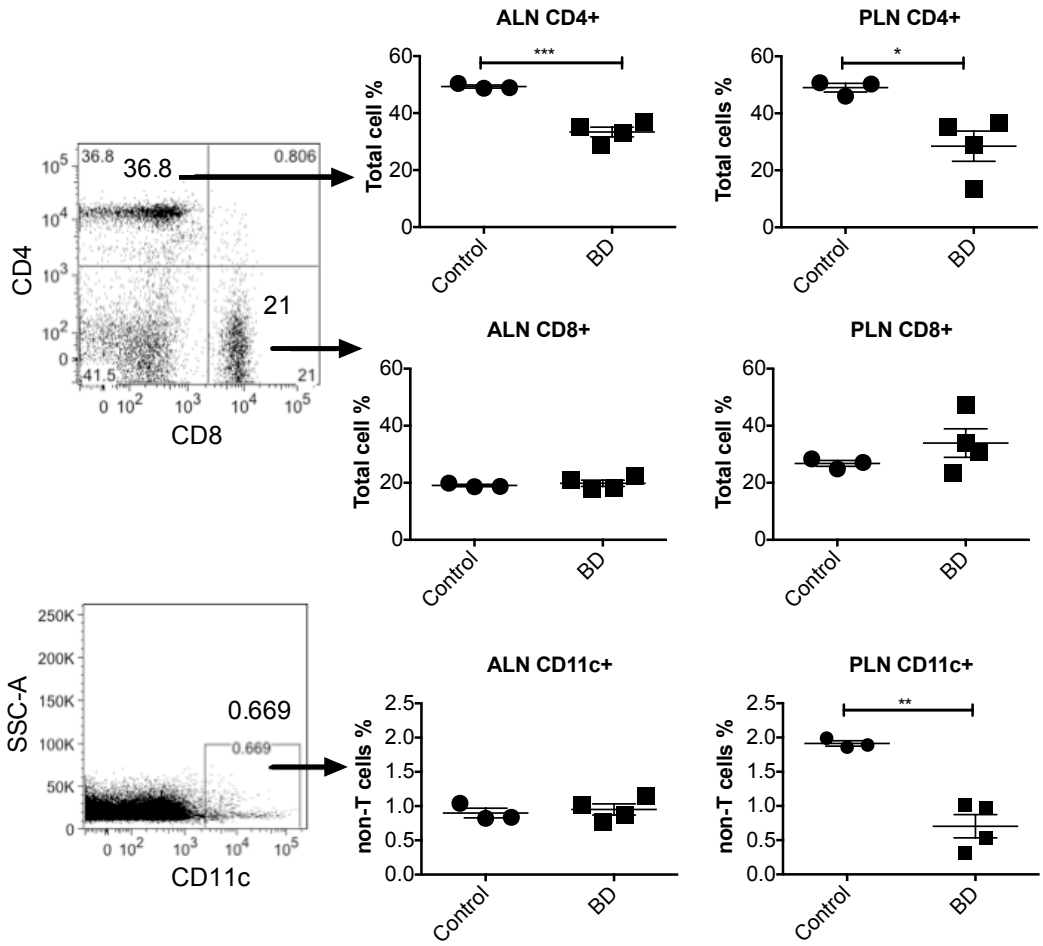

Figure 4.6 Effect of BD cream on T cell and DC population in the ALN and PLN. Cell isolated from ALN and PLN were stained with CD4, CD8 and CD11c to distinguish T cells and DCs. FACs gating strategies are shown on the left. $CD4^+$ and $CD8^+$ population were gated from total live cells and $CD11c^+$ population was gated from $CD4^-CD8^-$ population. Mean±SD. t test, *p<0.05, **p<0.01, ***p<0.001.

4.4.2.3. Titration of topical steroid for murine study

Section 4.4.2.2 confirmed that topical BD does have a depletion effect on $CD4^+$ T cells and $CD11c^+$ DCs. A titration experiment was then undertaken to determine the BD dosage, which would elicit minimal systemic effect. BD cream (0.05% w/w) was diluted to 0.005% w/w and 0.001% w/w using geometric dilution with Diprobase cream. Diprobase cream alone without BD, was applied as a control. Cells from the ALN, PLN and SP were analysed to determine the effect of topical BD on $CD4^+$ T cells. As seen in Figure 4.7 cream alone did not have any effect on $CD4^+$ T cell number or phenotype. Application of 0.05% w/w BD cream

caused a reduced $CD4^+$ T cell in both ALN and PLN (section 4.4.2.2. By reducing the dose of BD, the $CD4^+$ T cell depletion was significantly reduced. Interestingly, there was no significant change in the number of $CD4^+$ T cells in the SP with or without treatment using a BD cream.

BD cream also affected cell phenotypes in the LNs and SP (Figure 4.8). The summary of these changes is listed in Table 4.5. In general BD reduced the total $CD4^+$ population in both ALN and PLN but not in the SP. $CD4^+$ T cell subpopulations were also analysed. $CD4^+CD44^+$ can be recognised as a marker for memory/activated T cells (Henao-Tamayo et al., 2010, Pepper and Jenkins, 2011). CD69 is another marker for activated T cells. GITR can also be up-regulated on $CD4^+CD25^+$ Treg cells and was found to be expressed on the surface of effector T cells (Zhang et al., 2013a, Ronchetti et al., 2004, Shevach and Stephens, 2006). CD62L expression is related to T cell homing and activation. T cells shed CD62L when homing to the lymph nodes (Klinger et al., 2009). It has been demonstrated that $CD62L^{lo}$ and $CCR7^-$ CD4 T cells exhibit an effector memory cell function (Bingaman et al., 2005). In the ALN, $CD44^+$, $GITR^+$ and $CD69^+$ subpopulations were increased after BD cream application, while no obvious changes were seen in the CD62L population. A similar trend was observed in the PLN; however, no changes were found in the $CD44^+$ population but $CD62L^-$ was significantly increased. In the SP, BD cream had almost the opposite effect to $CD4^+$ T cells compared with the ALN and PLN. $CD44^+$, $GITR^+$ and $CD62L^-$ populations all showed a reduction in the SP. As in the ALN and PLN, the $CD69^+$ subpopulation was increased in the SP. Interestingly, $CD62L^+$ population was increased after BD cream treatment, with obvious changes in the other two lymphoid organs (ALN and PLN).

DC were also analysed following titration of the BD cream dose. BD cream did not influence $CD11c^+$ DCs in the ALN at different BD doses. In the PLN, $CD11c^+$ DCs decreased when using full dose BD and recovered to control levels when the BD was diluted 50 times. In both cases, vehicle alone did not have any effect on DC numbers.

With the titration of BD cream from 0.05% w/w to 0.005% w/w and 0.001% w/w, the systemic effects of BD cream on both $CD4^+$ T cells and DCs was reduced. A 50 times dilution had no effect on the $CD4^+$ T cell and $CD11c^+$ cell population when compared with the untreated and cream-only groups. Therefore for later experiments 1/50 diluted BD cream was used.

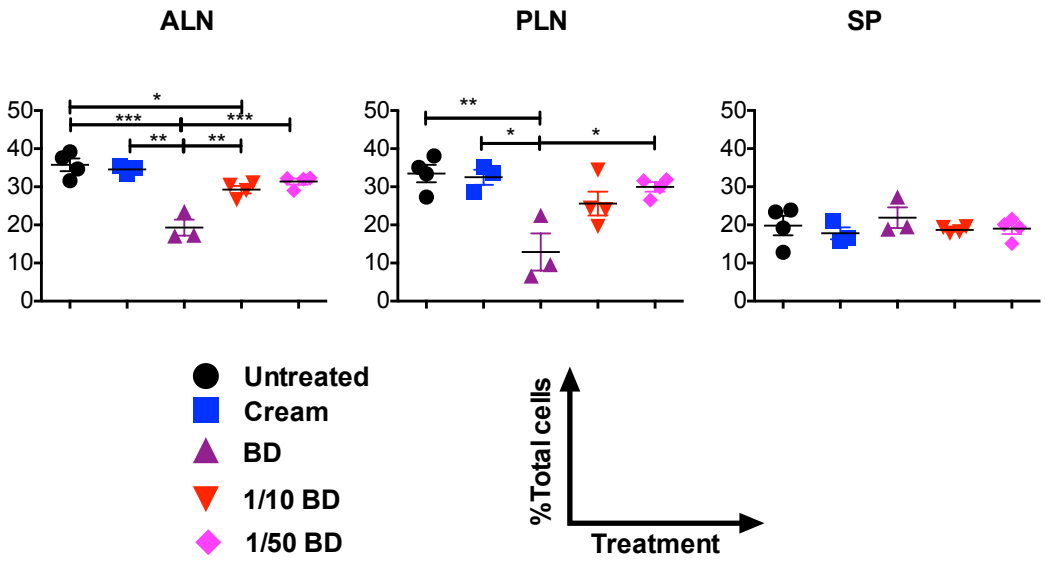

Figure 4.7 BD effect on $CD4^+$ T cell population. NOD mice were pre-treated with either full dose BD or diluted (1/10, 1/50) BD for two days and percentage of $CD4^+$ T cells as a percentage of total cell population were analysed by flow cytometry. N≥3. Mean±SD. Data were compiled from two separate experiments. One Way ANOVA with Tukey post test. *p<0.05, **p<0.01, ***p<0.001.

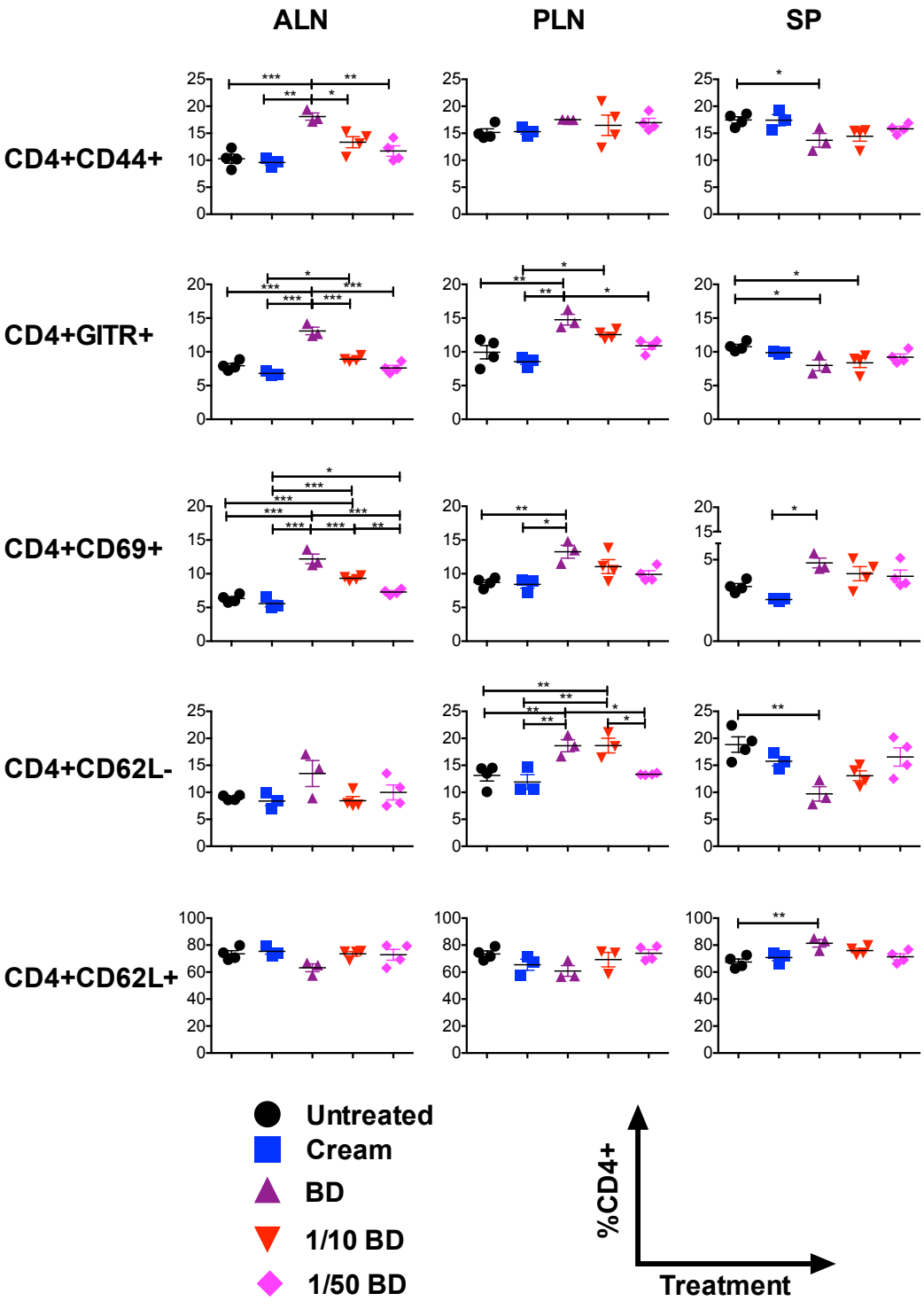

Figure 4.8 Effect of short term topical BD on CD4$^+$ T cell phenotypes. NOD mice were pre-treated with either full dose BD or diluted (1/10, 1/50) BD for two days and CD4$^+$ T cell phenotypes were analysed by flow cytometry. N≥3. Data were compiled from two separate experiments. Mean±SD. One Way ANOVA with Tukey post test. *p<0.05, **p<0.01, ***p<0.001.

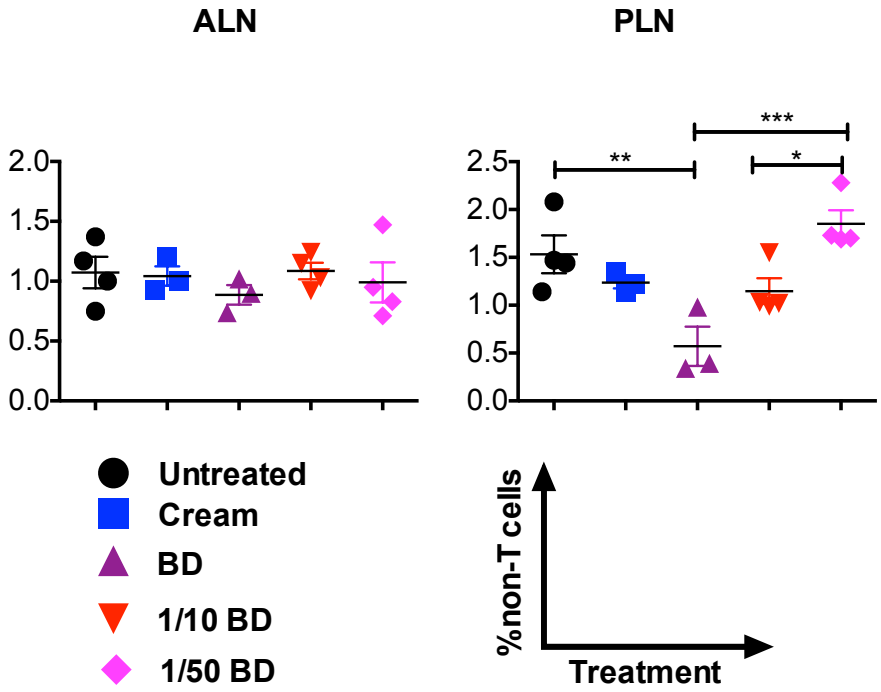

Figure 4.9 Effect of BD on CD11c$^+$ DCs population in ALN and PLN. NOD mice were pre-treated with either full dose BD or diluted (1/10, 1/50) BD for two days and CD11c$^+$ T cell population were analysed by flow cytometry. Data were compiled from two separate experiments. N≥3. Mean±SD. One Way ANOVA with Tukey post test. *p<0.05, **p<0.01, ***p<0.001.

Table 4.5 Effect of topical betamethasone on CD4$^+$ T cell subpopulation in ALN, PLN and SP. Summary of BD effect on CD4$^+$ populations as demonstrated in **Figure 4.8**. Topical BD showed different influence on the same CD4$^+$ T cell population in different lymphoid organs. Downwards arrow: BD reduced its population significantly (p<0.05); upwards arrow: BD increased its population significantly; horizontal line: BD showed no effect; horizontal line with downwards arrow: BD showed a small change on its population, but not significantly.

Phenotype / Organ	CD4+	CD4+ CD44+	CD4+ GITR+	CD4+ CD69+	CD4+ CD62L-	CD4+ CD62L+
ALN	↓	↑	↑	↑	—	—↓
PLN	↓	—	↑	↑	↑	—↓
SP	—	↓	↓	↑	↓	↑

4.4.3. Effect of short term topical BD on inducing antigen specific tolerance *in vivo*

Short term pretreatment with topical BD was then tested for its effect in inducing tolerance with or without ASI. Both BD cream (0.05% w/w) and 1/50 diluted BD cream (0.001% w/w) were used to induce tolerance as illustrated in Figure 4.10 A. When using BD cream for pre-treatment, no reduction of proliferation was observed when compared with the control group. However, a small increase was seen in the proliferation profile of mice that were treated with BD, with or without m31 (Figure 4.10 B). In order to eliminate the systemic effect of BD cream, 1/50 diluted BD was used to promote pre-conditioning of skin DCs into tol-DCs. When using potent m31 as an antigen, no sign of tolerance was observed with m31 alone. Diluted BD cream (1/50) pre-treatment together with m31 did not show any benefit with respect to inducing tolerance (Figure 4.10 C). The endogenous antigen, WE14, was then used to investigate whether the effect of topical BD in enhancing WE14 induced peptide-specific tolerance. However, despite the demonstrated efficacy of WE14 in inducing tolerance, 1/50 BD cream reversed proliferation back to control levels (Figure 4.10 E). One interesting observation was that 1/50 BD cream alone-down regulated BDC2.5 T cell proliferation significantly when compared to full dose BD cream (Figure 4.10 D).

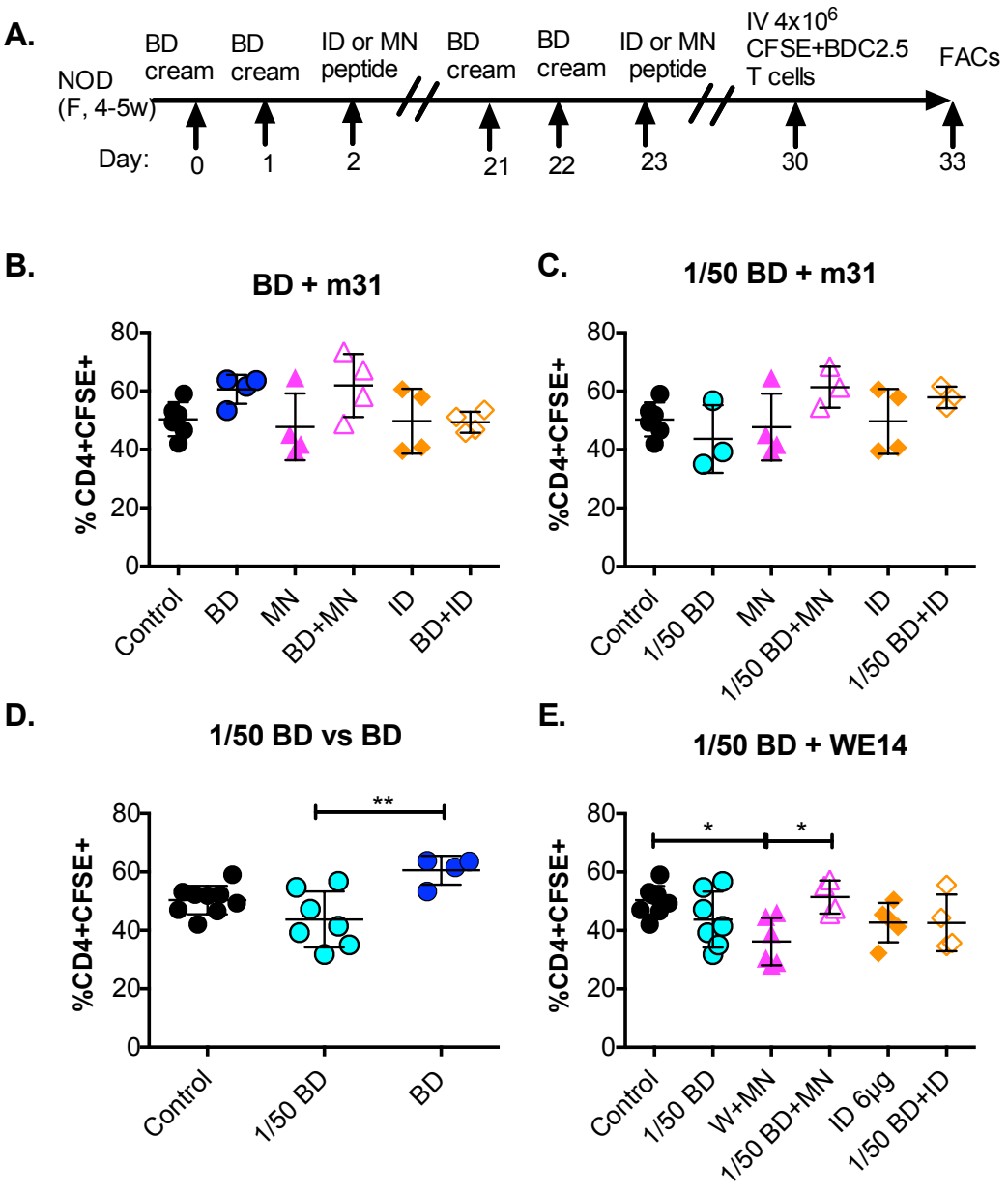

Figure 4.10 Effect of topical BD pre-treatment on inducing antigen specific tolerance *in vivo*. Both BD cream and 1/50 BD cream were tested. WE14 and m31 were used as an antigen for inducing tolerance and BDC2.5 T cell proliferation profile was used as an indicator of induced tolerance. **A.** Tolerance protocol with two days pre-treatment with BD cream. **B.** BDC2.5 T cell proliferation profile in PLN of mice that were treated with BD cream and m31. **C.** BDC2.5 T cell proliferation profile in PLN with mice that were treated with 1/50 BD cream and m31. **D.** Comparison of 1/50 diluted BD cream and full dose BD cream on BDC2.5 T cell proliferation (re-analysed data from Figure **B&E**). **E.** BDC2.5 T cell proliferation profile in PLN with mice that treated with 1/50 BD cream and WE14. n≥3. Data were compiled from three separate experiments, Mean±SD. One way ANOVA with Tukey post test, *p<0.05, **p<0.01. Control= without any treatment, ID=intradermal injection, MN=MN treatment for 10 minutes, BD=0.1ml BD cream treatment

4.5. Discussion

4.5.1. Effect of BD cream on epidermal cells

As demonstrated in Chapter 3, the local clearance rate of a peptide could be altered if the skin is hydrated with a topical formulation. Therefore, this study was designed to test the use of BSP-coated MNs to minimise this effect. The aqueous solubility of BD is very low, even when using an optimised formulation as described in Chapter 2. The phosphate salt form of betamethasone, BSP, was used to coat MNs. BSP is a water-soluble compound can be delivered using solid-coated MNs. On average, 18μg of BSP was delivered into human skin and 11μg into mouse skin using the same MN delivery system. This provides further evidence that the skin model can influence delivery efficiency when using a solid-coated MN system, as discussed in Chapter 2. We also demonstrated that HLA DR expression on human skin Langerin^{+}CD1a^{+} DCs (LCs) were down-regulated by topical BD cream compared to untreated skin from the same donor. BSP-coated MNs showed a similar effect on HLA DR expression compared with BD cream. Blank MNs alone had a variable influence on HLA DR. This variation was reduced after MNs were coated with BSP (Figure 4.3). This suggested that BSP could regulate skin DCs even if they were activated. A similar finding regarding down-regulation of HLA DR expression on human skin DCs has also been reported elsewhere (Piemonti et al., 1999b). Indeed, it has been shown that GCs can regulate the maturation process of human DCs by inhibiting co-stimulator (CD83 and CD86), HLA DR expression and secretion of cytokines such as IFNγ (Larange et al., 2012).

Mouse skin epidermal cells isolated from skin treated with 0.1ml BD cream were able to induce more IL10 with BDC2.5 T cells than untreated skin (Figure 4.4). IL10 is a cytokine, which can be released by both DCs and T cells. It functions

as an immune regulator, which can down regulate Th1 cytokines and co-stimulators (Ng et al., 2013, Ouyang et al., 2011, Saraiva and O'Garra, 2010). It has been shown that an inflammatory response can be suppressed by IL10 and lack of IL10 can aggravate development of autoimmune diseases (Hata et al., 2004). Therefore, the up regulation of IL10 can be viewed as an indicator of the promotion of immune tolerance. GCs have been shown to prevent the maturation of DCs and alter the DC activation pathway, resulting in generation of a tol-DC, which secretes IL10 (Rea et al., 2000). A genomic study also has been shown that expression of IFNγ-regulated genes in human keratinocytes were suppressed by GCs 24 hour post application (Stojadinovic et al., 2007). These findings support the hypothesis that GC treatment could result in a more tolerogenic skin environment. However, in a human epidermal cell function experiment, no obvious change in IL10 level was observed from a MLR compared to untreated skin (Figure 4.3). Interestingly, epidermal cells from the same patient were shown able to suppress the proliferation of MLR. The low response demonstrated may have been related to the age of the skin donor (Agrawal et al., 2008, Sprecher et al., 1990). Lower HLA DR expression was found on DCs when the skin donor age was greater than 60. As there is have limited controls over certain-parameters in human skin explant experiments, such as age and ethnic background of donors, it would be necessary to have a larger sample size than was used in this study in order to be able to draw a meaningful conclusion.

4.5.2. Titration of topical steroid for murine study

Mouse skin is approximately 10 times thinner than human skin and therefore less BD is retained in mouse skin than human skin when using the same dose. It has been shown that once BD was absorbed through skin, this absorption into the

system may be sufficient to cause systemic suppression. A reduction of $CD4^+$ T lymphocytes and $CD11c^+$ DCs in the PLN was observed after a 2-day BD cream treatment regime. This cell depletion had a beneficial effect on BDC2.5 T cell proliferation *in vivo* three days after the second BD treatment. This may be because BD is a potent GC with a biological half-life of between 36 and 54 hours (Gary, 2013). By systemic injection, GC together with proinsulin B9-23 can induce antigen specific Tregs *in vivo* and prolong survival rate of NOD mice (Zhang et al., 2013a). In this project, however, we intend to utilise GCs to induce tol-DCs rather than causing a systemic depletion of T cells or DCs. A titration study was carried out to minimise the systemic effect whilst retaining the local therapeutic effect over skin DCs.

In this study, BD had a depletion effect on $CD4^+$ T cells that migrated to LNs, ALN and PLN, but not on cells that in the SP. This may be because T cells, which migrated to LNs were in an activated state and they are more sensitive to the GC than when they are in a naïve state in the SP (Wu et al., 2013). GCs have been shown to cause apoptosis or functional changes to the lymphocytes (Herold et al., 2006, Wu et al., 2013). Apart from depletion of all $CD4^+$ T cells, topical BD also showed an effect on $CD4^+$ T cell subtypes. In LNs, phenotypically, a higher proportion of memory T cell subtypes was found after BD treatment. This could be due to GC induced apoptosis of the activated T cells and sparing of the effector/memory T cells (Wu et al., 2013, Tischner et al., 2011, Jamieson and Yamamoto, 2000). Thus the relative fraction of memory $CD4^+$ T cell subsets comprised a higher proportion of the BD treated group than the control group. Conversely, Tregs can be induced in the EAE (Experimental autoimmune encephalomyelitis) mouse model when using GCs (Chen et al., 2006). It was also suggested that $CD4^+CD62L^+$ central memory T cells are able to convert to $Foxp3^+$ T cells, which show suppressive function as iTregs (Zhang

et al., 2013b). This could explain the increased subpopulation of $CD4^{+}CD62L^{hi}$ in the SP. Nevertheless, systemic toxicity by over dosing with BD must be avoided in our experiments. After titration, 1/50w/w diluted BD cream showed no systemic adverse effects on either $CD4^{+}$ T cells or $CD11c^{+}$ DCs.

4.5.3. Effect of topical BD cream on inducing antigen specific tolerance *in vivo*

The primary approach was to use undiluted (0.05% w/w) BD cream together with m31 to induce tolerance. GCs have already been shown to have an immunoregulatory effect in the treatment of autoimmune disease in murine models (Chen et al., 2006, Zhang et al., 2013a). The question was whether topical BD treatment could enhance tolerance. However, no reduction in proliferation was observed in the BD treated groups. As described above, when using undiluted BD cream as a tolerogenic enhancer, activated T cell depletion would occur. It has been shown that after BD was cleared from the system, a non-specific T cell proliferation will occur because of cell homeostatic state after depletion (Ge et al., 2002). This could be the main reason that undiluted BD cream may not be suitable for induct tolerance using the current protocol.

The second approach was to use 1/50w/w diluted BD cream together with a high affinity antigen (m31) and a low affinity antigen (WE14) to induce tolerance *in vivo*. However, no suppression of proliferation was observed. This could be due to several factors. Although it has been shown that topical corticosteroids influence the maturation of skin DCs *in vivo*, GCs could have an adverse effect on the local skin immune system. It was reported that GCs down regulated the expression of MHCII and co-stimulators in the 2 days following topical GC treatments; meanwhile, it can promote apoptosis of LCs *in vivo* (Hoetzenecker et

al., 2004, Meingassner et al., 2003). LC depletion was also reported in an early murine skin study (Furue and Katz, 1989b). A study of topical BD also demonstrated a significant depletion of LCs in guinea pig skin (Belsito et al., 1982b). GCs also inhibit migration of DCs from skin to draining LNs after sensitization (Cumberbatch et al., 1999). In this project, the approach was to induce tolerance by targeting skin DCs with an autoantigen in a minimally invasive manner. If GCs did induce LC apoptosis and inhibit DC migration, this would then prevent the induction of Tregs in the draining LNs. An *in vivo* study in primates also suggested that topical GC treatment resulted in an increased mature DC population in the skin draining LNs (Koopman et al., 2001). When these matured DCs in draining LNs captured free-floating injected peptide, an immune response could be stimulated. Although some data suggests that GCs can cause an increased capacity for DCs endocytosis, an impaired antigen presentation and stimulation of T cells was also observed (Piemonti et al., 1999a, Pan et al., 2001b). Therefore, even if diluted BD cream with reduced potency was not sufficient to deplete DCs and antigen-carrying DC migrated to LNs, DCs may not be able to cross talk with T cells to induce antigen-specific Treg. Furthermore, T cells can be depolarised by GCs and reduce the interaction between APCs (Muller et al., 2013). The aforementioned experiment was not shown to enhance antigen specific Tregs. However, it is possible that under other circumstances the GCs could have a different effect. As demonstrated in this study, diluted GC alone had a minor non-antigen specific suppressive effect on BDC2.5 T cell proliferation.

Fundamental differences between species may have had an effect on the outcome of antigen immunotherapy, i.e. the unsuccessful prevention of BDC2.5 T cell proliferation in a murine study may not translate to the same effect (or lack thereof) in human studies. Factors such as the thickness of the stratum corneum

and different metabolism of BD, which has been demonstrated by another group to vary in different types of human skin cells, could influence the pharmacokinetics of BD and be further reflected as a change in pharmacodynamics (Gysler et al., 1999).

4.6. Conclusion

The results presented show that topical BD treatment can alter the phenotype of human LCs in the epidermis to a less mature phenotype, showing reduced HLA DR expression. Using BSP-coated MNs, a similar reduction of HLA DR expression on LCs was also observed. This suggested that it is possible to use solid-coated MNs to deliver betamethasone, targeting skin DCs. Human epidermal cells extracted from skin pre-treated with BD were able to regulate PBMC proliferation, however the level of IL10 secretion in the MLR was not shown to be influenced when using human epidermal cells, which may due to the small sample group size. In the murine study, topical BD was shown to be able to alter the IL10 level secreted by epidermal cells. These data suggested topical BD could potentially alter the maturation process of DCs and promote Tol-DCs.

When an undiluted (0.05% w/w) BD cream was used in murine studies, systemic toxicity was observed. This toxicity was reflected by $CD4^+$ T cell depletion in both ALN and PLN and $CD11c^+$ DC depletion in the PLN. A change to the $CD4^+$ T cell subtypes also suggested that BD went into the systemic circulation after absorption through the skin. The aim of this project was to induce antigen-specific tolerance by skin vaccination rather than induce systemic suppression. Therefore, it was deemed necessary to titrate 0.05% w/w BD cream to minimise the systemic suppressive effect of BD. Using $CD4^+$ T cell population and a change of $CD4^+$ T cell phenotype as an indicator, it was shown that 1/50 dilution (0.001% w/w) minimised the systemic effects of BD.

As shown in Chapter 3, tolerance can be induced in NOD mice when using an endogenous antigen, WE14. However, BD pre-treatment impaired the effect of inducing tolerance *in vivo* using WE14. This could potentially be due to a number

of individual or combined reasons summarised from other publications, including: 1. LC/DCs were depleted from skin by BD; 2. Following BD pre-treatment, skin DCs, which migrated to draining LNs showed an intermediate maturation; 3. GCs have a negative impact on DC antigen uptake and presentation to T cells. These hypotheses still need to be further tested in future studies, which are not included in this project. GCs have complex immunomodulatory mechanisms. Even though GCs have been shown to induce tolerance (Tregs and Tol-DCs *in vitro* and in some *in vivo* models), the non-specific immunosuppressive effect of GCs may cause side effects when used in this manner.

Chapter 5 General discussion

5.1. Brief overview

The aim of this thesis was to investigate whether peripheral tolerance can be induced using autoantigen delivered by MNs or ID injection. Further investigation was undertaken to determine whether short term pre-treatment with topical BD cream could enhance ASI-induced tolerance. Three main elements were involved in this project: developing an effective MN system, inducing peripheral tolerance using autoantigen and assessing the impact of pre-treatment with betamethasone on ASI.

5.2. Significance, limitations and future work

5.2.1. MN design and coating formulation

Solid-coated MNs have been shown to be an effective delivery system with which to target skin DCs, especially LCs located in the epidermis in both human skin and mouse skin models, when compared to hollow MNs (section 2.4.1.). One problem with using solid-coated MNs however, is the difficulty encountered in coating hydrophobic materials onto the MN surface and ensuring their efficient release upon skin insertion. A novel coating formulation was designed and tested to enable the effective delivery of hydrophobic peptides using a coated MN system. This formulation maximised delivery efficiency whilst using minimal additive ingredients. Of the excipients tested during this project low molecular weight PVA was shown to assist the delivery when used at a low (1:10) w:w ratio to peptide. This ratio is much lower than other reported coating formulations (1:165 excipient:drug) (Gill and Prausnitz, 2007c). A benefit of using a low amount of coating excipient is the ability to coat the desired amount of peptide without overloading the needles excessively with material, which may adversely

influence MN skin puncture performance by reducing the effective needle sharpness. No immune response (non-specific) was observed when using a PVA-only formulation in an *in vitro* T cell response assay, which ensured minimal trauma to the skin when using MN delivery, which in turn should encourage the immune system to respond by inducing tolerance rather than causing activation. Using a combination of a water-miscible alcohol (2M2B) with adjusted pH (using acetic acid), it was demonstrated that peptides with a broad spectrum of hydrophobicity could be dissolved and used to coat MNs. It has been estimated that approximately 40% of approved drugs are hydrophobic (Basavaraj and Betageri, 2014). The novel coating formulation developed in this project enabled a simple preparation process for both hydrophobic and hydrophilic peptides without using harsh solvents or exposing sensitive reagents to high temperatures (Gill and Prausnitz, 2007c). This approach could potentially, therefore, enable a wide range of therapeutic drugs to be delivered into the skin using a solid-coated MN system. Regarding the delivered dose, by lowering the excipient ratio, the amount of hydrophobic material coated onto the MNs is potentially increased without overloading the MNs and affecting skin puncture. A previous solid-coated study has shown that a peptide (salmon calcitonin) lost its bioactivity during the formulation preparation process, showing a low bioavailobility *in vivo* (Tas et al., 2012). Other MN studies on coated peptides have been undertaken (Zhu et al., 2014) (Mohammed et al., 2014), but no stability validation data is available in the published literature. In this study, we have demonstrated that it is possible to preserve peptide bioactivity during the dissolving, storage and coating processes involved in producing a peptide/drug formulation for solid-coated MN delivery. This provides two important pieces of information for future work: 1) the coating formulation outlined above ensured that no undesirable immune response was triggered due to the presence of denatured peptide; 2) this formulation could potentially be used to deliver other peptides using solid-coated

MNs. To provide optimal characteristics for clinical use, it will be important to characterise the storage stability of solid-coated formulation and to compare this with an equivalent peptide solution. This will help to provide information, which could help improve the shelf life of coated peptides and reduce cold chain costs.

Other factors known to influence peptide delivery efficiency include skin thickness and hydration state. Therefore, there are differences in delivery efficiency between model species. The optimised formulation on its own was unable to deliver the desired dose of hydrophobic peptide to mouse skin, due to the low water content and the thin structure of mouse skin compared to human skin (Wong et al., 2011). Differences in skin hydration will not be the only considerations when selecting appropriate biological models to test MN performance. For example, it has been demonstrated that the mechanical properties are different between mouse and human skin and it has been suggested that murine skin may not be a useful biomechanical model for human skin (Groves et al., 2013). This project has demonstrated for the first time the significant implications of using different skin models when testing the delivery efficiency of solid-coated MNs. Differences between models mean that it may be necessary to test MNs using an appropriate human skin model, in addition to the murine *in vivo* model, before transitioning to clinical trials.

This project has demonstrated that removing surface debris and cleaning the surface of stainless steel MNs by electro-polishing can significantly benefit delivery efficiency, especially for hydrophobic peptides such as proinsulin B9-23. The delivery efficiency of peptide can also be increased by increasing the number of needles per MN array, without increasing the amount of peptide coated on MNs. We believe that this is due to the increased dispersion of the hydrophobic material over a greater surface area, thus exposing the peptide to

sufficient moisture within the skin compartments to facilitate dissolution (Chapter 2). This approach could however be limited by size of the application area which requires treatment by the MNs and the optimum MN density on the array to allow sufficient skin penetration (Yan et al., 2010). It is suggested that future work should be conducted to test the combination of these three parameters (density, area and coating thickness) to assist in optimising the dosage for MN coated therapeutic drugs.

In order to target skin DCs, especially LCs effectively, MN shape and length were also considered. The needle shape design used was a wedge shape, which is thought to be able to release the model drug in the upper layer of the skin (Al-Qallaf et al., 2009). This MN design therefore increases the potential to release more substance into the epidermal layer and therefore maximise its facility to target tolerogenic LCs. A needle length of 500μm (before electro-polishing) was chosen for both human and murine studies. This is because previous publications suggested that skin sealed 35% faster when using short (500μm) rather than long (750μm) needles (Gupta et al., 2011a). It was suggested that use of 400μm long MNs will effectively penetrate skin without causing significantly increased skin irritation (Bal et al., 2008). This needle length was selected to provide for efficient puncture of both human and murine skin without causing significant trauma. Although the anatomy differences between species was taken into consideration during the MN design process, we finally considered that the most appropriate approach would be to use the same length for both human and murine studies for reasons including: The needle length would be too short to coat using the current coating method, if the needle length were scaled down for murine study according to the skin thickness. It is also difficult to manufacture a scaled down needle but keep the needle dimensions in the same proportion. Thirdly, because this project could lead to a clinical study, use of the

same needle length for murine and human studies may help to ensure more efficient translation from pre-clinical to clinical study.

As a result of these studies on device/formulation optimisation, the solid-coated MN system thereafter used in murine studies comprised three arrays of electro-polished MNs with 10x450µm long needles per array. By combining an optimised coating formulation with electro-polished MN arrays, we were able to achieve a delivery dose of 6µg (WE14) and 2µg (m31) to live mice *in vivo*. One drawback of the solid-coated MN approach is that it is difficult to dose precisely due to variations in skin morphology between individuals or the hydration status of the skin. We were, however, able to control the standard error for dosing to within a narrow range (Chapter 2). To better understand the dynamics of the delivery process and establish the likely clinical variation when using coated MNs, it will be important to test MN delivery against a range of measurable skin parameters, such as sex and age of donors, hydration status (as measured by TEWL) and body site skin was taken from. This could provide useful information for future clinical studies and help to establish meaningful guidelines for dosage and usage.

5.2.2. Inducing tolerance *in vivo* using solid-coated MNs

The local skin clearance of peptide following delivery was analysed using the Kodak *in vivo* imaging system. Clearance following ID injection of a TAMRA-labelled peptide was observed to be altered when the skin had been pre-treated with a topical BD cream, presumably as a result of the topical treatment occluding the skin and increasing tissue hydration. This hydration effect showed minimal effect on clearance when solid-coated MNs were used instead of ID injection. In fact, solid-coated MN delivery resulted in an increased retention of

the peptide m31 in skin compared to ID injection, both with and without topical corticosteroid pre-treatment. Clearance of peptide from the skin can be altered by factors such as temperature and peptide solubility (Nakayama et al., 1999, Higaki et al., 2002, Neelam, 2012, Trabaris et al., 2012). Indeed, in our study peptide m31 was cleared more rapidly from the skin at high temperature than in a controlled cool environment. The intensity of signal arising from the more hydrophilic peptide (WE14) was shown to decline more rapidly than in the low solubility peptide (m31) when administered either by ID injection or MNs. The prolonged retention of peptide in the skin when using MNs may be due to a solid depot of the peptide being deposited at the delivery site with subsequent slow dissolution in the locally restricted water content of the skin. These data suggested that during a 24-hour monitoring period, peptides remained in skin longer when delivered by MN than ID injection. One drawback of this measurement is that the detection level is limited by the sensitivity of the Kodak *in vivo* imaging system. Factors such as autofluorescence, light scattering within the tissue and noise from the detector are all known to influence the final result (Leblond et al., 2010). The Kodak *in vivo* imaging system was, therefore, only used to gain an understanding of the factors that can influence the clearance of the peptide from skin. A cellular tracking experiment, as discussed below, was also undertaken to help understand the peptide trafficking route; and determine whether peptide trafficked through a cellular route (i.e. uptake by skin DCs with subsequent trafficking to lymphoid organ) or through systemic circulation.

In order to investigate whether peptide delivery using coated MNs translated to a functional advantage, we conducted *in vivo* studies in a murine model where BDC2.5 T cells were transferred intravenously to non-obese diabetic (NOD) mice. Compared with intradermal injection, coated MNs appeared to more effectively target skin dendritic cells as a higher BDC2.5 T cell proliferation profile

was observed in the draining lymph node (ALN) in MN treated skin, than in skin treated with the same dose of peptide via. ID injection. In mice, BDC2.5 proliferation was observed 10 days post MN delivery but no proliferation was observed at this time following intradermal injection. These data further confirm the results from the clearance study in that MN delivery can target skin DCs more effectively than ID injection and that solid peptide delivered by MNs is retained in the skin for longer than peptide in solution delivered by ID injection. These kinetic differences could translate to differences in inducing tolerance *in vivo* and indicate that solid-coated MN delivery could be an effective intradermal delivery method for targeting skin DCs and minimising any undesirable systemic influences. If this were the case MN administration could potentially be useful for therapies such as ASI, vaccination and skin cancer therapy (Koutsonanos et al., 2012, Quan et al., 2013, Zaric et al., 2013, Mohammed et al., 2014).

BDC2.5 T cells from TCR-transgenic mice can recognise endogenous antigen in the pancreas of NOD mice (Haskins et al., 1988, Haskins et al., 1989). Induced tolerance can therefore be reflected in a change in the proliferation profile of BDC2.5 T cells in the PLN of recipient NOD mice. When using the high potency peptide m31 to immunise NOD mice, no suppression of BDC2.5 T cell proliferation was observed using either ID or MN delivery. This may be because m31 has high affinity with TCR of BDC2.5 T cells, and it activates T cells (Delong et al., 2013). Another explanation may be related to the solubility of m31. Relatively low solubility m31 may remain partially solid in the depot within the skin after delivery. DCs in skin could then be activated by this solid form peptide, becoming mature and activating T cells in subsequent processes. When using a hydrophilic peptide; WE14, a reduced BDC2.5 T cell proliferation profile was observed. WE14 is an endogenous antigen, which has been shown to be effective in delaying T1D disease progression (Haskins et al., 2012). Here, we

were able to demonstrate for the first time, that delivery by solid-coated MNs could enhance the tolerogenic effect of WE14 compared to ID injection; resulting in fewer proliferated BDC2.5 T cells in the PLN. Factors such as minimised trauma, DC targeted delivery and a relatively slow release profile, suggested that MN delivery could have advantages in inducing tolerance when compared to ID injection. Tolerance was also reflected in the changing phenotype of transferred BDC2.5 T cells. A greater proportion of antigen specific BDC2.5 T cells remained in a naïve state ($CD62L^{+}CD44^{-}$) when NOD mice were treated with MNs than when using ID with the same dose of WE14. No change was observed in the total $CD62L^{+}CD44^{-}$ population indicating that antigen-specific tolerance was induced using the solid-coated MN/WE14 system. Encouragingly, increasing the ID dose of WE14 from 6μg to 50μg enhanced the tolerance effect, demonstrating that antigen immunotherapy is dose responsive and could be further improved. It must be noted that the age of mice was a key factor in the effectiveness of this therapy in inducing tolerance. In the tolerance protocol NOD mice were treated with peptide at 4-5 weeks of age. When mice of older than 5 weeks were used, the experiment showed inconsistent results. NOD mice develop insulitis at approximately 3 weeks old and develop onset diabetes at the age of 12 weeks (Leiter et al., 1987, Atkinson and Leiter, 1999, Leiter, 2001, Solomon and Sarvetnick, 2004). The Tregs induced using WE14 may not be of sufficient quantity to suppress the growing population of effector T cells as the disease progresses. This is not to say that tolerance cannot be induced at later stages of disease progression, rather, this could be due to a limitation of the proliferation readout. When NOD mice were greater than 5 weeks old, the proliferation of Teffs could be enhanced by the increased level of endogenous antigen released and the increased level of proinflammatory signals due to the increased degree of insulitis. The induced antigen specific Tregs represent a small proportion of the total T cell population, therefore, the tolerogenic effect

could be undermined when Teff proliferation is above the detectable threshold of induced tolerance. In another experiment, it has been suggested that young mice vaccinated with recombinant DNA encoded insulin peptide lead to earlier onset of T1D, which contradicts results obtained in this project (Weaver et al., 2001). Although proliferation data suggests that tolerance was induced, it is still uncertain whether peptide treatment could alter natural disease progression. Therefore, future experiments need to be undertaken using female NOD mice treated with WE14 peptide delivered by ID injection or MN to monitor the whether this treatment can prevent or delay the progression of T1D. The tolerance protocol can also be optimised. A recent study has suggested that dose escalation was more effective in inducing IL10-secreting Tregs than a single high dose injection (Burton et al., 2014). It is also important to understand the tolerance mechanisms that iTregs exploit after ASI. As introduced in section 1.4.1.2, iTregs could induce Teff apoptosis, reduce Teff proliferation or cause indirect suppression through DCs (Vignali et al., 2008, Schmetterer et al., 2012). Based on current proliferation results, it is still uncertain which mechanism or combination of mechanisms any iTregs may use to exert their effect. One study demonstrated that BDC2.5-TCR-Tg mice could be protected from developing diabetes by injection of a soluble peptide, which was thought to be due to the apoptosis of activated Teffs (Judkowski et al., 2004). Full understanding of ASI mechanisms is essential to determine the treatment stage, dose and duration and the selection of appropriate combination therapies. In this project, we explored the use of betamethasone pre-treatment as a combined therapy with ASI.

5.2.3. Effect of short term topical BD on ASI

To investigate the effect of steroid on enhancing tolerance, we used topical betamethasone to educate skin DCs into a tolerogenic state. As discussed previously, the hydration effect caused by topical steroid application can influence the clearance of delivered peptide. Betamethasone coated MNs were tested against topical betamethasone application on human skin explants. HLA DR expression on human LCs was reduced when skin was treated with topical BD and BSP coated MNs. Proliferation of MLR was slightly reduced with betamethasone treated human skin epidermal cells; this however did not correlate with the level of anti-inflammatory cytokine IL10. Mouse skin epidermal cells, on the other hand, showed an increased level of IL10 when co-cultured with BDC2.5 T cells. Although it was demonstrated that topical BD could potentially down regulate the maturation of skin DCs, we found that the dose required to demonstrate this effect in the murine study caused some systemic toxicity (Piemonti et al., 1999b) (Shibata et al., 2009). This toxicity was reflected in the depletion of $CD4^+$ T cells and $CD11C^+$ DCs in LNs. Interestingly, betamethasone has been shown to have different effects on $CD4^+$ T cells in different lymphoid organs. Betamethasone can spare the memory/effector T cells and naïve T cells in LNs and in the SP, but induces apoptosis in activated T cells; therefore, the subpopulation of $CD4^+$ T cells was changed due to treatment with betamethasone (Wu et al., 2013, Tischner et al., 2011, Jamieson and Yamamoto, 2000). We found that when topical betamethasone was diluted to 0.001% w/w, systemic toxicity was minimised. NOD mice were therefore pre-treated with a reduced dose of topical betamethasone followed by peptide (m31 or WE14) treatment, but no enhanced tolerance was observed. This could be due to non-specific immunosuppressive effects and the complex mechanisms of glucocorticoids on both DCs and T cells (Furue and Katz, 1989b, Moser et al.,

1995, Koopman et al., 2001, Hoetzenecker et al., 2004, Rozkova et al., 2006, Herold et al., 2006). Increased BDC2.5 T cell proliferation was observed when using undiluted BD cream, which may due to the T cell re-reaching its homeostatic state after depletion. A 1/50 diluted cream also showed no effect on enhancing tolerance. One possible explanation for this is that betamethasone may deplete DCs and/or prevent DCs migrating from the skin (Hoetzenecker et al., 2004, Meingassner et al., 2003). This would have the effect of reducing effective DCs presentation of peptide and consequent interaction with T cells in LNs. In a primate study, DCs were also found in their matured state after skin was treated with a topical steroid (Koopman et al., 2001). These matured DCs were likely to trigger an immune response rather than to induce a tolerogenic immune response. The anti-inflammatory effect of betamethasone remains undisputed. As previously stated 1/50 diluted BD cream alone could reduce the proliferation of BDC2.5 T cells, showing that the dose we were using was able to suppress immune response *in vivo*. Betamethasone acts through its receptor in cells, which is expressed in a wide variety of cells (Danielsen et al., 1987, Barnes, 1998, Rhen and Cidlowski, 2005, Coutinho and Chapman, 2011). Therefore, it is very difficult to target one specific cell type using betamethasone. This non-specific targeting may cause complex cross talk between lymphocytes and non-lymphocytes. It is therefore very difficult to precisely predict the true effect of betamethasone on ASI.

5.3. Concluding remarks

In conclusion in this project the following was achieved:

1. A novel, universal solid MN coating formulation system was developed for materials with a wide range of hydrophobicity. This formulation system contains three co-solvents, water, 2-methyl-2-butanol and acetic acid, and one excipient, PVA2000. No loss of bioactivity was detected when peptides were formulated using this coating solution.
2. Solid stainless steel MNs were optimised for skin-targeted delivery to skin DCs. MNs with needle lengths of 500μm were chosen for effective skin delivery in both human and mouse skin. Electropolishing was performed to reduce the surface roughness from MN surface and hence enhance the delivery efficiency of hydrophobic peptides. The optimised MN device contained three arrays of MNs, 30 MNs in total, and was shown to be able to effectively deliver 2μg m31 and 6μg WE14 to mouse skin.
3. The clearance of peptides delivered to skin was shown to be influenced by environmental temperature, skin hydration, peptide hydrophobicity and delivery route. A key determining factor for clearance of peptide from skin is the delivery route; peptide delivered by solid-coated MNs remained in skin longer than ID injection. This prolonged effect was not influenced by the hydration state of the skin.
4. It was demonstrated for the first time that tolerance can be induced in NOD mice *in vivo* using an endogenous antigen administered either by ID or solid-coated MNs. Although reduced proliferation of transferred BDC2.5 T cells in NOD PLN was observed in both groups, the solid-coated MN treated group showed a dose sparing effect comparing with ID injection group. Therefore, the degree of induced tolerance was enhanced by using solid-coated MNs compared with ID injection when

delivering the same dose. The induced tolerance also showed a dose responsive effect, showing more BDC2.5 T cells were prevented from proliferation when using a high dose of WE14 (50µg).

5. Both topical and betamethasone coated MNs had an effect on skin DCs. A high dose of betamethasone induced apoptosis of T cells and upregulated T cell activation markers. Reduced proliferation of transferred BDC2.5 T cells in the PLN was observed when using diluted BD. However, tolerance induced using WE14 was not enhanced when combined with short term pre-treatment of topical corticosteroid.

Bibliography

ACHA-ORBEA, H. & MCDEVITT, H. O. 1987. The first external domain of the nonobese diabetic mouse class II I-A beta chain is unique. *Proc Natl Acad Sci U S A,* 84**,** 2435-9.

AGRAWAL, A., AGRAWAL, S., TAY, J. & GUPTA, S. 2008. Biology of dendritic cells in aging. *J Clin Immunol,* 28**,** 14-20.

AKBARI, O., DEKRUYFF, R. H. & UMETSU, D. T. 2001. Pulmonary dendritic cells producing IL-10 mediate tolerance induced by respiratory exposure to antigen. *Nat Immunol,* 2**,** 725-31.

AL-QALLAF, B., DAS, D. B. & DAVIDSON, A. 2009. Transdermal drug delivery by coated microneedles: geometry effects on drug concentration in blood. *Asia-Pacific Journal of Chemical Engineering,* 4**,** 845-857.

ALARCON, J. B., HARTLEY, A. W., HARVEY, N. G. & MIKSZTA, J. A. 2007. Preclinical evaluation of microneedle technology for intradermal delivery of influenza vaccines. *Clin Vaccine Immunol,* 14**,** 375-81.

ALEXANDRE, N., RIBEIRO, J., GARTNER, A., PEREIRA, T., AMORIM, I., FRAGOSO, J., LOPES, A., FERNANDES, J., COSTA, E., SANTOS-SILVA, A., RODRIGUES, M., SANTOS, J. D., MAURICIO, A. C. & LUIS, A. L. 2014. Biocompatibility and hemocompatibility of polyvinyl alcohol hydrogel used for vascular grafting-In vitro and in vivo studies. *J Biomed Mater Res A*.

ALMAWI, W. Y., BEYHUM, H. N., RAHME, A. A. & RIEDER, M. J. 1996. Regulation of cytokine and cytokine receptor expression by glucocorticoids. *J Leukoc Biol,* 60**,** 563-72.

AMERI, M., KADKHODAYAN, M., NGUYEN, J., BRAVO, J. A., SU, R., CHAN, K., SAMIEE, A. & DADDONA, P. E. 2014. Human Growth Hormone Delivery with a Microneedle Transdermal System: Preclinical Formulation, Stability, Delivery and PK of Therapeutically Relevant Doses. *Pharmaceutics,* 6**,** 220-34.

AMERICAN DIABETES, A. 2010. Diagnosis and classification of diabetes mellitus. *Diabetes Care,* 33 Suppl 1**,** S62-9.

AMMIRATI, E., CIANFLONE, D., VECCHIO, V., BANFI, M., VERMI, A. C., DE METRIO, M., GRIGORE, L., PELLEGATTA, F., PIRILLO, A., GARLASCHELLI, K., MANFREDI, A. A., CATAPANO, A. L., MASERI, A., PALINI, A. G. & NORATA, G. D. 2012. Effector Memory T cells Are Associated With Atherosclerosis in Humans and Animal Models. *J Am Heart Assoc,* 1**,** 27-41.

ANDERSON, R. P. & JABRI, B. 2013. Vaccine against autoimmune disease: antigen-specific immunotherapy. *Curr Opin Immunol,* 25**,** 410-7.

APPLEMAN, L. J. & BOUSSIOTIS, V. A. 2003. T cell anergy and costimulation. *Immunol Rev,* 192**,** 161-80.

ASCHENBRENNER, K., D'CRUZ, L. M., VOLLMANN, E. H., HINTERBERGER, M., EMMERICH, J., SWEE, L. K., ROLINK, A. & KLEIN, L. 2007. Selection of Foxp3+ regulatory T cells specific for self antigen expressed and presented by Aire+ medullary thymic epithelial cells. *Nat Immunol,* 8**,** 351-8.

ASHWORTH, J., BOOKER, J. & BREATHNACH, S. M. 1988. Effects of topical corticosteroid therapy on Langerhans cell antigen presenting function in human skin. *The British journal of dermatology,* 118**,** 457-69.

ATKINSON, M. A. & LEITER, E. H. 1999. The NOD mouse model of type 1 diabetes: as good as it gets? *Nature medicine,* 5**,** 601-4.

ATKINSON, M. A., MACLAREN, N. K. & LUCHETTA, R. 1990. Insulitis and diabetes in NOD mice reduced by prophylactic insulin therapy. *Diabetes,* 39**,** 933-7.

AZAR, S. T., TAMIM, H., BEYHUM, H. N., HABBAL, M. Z. & ALMAWI, W. Y. 1999. Type I (insulin-dependent) diabetes is a Th1- and Th2-mediated autoimmune disease. *Clin Diagn Lab Immunol,* 6**,** 306-10.

BAATEN, B. J., LI, C. R., DEIRO, M. F., LIN, M. M., LINTON, P. J. & BRADLEY, L. M. 2010. CD44 regulates survival and memory development in Th1 cells. *Immunity,* 32**,** 104-15.

BABAD, J., GELIEBTER, A. & DILORENZO, T. P. 2010. T-cell autoantigens in the non-obese diabetic mouse model of autoimmune diabetes. *Immunology,* 131**,** 459-65.

BADRAN, M. M., KUNTSCHE, J. & FAHR, A. 2009. Skin penetration enhancement by a microneedle device (Dermaroller) in vitro: dependency on needle size and applied formulation. *European journal of pharmaceutical sciences : official journal of the European Federation for Pharmaceutical Sciences,* 36**,** 511-23.

BAL, S. M., CAUSSIN, J., PAVEL, S. & BOUWSTRA, J. A. 2008. In vivo assessment of safety of microneedle arrays in human skin. *European journal of pharmaceutical sciences : official journal of the European Federation for Pharmaceutical Sciences,* 35**,** 193-202.

BAL, S. M., DING, Z., KERSTEN, G. F., JISKOOT, W. & BOUWSTRA, J. A. 2010. Microneedle-based transcutaneous immunisation in mice with N-

trimethyl chitosan adjuvanted diphtheria toxoid formulations. *Pharm Res,* 27**,** 1837-47.

BAO, M., YANG, Y., JUN, H. S. & YOON, J. W. 2002. Molecular mechanisms for gender differences in susceptibility to T cell-mediated autoimmune diabetes in nonobese diabetic mice. *J Immunol,* 168**,** 5369-75.

BARNES, P. J. 1998. Anti-inflammatory actions of glucocorticoids: molecular mechanisms. *Clin Sci (Lond),* 94**,** 557-72.

BASAVARAJ, S. & BETAGERI, G. V. 2014. Can formulation and drug delivery reduce attrition during drug discovery and development—review of feasibility, benefits and challenges. *Acta Pharmaceutica Sinica B,* 4**,** 3-17.

BAXTER, A. G., KOULMANDA, M. & MANDEL, T. E. 1991. High and low diabetes incidence nonobese diabetic (NOD) mice: origins and characterisation. *Autoimmunity,* 9**,** 61-7.

BELSITO, D. V., FLOTTE, T. J., LIM, H. W., BAER, R. L., THORBECKE, G. J. & GIGLI, I. 1982a. Effect of glucocorticosteroids on epidermal Langerhans cells. *The Journal of experimental medicine,* 155**,** 291-302.

BELSITO, D. V., FLOTTE, T. J., LIM, H. W., BAER, R. L., THORBECKE, G. J. & GIGLI, I. 1982b. Effect of glucocorticosteroids on epidermal Langerhans cells. *J Exp Med,* 155**,** 291-302.

BERAN, J., AMBROZAITIS, A., LAISKONIS, A., MICKUVIENE, N., BACART, P., CALOZET, Y., DEMANET, E., HEIJMANS, S., VAN BELLE, P., WEBER, F. & SALAMAND, C. 2009. Intradermal influenza vaccination of healthy adults using a new microinjection system: a 3-year randomised controlled safety and immunogenicity trial. *BMC Med,* 7**,** 13.

BERGER, T. G., SCHULZE-KOOPS, H., SCHAFER, M., MULLER, E. & LUTZ, M. B. 2009. Immature and maturation-resistant human dendritic cells generated from bone marrow require two stimulations to induce T cell anergy in vitro. *PLoS One,* 4**,** e6645.

BEVILACQUA, M., BUTCHER, E., FURIE, B., FURIE, B., GALLATIN, M., GIMBRONE, M., HARLAN, J., KISHIMOTO, K., LASKY, L., MCEVER, R. & ET AL. 1991. Selectins: a family of adhesion receptors. *Cell,* 67**,** 233.

BINGAMAN, A. W., PATKE, D. S., MANE, V. R., AHMADZADEH, M., NDEJEMBI, M., BARTLETT, S. T. & FARBER, D. L. 2005. Novel phenotypes and migratory properties distinguish memory CD4 T cell subsets in lymphoid and lung tissue. *Eur J Immunol,* 35**,** 3173-86.

BOND, J. R. & BARRY, B. W. 1988. Limitations of hairless mouse skin as a model for in vitro permeation studies through human skin: hydration damage. *J Invest Dermatol,* 90**,** 486-9.

BONNER, S. M., PIETROPAOLO, S. L., FAN, Y., CHANG, Y., SETHUPATHY, P., MORRAN, M. P., BEEMS, M., GIANNOUKAKIS, N., TRUCCO, G., PALUMBO, M. O., SOLIMENA, M., PUGLIESE, A., POLYCHRONAKOS, C., TRUCCO, M. & PIETROPAOLO, M. 2012. Sequence variation in promoter of Ica1 gene, which encodes protein implicated in type 1 diabetes, causes transcription factor autoimmune regulator (AIRE) to increase its binding and down-regulate expression. *J Biol Chem,* 287**,** 17882-93.

BOONMA, A., NARAYAN, R. J. & LEE, Y. S. 2012. Analytical Modeling and Evaluation of Microneedles Apparatus with Deformable Soft Tissues for Biomedical Applications.

BOSMA, M. J. & CARROLL, A. M. 1991. The SCID mouse mutant: definition, characterization, and potential uses. *Annu Rev Immunol,* 9**,** 323-50.

BRADLEY, L. M., ASENSIO, V. C., SCHIOETZ, L. K., HARBERTSON, J., KRAHL, T., PATSTONE, G., WOOLF, N., CAMPBELL, I. L. & SARVETNICK, N. 1999. Islet-specific Th1, but not Th2, cells secrete multiple chemokines and promote rapid induction of autoimmune diabetes. *J Immunol,* 162**,** 2511-20.

BRODE, S., RAINE, T., ZACCONE, P. & COOKE, A. 2006. Cyclophosphamide-induced type-1 diabetes in the NOD mouse is associated with a reduction of CD4+CD25+Foxp3+ regulatory T cells. *J Immunol,* 177**,** 6603-12.

BURTON, B. R., BRITTON, G. J., FANG, H., VERHAGEN, J., SMITHERS, B., SABATOS-PEYTON, C. A., CARNEY, L. J., GOUGH, J., STROBEL, S. & WRAITH, D. C. 2014. Sequential transcriptional changes dictate safe and effective antigen-specific immunotherapy. *Nat Commun,* 5**,** 4741.

CARUSO, A., LICENZIATI, S., CORULLI, M., CANARIS, A. D., DE FRANCESCO, M. A., FIORENTINI, S., PERONI, L., FALLACARA, F., DIMA, F., BALSARI, A. & TURANO, A. 1997. Flow cytometric analysis of activation markers on stimulated T cells and their correlation with cell proliferation. *Cytometry,* 27**,** 71-6.

CHAILLOUS, L., LEFEVRE, H., THIVOLET, C., BOITARD, C., LAHLOU, N., ATLAN-GEPNER, C., BOUHANICK, B., MOGENET, A., NICOLINO, M., CAREL, J. C., LECOMTE, P., MARECHAUD, R., BOUGNERES, P., CHARBONNEL, B. & SAI, P. 2000. Oral insulin administration and residual beta-cell function in recent-onset type 1 diabetes: a multicentre randomised controlled trial. Diabete Insuline Orale group. *Lancet,* 356**,** 545-9.

CHANDRASEKARAN, S., BRAZZLE, J. D. & FRAZIER, A. B. 2003. Surface micromachined metallic microneedles. *Microelectromechanical Systems, Journal of,* 12**,** 281-288.

CHATENOUD, L. 2011. Natural and induced T CD4+CD25+FOXP3+ regulatory T cells. *Methods Mol Biol,* 677**,** 3-13.

CHATENOUD, L., THERVET, E., PRIMO, J. & BACH, J. F. 1994. Anti-CD3 antibody induces long-term remission of overt autoimmunity in nonobese diabetic mice. *Proc Natl Acad Sci U S A,* 91**,** 123-7.

CHEN, J. & LEE, L. 2007. Clinical applications and new developments of optical coherence tomography: an evidence-based review. *Clin Exp Optom,* 90**,** 317-35.

CHEN, X., OPPENHEIM, J. J., WINKLER-PICKETT, R. T., ORTALDO, J. R. & HOWARD, O. M. 2006. Glucocorticoid amplifies IL-2-dependent expansion of functional FoxP3(+)CD4(+)CD25(+) T regulatory cells in vivo and enhances their capacity to suppress EAE. *Eur J Immunol,* 36**,** 2139-49.

CHONG, R. H., GONZALEZ-GONZALEZ, E., LARA, M. F., SPEAKER, T. J., CONTAG, C. H., KASPAR, R. L., COULMAN, S. A., HARGEST, R. & BIRCHALL, J. C. 2013. Gene silencing following siRNA delivery to skin via coated steel microneedles: In vitro and in vivo proof-of-concept. *J Control Release,* 166**,** 211-9.

CHOW, Z., BANERJEE, A. & HICKEY, M. J. 2015. Controlling the fire - tissue-specific mechanisms of effector regulatory T-cell homing. *Immunol Cell Biol,* 93**,** 355-363.

CHRISTIANSON, S. W., SHULTZ, L. D. & LEITER, E. H. 1993. Adoptive transfer of diabetes into immunodeficient NOD-scid/scid mice. Relative contributions of CD4+ and CD8+ T-cells from diabetic versus prediabetic NOD.NON-Thy-1a donors. *Diabetes,* 42**,** 44-55.

CHRISTIE, R. J., TADIELLO, C. J., CHAMBERLAIN, L. M. & GRAINGER, D. W. 2009. Optical properties and application of a reactive and bioreducible thiol-containing tetramethylrhodamine dimer. *Bioconjug Chem,* 20**,** 476-80.

CHU, L. Y., CHOI, S. O. & PRAUSNITZ, M. R. 2010. Fabrication of Dissolving Polymer Microneedles for Controlled Drug Encapsulation and Delivery: Bubble and Pedestal Microneedle Designs. *Journal of pharmaceutical sciences,* 99**,** 4228-4238.

CHUNG, D. J., ROMANO, E., PRONSCHINSKE, K. B., SHYER, J. A., MENNECOZZI, M., ST ANGELO, E. T. & YOUNG, J. W. 2013. Langerhans-type and monocyte-derived human dendritic cells have different

susceptibilities to mRNA electroporation with distinct effects on maturation and activation: implications for immunogenicity in dendritic cell-based immunotherapy. *J Transl Med,* 11**,** 166.

CORMIER, M., JOHNSON, B., AMERI, M., NYAM, K., LIBIRAN, L., ZHANG, D. D. & DADDONA, P. 2004. Transdermal delivery of desmopressin using a coated microneedle array patch system. *J Control Release,* 97**,** 503-11.

CORPER, A. L., STRATMANN, T., APOSTOLOPOULOS, V., SCOTT, C. A., GARCIA, K. C., KANG, A. S., WILSON, I. A. & TEYTON, L. 2000. A structural framework for deciphering the link between I-Ag7 and autoimmune diabetes. *Science,* 288**,** 505-11.

CORREIA, R. P., MATOS, E. S. F. A., BACAL, N. S., CAMPREGHER, P. V., HAMERSCHLAK, N. & AMARANTE-MENDES, G. P. 2014. Involvement of memory T-cells in the pathophysiology of chronic lymphocytic leukemia. *Rev Bras Hematol Hemoter,* 36**,** 60-4.

COTTA-DE-ALMEIDA, V., VILLA-VERDE, D. M., LEPAULT, F., PLEAU, J. M., DARDENNE, M. & SAVINO, W. 2004. Impaired migration of NOD mouse thymocytes: a fibronectin receptor-related defect. *Eur J Immunol,* 34**,** 1578-87.

COULMAN, S. A., ANSTEY, A., GATELEY, C., MORRISSEY, A., MCLOUGHLIN, P., ALLENDER, C. & BIRCHALL, J. C. 2009. Microneedle mediated delivery of nanoparticles into human skin. *Int J Pharm,* 366**,** 190-200.

COULMAN, S. A., BARROW, D., ANSTEY, A., GATELEY, C., MORRISSEY, A., WILKE, N., ALLENDER, C., BRAIN, K. & BIRCHALL, J. C. 2006. Minimally invasive cutaneous delivery of macromolecules and plasmid DNA via microneedles. *Curr Drug Deliv,* 3**,** 65-75.

COULMAN, S. A., BIRCHALL, J. C., ALEX, A., PEARTON, M., HOFER, B., O'MAHONY, C., DREXLER, W. & POVAZAY, B. 2011. In vivo, in situ imaging of microneedle insertion into the skin of human volunteers using optical coherence tomography. *Pharm Res,* 28**,** 66-81.

COUTINHO, A. E. & CHAPMAN, K. E. 2011. The anti-inflammatory and immunosuppressive effects of glucocorticoids, recent developments and mechanistic insights. *Mol Cell Endocrinol,* 335**,** 2-13.

CUDWORTH, A. G. & WOODROW, J. C. 1977. Classification of diabetes. *Lancet,* 1**,** 949-50.

CUMBERBATCH, M., DEARMAN, R. J. & KIMBER, I. 1999. Inhibition by dexamethasone of Langerhans cell migration: influence of epidermal cytokine signals. *Immunopharmacology,* 41**,** 235-43.

CURRY, W. J., BARKATULLAH, S. C., JOHANSSON, A. N., QUINN, J. G., NORLEN, P., CONNOLLY, C. K., MCCOLLUM, A. P. & MCVICAR, C. M. 2002. WE-14, a chromogranin a-derived neuropeptide. *Annals of the New York Academy of Sciences,* 971**,** 311-6.

DADDONA, P. E., MATRIANO, J. A., MANDEMA, J. & MAA, Y. F. 2011. Parathyroid hormone (1-34)-coated microneedle patch system: clinical pharmacokinetics and pharmacodynamics for treatment of osteoporosis. *Pharmaceutical research,* 28**,** 159-65.

DAI, Y. D., JENSEN, K. P., LEHUEN, A., MASTELLER, E. L., BLUESTONE, J. A., WILSON, D. B. & SERCARZ, E. E. 2005. A peptide of glutamic acid decarboxylase 65 can recruit and expand a diabetogenic T cell clone, BDC2.5, in the pancreas. *Journal of immunology,* 175**,** 3621-7.

DAIFOTIS, A. G., KOENIG, S., CHATENOUD, L. & HEROLD, K. C. 2013. Anti-CD3 clinical trials in type 1 diabetes mellitus. *Clin Immunol,* 149**,** 268-78.

DANIEL, D., GILL, R. G., SCHLOOT, N. & WEGMANN, D. 1995. Epitope specificity, cytokine production profile and diabetogenic activity of insulin-specific T cell clones isolated from NOD mice. *Eur J Immunol,* 25**,** 1056-62.

DANIEL, D. & WEGMANN, D. R. 1996. Protection of nonobese diabetic mice from diabetes by intranasal or subcutaneous administration of insulin peptide B-(9-23). *Proceedings of the National Academy of Sciences of the United States of America,* 93**,** 956-60.

DANIELSEN, M., NORTHROP, J. P., JONKLAAS, J. & RINGOLD, G. M. 1987. Domains of the glucocorticoid receptor involved in specific and nonspecific deoxyribonucleic acid binding, hormone activation, and transcriptional enhancement. *Mol Endocrinol,* 1**,** 816-22.

DAVIS, S. P., LANDIS, B. J., ADAMS, Z. H., ALLEN, M. G. & PRAUSNITZ, M. R. 2004. Insertion of microneedles into skin: measurement and prediction of insertion force and needle fracture force. *J Biomech,* 37**,** 1155-63.

DE FILIPPO, G., CAREL, J. C., BOITARD, C. & BOUGNERES, P. F. 1996. Long-term results of early cyclosporin therapy in juvenile IDDM. *Diabetes,* 45**,** 101-4.

DEL PRETE, G. 1992. Human Th1 and Th2 lymphocytes: their role in the pathophysiology of atopy. *Allergy,* 47**,** 450-5.

DELONG, T., BAKER, R. L., HE, J., BARBOUR, G., BRADLEY, B. & HASKINS, K. 2012. Diabetogenic T-cell clones recognize an altered peptide of chromogranin A. *Diabetes,* 61**,** 3239-46.

DELONG, T., BAKER, R. L., HE, J. & HASKINS, K. 2013. Novel autoantigens for diabetogenic CD4 T cells in autoimmune diabetes. *Immunologic research,* 55**,** 167-72.

DINARELLO, C. A. 2000. Proinflammatory cytokines. *Chest,* 118**,** 503-8.

DOBBS, C. & HASKINS, K. 2001. Comparison of a T cell clone and of T cells from a TCR transgenic mouse: TCR transgenic T cells specific for self-antigen are atypical. *J Immunol,* 166**,** 2495-504.

DONNELLY, R. F., GARLAND, M. J., MORROW, D. I., MIGALSKA, K., SINGH, T. R., MAJITHIYA, R. & WOOLFSON, A. D. 2010. Optical coherence tomography is a valuable tool in the study of the effects of microneedle geometry on skin penetration characteristics and in-skin dissolution. *J Control Release,* 147**,** 333-41.

DONNELLY, R. F., MAJITHIYA, R., SINGH, T. R., MORROW, D. I., GARLAND, M. J., DEMIR, Y. K., MIGALSKA, K., RYAN, E., GILLEN, D., SCOTT, C. J. & WOOLFSON, A. D. 2011. Design, optimization and characterisation of polymeric microneedle arrays prepared by a novel laser-based micromoulding technique. *Pharmaceutical Research,* 28**,** 41-57.

DONNELLY, R. F., MORROW, D. I., SINGH, T. R., MIGALSKA, K., MCCARRON, P. A., O'MAHONY, C. & WOOLFSON, A. D. 2009a. Processing difficulties and instability of carbohydrate microneedle arrays. *Drug Development and Industrial Pharmacy,* 35**,** 1242-54.

DONNELLY, R. F., SINGH, T. R., TUNNEY, M. M., MORROW, D. I., MCCARRON, P. A., O'MAHONY, C. & WOOLFSON, A. D. 2009b. Microneedle arrays allow lower microbial penetration than hypodermic needles in vitro. *Pharm Res,* 26**,** 2513-22.

EDWARDS, T. B. 1995. Effectiveness and safety of beclomethasone dipropionate, an intranasal corticosteroid, in the treatment of patients with allergic rhinitis. *Clin Ther,* 17**,** 1032-41.

ENGVALL, E. & PERLMANN, P. 1971. Enzyme-linked immunosorbent assay (ELISA). Quantitative assay of immunoglobulin G. *Immunochemistry,* 8**,** 871-4.

ERGUN-LONGMIRE, B., MARKER, J., ZEIDLER, A., RAPAPORT, R., RASKIN, P., BODE, B., SCHATZ, D., VARGAS, A., ROGERS, D., SCHWARTZ, S., MALONE, J., KRISCHER, J. & MACLAREN, N. K. 2004. Oral insulin therapy to prevent progression of immune-mediated (type 1) diabetes. *Ann N Y Acad Sci,* 1029**,** 260-77.

ERMANN, J., HOFFMANN, P., EDINGER, M., DUTT, S., BLANKENBERG, F. G., HIGGINS, J. P., NEGRIN, R. S., FATHMAN, C. G. & STROBER, S. 2005.

Only the CD62L+ subpopulation of CD4+CD25+ regulatory T cells protects from lethal acute GVHD. *Blood,* 105**,** 2220-6.

FAHIM, M. A. & AL-MUHTASEB, S. A. 1996. Liquid–Liquid Equilibria of the Ternary System Water + Acetic Acid + 2-Methyl-2-butanol. *Journal of Chemical & Engineering Data,* 41**,** 1311-1314.

FAINARU, O., HANTISTEANU, S., ROTFARB, N., MICHAELI, M., HALLAK, M. & ELLENBOGEN, A. 2012. CD11c+HLADR+ dendritic cells are present in human ovarian follicular fluid, and their maturity correlates with serum estradiol levels in response to gonadotropins. *Fertil Steril,* 97**,** 702-6.

FEUERER, M., HILL, J. A., MATHIS, D. & BENOIST, C. 2009. Foxp3+ regulatory T cells: differentiation, specification, subphenotypes. *Nat Immunol,* 10**,** 689-95.

FISCHER, A. H., JACOBSON, K. A., ROSE, J. & ZELLER, R. 2008. Hematoxylin and eosin staining of tissue and cell sections. *CSH Protoc,* 2008**,** pdb prot4986.

FONTENOT, J. D., GAVIN, M. A. & RUDENSKY, A. Y. 2003. Foxp3 programs the development and function of CD4+CD25+ regulatory T cells. *Nat Immunol,* 4**,** 330-6.

FORBES, J. M. & COOPER, M. E. 2013. Mechanisms of diabetic complications. *Physiol Rev,* 93**,** 137-88.

FOURLANOS, S., PERRY, C., GELLERT, S. A., MARTINUZZI, E., MALLONE, R., BUTLER, J., COLMAN, P. G. & HARRISON, L. C. 2011. Evidence that nasal insulin induces immune tolerance to insulin in adults with autoimmune diabetes. *Diabetes,* 60**,** 1237-45.

FOUSTERI, G., DAVE, A., BOT, A., JUNTTI, T., OMID, S. & VON HERRATH, M. 2010. Subcutaneous insulin B:9-23/IFA immunisation induces Tregs that control late-stage prediabetes in NOD mice through IL-10 and IFNgamma. *Diabetologia,* 53**,** 1958-70.

FUKUNAGA, A., KHASKHELY, N. M., SREEVIDYA, C. S., BYRNE, S. N. & ULLRICH, S. E. 2008. Dermal dendritic cells, and not Langerhans cells, play an essential role in inducing an immune response. *J Immunol,* 180**,** 3057-64.

FURUE, M. & KATZ, S. I. 1989a. Direct effects of glucocorticosteroids on epidermal Langerhans cells. *The Journal of investigative dermatology,* 92**,** 342-7.

FURUE, M. & KATZ, S. I. 1989b. Direct effects of glucocorticosteroids on epidermal Langerhans cells. *J Invest Dermatol,* 92**,** 342-7.

GAGNERAULT, M. C., LUAN, J. J., LOTTON, C. & LEPAULT, F. 2002. Pancreatic lymph nodes are required for priming of beta cell reactive T cells in NOD mice. *J Exp Med,* 196**,** 369-77.

GARBI, N., HAMMERLING, G. J., PROBST, H. C. & VAN DEN BROEK, M. 2010. Tonic T cell signalling and T cell tolerance as opposite effects of self-recognition on dendritic cells. *Curr Opin Immunol,* 22**,** 601-8.

GARY, S. F. R., C. BUDD; SHERINE, E. GABRIEL; IAIN, B. MCLNNES; JAMES, R. O'DELL 2013. Glucocorticoid Therapy. *Kelley's Textbook of Rheumatology.*

GASPARI, A. A. & KATZ, S. I. 1991. Induction of in vivo hyporesponsiveness to contact allergens by hapten-modified Ia+ keratinocytes. *Journal of immunology,* 147**,** 4155-61.

GE, Q., PALLISER, D., EISEN, H. N. & CHEN, J. 2002. Homeostatic T cell proliferation in a T cell-dendritic cell coculture system. *Proc Natl Acad Sci U S A,* 99**,** 2983-8.

GEGINAT, J., PARONI, M., MAGLIE, S., ALFEN, J. S., KASTIRR, I., GRUARIN, P., DE SIMONE, M., PAGANI, M. & ABRIGNANI, S. 2014. Plasticity of human CD4 T cell subsets. *Front Immunol,* 5**,** 630.

GEPTS, W. 1965. Pathologic anatomy of the pancreas in juvenile diabetes mellitus. *Diabetes,* 14**,** 619-33.

GERLACH, K., HWANG, Y., NIKOLAEV, A., ATREYA, R., DORNHOFF, H., STEINER, S., LEHR, H. A., WIRTZ, S., VIETH, M., WAISMAN, A., ROSENBAUER, F., MCKENZIE, A. N., WEIGMANN, B. & NEURATH, M. F. 2014. TH9 cells that express the transcription factor PU.1 drive T cell-mediated colitis via IL-9 receptor signaling in intestinal epithelial cells. *Nat Immunol,* 15**,** 676-86.

GERSTEL, M. S. 1976. Drug delivery device. Google Patents.

GHOSH, B., REDDY, L. H., KULKARNI, R. V. & KHANAM, J. 2000. Comparison of skin permeability of drugs in mice and human cadaver skin. *Indian J Exp Biol,* 38**,** 42-5.

GHOSH, T. K., HABIB, M. J., CHILDS, K. & ALEXANDER, M. 1992. Transdermal delivery of metoprolol I: Comparison between hairless mouse and human cadaver skin and effect of n-decylmethyl sulfoxide. *International Journal of Pharmaceutics,* 88**,** 391-396.

GILL, H. S. & PRAUSNITZ, M. R. 2007a. Coated microneedles for transdermal delivery. *Journal of controlled release : official journal of the Controlled Release Society,* 117**,** 227-37.

GILL, H. S. & PRAUSNITZ, M. R. 2007b. Coated microneedles for transdermal delivery. *J Control Release,* 117**,** 227-37.

GILL, H. S. & PRAUSNITZ, M. R. 2007c. Coating formulations for microneedles. *Pharmaceutical research,* 24**,** 1369-80.

GILLIS, S., FERM, M. M., OU, W. & SMITH, K. A. 1978. T cell growth factor: parameters of production and a quantitative microassay for activity. *J Immunol,* 120**,** 2027-32.

GIRVIN, A. M., DAL CANTO, M. C., RHEE, L., SALOMON, B., SHARPE, A., BLUESTONE, J. A. & MILLER, S. D. 2000. A critical role for B7/CD28 costimulation in experimental autoimmune encephalomyelitis: a comparative study using costimulatory molecule-deficient mice and monoclonal antibody blockade. *J Immunol,* 164**,** 136-43.

GODFREY, D. I. & ZLOTNIK, A. 1993. Control points in early T-cell development. *Immunol Today,* 14**,** 547-53.

GONZALEZ, A., ANDRE-SCHMUTZ, I., CARNAUD, C., MATHIS, D. & BENOIST, C. 2001. Damage control, rather than unresponsiveness, effected by protective DX5+ T cells in autoimmune diabetes. *Nat Immunol,* 2**,** 1117-25.

GONZALEZ, A., KATZ, J. D., MATTEI, M. G., KIKUTANI, H., BENOIST, C. & MATHIS, D. 1997. Genetic control of diabetes progression. *Immunity,* 7**,** 873-83.

GOTTLIEB, P. A., DELONG, T., BAKER, R. L., FITZGERALD-MILLER, L., WAGNER, R., COOK, G., REWERS, M. R., MICHELS, A. & HASKINS, K. 2014. Chromogranin A is a T cell antigen in human type 1 diabetes. *J Autoimmun,* 50**,** 38-41.

GRABBE, S., STEINBRINK, K., STEINERT, M., LUGER, T. A. & SCHWARZ, T. 1995. Removal of the majority of epidermal Langerhans cells by topical or systemic steroid application enhances the effector phase of murine contact hypersensitivity. *Journal of immunology,* 155**,** 4207-17.

GRAHAM, V. A., MARZO, A. L. & TOUGH, D. F. 2007. A role for CD44 in T cell development and function during direct competition between CD44+ and CD44- cells. *Eur J Immunol,* 37**,** 925-34.

GROVES, R. B., COULMAN, S. A., BIRCHALL, J. C. & EVANS, S. L. 2013. An anisotropic, hyperelastic model for skin: experimental measurements, finite element modelling and identification of parameters for human and murine skin. *J Mech Behav Biomed Mater,* 18**,** 167-80.

GUPTA, H., BHANDARI, D. & SHARMA, A. 2009a. Recent trends in oral drug delivery: a review. *Recent Pat Drug Deliv Formul,* 3**,** 162-73.

GUPTA, J., FELNER, E. I. & PRAUSNITZ, M. R. 2009b. Minimally invasive insulin delivery in subjects with type 1 diabetes using hollow microneedles. *Diabetes Technol Ther,* 11**,** 329-37.

GUPTA, J., FELNER, E. I. & PRAUSNITZ, M. R. 2009c. Minimally invasive insulin delivery in subjects with type 1 diabetes using hollow microneedles. *Diabetes technology & therapeutics,* 11**,** 329-37.

GUPTA, J., GILL, H. S., ANDREWS, S. N. & PRAUSNITZ, M. R. 2011a. Kinetics of skin resealing after insertion of microneedles in human subjects. *J Control Release,* 154**,** 148-55.

GUPTA, J., PARK, S. S., BONDY, B., FELNER, E. I. & PRAUSNITZ, M. R. 2011b. Infusion pressure and pain during microneedle injection into skin of human subjects. *Biomaterials,* 32**,** 6823-31.

GYSLER, A., KLEUSER, B., SIPPL, W., LANGE, K., KORTING, H. C., HOLTJE, H. D. & KORTING, H. C. 1999. Skin penetration and metabolism of topical glucocorticoids in reconstructed epidermis and in excised human skin. *Pharm Res,* 16**,** 1386-91.

HAQ, M. I., SMITH, E., JOHN, D. N., KALAVALA, M., EDWARDS, C., ANSTEY, A., MORRISSEY, A. & BIRCHALL, J. C. 2009. Clinical administration of microneedles: skin puncture, pain and sensation. *Biomed Microdevices,* 11**,** 35-47.

HARJUTSALO, V., SJOBERG, L. & TUOMILEHTO, J. 2008. Time trends in the incidence of type 1 diabetes in Finnish children: a cohort study. *Lancet,* 371**,** 1777-82.

HASKINS, K. & COOKE, A. 2011. CD4 T cells and their antigens in the pathogenesis of autoimmune diabetes. *Current opinion in immunology,* 23**,** 739-45.

HASKINS, K., DELONG, T., KAPPLER, J. W., STADINSKI, B., REISDORPH, N. & REISDORPH, R. 2012. Methods and compositions for the treatment of autoimmune disease. Google Patents.

HASKINS, K., PORTAS, M., BERGMAN, B., LAFFERTY, K. & BRADLEY, B. 1989. Pancreatic islet-specific T-cell clones from nonobese diabetic mice. *Proc Natl Acad Sci U S A,* 86**,** 8000-4.

HASKINS, K., PORTAS, M., BRADLEY, B., WEGMANN, D. & LAFFERTY, K. 1988. T-lymphocyte clone specific for pancreatic islet antigen. *Diabetes,* 37**,** 1444-8.

HATA, H., SAKAGUCHI, N., YOSHITOMI, H., IWAKURA, Y., SEKIKAWA, K., AZUMA, Y., KANAI, C., MORIIZUMI, E., NOMURA, T., NAKAMURA, T. & SAKAGUCHI, S. 2004. Distinct contribution of IL-6, TNF-alpha, IL-1,

and IL-10 to T cell-mediated spontaneous autoimmune arthritis in mice. *J Clin Invest,* 114**,** 582-8.

HATTON, R. D. 2011. TGF-beta in Th17 cell development: the truth is out there. *Immunity,* 34**,** 288-90.

HAWRYLOWICZ, C. M. & O'GARRA, A. 2005. Potential role of interleukin-10-secreting regulatory T cells in allergy and asthma. *Nat Rev Immunol,* 5**,** 271-83.

HENAO-TAMAYO, M. I., ORDWAY, D. J., IRWIN, S. M., SHANG, S., SHANLEY, C. & ORME, I. M. 2010. Phenotypic definition of effector and memory T-lymphocyte subsets in mice chronically infected with Mycobacterium tuberculosis. *Clin Vaccine Immunol,* 17**,** 618-25.

HEROLD, K. C., GITELMAN, S. E., EHLERS, M. R., GOTTLIEB, P. A., GREENBAUM, C. J., HAGOPIAN, W., BOYLE, K. D., KEYES-ELSTEIN, L., AGGARWAL, S., PHIPPARD, D., SAYRE, P. H., MCNAMARA, J., BLUESTONE, J. A. & AB, A. T. E. S. T. 2013. Teplizumab (anti-CD3 mAb) treatment preserves C-peptide responses in patients with new-onset type 1 diabetes in a randomized controlled trial: metabolic and immunologic features at baseline identify a subgroup of responders. *Diabetes,* 62**,** 3766-74.

HEROLD, K. C., HAGOPIAN, W., AUGER, J. A., POUMIAN-RUIZ, E., TAYLOR, L., DONALDSON, D., GITELMAN, S. E., HARLAN, D. M., XU, D., ZIVIN, R. A. & BLUESTONE, J. A. 2002. Anti-CD3 monoclonal antibody in new-onset type 1 diabetes mellitus. *N Engl J Med,* 346**,** 1692-8.

HEROLD, M. J., MCPHERSON, K. G. & REICHARDT, H. M. 2006. Glucocorticoids in T cell apoptosis and function. *Cell Mol Life Sci,* 63**,** 60-72.

HIGAKI, K., ASAI, M., SUYAMA, T., NAKAYAMA, K., OGAWARA, K. & KIMURA, T. 2002. Estimation of intradermal disposition kinetics of drugs: II. Factors determining penetration of drugs from viable skin to muscular layer. *Int J Pharm,* 239**,** 129-41.

HOARAU, C., LAGARAINE, C., MARTIN, L., VELGE-ROUSSEL, F. & LEBRANCHU, Y. 2006. Supernatant of Bifidobacterium breve induces dendritic cell maturation, activation, and survival through a Toll-like receptor 2 pathway. *J Allergy Clin Immunol,* 117**,** 696-702.

HOETZENECKER, W., MEINGASSNER, J. G., ECKER, R., STINGL, G., STUETZ, A. & ELBE-BURGER, A. 2004. Corticosteroids but not pimecrolimus affect viability, maturation and immune function of murine epidermal Langerhans cells. *J Invest Dermatol,* 122**,** 673-84.

HOGQUIST, K. A., BALDWIN, T. A. & JAMESON, S. C. 2005. Central tolerance: learning self-control in the thymus. *Nat Rev Immunol,* 5**,** 772-82.

HORI, S., HAURY, M., COUTINHO, A. & DEMENGEOT, J. 2002. Specificity requirements for selection and effector functions of CD25+4+ regulatory T cells in anti-myelin basic protein T cell receptor transgenic mice. *Proc Natl Acad Sci U S A,* 99**,** 8213-8.

HORI, S., NOMURA, T. & SAKAGUCHI, S. 2003. Control of regulatory T cell development by the transcription factor Foxp3. *Science,* 299**,** 1057-61.

HORI, S. & SAKAGUCHI, S. 2004. Foxp3: a critical regulator of the development and function of regulatory T cells. *Microbes Infect,* 6**,** 745-51.

HSIEH, C. S., LIANG, Y., TYZNIK, A. J., SELF, S. G., LIGGITT, D. & RUDENSKY, A. Y. 2004. Recognition of the peripheral self by naturally arising CD25+ CD4+ T cell receptors. *Immunity,* 21**,** 267-77.

HUANG, D., SWANSON, E. A., LIN, C. P., SCHUMAN, J. S., STINSON, W. G., CHANG, W., HEE, M. R., FLOTTE, T., GREGORY, K., PULIAFITO, C. A. & ET AL. 1991. Optical coherence tomography. *Science,* 254**,** 1178-81.

INABA, K., INABA, M., NAITO, M. & STEINMAN, R. M. 1993. Dendritic cell progenitors phagocytose particulates, including bacillus Calmette-Guerin organisms, and sensitize mice to mycobacterial antigens in vivo. *The Journal of experimental medicine,* 178**,** 479-88.

IRVINE, W. J. 1977. Classification of diabetes mellitus. *Lancet,* 1**,** 1202-3.

ITO, Y., KASHIWARA, S., FUKUSHIMA, K. & TAKADA, K. 2011a. Two-layered dissolving microneedles for percutaneous delivery of sumatriptan in rats. *Drug Development and Industrial Pharmacy,* 37**,** 1387-1393.

ITO, Y., MURANO, H., HAMASAKI, N., FUKUSHIMA, K. & TAKADA, K. 2011b. Incidence of low bioavailability of leuprolide acetate after percutaneous administration to rats by dissolving microneedles. *Int J Pharm,* 407**,** 126-31.

JAECKEL, E., VON BOEHMER, H. & MANNS, M. P. 2005. Antigen-specific FoxP3-transduced T-cells can control established type 1 diabetes. *Diabetes,* 54**,** 306-10.

JAMIESON, C. A. & YAMAMOTO, K. R. 2000. Crosstalk pathway for inhibition of glucocorticoid-induced apoptosis by T cell receptor signaling. *Proc Natl Acad Sci U S A,* 97**,** 7319-24.

JENSEN, E. C. 2012. Types of imaging, Part 1: Electron microscopy. *Anat Rec (Hoboken),* 295**,** 716-21.

JING JI, F. E. H. T. A. J. M. 2006. Microfabricated hollow microneedle array using ICP etcher. *J. Phys.: Conf. Ser.,* 34.

JOLLES, S. 2002. Paul Langerhans. *J Clin Pathol,* 55**,** 243.

JONULEIT, H. & SCHMITT, E. 2003. The regulatory T cell family: distinct subsets and their interrelations. *Journal of immunology,* 171**,** 6323-7.

JUDKOWSKI, V., PINILLA, C., SCHRODER, K., TUCKER, L., SARVETNICK, N. & WILSON, D. B. 2001. Identification of MHC class II-restricted peptide ligands, including a glutamic acid decarboxylase 65 sequence, that stimulate diabetogenic T cells from transgenic BDC2.5 nonobese diabetic mice. *Journal of immunology,* 166**,** 908-17.

JUDKOWSKI, V., RODRIGUEZ, E., PINILLA, C., MASTELLER, E., BLUESTONE, J. A., SARVETNICK, N. & WILSON, D. B. 2004. Peptide specific amelioration of T cell mediated pathogenesis in murine type 1 diabetes. *Clin Immunol,* 113**,** 29-37.

KALLURI, H. & BANGA, A. K. 2011. Formation and closure of microchannels in skin following microporation. *Pharm Res,* 28**,** 82-94.

KALLURI, H., KOLLI, C. S. & BANGA, A. K. 2011. Characterization of microchannels created by metal microneedles: formation and closure. *AAPS J,* 13**,** 473-81.

KALTHOFF, F. S., CHUNG, J., MUSSER, P. & STUETZ, A. 2003. Pimecrolimus does not affect the differentiation, maturation and function of human monocyte-derived dendritic cells, in contrast to corticosteroids. *Clin Exp Immunol,* 133**,** 350-9.

KAMINITZ, A., MIZRAHI, K. & ASKENASY, N. 2014. Surge in regulatory T cells does not prevent onset of hyperglycemia in NOD mice: immune profiles do not correlate with disease severity. *Autoimmunity,* 47**,** 105-12.

KANITAKIS, J. 2002. Anatomy, histology and immunohistochemistry of normal human skin. *European journal of dermatology : EJD,* 12**,** 390-9; quiz 400-1.

KASHIHARA, M., UEDA, M., HORIGUCHI, Y., FURUKAWA, F., HANAOKA, M. & IMAMURA, S. 1986. A monoclonal antibody specifically reactive to human Langerhans cells. *J Invest Dermatol,* 87**,** 602-7.

KATZ, J. D., WANG, B., HASKINS, K., BENOIST, C. & MATHIS, D. 1993. Following a diabetogenic T cell from genesis through pathogenesis. *Cell,* 74**,** 1089-100.

KAUSHIK, S., HORD, A. H., DENSON, D. D., MCALLISTER, D. V., SMITRA, S., ALLEN, M. G. & PRAUSNITZ, M. R. 2001. Lack of pain associated with microfabricated microneedles. *Anesth Analg,* 92**,** 502-4.

KENNEY, R. T., FRECH, S. A., MUENZ, L. R., VILLAR, C. P. & GLENN, G. M. 2004. Dose sparing with intradermal injection of influenza vaccine. *N Engl J Med,* 351**,** 2295-301.

KERZERHO, J., WUNSCH, D., SZELY, N., MEYER, H. A., LURZ, L., ROSE, L., WAHN, U., AKBARI, O. & STOCK, P. 2012. Effects of systemic versus local administration of corticosteroids on mucosal tolerance. *Journal of immunology,* 188**,** 470-6.

KIM, J., LAHL, K., HORI, S., LODDENKEMPER, C., CHAUDHRY, A., DEROOS, P., RUDENSKY, A. & SPARWASSER, T. 2009a. Cutting edge: depletion of Foxp3+ cells leads to induction of autoimmunity by specific ablation of regulatory T cells in genetically targeted mice. *J Immunol,* 183**,** 7631-4.

KIM, Y. C., PARK, J. H. & PRAUSNITZ, M. R. 2012. Microneedles for drug and vaccine delivery. *Adv Drug Deliv Rev,* 64**,** 1547-68.

KIM, Y. C., QUAN, F. S., COMPANS, R. W., KANG, S. M. & PRAUSNITZ, M. R. 2010a. Formulation and coating of microneedles with inactivated influenza virus to improve vaccine stability and immunogenicity. *J Control Release,* 142**,** 187-95.

KIM, Y. C., QUAN, F. S., COMPANS, R. W., KANG, S. M. & PRAUSNITZ, M. R. 2010b. Formulation of microneedles coated with influenza virus-like particle vaccine. *AAPS PharmSciTech,* 11**,** 1193-201.

KIM, Y. C., QUAN, F. S., YOO, D. G., COMPANS, R. W., KANG, S. M. & PRAUSNITZ, M. R. 2009b. Improved influenza vaccination in the skin using vaccine coated microneedles. *Vaccine,* 27**,** 6932-8.

KING, A. J. 2012. The use of animal models in diabetes research. *Br J Pharmacol,* 166**,** 877-94.

KISSENPFENNIG, A., HENRI, S., DUBOIS, B., LAPLACE-BUILHE, C., PERRIN, P., ROMANI, N., TRIPP, C. H., DOUILLARD, P., LESERMAN, L., KAISERLIAN, D., SAELAND, S., DAVOUST, J. & MALISSEN, B. 2005. Dynamics and function of Langerhans cells in vivo: dermal dendritic cells colonize lymph node areas distinct from slower migrating Langerhans cells. *Immunity,* 22**,** 643-54.

KLEIJWEGT, F. S., LABAN, S., DUINKERKEN, G., JOOSTEN, A. M., ZALDUMBIDE, A., NIKOLIC, T. & ROEP, B. O. 2010. Critical role for TNF in the induction of human antigen-specific regulatory T cells by tolerogenic dendritic cells. *J Immunol,* 185**,** 1412-8.

KLEIN, L., HINTERBERGER, M., WIRNSBERGER, G. & KYEWSKI, B. 2009. Antigen presentation in the thymus for positive selection and central tolerance induction. *Nat Rev Immunol,* 9**,** 833-44.

KLINGER, A., GEBERT, A., BIEBER, K., KALIES, K., AGER, A., BELL, E. B. & WESTERMANN, J. 2009. Cyclical expression of L-selectin (CD62L) by recirculating T cells. *Int Immunol,* 21**,** 443-55.

KOBAYASHI, Y. 1997. Langerhans' cells produce type IV collagenase (MMP-9) following epicutaneous stimulation with haptens. *Immunology,* 90**,** 496-501.

KONRADI, S., YASMIN, N., HASLWANTER, D., WEBER, M., GESSLBAUER, B., SIXT, M. & STROBL, H. 2014. Langerhans cell maturation is accompanied by induction of N-cadherin and the transcriptional regulators of epithelial-mesenchymal transition ZEB1/2. *Eur J Immunol,* 44**,** 553-60.

KOOPMAN, G., DALGLEISH, A. G., BHOGAL, B. S., HAAKSMA, A. G. & HEENEY, J. L. 2001. Changes in dendritic cell subsets in the lymph nodes of rhesus macaques after application of glucocorticoids. *Human immunology,* 62**,** 208-14.

KOUTSONANOS, D. G., VASSILIEVA, E. V., STAVROPOULOU, A., ZARNITSYN, V. G., ESSER, E. S., TAHERBHAI, M. T., PRAUSNITZ, M. R., COMPANS, R. W. & SKOUNTZOU, I. 2012. Delivery of subunit influenza vaccine to skin with microneedles improves immunogenicity and long-lived protection. *Scientific reports,* 2**,** 357.

KUKREJA, A., COST, G., MARKER, J., ZHANG, C., SUN, Z., LIN-SU, K., TEN, S., SANZ, M., EXLEY, M., WILSON, B., PORCELLI, S. & MACLAREN, N. 2002. Multiple immuno-regulatory defects in type-1 diabetes. *J Clin Invest,* 109**,** 131-40.

KURITA, S., KOYAMA, J., ONIZUKA, S., MOTOMURA, K., WATANABE, H., WATANABE, K., SENBA, M., APICELLA, M. A., MURPHY, T. F., YONEYAMA, H., MATSUSHIMA, K., NAGATAKE, T. & OISHI, K. 2006. Dynamics of dendritic cell migration and the subsequent induction of protective immunity in the lung after repeated airway challenges by nontypeable Haemophilus influenzae outer membrane protein. *Vaccine,* 24**,** 5896-903.

KURU, K. 2014. Optimization and enhancement of H&E stained microscopical images by applying bilinear interpolation method on lab color mode. *Theor Biol Med Model,* 11**,** 9.

KUSHWAH, R. & HU, J. 2011. Role of dendritic cells in the induction of regulatory T cells. *Cell & bioscience,* 1**,** 20.

KUZMANICH, G., SIMONCELLI, S., GARD, M. N., SPANIG, F., HENDERSON, B. L., GULDI, D. M. & GARCIA-GARIBAY, M. A. 2011. Excited state kinetics in crystalline solids: self-quenching in nanocrystals of 4,4'-disubstituted

benzophenone triplets occurs by a reductive quenching mechanism. *J Am Chem Soc,* 133**,** 17296-306.

LARANGE, A., ANTONIOS, D., PALLARDY, M. & KERDINE-ROMER, S. 2012. Glucocorticoids inhibit dendritic cell maturation induced by Toll-like receptor 7 and Toll-like receptor 8. *J Leukoc Biol,* 91**,** 105-17.

LAURENT, A., MISTRETTA, F., BOTTIGIOLI, D., DAHEL, K., GOUJON, C., NICOLAS, J. F., HENNINO, A. & LAURENT, P. E. 2007. Echographic measurement of skin thickness in adults by high frequency ultrasound to assess the appropriate microneedle length for intradermal delivery of vaccines. *Vaccine,* 25**,** 6423-30.

LEBLOND, F., DAVIS, S. C., VALDES, P. A. & POGUE, B. W. 2010. Pre-clinical whole-body fluorescence imaging: Review of instruments, methods and applications. *J Photochem Photobiol B,* 98**,** 77-94.

LEBRE, M. C., ANTONS, J. C., KALINSKI, P., SCHUITEMAKER, J. H., VAN CAPEL, T. M., KAPSENBERG, M. L. & DE JONG, E. C. 2003. Double-stranded RNA-exposed human keratinocytes promote Th1 responses by inducing a Type-1 polarized phenotype in dendritic cells: role of keratinocyte-derived tumor necrosis factor alpha, type I interferons, and interleukin-18. *J Invest Dermatol,* 120**,** 990-7.

LEBRUN-VIGNES, B., LEGRAIN, V., AMORIC, J. & TAIEB, A. 2000. [Comparative study of efficacy and effect on plasma cortisol levels of micronised desonide cream 0.1 p. 100 versus betamethasone dipropionate cream 0.05 p. 100 In the treatment of childhood atopic dermatitis]. *Ann Dermatol Venereol,* 127**,** 590-5.

LEE, E. S. 2000. Machining Characteristics of the Electropolishing of Stainless Steel (STS316L). *The International Journal of Advanced Manufacturing Technology,* 16**,** 591-599.

LEE, J. W., CHOI, S. O., FELNER, E. I. & PRAUSNITZ, M. R. 2011. Dissolving microneedle patch for transdermal delivery of human growth hormone. *Small,* 7**,** 531-9.

LEE, J. W., PARK, J. H. & PRAUSNITZ, M. R. 2008. Dissolving microneedles for transdermal drug delivery. *Biomaterials,* 29**,** 2113-24.

LEITER, E. H. 2001. The NOD mouse: a model for insulin-dependent diabetes mellitus. *Current protocols in immunology / edited by John E. Coligan ... [et al.],* Chapter 15**,** Unit 15 9.

LEITER, E. H., PROCHAZKA, M. & COLEMAN, D. L. 1987. The non-obese diabetic (NOD) mouse. *The American journal of pathology,* 128**,** 380-3.

LENG, S. X., MCELHANEY, J. E., WALSTON, J. D., XIE, D., FEDARKO, N. S. & KUCHEL, G. A. 2008. ELISA and multiplex technologies for cytokine measurement in inflammation and aging research. *J Gerontol A Biol Sci Med Sci,* 63**,** 879-84.

LERNMARK, A. & LARSSON, H. E. 2013. Immune therapy in type 1 diabetes mellitus. *Nat Rev Endocrinol,* 9**,** 92-103.

LETOURNEAU, S., KRIEG, C., PANTALEO, G. & BOYMAN, O. 2009. IL-2- and CD25-dependent immunoregulatory mechanisms in the homeostasis of T-cell subsets. *J Allergy Clin Immunol,* 123**,** 758-62.

LI, W. Z., HUO, M. R., ZHOU, J. P., ZHOU, Y. Q., HAO, B. H., LIU, T. & ZHANG, Y. 2010. Super-short solid silicon microneedles for transdermal drug delivery applications. *Int J Pharm,* 389**,** 122-9.

LINDSEY, W. B., LOWDELL, M. W., MARTI, G. E., ABBASI, F., ZENGER, V., KING, K. M. & LAMB, L. S., JR. 2007. CD69 expression as an index of T-cell function: assay standardization, validation and use in monitoring immune recovery. *Cytotherapy,* 9**,** 123-32.

LIO, C. W., DODSON, L. F., DEPPONG, C. M., HSIEH, C. S. & GREEN, J. M. 2010. CD28 facilitates the generation of Foxp3(-) cytokine responsive regulatory T cell precursors. *J Immunol,* 184**,** 6007-13.

LIO, C. W. & HSIEH, C. S. 2008. A two-step process for thymic regulatory T cell development. *Immunity,* 28**,** 100-11.

LIPTON, S. H. & BODWELL, C. E. 1973. Oxidation of amino acids by dimethyl sulfoxide. *J Agric Food Chem,* 21**,** 235-7.

LISTON, A., LESAGE, S., WILSON, J., PELTONEN, L. & GOODNOW, C. C. 2003. Aire regulates negative selection of organ-specific T cells. *Nat Immunol,* 4**,** 350-4.

LIU, Y., ZHANG, P., LI, J., KULKARNI, A. B., PERRUCHE, S. & CHEN, W. 2008. A critical function for TGF-beta signaling in the development of natural CD4+CD25+Foxp3+ regulatory T cells. *Nat Immunol,* 9**,** 632-40.

LUCKHEERAM, R. V., ZHOU, R., VERMA, A. D. & XIA, B. 2012. CD4(+)T cells: differentiation and functions. *Clin Dev Immunol,* 2012**,** 925135.

LUDVIGSSON, J., CHERAMY, M., AXELSSON, S., PIHL, M., AKERMAN, L., CASAS, R. & CLINICAL, G. A. D. S. G. I. S. 2014. GAD-treatment of children and adolescents with recent-onset type 1 diabetes preserves residual insulin secretion after 30 months. *Diabetes Metab Res Rev,* 30**,** 405-14.

LUDVIGSSON, J., FARESJO, M., HJORTH, M., AXELSSON, S., CHERAMY, M., PIHL, M., VAARALA, O., FORSANDER, G., IVARSSON, S., JOHANSSON, C.,

LINDH, A., NILSSON, N. O., AMAN, J., ORTQVIST, E., ZERHOUNI, P. & CASAS, R. 2008. GAD treatment and insulin secretion in recent-onset type 1 diabetes. *N Engl J Med,* 359**,** 1909-20.

LUTZ, M. B. & SCHULER, G. 2002. Immature, semi-mature and fully mature dendritic cells: which signals induce tolerance or immunity? *Trends Immunol,* 23**,** 445-9.

MACLEOD, M. K., CLAMBEY, E. T., KAPPLER, J. W. & MARRACK, P. 2009. CD4 memory T cells: what are they and what can they do? *Semin Immunol,* 21**,** 53-61.

MACLEOD, M. K., KAPPLER, J. W. & MARRACK, P. 2010. Memory CD4 T cells: generation, reactivation and re-assignment. *Immunology,* 130**,** 10-5.

MAKINO, S., KUNIMOTO, K., MURAOKA, Y., MIZUSHIMA, Y., KATAGIRI, K. & TOCHINO, Y. 1980. Breeding of a non-obese, diabetic strain of mice. *Jikken Dobutsu,* 29**,** 1-13.

MARC, P. S.-M., KANG; JAE-MIN, SONG;ALEXANDER, V. ANSTEY;MATTHEW, IVORY;RICHARD, W. COMPANS;JAMES, C. BIRCHALL 2010. Changes in Human Langerhans Cells Following Intradermal Injection of Influenza Virus-Like Particle Vaccines. *PLoS ONE* 5.

MAREK-TRZONKOWSKA, N., MYSLIWIEC, M., DOBYSZUK, A., GRABOWSKA, M., TECHMANSKA, I., JUSCINSKA, J., WUJTEWICZ, M. A., WITKOWSKI, P., MLYNARSKI, W., BALCERSKA, A., MYSLIWSKA, J. & TRZONKOWSKI, P. 2012. Administration of CD4+CD25highCD127- regulatory T cells preserves beta-cell function in type 1 diabetes in children. *Diabetes Care,* 35**,** 1817-20.

MARKLE, J. G., FRANK, D. N., MORTIN-TOTH, S., ROBERTSON, C. E., FEAZEL, L. M., ROLLE-KAMPCZYK, U., VON BERGEN, M., MCCOY, K. D., MACPHERSON, A. J. & DANSKA, J. S. 2013. Sex differences in the gut microbiome drive hormone-dependent regulation of autoimmunity. *Science,* 339**,** 1084-8.

MARTIN, C. J., ALLENDER, C. J., BRAIN, K. R., MORRISSEY, A. & BIRCHALL, J. C. 2012. Low temperature fabrication of biodegradable sugar glass microneedles for transdermal drug delivery applications. *Journal of controlled release : official journal of the Controlled Release Society,* 158**,** 93-101.

MARTIN, P., GOMEZ, M., LAMANA, A., CRUZ-ADALIA, A., RAMIREZ-HUESCA, M., URSA, M. A., YANEZ-MO, M. & SANCHEZ-MADRID, F. 2010. CD69 association with Jak3/Stat5 proteins regulates Th17 cell differentiation. *Mol Cell Biol,* 30**,** 4877-89.

MASTELLER, E. L., WARNER, M. R., TANG, Q., TARBELL, K. V., MCDEVITT, H. & BLUESTONE, J. A. 2005. Expansion of functional endogenous antigen-specific CD4+CD25+ regulatory T cells from nonobese diabetic mice. *J Immunol,* 175**,** 3053-9.

MATSUMURA, Y., KOBAYASHI, T., ICHIYAMA, K., YOSHIDA, R., HASHIMOTO, M., TAKIMOTO, T., TANAKA, K., CHINEN, T., SHICHITA, T., WYSS-CORAY, T., SATO, K. & YOSHIMURA, A. 2007. Selective expansion of foxp3-positive regulatory T cells and immunosuppression by suppressors of cytokine signaling 3-deficient dendritic cells. *J Immunol,* 179**,** 2170-9.

MATSUO, M., NAGATA, Y., SATO, E., ATANACKOVIC, D., VALMORI, D., CHEN, Y. T., RITTER, G., MELLMAN, I., OLD, L. J. & GNJATIC, S. 2004. IFN-gamma enables cross-presentation of exogenous protein antigen in human Langerhans cells by potentiating maturation. *Proc Natl Acad Sci U S A,* 101**,** 14467-72.

MCCAUGHTRY, T. M. & HOGQUIST, K. A. 2008. Central tolerance: what have we learned from mice? *Semin Immunopathol,* 30**,** 399-409.

MCGRATH, M. G., VRDOLJAK, A., O'MAHONY, C., OLIVEIRA, J. C., MOORE, A. C. & CREAN, A. M. 2011. Determination of parameters for successful spray coating of silicon microneedle arrays. *International journal of pharmaceutics,* 415**,** 140-9.

MEINGASSNER, J. G., KOWALSKY, E., SCHWENDINGER, H., ELBE-BURGER, A. & STUTZ, A. 2003. Pimecrolimus does not affect Langerhans cells in murine epidermis. *Br J Dermatol,* 149**,** 853-7.

MELLOR, A. L. & MUNN, D. H. 2004. IDO expression by dendritic cells: tolerance and tryptophan catabolism. *Nat Rev Immunol,* 4**,** 762-74.

MEMPEL, T. R., HENRICKSON, S. E. & VON ANDRIAN, U. H. 2004. T-cell priming by dendritic cells in lymph nodes occurs in three distinct phases. *Nature,* 427**,** 154-9.

MENDES-DA-CRUZ, D. A., SMANIOTTO, S., KELLER, A. C., DARDENNE, M. & SAVINO, W. 2008. Multivectorial abnormal cell migration in the NOD mouse thymus. *J Immunol,* 180**,** 4639-47.

MENTER, A., ABRAMOVITS, W., COLON, L. E., JOHNSON, L. A. & GOTTSCHALK, R. W. 2009. Comparing clobetasol propionate 0.05% spray to calcipotriene 0.005% betamethasone dipropionate 0.064% ointment for the treatment of moderate to severe plaque psoriasis. *J Drugs Dermatol,* 8**,** 52-7.

MERAD, M. & MANZ, M. G. 2009. Dendritic cell homeostasis. *Blood,* 113**,** 3418-27.

MERAD, M., SATHE, P., HELFT, J., MILLER, J. & MORTHA, A. 2013. The dendritic cell lineage: ontogeny and function of dendritic cells and their subsets in the steady state and the inflamed setting. *Annu Rev Immunol,* 31**,** 563-604.

MIKI-HOSOKAWA, T., HASEGAWA, A., IWAMURA, C., SHINODA, K., TOFUKUJI, S., WATANABE, Y., HOSOKAWA, H., MOTOHASHI, S., HASHIMOTO, K., SHIRAI, M., YAMASHITA, M. & NAKAYAMA, T. 2009. CD69 controls the pathogenesis of allergic airway inflammation. *J Immunol,* 183**,** 8203-15.

MILLER, M. J., SAFRINA, O., PARKER, I. & CAHALAN, M. D. 2004. Imaging the single cell dynamics of CD4+ T cell activation by dendritic cells in lymph nodes. *J Exp Med,* 200**,** 847-56.

MILLER, S. D., TURLEY, D. M. & PODOJIL, J. R. 2007. Antigen-specific tolerance strategies for the prevention and treatment of autoimmune disease. *Nat Rev Immunol,* 7**,** 665-77.

MILOUD, T., HAMMERLING, G. J. & GARBI, N. 2010. Review of murine dendritic cells: types, location, and development. *Methods in molecular biology,* 595**,** 21-42.

MOHAMMED, Y. H., YAMADA, M., LIN, L. L., GRICE, J. E., ROBERTS, M. S., RAPHAEL, A. P., BENSON, H. A. & PROW, T. W. 2014. Microneedle enhanced delivery of cosmeceutically relevant peptides in human skin. *PLoS One,* 9**,** e101956.

MOLL, H., FUCHS, H., BLANK, C. & ROLLINGHOFF, M. 1993. Langerhans cells transport Leishmania major from the infected skin to the draining lymph node for presentation to antigen-specific T cells. *European journal of immunology,* 23**,** 1595-601.

MOMMAAS, A. M., MULDER, A. A., OUT, C. J., GIROLOMONI, G., KOERTEN, H. K., VERMEER, B. J. & KONING, F. 1995. Distribution of HLA class II molecules in epidermal Langerhans cells in situ. *Eur J Immunol,* 25**,** 520-5.

MONTERO-HADJADJE, M., VAUDRY, H., TURQUIER, V., LEPRINCE, J., DO REGO, J. L., YON, L., GALLO-PAYET, N., PLOUIN, P. F. & ANOUAR, Y. 2002. Localization and characterization of evolutionarily conserved chromogranin A-derived peptides in the rat and human pituitary and adrenal glands. *Cell Tissue Res,* 310**,** 223-36.

MORDES, J. P., BORTELL, R., BLANKENHORN, E. P., ROSSINI, A. A. & GREINER, D. L. 2004. Rat models of type 1 diabetes: genetics, environment, and autoimmunity. *ILAR J,* 45**,** 278-91.

MORISHITA, M. & PEPPAS, N. A. 2006. Is the oral route possible for peptide and protein drug delivery? *Drug Discov Today,* 11**,** 905-10.

MOSER, M., DE SMEDT, T., SORNASSE, T., TIELEMANS, F., CHENTOUFI, A. A., MURAILLE, E., VAN MECHELEN, M., URBAIN, J. & LEO, O. 1995. Glucocorticoids down-regulate dendritic cell function in vitro and in vivo. *Eur J Immunol,* 25**,** 2818-24.

MOSMANN, T. 1983. Rapid colorimetric assay for cellular growth and survival: application to proliferation and cytotoxicity assays. *J Immunol Methods,* 65**,** 55-63.

MOSMANN, T. R., CHERWINSKI, H., BOND, M. W., GIEDLIN, M. A. & COFFMAN, R. L. 1986. Two types of murine helper T cell clone. I. Definition according to profiles of lymphokine activities and secreted proteins. *J Immunol,* 136**,** 2348-57.

MULLER, N., FISCHER, H. J., TISCHNER, D., VAN DEN BRANDT, J. & REICHARDT, H. M. 2013. Glucocorticoids induce effector T cell depolarization via ERM proteins, thereby impeding migration and APC conjugation. *J Immunol,* 190**,** 4360-70.

MURAT, J. C., GAMET, L., CAZENAVE, Y. & TROCHERIS, V. 1990. Questions about the use of [3H]thymidine incorporation as a reliable method to estimate cell proliferation rate. *Biochem J,* 270**,** 563-4.

N WILKE, A. M. 2007. Silicon microneedle formation using modified mask designs based on convex corner undercut. *J. Micromech. Microeng. ,* 17.

NAKAYAMA, K., MATSUURA, H., ASAI, M., OGAWARA, K., HIGAKI, K. & KIMURA, T. 1999. Estimation of intradermal disposition kinetics of drugs: I. Analysis by compartment model with contralateral tissues. *Pharm Res,* 16**,** 302-8.

NANTO-SALONEN, K., KUPILA, A., SIMELL, S., SILJANDER, H., SALONSAARI, T., HEKKALA, A., KORHONEN, S., ERKKOLA, R., SIPILA, J. I., HAAVISTO, L., SILTALA, M., TUOMINEN, J., HAKALAX, J., HYOTY, H., ILONEN, J., VEIJOLA, R., SIMELL, T., KNIP, M. & SIMELL, O. 2008. Nasal insulin to prevent type 1 diabetes in children with HLA genotypes and autoantibodies conferring increased risk of disease: a double-blind, randomised controlled trial. *Lancet,* 372**,** 1746-55.

NATARAJAN, K., SAWICKI, M. W., MARGULIES, D. H. & MARIUZZA, R. A. 2000. Crystal structure of human CD69: a C-type lectin-like activation marker of hematopoietic cells. *Biochemistry,* 39**,** 14779-86.

NEELAM, P. S. N. A. S. V. S. 2012. Skin kinetics and dermal clearance. *International Research Journal of Pharmacy,* 3**,** 6.

NELSON, B. H. & WILLERFORD, D. M. 1998. Biology of the interleukin-2 receptor. *Adv Immunol,* 70**,** 1-81.

NESTLE, F. O., DI MEGLIO, P., QIN, J. Z. & NICKOLOFF, B. J. 2009. Skin immune sentinels in health and disease. *Nature reviews. Immunology,* 9**,** 679-91.

NG, K. W., PEARTON, M., COULMAN, S., ANSTEY, A., GATELEY, C., MORRISSEY, A., ALLENDER, C. & BIRCHALL, J. 2009. Development of an ex vivo human skin model for intradermal vaccination: tissue viability and Langerhans cell behaviour. *Vaccine,* 27**,** 5948-55.

NG, T. H., BRITTON, G. J., HILL, E. V., VERHAGEN, J., BURTON, B. R. & WRAITH, D. C. 2013. Regulation of adaptive immunity; the role of interleukin-10. *Front Immunol,* 4**,** 129.

NICKOLOFF, B. J. & TURKA, L. A. 1994. Immunological functions of non-professional antigen-presenting cells: new insights from studies of T-cell interactions with keratinocytes. *Immunology today,* 15**,** 464-9.

NORMAN, J. J., BROWN, M. R., RAVIELE, N. A., PRAUSNITZ, M. R. & FELNER, E. I. 2013. Faster pharmacokinetics and increased patient acceptance of intradermal insulin delivery using a single hollow microneedle in children and adolescents with type 1 diabetes. *Pediatr Diabetes,* 14**,** 459-65.

OLATUNJI, O., DAS, D. B., GARLAND, M. J., BELAID, L. & DONNELLY, R. F. 2013. Influence of array interspacing on the force required for successful microneedle skin penetration: theoretical and practical approaches. *J Pharm Sci,* 102**,** 1209-21.

OLATUNJI, O., DAS, D. B. & NASSEHI, V. 2012. Modelling transdermal drug delivery using microneedles: effect of geometry on drug transport behaviour. *Journal of pharmaceutical sciences,* 101**,** 164-75.

ORBAN, T., FARKAS, K., JALAHEJ, H., KIS, J., TRESZL, A., FALK, B., REIJONEN, H., WOLFSDORF, J., RICKER, A., MATTHEWS, J. B., TCHAO, N., SAYRE, P. & BIANCHINE, P. 2010. Autoantigen-specific regulatory T cells induced in patients with type 1 diabetes mellitus by insulin B-chain immunotherapy. *J Autoimmun,* 34**,** 408-15.

OUYANG, W., BECKETT, O., MA, Q. & LI, M. O. 2010. Transforming growth factor-beta signaling curbs thymic negative selection promoting regulatory T cell development. *Immunity,* 32**,** 642-53.

OUYANG, W., RUTZ, S., CRELLIN, N. K., VALDEZ, P. A. & HYMOWITZ, S. G. 2011. Regulation and functions of the IL-10 family of cytokines in inflammation and disease. *Annu Rev Immunol,* 29**,** 71-109.

PALMER, E. & NAEHER, D. 2009. Affinity threshold for thymic selection through a T-cell receptor-co-receptor zipper. *Nat Rev Immunol,* 9**,** 207-13.

PALOMARES, O., O'MAHONY, L. & AKDIS, C. A. 2011. The many routes of dendritic cells to ensure immune regulation. *The Journal of allergy and clinical immunology,* 127**,** 1541-2.

PALUCKA, A. K., PEDROZA, A., ASPORD, C., BURTON, L. & BANCHEREAU, J. 2009. Abstract# 1167: Breast cancer instructs human myeloid dendritic cells to express OX40 ligand and to prime pro-inflammatory Th13 cells that facilitate tumor development. *Cancer Research,* 69**,** 1167-1167.

PAN, J., JU, D., WANG, Q., ZHANG, M., XIA, D., ZHANG, L., YU, H. & CAO, X. 2001a. Dexamethasone inhibits the antigen presentation of dendritic cells in MHC class II pathway. *Immunology letters,* 76**,** 153-61.

PAN, J., JU, D., WANG, Q., ZHANG, M., XIA, D., ZHANG, L., YU, H. & CAO, X. 2001b. Dexamethasone inhibits the antigen presentation of dendritic cells in MHC class II pathway. *Immunol Lett,* 76**,** 153-61.

PARK, J. H., ALLEN, M. G. & PRAUSNITZ, M. R. 2006. Polymer microneedles for controlled-release drug delivery. *Pharmaceutical research,* 23**,** 1008-19.

PEARTON, M., ALLENDER, C., BRAIN, K., ANSTEY, A., GATELEY, C., WILKE, N., MORRISSEY, A. & BIRCHALL, J. 2008. Gene delivery to the epidermal cells of human skin explants using microfabricated microneedles and hydrogel formulations. *Pharm Res,* 25**,** 407-16.

PEARTON, M., KANG, S. M., SONG, J. M., ANSTEY, A. V., IVORY, M., COMPANS, R. W. & BIRCHALL, J. C. 2010a. Changes in human Langerhans cells following intradermal injection of influenza virus-like particle vaccines. *PloS one,* 5**,** e12410.

PEARTON, M., KANG, S. M., SONG, J. M., KIM, Y. C., QUAN, F. S., ANSTEY, A., IVORY, M., PRAUSNITZ, M. R., COMPANS, R. W. & BIRCHALL, J. C. 2010b. Influenza virus-like particles coated onto microneedles can elicit stimulatory effects on Langerhans cells in human skin. *Vaccine,* 28**,** 6104-13.

PEARTON, M., SALLER, V., COULMAN, S. A., GATELEY, C., ANSTEY, A. V., ZARNITSYN, V. & BIRCHALL, J. C. 2012. Microneedle delivery of plasmid DNA to living human skin: Formulation coating, skin insertion and gene expression. *J Control Release,* 160**,** 561-9.

PENNA, G. & ADORINI, L. 2000. 1 Alpha,25-dihydroxyvitamin D3 inhibits differentiation, maturation, activation, and survival of dendritic cells

leading to impaired alloreactive T cell activation. *J Immunol,* 164**,** 2405-11.

PEPPER, M. & JENKINS, M. K. 2011. Origins of CD4(+) effector and central memory T cells. *Nat Immunol,* 12**,** 467-71.

PETERSON, J. D. & HASKINS, K. 1996. Transfer of diabetes in the NOD-scid mouse by CD4 T-cell clones. Differential requirement for CD8 T-cells. *Diabetes,* 45**,** 328-36.

PETTUS, J. & VON HERRATH, M. 2013. Keeping the patient perspective: Where are we in the world of type 1 diabetes? *Clin Immunol,* 149**,** 265-7.

PETZOLD, C., RIEWALDT, J., WATTS, D., SPARWASSER, T., SCHALLENBERG, S. & KRETSCHMER, K. 2013. Foxp3(+) regulatory T cells in mouse models of type 1 diabetes. *J Diabetes Res,* 2013**,** 940710.

PHILLIPS, J. M., PARISH, N. M., RAINE, T., BLAND, C., SAWYER, Y., DE LA PENA, H. & COOKE, A. 2009. Type 1 diabetes development requires both CD4+ and CD8+ T cells and can be reversed by non-depleting antibodies targeting both T cell populations. *Rev Diabet Stud,* 6**,** 97-103.

PIEMONTI, L., MONTI, P., ALLAVENA, P., LEONE, B. E., CAPUTO, A. & DI CARLO, V. 1999a. Glucocorticoids increase the endocytic activity of human dendritic cells. *Int Immunol,* 11**,** 1519-26.

PIEMONTI, L., MONTI, P., ALLAVENA, P., SIRONI, M., SOLDINI, L., LEONE, B. E., SOCCI, C. & DI CARLO, V. 1999b. Glucocorticoids affect human dendritic cell differentiation and maturation. *J Immunol,* 162**,** 6473-81.

PIROT, P., CARDOZO, A. K. & EIZIRIK, D. L. 2008. Mediators and mechanisms of pancreatic beta-cell death in type 1 diabetes. *Arq Bras Endocrinol Metabol,* 52**,** 156-65.

PIVARCSI, A., KEMENY, L. & DOBOZY, A. 2004. Innate immune functions of the keratinocytes. A review. *Acta microbiologica et immunologica Hungarica,* 51**,** 303-10.

POLIGONE, B., WEAVER, D. J., JR., SEN, P., BALDWIN, A. S., JR. & TISCH, R. 2002. Elevated NF-kappaB activation in nonobese diabetic mouse dendritic cells results in enhanced APC function. *J Immunol,* 168**,** 188-96.

QUAH, B. J. & PARISH, C. R. 2012. New and improved methods for measuring lymphocyte proliferation in vitro and in vivo using CFSE-like fluorescent dyes. *Journal of immunological methods,* 379**,** 1-14.

QUAH, B. J., WARREN, H. S. & PARISH, C. R. 2007. Monitoring lymphocyte proliferation in vitro and in vivo with the intracellular fluorescent dye carboxyfluorescein diacetate succinimidyl ester. *Nat Protoc,* 2**,** 2049-56.

QUAN, F. S., KIM, Y. C., SONG, J. M., HWANG, H. S., COMPANS, R. W., PRAUSNITZ, M. R. & KANG, S. M. 2013. Long-term protective immunity from an influenza virus-like particle vaccine administered with a microneedle patch. *Clinical and vaccine immunology : CVI,* 20**,** 1433-9.

QUAN, F. S., KIM, Y. C., YOO, D. G., COMPANS, R. W., PRAUSNITZ, M. R. & KANG, S. M. 2009. Stabilization of influenza vaccine enhances protection by microneedle delivery in the mouse skin. *PLoS One,* 4**,** e7152.

RANDOLPH, G. J., ANGELI, V. & SWARTZ, M. A. 2005. Dendritic-cell trafficking to lymph nodes through lymphatic vessels. *Nat Rev Immunol,* 5**,** 617-28.

RAPHAEL, A. P., PROW, T. W., CRICHTON, M. L., CHEN, X., FERNANDO, G. J. & KENDALL, M. A. 2010. Targeted, needle-free vaccinations in skin using multilayered, densely-packed dissolving microprojection arrays. *Small,* 6**,** 1785-93.

RATTANAPAK, T., BIRCHALL, J. C., YOUNG, K., KUBO, A., FUJIMORI, S., ISHII, M. & HOOK, S. 2014. Dynamic visualization of dendritic cell-antigen interactions in the skin following transcutaneous immunization. *PLoS One,* 9**,** e89503.

REA, D., VAN KOOTEN, C., VAN MEIJGAARDEN, K. E., OTTENHOFF, T. H., MELIEF, C. J. & OFFRINGA, R. 2000. Glucocorticoids transform CD40-triggering of dendritic cells into an alternative activation pathway resulting in antigen-presenting cells that secrete IL-10. *Blood,* 95**,** 3162-7.

REED, J. M., BRANIGAN, P. J. & BAMEZAI, A. 2008. Interferon gamma enhances clonal expansion and survival of CD4+ T cells. *J Interferon Cytokine Res,* 28**,** 611-22.

REIS E SOUSA, C., STAHL, P. D. & AUSTYN, J. M. 1993. Phagocytosis of antigens by Langerhans cells in vitro. *The Journal of experimental medicine,* 178**,** 509-19.

REIZIS, B., BUNIN, A., GHOSH, H. S., LEWIS, K. L. & SISIRAK, V. 2011. Plasmacytoid dendritic cells: recent progress and open questions. *Annu Rev Immunol,* 29**,** 163-83.

RHEN, T. & CIDLOWSKI, J. A. 2005. Antiinflammatory action of glucocorticoids--new mechanisms for old drugs. *N Engl J Med,* 353**,** 1711-23.

ROEP, B. O. 2003. The role of T-cells in the pathogenesis of Type 1 diabetes: from cause to cure. *Diabetologia,* 46**,** 305-21.

ROEP, B. O. & PEAKMAN, M. 2012. Antigen targets of type 1 diabetes autoimmunity. *Cold Spring Harb Perspect Med,* 2**,** a007781.

ROMAGNANI, S. 1999. Th1/Th2 cells. *Inflamm Bowel Dis,* 5**,** 285-94.

ROMANI, N., RATZINGER, G., PFALLER, K., SALVENMOSER, W., STOSSEL, H., KOCH, F. & STOITZNER, P. 2001. Migration of dendritic cells into lymphatics-the Langerhans cell example: routes, regulation, and relevance. *Int Rev Cytol,* 207**,** 237-70.

RONCHETTI, S., ZOLLO, O., BRUSCOLI, S., AGOSTINI, M., BIANCHINI, R., NOCENTINI, G., AYROLDI, E. & RICCARDI, C. 2004. GITR, a member of the TNF receptor superfamily, is costimulatory to mouse T lymphocyte subpopulations. *Eur J Immunol,* 34**,** 613-22.

ROY, S. D., HOU, S. Y., WITHAM, S. L. & FLYNN, G. L. 1994. Transdermal delivery of narcotic analgesics: comparative metabolism and permeability of human cadaver skin and hairless mouse skin. *J Pharm Sci,* 83**,** 1723-8.

ROZKOVA, D., HORVATH, R., BARTUNKOVA, J. & SPISEK, R. 2006. Glucocorticoids severely impair differentiation and antigen presenting function of dendritic cells despite upregulation of Toll-like receptors. *Clin Immunol,* 120**,** 260-71.

RYBA, M., RYBARCZYK-KAPTURSKA, K., ZORENA, K., MYSLIWIEC, M. & MYSLIWSKA, J. 2011. Lower frequency of CD62L(high) and higher frequency of TNFR2(+) Tregs are associated with inflammatory conditions in type 1 diabetic patients. *Mediators Inflamm,* 2011**,** 645643.

SABATOS-PEYTON, C. A., VERHAGEN, J. & WRAITH, D. C. 2010. Antigen-specific immunotherapy of autoimmune and allergic diseases. *Curr Opin Immunol,* 22**,** 609-15.

SAKUMAI, M., YACHIE, A. & KASAHARA, Y. 2007. [Role of T cells in the pathogenesis of type I diabetes mellitus: structure analysis of complementarity determining region 3 of circulating T cells]. *Rinsho Byori,* 55**,** 112-9.

SARAIVA, M. & O'GARRA, A. 2010. The regulation of IL-10 production by immune cells. *Nat Rev Immunol,* 10**,** 170-81.

SAVINA, A. & AMIGORENA, S. 2007. Phagocytosis and antigen presentation in dendritic cells. *Immunol Rev,* 219**,** 143-56.

SAXENA, V., ONDR, J. K., MAGNUSEN, A. F., MUNN, D. H. & KATZ, J. D. 2007. The countervailing actions of myeloid and plasmacytoid dendritic cells control autoimmune diabetes in the nonobese diabetic mouse. *J Immunol,* 179**,** 5041-53.

SCAGLIA, L., CAHILL, C. J., FINEGOOD, D. T. & BONNER-WEIR, S. 1997. Apoptosis participates in the remodeling of the endocrine pancreas in the neonatal rat. *Endocrinology,* 138**,** 1736-41.

SCHMETTERER, K. G., NEUNKIRCHNER, A. & PICKL, W. F. 2012. Naturally occurring regulatory T cells: markers, mechanisms, and manipulation. *FASEB J,* 26**,** 2253-76.

SCHRODER, K., HERTZOG, P. J., RAVASI, T. & HUME, D. A. 2004. Interferon-gamma: an overview of signals, mechanisms and functions. *J Leukoc Biol,* 75**,** 163-89.

SENESCHAL, J., JIANG, X. & KUPPER, T. S. 2014. Langerin(+) Dermal DC, but Not Langerhans Cells, Are Required for Effective CD8-Mediated Immune Responses after Skin Scarification with Vaccinia Virus. *J Invest Dermatol,* 134**,** 686-94.

SERREZE, D. V. & LEITER, E. H. 1994. Genetic and pathogenic basis of autoimmune diabetes in NOD mice. *Current opinion in immunology,* 6**,** 900-6.

SHAO, S., HE, F., YANG, Y., YUAN, G., ZHANG, M. & YU, X. 2012. Th17 cells in type 1 diabetes. *Cell Immunol,* 280**,** 16-21.

SHARPE, A. H. & FREEMAN, G. J. 2002. The B7-CD28 superfamily. *Nat Rev Immunol,* 2**,** 116-26.

SHEVACH, E. M. & STEPHENS, G. L. 2006. The GITR-GITRL interaction: co-stimulation or contrasuppression of regulatory activity? *Nat Rev Immunol,* 6**,** 613-8.

SHEVACH, E. M. & THORNTON, A. M. 2014. tTregs, pTregs, and iTregs: similarities and differences. *Immunol Rev,* 259**,** 88-102.

SHIBATA, M., KATSUYAMA, M., ONODERA, T., EHAMA, R., HOSOI, J. & TAGAMI, H. 2009. Glucocorticoids enhance Toll-like receptor 2 expression in human keratinocytes stimulated with Propionibacterium acnes or proinflammatory cytokines. *J Invest Dermatol,* 129**,** 375-82.

SHKLOVSKAYA, E., O'SULLIVAN, B. J., NG, L. G., ROEDIGER, B., THOMAS, R., WENINGER, W. & FAZEKAS DE ST GROTH, B. 2011. Langerhans cells are precommitted to immune tolerance induction. *Proceedings of the*

National Academy of Sciences of the United States of America, 108**,** 18049-54.

SIVAMANI, R. K., STOEBER, B., WU, G. C., ZHAI, H., LIEPMANN, D. & MAIBACH, H. 2005. Clinical microneedle injection of methyl nicotinate: stratum corneum penetration. *Skin Res Technol,* 11**,** 152-6.

SKYLER, J. S., KRISCHER, J. P., WOLFSDORF, J., COWIE, C., PALMER, J. P., GREENBAUM, C., CUTHBERTSON, D., RAFKIN-MERVIS, L. E., CHASE, H. P. & LESCHEK, E. 2005. Effects of oral insulin in relatives of patients with type 1 diabetes: The Diabetes Prevention Trial--Type 1. *Diabetes Care,* 28**,** 1068-76.

SMITH, E. B., BRENEMAN, D. L., GRIFFITH, R. F., HEBERT, A. A., HICKMAN, J. G., MALONEY, J. M., MILLIKAN, L. E., SULICA, V. I., DROMGOOLE, S. H., SEFTON, J. & ET AL. 1992. Double-blind comparison of naftifine cream and clotrimazole/betamethasone dipropionate cream in the treatment of tinea pedis. *J Am Acad Dermatol,* 26**,** 125-7.

SO, J. W., PARK, H. H., LEE, S. S., KIM, D. C., SHIN, S. C. & CHO, C. W. 2009. Effect of microneedle on the pharmacokinetics of ketoprofen from its transdermal formulations. *Drug delivery,* 16**,** 52-6.

SOLOMON, M. & SARVETNICK, N. 2004. The pathogenesis of diabetes in the NOD mouse. *Advances in immunology,* 84**,** 239-64.

SONG, J. M., KIM, Y. C., LIPATOV, A. S., PEARTON, M., DAVIS, C. T., YOO, D. G., PARK, K. M., CHEN, L. M., QUAN, F. S., BIRCHALL, J. C., DONIS, R. O., PRAUSNITZ, M. R., COMPANS, R. W. & KANG, S. M. 2010. Microneedle delivery of H5N1 influenza virus-like particles to the skin induces long-lasting B- and T-cell responses in mice. *Clin Vaccine Immunol,* 17**,** 1381-9.

SPRECHER, E., BECKER, Y., KRAAL, G., HALL, E., HARRISON, D. & SHULTZ, L. D. 1990. Effect of aging on epidermal dendritic cell populations in C57BL/6J mice. *J Invest Dermatol,* 94**,** 247-53.

STADINSKI, B. D., DELONG, T., REISDORPH, N., REISDORPH, R., POWELL, R. L., ARMSTRONG, M., PIGANELLI, J. D., BARBOUR, G., BRADLEY, B., CRAWFORD, F., MARRACK, P., MAHATA, S. K., KAPPLER, J. W. & HASKINS, K. 2010. Chromogranin A is an autoantigen in type 1 diabetes. *Nature immunology,* 11**,** 225-31.

STARY, G., KLEIN, I., BAUER, W., KOSZIK, F., REININGER, B., KOHLHOFER, S., GRUBER, K., SKVARA, H., JUNG, T. & STINGL, G. 2011a. Glucocorticosteroids modify Langerhans cells to produce TGF-beta and expand regulatory T cells. *J Immunol,* 186**,** 103-12.

STARY, G., KLEIN, I., BAUER, W., KOSZIK, F., REININGER, B., KOHLHOFER, S., GRUBER, K., SKVARA, H., JUNG, T. & STINGL, G. 2011b. Glucocorticosteroids modify Langerhans cells to produce TGF-beta and expand regulatory T cells. *Journal of immunology,* 186**,** 103-12.

STEINMAN, R. M. & COHN, Z. A. 1973. Identification of a novel cell type in peripheral lymphoid organs of mice. I. Morphology, quantitation, tissue distribution. *J Exp Med,* 137**,** 1142-62.

STOJADINOVIC, O., LEE, B., VOUTHOUNIS, C., VUKELIC, S., PASTAR, I., BLUMENBERG, M., BREM, H. & TOMIC-CANIC, M. 2007. Novel genomic effects of glucocorticoids in epidermal keratinocytes: inhibition of apoptosis, interferon-gamma pathway, and wound healing along with promotion of terminal differentiation. *J Biol Chem,* 282**,** 4021-34.

STOREY, M. & JORDAN, S. 2008. An overview of the immune system. *Nurs Stand,* 23**,** 47-56; quiz 58, 60.

STRATMANN, T., APOSTOLOPOULOS, V., MALLET-DESIGNE, V., CORPER, A. L., SCOTT, C. A., WILSON, I. A., KANG, A. S. & TEYTON, L. 2000. The I-Ag7 MHC class II molecule linked to murine diabetes is a promiscuous peptide binder. *J Immunol,* 165**,** 3214-25.

SULLIVAN, S. P., KOUTSONANOS, D. G., DEL PILAR MARTIN, M., LEE, J. W., ZARNITSYN, V., CHOI, S. O., MURTHY, N., COMPANS, R. W., SKOUNTZOU, I. & PRAUSNITZ, M. R. 2010. Dissolving polymer microneedle patches for influenza vaccination. *Nature medicine,* 16**,** 915-20.

SZELES, L., KERESZTES, G., TOROCSIK, D., BALAJTHY, Z., KRENACS, L., POLISKA, S., STEINMEYER, A., ZUEGEL, U., PRUENSTER, M., ROT, A. & NAGY, L. 2009. 1,25-dihydroxyvitamin D3 is an autonomous regulator of the transcriptional changes leading to a tolerogenic dendritic cell phenotype. *J Immunol,* 182**,** 2074-83.

TAKAHASHI, T., KUNIYASU, Y., TODA, M., SAKAGUCHI, N., ITOH, M., IWATA, M., SHIMIZU, J. & SAKAGUCHI, S. 1998. Immunologic self-tolerance maintained by CD25+CD4+ naturally anergic and suppressive T cells: induction of autoimmune disease by breaking their anergic/suppressive state. *Int Immunol,* 10**,** 1969-80.

TANG, Q. & BLUESTONE, J. A. 2013. Regulatory T-cell therapy in transplantation: moving to the clinic. *Cold Spring Harb Perspect Med,* 3.

TANG, Q., HENRIKSEN, K. J., BI, M., FINGER, E. B., SZOT, G., YE, J., MASTELLER, E. L., MCDEVITT, H., BONYHADI, M. & BLUESTONE, J. A. 2004. In vitro-expanded antigen-specific regulatory T cells suppress autoimmune diabetes. *J Exp Med,* 199**,** 1455-65.

TAPLIN, C. E., CRAIG, M. E., LLOYD, M., TAYLOR, C., CROCK, P., SILINK, M. & HOWARD, N. J. 2005. The rising incidence of childhood type 1 diabetes in New South Wales, 1990-2002. *Med J Aust,* 183**,** 243-6.

TARBELL, K. V., PETIT, L., ZUO, X., TOY, P., LUO, X., MQADMI, A., YANG, H., SUTHANTHIRAN, M., MOJSOV, S. & STEINMAN, R. M. 2007. Dendritic cell-expanded, islet-specific CD4+ CD25+ CD62L+ regulatory T cells restore normoglycemia in diabetic NOD mice. *J Exp Med,* 204**,** 191-201.

TAS, C., MANSOOR, S., KALLURI, H., ZARNITSYN, V. G., CHOI, S. O., BANGA, A. K. & PRAUSNITZ, M. R. 2012. Delivery of salmon calcitonin using a microneedle patch. *International journal of pharmaceutics,* 423**,** 257-63.

TESTI, R., D'AMBROSIO, D., DE MARIA, R. & SANTONI, A. 1994. The CD69 receptor: a multipurpose cell-surface trigger for hematopoietic cells. *Immunol Today,* 15**,** 479-83.

THOMPSON, C. B., LINDSTEN, T., LEDBETTER, J. A., KUNKEL, S. L., YOUNG, H. A., EMERSON, S. G., LEIDEN, J. M. & JUNE, C. H. 1989. CD28 activation pathway regulates the production of multiple T-cell-derived lymphokines/cytokines. *Proc Natl Acad Sci U S A,* 86**,** 1333-7.

THROWER, S. L., JAMES, L., HALL, W., GREEN, K. M., ARIF, S., ALLEN, J. S., VAN-KRINKS, C., LOZANOSKA-OCHSER, B., MARQUESINI, L., BROWN, S., WONG, F. S., DAYAN, C. M. & PEAKMAN, M. 2009. Proinsulin peptide immunotherapy in type 1 diabetes: report of a first-in-man Phase I safety study. *Clin Exp Immunol,* 155**,** 156-65.

TISCHNER, D., THEISS, J., KARABINSKAYA, A., VAN DEN BRANDT, J., REICHARDT, S. D., KAROW, U., HEROLD, M. J., LUHDER, F., UTERMOHLEN, O. & REICHARDT, H. M. 2011. Acid sphingomyelinase is required for protection of effector memory T cells against glucocorticoid-induced cell death. *J Immunol,* 187**,** 4509-16.

TIVOL, E. A., BORRIELLO, F., SCHWEITZER, A. N., LYNCH, W. P., BLUESTONE, J. A. & SHARPE, A. H. 1995. Loss of CTLA-4 leads to massive lymphoproliferation and fatal multiorgan tissue destruction, revealing a critical negative regulatory role of CTLA-4. *Immunity,* 3**,** 541-7.

TORRISI, B. M., ZARNITSYN, V., PRAUSNITZ, M. R., ANSTEY, A., GATELEY, C., BIRCHALL, J. C. & COULMAN, S. A. 2013. Pocketed microneedles for rapid delivery of a liquid-state botulinum toxin A formulation into human skin. *J Control Release,* 165**,** 146-52.

TRABARIS, M., LASKIN, J. D. & WEISEL, C. P. 2012. Effects of temperature, surfactants and skin location on the dermal penetration of haloacetonitriles and chloral hydrate. *Journal of exposure science & environmental epidemiology,* 22**,** 393-7.

TRUDEAU, J. D., DUTZ, J. P., ARANY, E., HILL, D. J., FIELDUS, W. E. & FINEGOOD, D. T. 2000. Neonatal beta-cell apoptosis: a trigger for autoimmune diabetes? *Diabetes,* 49**,** 1-7.

TUAN-MAHMOOD, T. M., MCCRUDDEN, M. T., TORRISI, B. M., MCALISTER, E., GARLAND, M. J., SINGH, T. R. & DONNELLY, R. F. 2013. Microneedles for intradermal and transdermal drug delivery. *Eur J Pharm Sci,* 50**,** 623-37.

UCHIZONO, Y., ALARCON, C., WICKSTEED, B. L., MARSH, B. J. & RHODES, C. J. 2007. The balance between proinsulin biosynthesis and insulin secretion: where can imbalance lead? *Diabetes Obes Metab,* 9 Suppl 2**,** 56-66.

UEDA, H., HOWSON, J. M., ESPOSITO, L., HEWARD, J., SNOOK, H., CHAMBERLAIN, G., RAINBOW, D. B., HUNTER, K. M., SMITH, A. N., DI GENOVA, G., HERR, M. H., DAHLMAN, I., PAYNE, F., SMYTH, D., LOWE, C., TWELLS, R. C., HOWLETT, S., HEALY, B., NUTLAND, S., RANCE, H. E., EVERETT, V., SMINK, L. J., LAM, A. C., CORDELL, H. J., WALKER, N. M., BORDIN, C., HULME, J., MOTZO, C., CUCCA, F., HESS, J. F., METZKER, M. L., ROGERS, J., GREGORY, S., ALLAHABADIA, A., NITHIYANANTHAN, R., TUOMILEHTO-WOLF, E., TUOMILEHTO, J., BINGLEY, P., GILLESPIE, K. M., UNDLIEN, D. E., RONNINGEN, K. S., GUJA, C., IONESCU-TIRGOVISTE, C., SAVAGE, D. A., MAXWELL, A. P., CARSON, D. J., PATTERSON, C. C., FRANKLYN, J. A., CLAYTON, D. G., PETERSON, L. B., WICKER, L. S., TODD, J. A. & GOUGH, S. C. 2003. Association of the T-cell regulatory gene CTLA4 with susceptibility to autoimmune disease. *Nature,* 423**,** 506-11.

UNGER, W. W., LABAN, S., KLEIJWEGT, F. S., VAN DER SLIK, A. R. & ROEP, B. O. 2009. Induction of Treg by monocyte-derived DC modulated by vitamin D3 or dexamethasone: differential role for PD-L1. *Eur J Immunol,* 39**,** 3147-59.

VALLADEAU, J., DUVERT-FRANCES, V., PIN, J. J., DEZUTTER-DAMBUYANT, C., VINCENT, C., MASSACRIER, C., VINCENT, J., YONEDA, K., BANCHEREAU, J., CAUX, C., DAVOUST, J. & SAELAND, S. 1999. The monoclonal antibody DCGM4 recognizes Langerin, a protein specific of Langerhans cells, and is rapidly internalized from the cell surface. *Eur J Immunol,* 29**,** 2695-704.

VAN BELLE, T. L., COPPIETERS, K. T. & VON HERRATH, M. G. 2011. Type 1 diabetes: etiology, immunology, and therapeutic strategies. *Physiological reviews,* 91**,** 79-118.

VAN DAMME, P., OOSTERHUIS-KAFEJA, F., VAN DER WIELEN, M., ALMAGOR, Y., SHARON, O. & LEVIN, Y. 2009. Safety and efficacy of a novel microneedle device for dose sparing intradermal influenza vaccination in healthy adults. *Vaccine,* 27**,** 454-9.

VAN DEN BROECK, W., DERORE, A. & SIMOENS, P. 2006. Anatomy and nomenclature of murine lymph nodes: Descriptive study and nomenclatory standardization in BALB/cAnNCrl mice. *J Immunol Methods,* 312**,** 12-9.

VAN DER AAR, A. M., PICAVET, D. I., MULLER, F. J., DE BOER, L., VAN CAPEL, T. M., ZAAT, S. A., BOS, J. D., JANSSEN, H., GEORGE, T. C., KAPSENBERG, M. L., VAN HAM, S. M., TEUNISSEN, M. B. & DE JONG, E. C. 2013. Langerhans cells favor skin flora tolerance through limited presentation of bacterial antigens and induction of regulatory T cells. *J Invest Dermatol,* 133**,** 1240-9.

VAN WILSEM, E. J., BREVE, J., KLEIJMEER, M. & KRAAL, G. 1994. Antigen-bearing Langerhans cells in skin draining lymph nodes: phenotype and kinetics of migration. *J Invest Dermatol,* 103**,** 217-20.

VANDEMEULEBROUCKE, E., GORUS, F. K., DECOCHEZ, K., WEETS, I., KEYMEULEN, B., DE BLOCK, C., TITS, J., PIPELEERS, D. G., MATHIEU, C. & BELGIAN DIABETES, R. 2009. Insulin treatment in IA-2A-positive relatives of type 1 diabetic patients. *Diabetes Metab,* 35**,** 319-27.

VERBAAN, F. J., BAL, S. M., VAN DEN BERG, D. J., GROENINK, W. H., VERPOORTEN, H., LUTTGE, R. & BOUWSTRA, J. A. 2007. Assembled microneedle arrays enhance the transport of compounds varying over a large range of molecular weight across human dermatomed skin. *Journal of controlled release : official journal of the Controlled Release Society,* 117**,** 238-45.

VIGNALI, D. A., COLLISON, L. W. & WORKMAN, C. J. 2008. How regulatory T cells work. *Nat Rev Immunol,* 8**,** 523-32.

WALKER, L. S. 2004. CD4+ CD25+ Treg: divide and rule? *Immunology,* 111**,** 129-37.

WALUNAS, T. L., BAKKER, C. Y. & BLUESTONE, J. A. 1996. CTLA-4 ligation blocks CD28-dependent T cell activation. *J Exp Med,* 183**,** 2541-50.

WAN, Y. Y. & FLAVELL, R. A. 2005. Identifying Foxp3-expressing suppressor T cells with a bicistronic reporter. *Proc Natl Acad Sci U S A,* 102**,** 5126-31.

WEAVER, D. J., JR., LIU, B. & TISCH, R. 2001. Plasmid DNAs encoding insulin and glutamic acid decarboxylase 65 have distinct effects on the progression of autoimmune diabetes in nonobese diabetic mice. *J Immunol,* 167**,** 586-92.

WERMELING, D. P., BANKS, S. L., HUDSON, D. A., GILL, H. S., GUPTA, J., PRAUSNITZ, M. R. & STINCHCOMB, A. L. 2008. Microneedles permit

transdermal delivery of a skin-impermeant medication to humans. *Proc Natl Acad Sci U S A,* 105**,** 2058-63.

WESTON, S. A. & PARISH, C. R. 1990. New fluorescent dyes for lymphocyte migration studies. Analysis by flow cytometry and fluorescence microscopy. *J Immunol Methods,* 133**,** 87-97.

WIDELITZ, R. B., JIANG, T. X., NOVEEN, A., TING-BERRETH, S. A., YIN, E., JUNG, H. S. & CHUONG, C. M. 1997. Molecular histology in skin appendage morphogenesis. *Microscopy research and technique,* 38**,** 452-65.

WIDERA, G., JOHNSON, J., KIM, L., LIBIRAN, L., NYAM, K., DADDONA, P. E. & CORMIER, M. 2006. Effect of delivery parameters on immunization to ovalbumin following intracutaneous administration by a coated microneedle array patch system. *Vaccine,* 24**,** 1653-64.

WONG, V. W., SORKIN, M., GLOTZBACH, J. P., LONGAKER, M. T. & GURTNER, G. C. 2011. Surgical approaches to create murine models of human wound healing. *J Biomed Biotechnol,* 2011**,** 969618.

WU, I., SHIN, S. C., CAO, Y., BENDER, I. K., JAFARI, N., FENG, G., LIN, S., CIDLOWSKI, J. A., SCHLEIMER, R. P. & LU, N. Z. 2013. Selective glucocorticoid receptor translational isoforms reveal glucocorticoid-induced apoptotic transcriptomes. *Cell Death Dis,* 4**,** e453.

XING, Y. & HOGQUIST, K. A. 2012. T-cell tolerance: central and peripheral. *Cold Spring Harb Perspect Biol,* 4.

YALOW, R. S. & BERSON, S. A. 1960. Immunoassay of endogenous plasma insulin in man. *J Clin Invest,* 39**,** 1157-75.

YAN, G., WARNER, K. S., ZHANG, J., SHARMA, S. & GALE, B. K. 2010. Evaluation needle length and density of microneedle arrays in the pretreatment of skin for transdermal drug delivery. *International journal of pharmaceutics,* 391**,** 7-12.

YESHURUN, Y., LEVIN, Y., ALMAGOR, Y., LAVI, G., HEFETZ, M., SEFI, Y. & CATCHPOLE, R. I. 2009. Intradermal delivery of biological agents. Google Patents.

YI, Z., DIZ, R., MARTIN, A. J., MORILLON, Y. M., KLINE, D. E., LI, L., WANG, B. & TISCH, R. 2012. Long-term remission of diabetes in NOD mice is induced by nondepleting anti-CD4 and anti-CD8 antibodies. *Diabetes,* 61**,** 2871-80.

YOU, S., SLEHOFFER, G., BARRIOT, S., BACH, J. F. & CHATENOUD, L. 2004. Unique role of CD4+CD62L+ regulatory T cells in the control of autoimmune diabetes in T cell receptor transgenic mice. *Proc Natl Acad Sci U S A,* 101 Suppl 2**,** 14580-5.

ZARIC, M., LYUBOMSKA, O., TOUZELET, O., POUX, C., AL-ZAHRANI, S., FAY, F., WALLACE, L., TERHORST, D., MALISSEN, B., HENRI, S., POWER, U. F., SCOTT, C. J., DONNELLY, R. F. & KISSENPFENNIG, A. 2013. Skin Dendritic Cell Targeting via Microneedle Arrays Laden with Antigen-Encapsulated Poly-d,l-lactide-co-Glycolide Nanoparticles Induces Efficient Antitumor and Antiviral Immune Responses. *ACS nano,* 7**,** 2042-55.

ZHAN, Y., FUNDA, D. P., EVERY, A. L., FUNDOVA, P., PURTON, J. F., LIDDICOAT, D. R., COLE, T. J., GODFREY, D. I., BRADY, J. L., MANNERING, S. I., HARRISON, L. C. & LEW, A. M. 2004. TCR-mediated activation promotes GITR upregulation in T cells and resistance to glucocorticoid-induced death. *Int Immunol,* 16**,** 1315-21.

ZHANG, H., PODOJIL, J. R., CHANG, J., LUO, X. & MILLER, S. D. 2010. TGF-beta-induced myelin peptide-specific regulatory T cells mediate antigen-specific suppression of induction of experimental autoimmune encephalomyelitis. *J Immunol,* 184**,** 6629-36.

ZHANG, J., GAO, W., YANG, X., KANG, J., ZHANG, Y., GUO, Q., HU, Y., XIA, G. & KANG, Y. 2013a. Tolerogenic vaccination reduced effector memory CD4 T cells and induced effector memory Treg cells for type I diabetes treatment. *PLoS One,* 8**,** e70056.

ZHANG, N. & BEVAN, M. J. 2011. CD8(+) T cells: foot soldiers of the immune system. *Immunity,* 35**,** 161-8.

ZHANG, X., CHANG LI, X., XIAO, X., SUN, R., TIAN, Z. & WEI, H. 2013b. CD4(+)CD62L(+) central memory T cells can be converted to Foxp3(+) T cells. *PLoS One,* 8**,** e77322.

ZHOU, C. P., LIU, Y. L., WANG, H. L., ZHANG, P. X. & ZHANG, J. L. 2010. Transdermal delivery of insulin using microneedle rollers in vivo. *Int J Pharm,* 392**,** 127-33.

ZHU, J. & PAUL, W. E. 2008. CD4 T cells: fates, functions, and faults. *Blood,* 112**,** 1557-69.

ZHU, Q., ZARNITSYN, V. G., YE, L., WEN, Z., GAO, Y., PAN, L., SKOUNTZOU, I., GILL, H. S., PRAUSNITZ, M. R., YANG, C. & COMPANS, R. W. 2009. Immunization by vaccine-coated microneedle arrays protects against lethal influenza virus challenge. *Proceedings of the National Academy of Sciences of the United States of America,* 106**,** 7968-73.

ZHU, Z., LUO, H., LU, W., LUAN, H., WU, Y., LUO, J., WANG, Y., PI, J., LIM, C. Y. & WANG, H. 2014. Rapidly dissolvable microneedle patches for transdermal delivery of exenatide. *Pharm Res,* 31**,** 3348-60.